



Durham E-Theses

Synthesis and Characterisation of Poly(vinyl alcohol) based materials for use within Personal Products

KING, PETER,ANDREW

How to cite:

KING, PETER,ANDREW (2015) *Synthesis and Characterisation of Poly(vinyl alcohol) based materials for use within Personal Products*, Durham theses, Durham University. Available at Durham E-Theses Online: <http://etheses.dur.ac.uk/11355/>

Use policy

The full-text may be used and/or reproduced, and given to third parties in any format or medium, without prior permission or charge, for personal research or study, educational, or not-for-profit purposes provided that:

- a full bibliographic reference is made to the original source
- a [link](#) is made to the metadata record in Durham E-Theses
- the full-text is not changed in any way

The full-text must not be sold in any format or medium without the formal permission of the copyright holders.

Please consult the [full Durham E-Theses policy](#) for further details.

Academic Support Office, Durham University, University Office, Old Elvet, Durham DH1 3HP
e-mail: e-theses.admin@dur.ac.uk Tel: +44 0191 334 6107
<http://etheses.dur.ac.uk>

Synthesis and Characterisation of Poly(vinyl alcohol) based materials for use within Personal Products

A thesis submitted for the degree of

Doctor of Philosophy

by

Peter Andrew King



Department of Chemistry

Durham University

England

Abstract

Cationic polymers based upon poly(vinyl alcohol) (PVA) are synthesised with various levels of charge densities, molecular architectures and hydrophobicities. Furthermore, macroinitiators incorporating PVA segments are synthesised and subsequently used for single electron transfer - living radical polymerisation (SET-LRP) for the synthesis of a range of graft copolymers.

Chapter 1 is a general introduction on cationic polymers, their use within conditioning shampoo formulations and the chemical properties required for this application. The polymerisation techniques: ring-opening polymerisation and reversible deactivation radical polymerisation (RDRP); as well as the polymeric materials: PVA and polyglycerol are also discussed.

Chapter 2 involves the synthesis of cationic PVA through either etherification or esterification reactions. The etherification of PVA using either glycidyltrimethylammonium chloride (GTMAC) or 1,2-chlorohydroxypropyltrimethylammonium chloride (CHPTMAC) to synthesise poly[(vinyl alcohol)-*ran*-(vinyl, 2-hydroxypropyl ether trimethylammonium chloride)] (P[VA]-*r*-(VETMAC)) is investigated. The charge densities of the polymers synthesised by slowing the rate of reaction with GTMAC were determined to be greater than the charge densities claimed in the literature. The synthesis of poly(vinyl betaine) (PVB) *via* the synthesis of poly(vinyl chloroacetate) as an intermediate is discussed, as well as attempts to control the charge density of the resulting PVB. The charge density of the synthesised polymers were determined using UV-Vis spectroscopy and by nuclear magnetic resonance (NMR) spectroscopy.

Chapter 3 discusses the synthesis of a novel hyperbranched graft copolymer, poly[(vinyl alcohol)-*graft*-(hyperbranched glycerol)] (P[(VA)-*g*-(hPG)]). The effects of the reaction conditions on the mole fraction of hyperbranched polyglycerol ($x_{(hPG)}$), the degree of branching (%DB) and the degree of substitution (%DS) were all monitored for the water solvated reactions. The synthesis of P[(VA)-*g*-(hPG)] in organic solvents is also discussed. Furthermore, comparisons between P[(VA)-*g*-(hPG)] and physical blends of PVA and hyperbranched polyglycerol are also made.

Chapter 4 entails the synthesis of cationic polymers based upon P[(VA)-*g*-(hPG)] synthesised in Chapter 3. Poly[(vinyl alcohol)-*ran*-(vinyl,2-hydroxypropyl ether trimethylammonium chloride)-*graft*-(hyperbranched polyglycerol-2-hydroxypropyl ether

trimethylammonium chloride)] (P[(VA)-*r*-(VETMAC)-*g*-(hPG-PETMAC)]) was synthesised from the reaction between P[(VA)-*g*-(hPG)] as the macroinitiator and GTMAC. The charge density of the resulting polymer was found to increase with increasing $x_{(hPG)}$ in the macroinitiator; charge densities up to 5.4 meq g⁻¹ were determined. Furthermore, the synthesis of poly[(vinyl betaine)-*graft*-(hyperbranched polyglycerol betaine)] is also discussed.

Chapter 5 describes the synthesis of hydrophobic derivatives of the polymers synthesised in the previous chapters using epoxyoctane to synthesise poly[(vinyl alcohol)-*ran*-(vinyl, 2-hydroxy octyl ether)], poly[(vinyl alcohol)-*ran*-(vinyl, 2-hydroxy octyl ether)-*ran*-(vinyl, 2-hydroxypropyl ether trimethylammonium chloride)], poly[(vinyl alcohol)-*ran*-(vinyl, 2-hydroxy octyl ether)-*graft*-(hyperbranched polyglycerol-2-hydroxyoctyl ether)] and poly[(vinyl, 2-hydroxy octyl ether)-*ran*-(vinyl, 2-hydroxypropyl ether trimethylammonium chloride)-*ran*-(vinyl alcohol)-*graft*-(hyperbranched polyglycerol)-(2-hydroxypropyl ether trimethylammonium chloride)/(2-hydroxy octyl ether)]. The hydrophobicity of the synthesised polymers is measured based upon their contact angle and aqueous solubility.

Chapter 6 focuses on the synthesis of macroinitiators for RDRP containing PVA and poly(vinyl, 2-bromopropionate) (PVBrP) repeat units. 2-bromopropionic anhydride was synthesised for the reaction with PVA. Poly[(vinyl, 2-bromopropionate)-*ran*-(vinyl 2-butyral)] was synthesised when the reaction was carried out in butanone. However when 1,4-dioxane was used as the reaction solvent poly[(vinyl alcohol)-*ran*-(vinyl, 2-bromopropionate)] (P[(VA)-*r*-(VBrP)]) was successfully synthesised, with 62% or 79% initiating groups (PVBrP groups).

Chapter 7 details the synthesis of graft copolymers by SET-LRP, using P[(VA)-*r*-(VBrP)] macroinitiators which were synthesised in Chapter 6. Methyl acrylate was polymerised with P[(VA)-*r*-(VBrP)] macroinitiators containing 62% or 79% initiating sites (PVBrP), with a molecular weight of 2.31×10^6 gmol⁻¹ determined by atomic force microscopy. Hydroxyethyl acrylate was polymerised with P[(VA)-*r*-(VBrP)] macroinitiator containing 62% initiating sites to synthesise poly[(vinyl alcohol)-*ran*-(vinyl 2-bromopropionate)-*graft*-(hydroxyethyl acrylate)] (P[(VA)-*r*-(VBrP)-*g*-(HEA)]), a water soluble polymer. When unpurified HEA monomer was polymerised, a cross-linked material was recovered with a 50% swelling ratio. N-isopropylacrylamide was also polymerised using P[(VA)-*r*-(VBrP)] macroinitiator containing 62% initiating sites, to synthesise a thermoresponsive polymer with a lower critical saturation temperature of 36 °C.

Chapter 8 surmises and concludes the work covered in Chapters 2 - 7, and further work is also suggested.

Acknowledgements

I would like to thank Dr. Ezat Khosravi for his contributions during my PhD studies. I also would like to acknowledge my industrial sponsor Dr. Osama Musa for his insight regarding my research. I want to thank Doug Carswell, for running the DSC and TGA experiments; Dr. Richard Thompson and Dr. Stephen Boothroyd, for their help with help with AFM measurements; and Dr. Juan Aguilar, Dr. Alan Kenwright and Dr. Catherine Heffernan for their assistance with NMR analysis. I am also grateful towards the members of the mechanical and electrical workshops, CIS department, lab technicians in stores and lab attendants for their assistance.

I am also going to thank the members of Khosravi research group, Dr. David Cole, Dr. Iain Johnson, Shenghui Hou, Russell Balster, Andrew Longstaff, Rose Simnett, Kieran Atter, Ejaz Ahmed and Danny Clee. Further thanks to the people of CG156 and CG165 past and present, in particularly Asahi Cano-Marques, Alex Hudson, Paul Brooks, Serena Agostini, Tatiana Lovato and Sam Lear. Thanks also to Ustinov College AFC; Van Mildert MCR; and my housemates Judith Evans and Martin Brader for their support.

I am also grateful for my family's support during my PhD, my mother, father and reluctantly my brother as well. Finally, special thanks to my partner Cat Blackwell who did the contact angle measurements for me.

Memorandum

The work reported in this thesis was carried out in the Department of Chemistry, Durham University, between October 2011 and December 2014. This work has not been submitted for any other degree in Durham and is the original work of the author except where acknowledged by means of appropriate reference.

Signed: _____

Date: _____

Statement of Copyright

The copyright of this thesis rests with the author. No quotation from it should be published without their prior written consent and information derived from it should be acknowledged.

Financial Support

I gratefully acknowledge Ashland Inc. and Engineering and Physical Sciences Research Council (EPSRC) for their funding of this research.

Contents

Abstract.....	ii
Acknowledgements.....	v
Memorandum	vi
Statement of Copyright.....	vi
Financial Support	vi
Contents.....	vii
Abbreviations.....	xvi

Chapter 1: General Background

1.1. Cationic polymers overview.....	2
1.1.1. Application of cationic polymers in personal products	2
1.2. Charge density	9
1.2.1. Charge density calculations	9
1.2.1.1. Spectrophotometric colloid titrations	9
1.2.1.2. Nuclear Magnetic Resonance spectroscopy	11
1.3. Polymerisation methods.....	11
1.3.1. Ring-opening Polymerisation.....	11
1.3.2. Radical polymerisations	13
1.3.2.1. Controlled radical polymerisations	15
1.3.2.1.1. Atom Transfer Radical Polymerisation	16

1.3.2.1.2. Single Electron Transfer - Living Radical Polymerisation	17
1.3.3. Graft Copolymerisation.....	19
1.4. Polymeric materials	21
1.4.1 Poly(vinyl alcohol)	21
1.4.1.1. Synthesis of cationic Poly(vinyl alcohol)	23
1.4.2. Synthesis of graft copolymers with polyglycerol side chains.....	25
1.5. Aims and objectives	29
1.6. References	30
<u>Chapter 2: Synthesis and characterisation of cationic poly(vinyl alcohol)</u>	
2.1. Introduction	35
2.2. Experimental	36
2.2.1. Materials	36
2.2.2. Instrumentation	37
2.2.3. Synthesis of poly[(vinyl alcohol)- <i>ran</i> -(vinyl, 2-hydroxypropyl ether trimethylammonium chloride)]	37
2.2.3.1. Using Glycidyltrimethylammonium chloride	37
2.2.3.2. Using 1,2-Chlorohydroxypropyltrimethylammonium chloride	38
2.2.4. Synthesis of Poly(vinyl chloroacetate)	38
2.2.5. Synthesis of Poly(vinyl betaine)	39
2.2.7. Synthesis of Poly[(vinyl alcohol)- <i>ran</i> -(vinyl betaine)]	39

2.2.8. Colloid titration monitored by UV-Vis spectroscopy	40
2.3. Results and Discussion	40
2.3.1. Synthesis of poly[(vinyl alcohol)- <i>ran</i> -(vinyl, 2-hydroxypropyl ether trimethylammonium chloride)]	40
2.3.1.1. Synthesis of P[(VA)- <i>r</i> -(VETMAC)] with GTMAC	40
2.3.1.2. Synthesis of P[(VA)- <i>r</i> -(VETMAC)] with CHPTMAC	45
2.3.1.3. Determining charge density of P[(VA)- <i>r</i> -(VETMAC)]	46
2.3.1.3.1. Colloid titration of P[(VA)- <i>r</i> -(VETMAC)]	46
2.3.1.3.2. ¹ H NMR spectroscopy	50
2.3.1.4. Effects of reaction conditions on charge density of P[(VA)- <i>r</i> -(VETMAC)]	51
2.3.1.4.1. Molar equivalents of GTMAC	51
2.3.1.4.2. Addition of inert diluent	52
2.3.1.4.3. Addition time of GTMAC	52
2.3.1.4.5. Reproducibility	54
2.3.3. Synthesis of poly(vinyl chloroacetate)	54
2.3.5. Synthesis of Poly(vinyl betaine)	61
2.3.6. Synthesis of Poly[(vinyl betaine)- <i>ran</i> -(vinyl alcohol)]	67
2.4. Conclusion	68
2.5. Reference	69

Chapter 3: Synthesis and characterisation of poly[(vinyl alcohol)-graft-(hyperbranched polyglycerol)]

3.1. Introduction	71
3.2. Experimental	73
3.2.1. Materials	73
3.2.2. Instrumentation	73
3.2.3. Synthesis of hyperbranched polyglycerol	73
3.2.4. Synthesis of poly[(vinyl alcohol)-graft-(hyperbranched glycerol)] in water	74
3.2.5. Synthesis of Poly[(vinyl alcohol)-graft-(hyperbranched glycerol)] in organic solvents	74
3.2.6. Preparation of Poly(vinyl alcohol)/hyperbranched polyglycerol blends	75
3.3. Results and Discussion	75
3.3.1. Synthesis of hyperbranched polyglycerol	75
3.3.2. Synthesis of Poly[(vinyl alcohol)-graft-(hyperbranched glycerol)] in water	81
3.3.2.1. Effects of reaction conditions	89
3.3.2.1.1. Reaction time	90
3.3.2.1.2. Molar equivalence of NaOH.....	90
3.3.2.1.3. Molar equivalence of glycidol	91
3.3.2.1.4. Reaction temperature.....	92
3.3.2.1.5. Glycidol addition time.....	94

3.3.3. Synthesis of Poly[(vinyl alcohol)- <i>graft</i> -(hyperbranched glycerol)] in organic solvents	97
3.3.4. Physical Properties of Poly[(vinyl alcohol)- <i>graft</i> -(hyperbranched glycerol)].....	97
3.3.5. Poly(vinyl alcohol)/hyperbranched polyglycerol blends.....	100
3.4. Conclusion.....	101
3.5. References	102
 <u>Chapter 4: Synthesis and characterisation of cationic poly[(vinyl alcohol)-<i>graft</i>-(hyperbranched polyglycerol)]</u>	
4.1. Introduction	104
4.2. Experimental	105
4.2.1 Materials	105
4.2.2 Instrumentation	105
4.2.3. Synthesis of Poly[(vinyl alcohol)- <i>ran</i> -(vinyl,2-hydroxypropyl ether trimethylammonium chloride)- <i>graft</i> -(hyperbranched polyglycerol-2-hydroxypropyl ether trimethylammonium chloride)].....	106
4.2.4. Synthesis of Poly[(vinyl chloroacetate)- <i>graft</i> -(hyperbranched polyglycerol 2-chloroacetate)]	106
4.2.5. Synthesis of Poly[(vinyl betaine)- <i>graft</i> -(hyperbranched polyglycerol betaine)]	107
4.3. Results and Discussion	107
4.3.1. Synthesis Poly[(vinyl alcohol)- <i>ran</i> -(vinyl,2-hydroxypropyl ether trimethylammonium chloride)- <i>graft</i> -(hyperbranched polyglycerol-2-hydroxypropyl ether trimethylammonium chloride)].....	107

4.3.2. Synthesis of Poly[(vinyl betaine)- <i>graft</i> -(hyperbranched polyglycerol betaine)]	112
4.3.2.1. Synthesis of Poly[(vinyl chloroacetate)- <i>graft</i> -(hyperbranched polyglycerol 2-chloroacetate)]	113
4.3.2.2. Quarternisation of poly[(vinyl chloroacetate)- <i>graft</i> -(hyperbranched polyglycerol 2-chloroacetate)]	118
4.4. Conclusion	121
4.5. References	122

Chapter 5: Synthesis and Characterisation of hydrophobic poly(vinyl alcohol) derivatives

5.1. Introduction	124
5.2. Experimental	125
5.2.1. Materials	125
5.2.2. Instrumentation	126
5.2.4. Synthesis of Poly[(vinyl alcohol)- <i>ran</i> -(vinyl, 2-hydroxy octyl ether)]	127
5.2.5. Synthesis of Poly[(vinyl alcohol)- <i>ran</i> -(vinyl, 2-hydroxy octyl ether)- <i>ran</i> -(vinyl, 2-hydroxypropyl ether trimethylammonium chloride)]	127
5.2.6. Synthesis of Poly[(vinyl alcohol)- <i>ran</i> -(vinyl, 2-hydroxy octyl ether)- <i>graft</i> -(hyperbranched polyglycerol-2-hydroxyoctyl ether)]	128
5.2.7. Synthesis of Poly[(vinyl, 2-hydroxy octyl ether)- <i>ran</i> -(vinyl, 2-hydroxypropyl ether trimethylammonium chloride)- <i>ran</i> -(vinyl alcohol)- <i>graft</i> -(hyperbranched polyglycerol)-(2-hydroxypropyl ether trimethylammonium chloride)/(2-hydroxy octyl ether)]	128
5.3. Results and Discussion	129

5.3.1. Synthesis of Poly[(vinyl alcohol)- <i>ran</i> -(vinyl, 2-hydroxy octyl ether)]	129
5.3.2. Synthesis of Poly[(vinyl alcohol)- <i>ran</i> -(vinyl, 2-hydroxy octyl ether)- <i>ran</i> -(vinyl, 2-hydroxypropyl ether trimethylammonium chloride)]	135
5.3.3. Synthesis of Poly[(vinyl alcohol)- <i>ran</i> -(vinyl, 2-hydroxy octyl ether)- <i>graft</i> -(hyperbranched polyglycerol-2-hydroxyoctyl ether)].....	139
5.3.4. Synthesis of Poly[(vinyl, 2-hydroxy octyl ether)- <i>ran</i> -(vinyl, 2-hydroxypropyl ether trimethylammonium chloride)- <i>ran</i> -(vinyl alcohol)- <i>graft</i> -(hyperbranched polyglycerol)-(2-hydroxypropyl ether trimethylammonium chloride)/(2-hydroxy octyl ether)]	143
5.3.5. Hydrophobic character analysis.....	147
5.4. Conclusion.....	154
5.5. References	155

Chapter 6: Synthesis and characterisation of poly(vinyl alcohol)-based Reversible-deactivation radical polymerisation initiators

6.1. Introduction	157
6.2. Experimental	158
6.2.1. Materials	158
6.2.2. Instrumentation	158
6.2.3. Synthesis of 2-bromopropionic anhydride	159
6.2.4. Synthesis of poly[(vinyl, 2-bromopropionate)- <i>ran</i> -(vinyl, 2-butyral)]	159
6.2.5. Synthesis of poly[(vinyl alcohol)- <i>ran</i> -(vinyl, 2-bromopropionate)]	160
6.3. Results & Discussion	160
6.3.1. Synthesis of 2-bromopropionic anhydride	160

6.3.2. Synthesis of poly[(vinyl, 2-bromopropionate)- <i>ran</i> -(vinyl, 2-butyral)]	164
6.3.3. Synthesis of poly[(vinyl alcohol)- <i>ran</i> -(vinyl, 2-bromopropionate)]	171
6.4. Conclusion	178
6.5. References	179

Chapter 7: Reversible-deactivation radical polymerisation of poly(vinyl alcohol)-based initiators

7.1. Introduction	181
7.2. Experimental	182
7.2.1. Materials	182
7.2.2. Instrumentation	183
7.2.3. Synthesis of poly[(vinyl alcohol)- <i>ran</i> -(vinyl 2-bromopropionate)- <i>graft</i> -(methyl acrylate)]	184
7.2.4. Synthesis of poly[(vinyl alcohol)- <i>ran</i> -(vinyl 2-bromopropionate)- <i>graft</i> -(hydroxyethyl acrylate)]	184
7.2.5. Synthesis of poly[(vinyl alcohol)- <i>ran</i> -(vinyl 2-bromopropionate)- <i>graft</i> -(N-isopropylacrylamide)]	185
7.3. Results & Discussion	186
7.3.1. Synthesis of poly[(vinyl alcohol)- <i>ran</i> -(vinyl 2-bromopropionate)- <i>graft</i> -(methyl acrylate)]	186
7.3.2. Synthesis of poly[(vinyl alcohol)- <i>ran</i> -(vinyl 2-bromopropionate)- <i>graft</i> -(hydroxyethyl acrylate)]	194

7.3.3. Synthesis of poly[(vinyl alcohol)- <i>ran</i> -(vinyl 2-bromopropionate)- <i>graft</i> -(N-isopropylacrylamide)]	197
7.4. Conclusion.....	201
7.5. References	202
<u>Chapter 8: Conclusions and future perspectives</u>	
8.1. Summary of work and general conclusions	204
8.2. Preliminary evaluation of poly(vinyl alcohol)-based materials applicability for use with shampoo formulations.....	213
8.3. Future perspectives	214
8.3.1. Application evaluation	214
8.3.2. Synthetic work	215
8.3. References	216
Appendix 1 - Appendices for Chapter 2.....	218
Appendix 2 - Appendices for Chapter 7.....	219

Abbreviations

%conv	Conversion
%DB	Degree of branching
%DS	Degree of substitution
%GE	Grafting efficiency
%HS	Degree of hydrophobic substitution
%mol	Molar equivalents
%QNC	Quaternary nitrogen content
%wt	Weight percentage
[M] _{eq}	Monomer concentration at equilibrium
[surf]	Surfactant concentration
1CAC	First critical aggregation concentration
2CAC	Second critical aggregation concentration
AFM	Atomic force microscopy
ASAP	Atmospheric solids analysis probe
ATRP	Atom transfer radical polymerisation
B.p.	Boiling point
BDH	β-diketone hydrolase
BPAnh	2-Bromopropionic anhydride
CAA	Chloroacetic anhydride
CAC	Critical aggregation concentration
CD	Charge density
CHPTMAC	1,2-Chlorohydroxypropylammonium chloride

cm	Centimetre
CMC	Critical micelle concentration
COSY	Correlation spectroscopy
CRP	Controlled radical polymerisation
CTAB	Hexadecyltrimethylammonium bromide
Cu	Copper
Cu(II)Br ₂	Copper (II) bromide
D	Dendritic
Đ	Dispersity
D ₂ O	Deuterium oxide
DCC	Dicyclocarbodiimide
DCM	Dichloromethane
dd	Double doublet
DEPT-135	Distortionless enhancement by polarization transfer-135
DMAP	4-Dimethylaminopyridine
DMF	Dimethylformamide
DMPU	1,3-Dimethyl-3,4,5,6-tetrahydro-2(1H)-pyrimidinone
DMSO	Dimethyl sulfoxide
DOWEX	DOWEX® MARATHON MR-3 mixed bed ion-exchange
DP	Degree of polymerisation
dq	Double quartet
DSC	Differential scanning calorimetry
<i>e.g.</i>	<i>exempli gratia</i>

<i>et al.</i>	<i>et alii, et alia</i>
FRP	Free radical polymerisation
FT-IR	Fourier transform infra-red spectroscopy
g	Gram(s)
GTMAC	Glycidyltrimethylammonium chloride
h	Hour(s)
H ₂ O	Water
HCl	Hydrochloric acid
HEA	Hydroxyethyl acrylate
HMBC	Heteronuclear multiple-bond correlation
HMW	High molecular weight
hPG	Hyperbranched polyglycerol
HSQC	Heteronuclear single quantum coherence
Hz	Hertz
<i>i.e.</i>	<i>id est</i>
ICAR	Initiators for continuous activator regeneration
INCI	International nomenclature of cosmetic ingredients
ISCT	Inner sphere electron transfer
J	Joules
J _#	Coupling constant
kHz	Kilohertz
KPVS	Potassium poly(vinyl sulphate)
L _{1,3}	Linear-1,3

L _{1,4}	Linear-1,4
LCST	Lower critical solution temperature
LiBr	Lithium bromide
LMW	Low molecular weight
M	Molarity
MA	Methyl acrylate
MeOH	Methanol
meq	Milliequivalent(s)
MgSO ₄	Magnesium sulphate
MHz	Megahertz
mmol	Millimole(s)
min	Minute(s)
mL	Millilitre(s)
mol	Moles
M _p	Peak molecular weight
M _w	Weight-average molar mass
MW	Molecular weight
MWCO	Molecular weight cut-off
N	Newton(s)
NaCl	Sodium chloride
NaHCO ₃	Sodium carbonate
NaOH	Sodium hydroxide
NaOMe	Sodium methoxide

NIPAM	N-isopropylacrylamide
nm	Nanometre(s)
NMe ₃	Trimethylamine
NMP	N-methyl-2-pyrrolidone
NMR	Nuclear magnetic resonance
OSET	Outer sphere electron transfer
<i>o</i> -Tb	<i>o</i> -Toluidine blue
P[(VBrP)- <i>r</i> -(VByl)]	Poly[(vinyl, 2-bromopropionate)- <i>ran</i> -(vinyl, 2-butyral)]
PVA	Poly(vinyl alcohol)
P[(VA)- <i>g</i> -(hPG)]	Poly[(vinyl alcohol)- <i>graft</i> -(hyperbranched polyglycerol)]
P[(VA)- <i>g</i> -(VAc)]	Poly[(vinyl alcohol)- <i>graft</i> -(vinyl acetate)]
P[(VA)- <i>r</i> -(VBrP)]	Poly[(vinyl alcohol)- <i>ran</i> -(vinyl, 2-bromopropionate)]
P[(VA)- <i>r</i> -(VBrP)- <i>g</i> -(HEA)]	Poly[(vinyl alcohol)- <i>ran</i> -(vinyl, 2-bromopropionate)- <i>graft</i> -(hydroxyethyl acrylate)]
P[(VA)- <i>r</i> -(VBrP)- <i>g</i> -(MA)]	Poly[(vinyl alcohol)- <i>ran</i> -(vinyl, 2-bromopropionate)- <i>graft</i> -(methyl acrylate)]
P[(VA)- <i>r</i> -(VBrP)- <i>g</i> -(NIPAM)]	Poly[(vinyl alcohol)- <i>ran</i> -(vinyl, 2-bromopropionate)- <i>graft</i> -(N-isopropylacrylamide)]
P[(VA)- <i>r</i> -(VETMAC)]	Poly[(vinyl alcohol)- <i>ran</i> -(vinyl, 2-hydroxypropyl ether trimethylammonium chloride)]
P[(VA)- <i>r</i> -(VETMAC)- <i>g</i> -(hPG-PETMAC)]	Poly[(vinyl alcohol)- <i>ran</i> -(vinyl, 2-hydroxypropyl ether trimethylammonium chloride)- <i>graft</i> -(hyperbranched polyglycerol-2-hydroxypropyl ether trimethylammonium chloride)]
P[(VA)- <i>r</i> -(VOE)]	Poly[(vinyl alcohol)- <i>ran</i> -(vinyl, 2-hydroxy octyl ether)]
P[(VA)- <i>r</i> -(VOE)- <i>g</i> -(hPG-OE)]	Poly[(vinyl alcohol)- <i>ran</i> -(vinyl, 2-hydroxy octyl ether)- <i>graft</i> -(hyperbranched polyglycerol-2-hydroxyoctyl ether)]
P[(VA)- <i>r</i> -(VOE)- <i>r</i> -	Poly[(vinyl alcohol)- <i>ran</i> -(vinyl, 2-hydroxy octyl ether)- <i>ran</i> -

(VETMAC)]	(vinyl,2-hydroxypropyl ether trimethylammonium chloride)]
P[(VB)- <i>g</i> -(hPG-B)]	Poly[(vinyl betaine)- <i>graft</i> -(hyperbranched polyglycerol betaine)]
P[(VCA)- <i>g</i> -(hPG-CA)]	Poly[(vinyl chloroacetate)- <i>graft</i> -(hyperbranched polyglycerol 2-chloroacetate)]
P[(VOE)- <i>r</i> -(VETMAC)- <i>r</i> -(VA)- <i>g</i> -(hPG-PETMAC/OE)]	Poly[(vinyl, 2-hydroxy octyl ether)- <i>ran</i> -(vinyl, 2-hydroxypropyl ether trimethylammonium chloride)- <i>ran</i> -(vinyl alcohol)- <i>graft</i> -(hyperbranched polyglycerol)-(2-hydroxypropyl ether trimethylammonium chloride)/(2-hydroxy octyl ether)])
ppm	Parts per million
PETMAC	2-Hydroxypropyl ether]trimethylammonium chloride
PHOS	Poly(4-hydroxystyrene)
PMA	Poly(methyl acrylate)
polyquat	Polyquaternium
PVAc	Poly(vinyl acetate)
PVBrP	Poly(vinyl, 2-bromopropionate)
PVByl	Poly(vinyl, 2-butyral)
PVCA	Poly(vinyl chloroacetate)
PVETMAC	Poly(vinyl, 2-hydroxypropyl ether trimethylammonium chloride)
PVPyl	Poly(vinyl, 2-propyl)
<i>r</i>	Correlation coefficient
RAFT	Reversible addition fragmentation chain transfer
RDRP	Reversible - deactivation radical polymerisation
RI	Refractive index
ROMP	Ring-opening metathesis polymerisation

ROP	Ring-opening polymerisation
RT	Ambient temperature
s	Second(s)
SAO	Secondary alcohol oxidase
SARA	Supplemental activator and reducing agent
SEC	Size exclusion chromatography
T	Terminal
T_c	Crystallisation temperature
T_d	Degradation temperature
T_g	Glass transition temperature
TGA	Thermogravimetric analysis
THMP	1,1,1-Tris(hydroxymethyl)propane
T_m	Melting point
TREN	Tris(2-aminoethyl)amine
v/v	Volume in volume
w/v	Weight in volume
$x_{(hPG)}$	Mole fraction of hyperbranched polyglycerol
λ	Wavelength
μL	Microlitre(s)
ν	Wavenumber
χ_c	Degree of crystallinity

Chapter 1

General Background

1.1. Cationic polymers overview

Cationic polymers are an important commodity polymer due to their adsorptive and biocidal properties. Generally polymers, unlike small molecules, have strong adsorptive properties; the adsorption energy of each segment is multiplied over the length of the entire polymer chain. If one segment desorbs from the surface it is more likely to re-adsorb than the remaining segments to desorb.¹ For cationic polymers adsorption is enhanced by the electrostatic interactions with anionic surfaces, *i.e.* damaged hair. Cationic polymers also have biocidal properties as the cationic charge can interfere with the cell membrane, displacing cationic species which results in fatal leakage of cytoplasm.²

Cationic polymers are used in an array of applications; such as water treatment, anti-fouling coatings, paper milling, pharmaceuticals and personal products.^{3,4,5,6} The adsorptive properties of cationic polymers make them desirable for use in personal products, such as moisturisers and conditioning shampoos. This thesis will mainly be focusing on their use as a conditioning agent in shampoo, as the materials developed during this project are for potential use in shampoo.

1.1.1. Application of cationic polymers in personal products

Cationic polymers play an important, but minor role, in modern day shampoos typically only making up 0.5% of formulations. Shampoos primarily consist of water (77%); the remainder of the formulation contains surfactants; conditioning ingredients (including silicone emulsion and cationic polymers); fragrance and other additives, which optimise performance, Figure 1.1.⁶

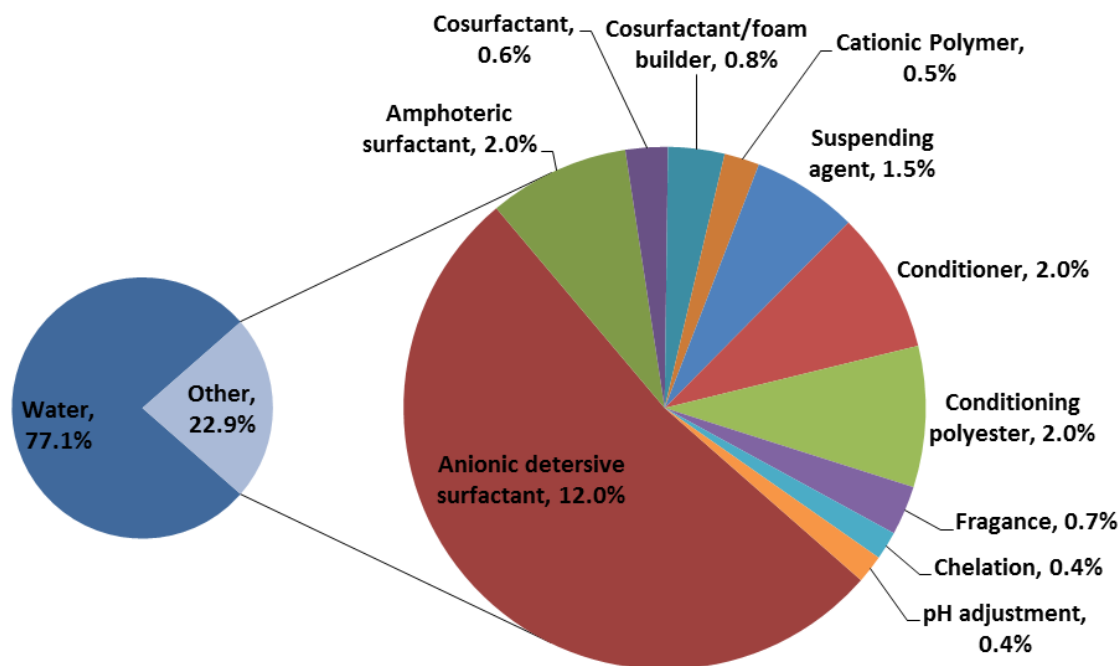


Figure 1.1: Composition of an idealised shampoo formulation.⁶

Surfactants are the second largest ingredient in formulations (15.4%) as they perform the primary task of shampoo of cleaning hair by removing dirt, skin particles and sebum. Sebum is a naturally occurring oil that is secreted onto the cuticle to protect the surface. However, excess sebum gives hair a lank and greasy appearance; therefore, its removal improves the appearance of hair.⁷ Sebum is hydrophobic and therefore cannot be solely removed using water, so surfactants are used. Surfactants are amphiphilic molecules containing a hydrophilic 'head' group and a hydrophobic 'tail' group. The hydrophilicity of the 'head' group is sufficient for surfactants to be water soluble; however the 'tail' groups remain in a 'hostile' aqueous environment. In water/oil systems, to reduce the interaction with the unfavourable aqueous phase, surfactants will adsorb at oily interfaces and form aggregates known as micelles consisting of an exterior of 'head' groups which protects the 'tail' group interior from water. The adsorption of surfactants at the interface between water and sebum reduces the surface tension allowing for better mixing; which enables sebum, and other hydrophobic impurities adsorbed in sebum, to be rinsed away with water during shampooing. A multitude of surfactants are used in conjunction with the primary surfactant (commonly lauryl sulphates), this is to affect the shape of the micelles formed. Instead of forming spherical micelles, the

cosurfactants reduce the curvature changing the architecture into a more 'worm' like shape, increasing the viscosity of the shampoo giving a more desired texture.⁷

The removal of sebum from hair can damage the cuticle so components are included into shampoo to repair the surface of the follicle. This is achieved by a silicone emulsion coating the cuticle and smoothing the hair surface which reduces its roughness. This deposition leaves hair feeling softer, more manageable (reducing the number of split ends, friction between shafts of hair and increasing combability) and more damage resistant.⁸

The deposition efficiency of expensive silicone is low; as conditioning shampoos perform two competing tasks; they remove dirt from hair whilst also depositing silicone emulsion. However, a small quantity of cationic polymer has been shown to improve silicone deposition and other particulates (*e.g.* anti-dandruff, styling agents), by adsorbing onto the hair strand.⁹ The adsorbed cationic polymer aids the formation of seam welds; which are thin layers of water between two hair shafts. Seam welds allow silicone emulsions to travel by capillary force closer to the root of the hair providing more uniform coverage.⁶

Cationic polymers deposit onto hair *via* the dilution-deposition mechanism. They form polymer/surfactant complexes, known as coacervates, with the detergent anionic surfactant molecules, already present in shampoo formulations. The surface activity of a coacervate is markedly greater than the original polymer, increasing its efficacy.¹⁰ Coacervate formation has been proven by measuring the surface tension of a polymer/surfactant system in comparison to a surfactant only system. The surface tension of both systems decrease with increasing surfactant concentration ([surf]), until aggregates begin to form and a plateau in surface tension is observed, Figure 1.2. In the surfactant only system, the plateau occurs at the critical micelle concentration (CMC), which is the [surf] when micelles begin to form. In the polymer/surfactant system, the plateau is observed at a lower [surf], due to coacervate formation known as the critical aggregation concentration (CAC), but the surface tension is greater. This phenomenon is also observed in some charge neutral polymer/surfactant systems (*e.g.* Poly[vinyl acetate] (PVAc), poly[ethylene oxide] and poly[vinyl pyrrolidone]).¹ Hemimicelles and micelles form along the polymer in the coacervate. However, once the polymer binding sites have been exhausted the surface tension begins to decrease again to another plateau in surface tension in line with the surfactant only system as solitary micelles begin to form. As the CAC occurs at lower concentrations than the CMC, the formation of coacervates is energetically more favourable than micellisation.

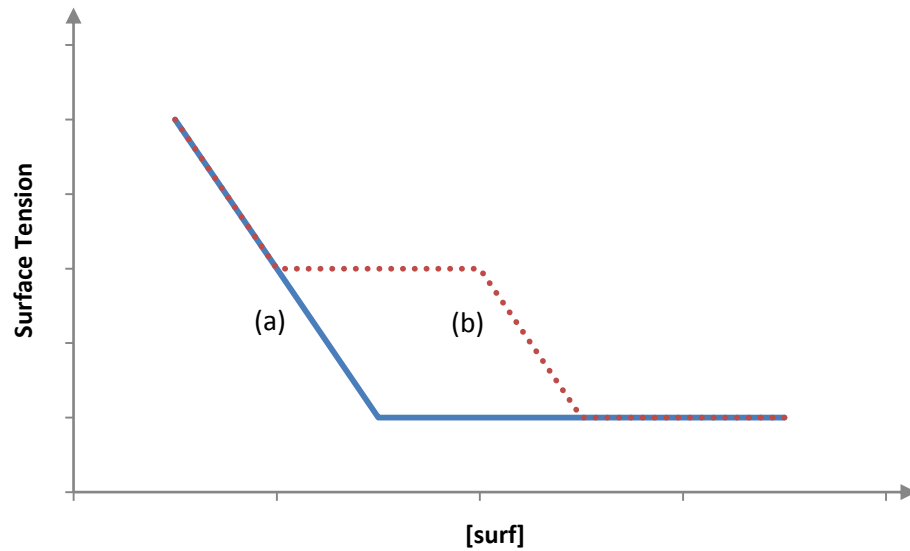


Figure 1.2: The decrease in surface tension of a solution with increasing [surf] (a) Surfactant only system (b) Polymer and surfactant system

Coacervate formation in shampoos is driven by the initial electrostatic interaction between the polyion and surfactant molecules; the first adsorbed surfactant molecules become nucleation site for micellular aggregates to form.¹¹ Once the coacervate is formed, the [surf] determines the complex's solubility and conformation, Figure 1.3. Two CACs are observed for coacervates; the first CAC (1CAC) is when the micellular structures initially form, creating a charge neutral complex. In this state, the coacervate becomes insoluble in water and therefore precipitates. In some formulations a second CAC (2CAC) is observed, when the [surf] increases and excess anionic surfactant binds to the coacervate; the complex becomes negatively charged and water soluble.^{6,12} The 2CAC is only observed with polymers with sufficient hydrophobic character.¹² The polymer's physical properties also impact the value of the 1CAC, with the concentration being affected by the polymer's charge density and hydrophobic character (see later).

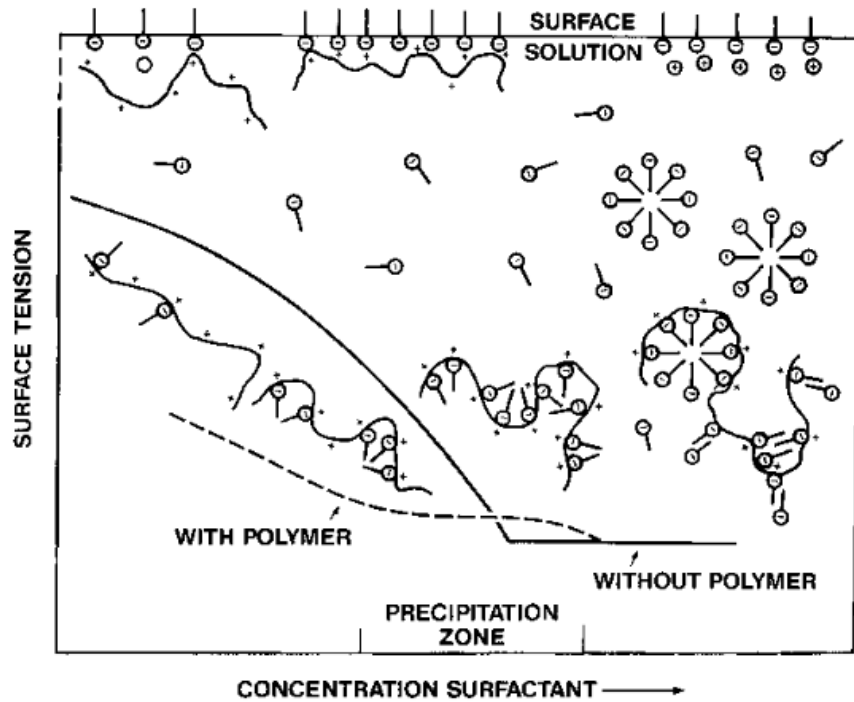


Figure 1.3: The effect of [surf] as surface tension, polymer conformation and solubility.¹

The high [surf] in shampoo formulations means that cationic polymers are present in negatively charged coacervates ($[\text{surf}] > 2\text{CAC}$). So when the shampooed hair is rinsed, the [surf] decreases below the 2CAC, precipitating the coacervate which then adsorbs on to follicle's surface. This was illustrated by Johnson *et al.* who simultaneously measured the turbidity of a solution and the mass of the adsorbed polymer in relation to the [surf]. A peak in the turbidity of the solution, due to the precipitation of the coacervate, coincides with a maxima in adsorbed polymer, Figure 1.4.¹³ It should be noted that polymers can still adsorb onto a surface without any surfactant present, but at a lesser extent. It is whilst the coacervate is adsorbed on the surface that seam welds are formed, aiding in the deposition of the active ingredients, particularly silicone emulsion.

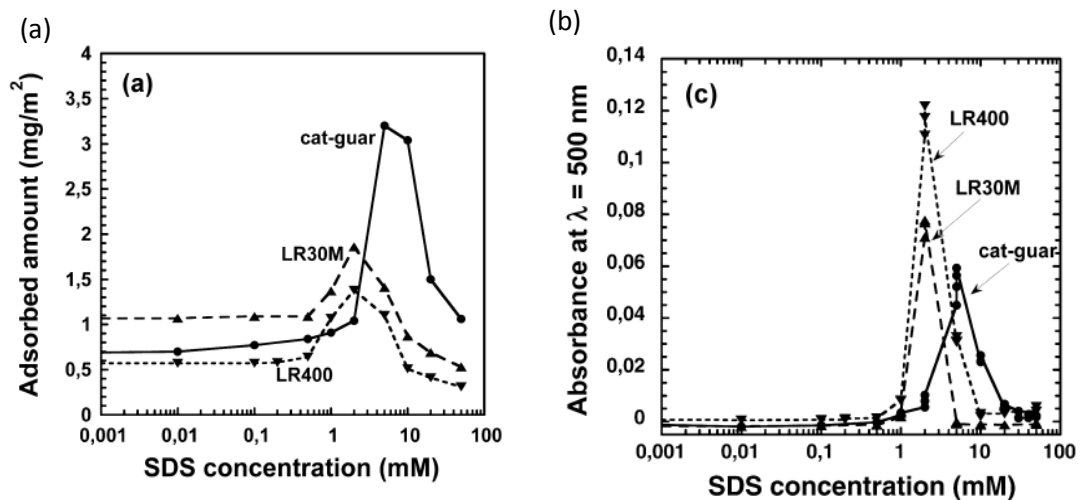


Figure 1.4: Graphs showing the effect on increasing [surf] has on (a) absorbed polymer amount and (b) turbidity of solution for various cationic polymers.¹⁴

As rinsing continues, the [surf] decreases below the 1CAC and the coacervate solubilises and desorbs from the surface. However, removal of the coacervate by increasing the [surf] above the 2CAC has proven to be more effective.¹⁵ Complete desorption is ideal as residual polymer left on the cuticle surface results in added weight making hair sag giving it an unwanted lank appearance of appearing low in volume, and flat.¹⁶

A secondary role of cationic polymers is that they can also improve the creaminess of the shampoo lathers by adsorbing across the foam lamella, hindering drainage, and blocking the plateau border, stabilising the foam.¹⁷

Conditioning shampoos were introduced by Balsam Shampoos in the 1960s, but it was not until the 1980s that coacervates were used as delivery agents.⁶ Nearly 100 polyquaterniums (polyquats) are registered with the International Nomenclature of Cosmetic Ingredients (INCI) after approval by the Personal Care Products Council.^{18,19} Polyquats are differentiated by their assigned number, designated by registration date not the chemical structure. A range of polyquats are shown in Figure 1.5.

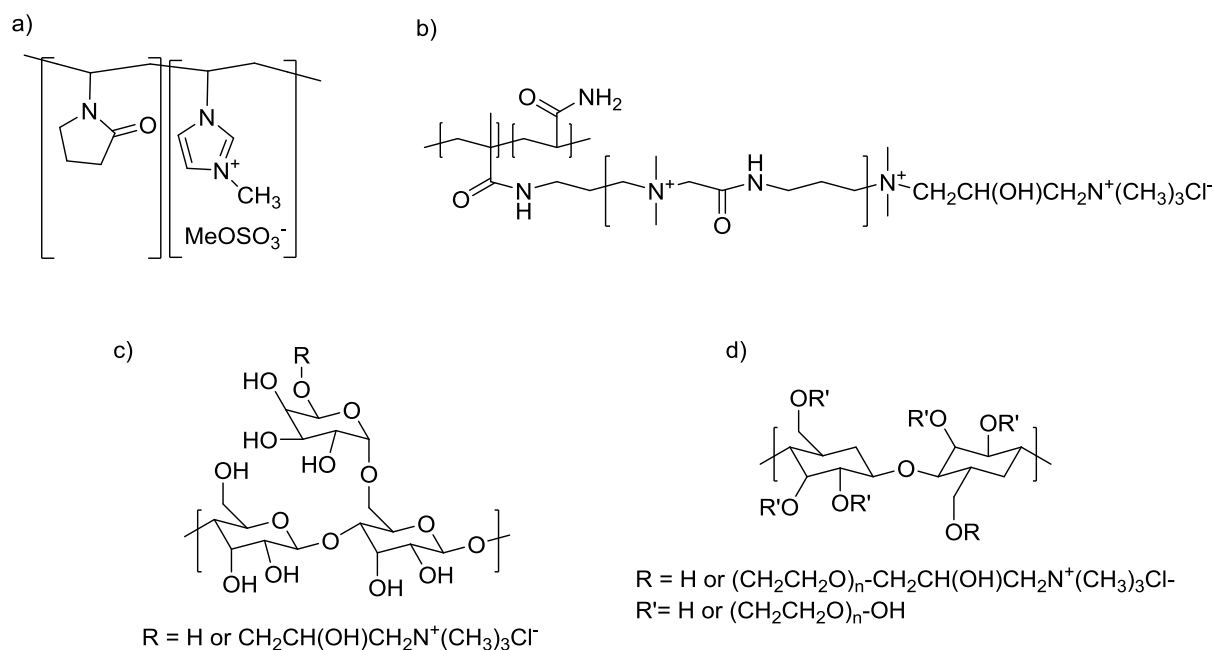


Figure 1.5: The structures of selected commercial cationic polymers (a) Polyquat-44 (b) Polyquat-76 (c) cationic-guar (d) polyquat-10

The efficacy of the cationic polymer to deposit a silicone emulsion followed by desorption of the polymer, depends on its properties. The molecular weight plays a vital role in the formation of the coacervate, as a minimum molecular weight of the cationic polymer is required for the formation of the surfactant/polymer complex at a given polymer concentration.^{1,20} Furthermore, an increase in the molecular weight results in an increase in the interaction between the polymer and the surfactant, and therefore improved coacervation. This is because polymers with a higher molecular weight deposit more silicone.¹⁶ The molecular weight also has an effect on the desorption of the polymer, it has been shown that polymers with a higher molecular weight will desorb more completely than lower molecular weight polymers.²¹

The hydrophobicity of the polymer impacts the 1CAC and it is the sole factor in the important 2CAC.¹² When the 2CAC is just below the concentration of the surfactant in the formulations is when superior deposition has been observed.²² However, a reduction in the deposited amount was observed with increased hydrophobicity, in polyions with equal charge densities, by Piculles *et al.*²³

The polymer architecture affects the imbued properties on hair. A branched polymer has been shown to compare favourably against linear polymers, it was theorised that the more

coiled and less hydrated branched structure was more readily deposited. The coiled polymer conformation also aides desorption from the surface.⁸ The flexibility of the polymer chain is important as more flexible synthetic polymers condition hair more effectively, compared to more rigid natural product based polymers; as the polymer chain flexibility affects the conformation of the polymer in solution.²⁴

1.2. Charge density

The charge density of a polymer is important as the electrostatic interactions between the surfactant and the polyion impact the 1CAC. A minimum charge density is required for most polymers to form a coacervate. There are some non-ionic polymers (mentioned earlier) that can form polymer/surfactant complexes, due to their hydrophobicity, but the interactions between oppositely charged polymers and surfactants is much greater.¹ The charge density also affects the conformation of the absorbed polymer; high charge density polyions will absorb parallel to the surface so a lower mass quantity is required to cover the same area.²¹ However, the desorption of the polyion increases with decreasing charge density.¹⁵ The charge density can affect the water content of the coacervate; the higher water content with low charge density polymers provides softer feel and volume enhancement in comparison to high charge density polymer.¹⁶

1.2.1. Charge density calculations

1.2.1.1. Spectrophotometric colloid titrations

The charge density of a polyion can be determined by titrating against a polyion with an opposite charge and using a small molecule as an indicator. For colloid titrations of cationic polymers a cationic dye as the indicator and an anionic polymer as the titrant are used.

The anionic polymer is added to the titrand containing the cationic polymer and indicator. The binding of the anionic polymer with the cationic polymer is favoured over the cationic dye, as the binding affinity increases with number of possible sites on the molecule. Which is seen as a molecular weight dependence in comparisons between charged species.²⁵ Once the added anionic polymer has finished forming a complex with the cationic polymer, the added anionic polymer begins to complex with the cationic dye. The indicator molecules are now bound to the same polymer molecule increasing interaction between dye molecules therefore a colour change is observed.²⁶

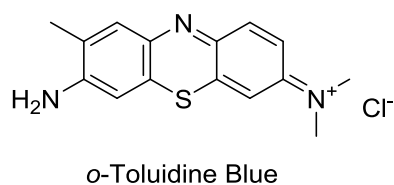
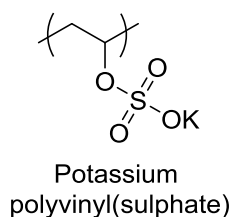


Figure 1.6: Components of spectrophotometric colloid titrations

To accurately gauge the end point the titration is monitored by UV-Vis spectroscopy. In the case of using *o*-Toluidine blue and potassium poly(vinyl sulphate) as the indicator and titrant, respectively, shown in Figure 1.6. The absorbance is measured at a single wavelength at 645 nm. Therefore, as the solution turns from blue to red/violet the absorbance decreases.²⁷ The end point is determined by a sudden drop in absorbance, known as a break point (Figure 1.7).

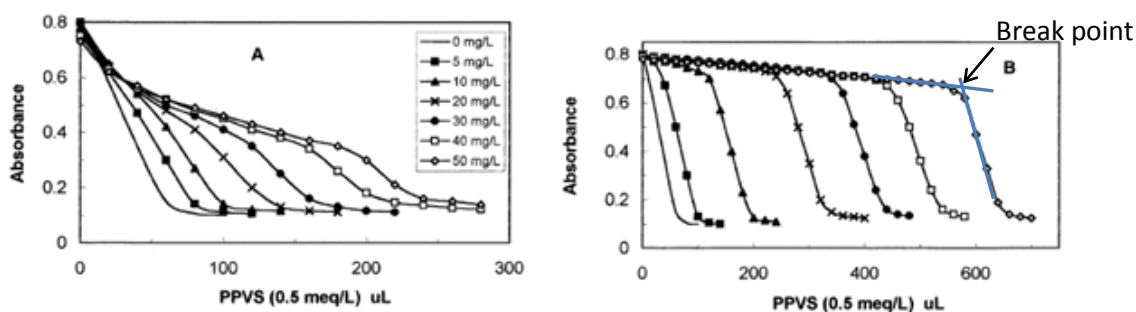


Figure 1.7 Change in absorbance with added titrant a) Low charge density polymer b) High charge density polymer²⁷

The end point of the reaction is less clearly defined in low charge density polymers ($< 1 \text{ meq g}^{-1}$) (Figure 1.7.a) than in high charge density polymers ($> 4 \text{ meq g}^{-1}$) (Figure 1.7.b). This is because in low charge density polymers the anionic polymer and cationic dye begin binding before the equivalence point.²⁷

To calculate the charge density, titrations using several different concentrations of cationic polymer are carried out. The concentration of the cationic polymer solution is plotted against the total amount of anionic polymer added at the end point of the titration. A linear graph is produced and the charge density is determined from the gradient; polymers with greater charge densities will have steeper gradients.²⁷ The correlation coefficient (r) reveals the precision of the method, with $r \geq 0.98$ even for low charge density polymers indicates the robustness of the method.²⁷

The accuracy of this method is dependent on the pH of the titrand for certain polymers, as well as the ionic strength of the solution. Kam *et al.* have shown that, at high pH levels, certain polymers will be hydrolysed which decreases the calculated charge density.²⁷ Determination of the end point can also be made more difficult with an increase in ionic strength, with the dissolved salts screening the electrostatic interactions flattening the break points.²⁷

1.2.1.2. Nuclear Magnetic Resonance spectroscopy


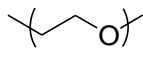
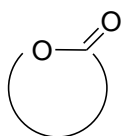
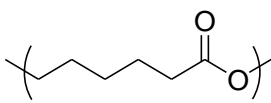

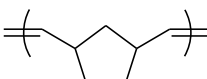
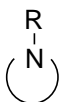
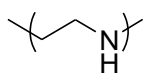
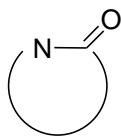
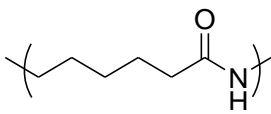
The charge density of a polymer can be predicted using nuclear magnetic resonance (NMR) spectroscopy. Analysis of the polyion's spectrum can be used to determine the ratio of charged moieties in relation to the polymer backbone. Fatehi *et al.*, have used the percentage of quaternary nitrogen atoms in the structure to predict the charge density of the polymer with good accuracy.²⁸ However, the equation used was not supplied and is not published as far as we are aware.

1.3. Polymerisation methods

1.3.1. Ring-opening Polymerisation

Ring-opening polymerisation (ROP) is a chain polymerisation technique of cyclic monomers. The relief of the bond angle strain as the cyclic monomer attaches to the propagating chain end is the driving force of the reaction.²⁹ ROP can be subdivided depending upon the active centre of the propagating chain end, into anionic, cationic or radical ROP; as well as ring-opening metathesis polymerisation (ROMP) where an olefin is the active chain end. A variety of possible monomers can be polymerised by these techniques as surmised in Table 1.1.

Table 1.1: List of viable monomers for ROP

Structure of Monomer	Technique	Example
 Ether	Anionic, cationic	 Poly(ethylene glycol)
 Esters	Anionic, cationic	 Poly(ϵ -caprolactone)
 Olefin	ROMP	 Poly(norbornene)
 Amine	Cationic	 Polyethylene imine
 Amide	Anionic, cationic	 Nylon 6

Anionic ROP will be the focus of this discussion. Derivatives of alkali metals are commonly used to initiate reactions *e.g.* hydrides, alkoxides and aryl species.³⁰ The growing polymer chain propagates *via* an S_N2 reaction. Creating a new active centre at the end of the molecule, this then becomes the new propagating chain end.

The rate of propagation is mainly dependent on the bond angle strain in the cyclic monomer. This can be seen by the increased monomer concentrations at equilibrium ($[M]_{eq}$) for less strained cyclic monomers, *e.g.* $[M]_{eq} = 7.9 \times 10^{-15} \text{ mol L}^{-1}$ for ethylene oxide and 3.3 mol L^{-1} for tetrahydrofuran. Therefore, greater the bond angle strain the more facile the polymerisation.²⁹

Another factor on rate of reaction is the dissociation of the counter-ion. Large counter-ions will dissociate further from the anion increasing the rate of reaction. Furthermore, the addition of crown ether, by aiding the dissociation of the counter-ion, has been shown to increase the rate of reaction.³⁰

The anionic ROP is terminated by addition of an acid to neutralise the anion. The propagating chain can also be unwillingly terminated by chain transfer. The strength of the anion can result in the abstraction of protons initiating the growth of a new chain. The chain can be transferred intramolecularly to the polymer or intermolecularly to the monomer or solvent.³¹ However, 'living' anionic ROP is possible. 'Living' polymerisations are highly controlled reactions devoid of chain transfer and chain termination and therefore produce well defined polymers. The original 'living' ROP was carried out by Szwarc *et al.* using sodium naphthalene as the initiator for the polymerisation of ethylene oxide.³²

1.3.2. Radical polymerisations

Uncontrolled free radical addition polymerisations (FRP) are capable of synthesising high molecular weight polymers with short reaction times; however, it is hindered by lack of control over the polymer's structure. FRP proceeds through three stages: initiation, propagation and termination. The formation of a radical to start the reaction can be formed in several different ways, such as thermal decomposition, photolysis and redox reactions amongst others. The radical attacks the alkene on the vinyl monomer, leaving a propagating radical on the monomer, Figure 1.8.a. The chain grows *via* the repeat propagation step of the propagating radical reacting with subsequent monomers, Figure 1.8.b.³³

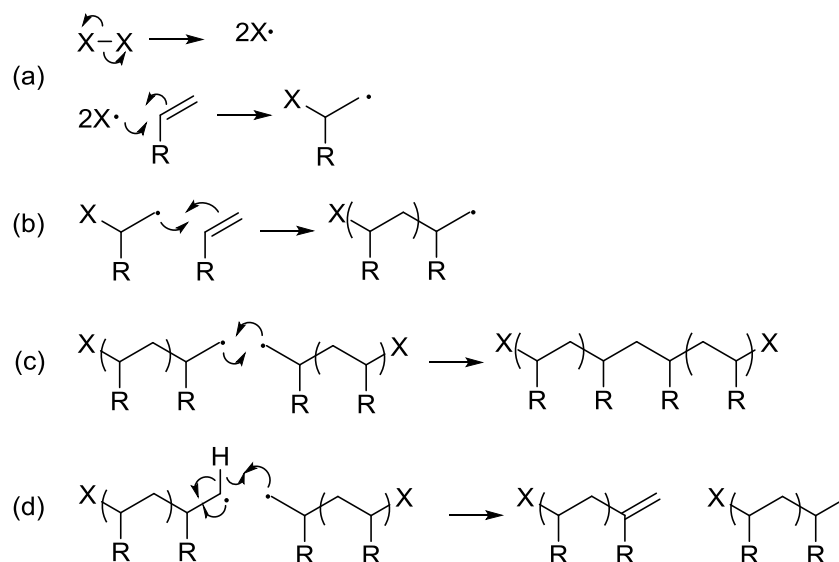


Figure 1.8: The mechanism of the steps in FRP (a) Initiation (b) Propagation (c) Combination (d) Disproportionation

Termination of the propagating chain can occur between two different polymer chains either by combination (Figure 1.8.c), where a single polymer chain is formed, or disproportionation (Figure 1.8.d), where the two end groups will rearrange to form an alkane and an alkene on either polymer. The propagating radical can also be transferred from the chain end (chain transfer), to an initiator, monomer, polymer (forming branched polymers) or polymerisation solvent. The uncontrolled termination and chain transfer of FRP lowers the tunability of polymers produced and increases the range of molecular weights present in a sample; this limits their usage for more refined applications.³³

Dispersity (\mathcal{D}) is a measure of the distribution of molecular weights evident in a polymer sample. \mathcal{D} is determined from the ratio of number-average molar mass (M_n) and weight-average molar mass (M_w) (Equation 1.1).³³

$$\mathcal{D} = \frac{M_w}{M_n} \quad \text{Equation 1.1}$$

M_n and M_w are both measures of the molecular weight of the polymer chains comprising the sample, which can be determined from Equation 1.2 and Equation 1.3.³³

$$M_n = \frac{\sum N_i \cdot M_i}{\sum N_i} \quad \text{Equation 1.2}$$

$$M_w = \frac{\sum N_i \cdot M_i^2}{\sum N_i \cdot M_i} \quad \text{Equation 1.3}$$

Where M_i is molar mass of species i and N_i is the number of molecules of species i , of molar mass M_i . Where $\mathcal{D} = 1$ is a monodisperse sample and greater values are less desired as the polymer's properties become less uniform. Unfortunately, FRP produces $\mathcal{D} = 2 - 10$, so precise prediction of properties is difficult.³³

Another negative property associated with FRP is the range of possible polymer conformations. The different types of copolymers are limited to only random copolymers, due to the one pot nature of FRP and short reaction times. Moreover, the high rate of termination means there is an increased likelihood of forming cross-linked materials when using multi-armed initiators are used.

A remedy to these problems has been suggested by lowering the radical concentration during the polymerisation. Several techniques have been developed based on this principle; collectively these techniques are named controlled radical polymerisations (CRP).

1.3.2.1. Controlled radical polymerisations

In CRP, equilibrium is established between a radical species and a dormant species (*i.e.* protected radical), reducing the concentration of active radicals in the polymerisation. This limits unwanted termination and chain transfer reactions. Consequently the control over the molecular weight and \mathcal{D} increases as well as possible polymer architectures, allowing for more specialised applications.

CRP methods can be characterised by the type of equilibrium that is established, such as dissociation-combination, *e.g.* nitroxide mediated polymerisation,³² reversible-deactivation, *e.g.* atom transfer radical polymerisation (ATRP)³⁴ and single electron transfer-living radical polymerisation (SET-LRP);³⁵ and degenerative chain transfer, reversible addition-fragmentation chain transfer (RAFT).³⁶

Reversible-deactivation radical polymerisations (RDRP), are based on the reversible formation and activation of an alkyl halide bond using a metal halide catalyst. The catalyst is oxidised when it abstracts the halide forming the radical, which can then propagate the growing chain. Control over the polymerisation is observed due to the favoured formation of the alkyl halide bond in the dormant species.³⁷

1.3.2.1.1. Atom Transfer Radical Polymerisation

ATRP, developed by Matyjaszewski and Sawamoto,^{38,39} is based on a synthetic technique called atom transfer radical addition, which is used to synthesis carbon-carbon bonds.³⁴ Synthesis of polymers using this method requires a transition metal catalyst capable of expanding its coordination sphere, commonly a copper halide; a ligand to stabilise the catalyst, this tends to be multidentate nitrogen containing molecule (Figure 1.9); and an alkyl halide initiator, with a low bond disassociation constant. ATRP can polymerise a wide range of monomers, *e.g.* (meth)acrylates, styrenes and (meth)acrylamides.³⁷

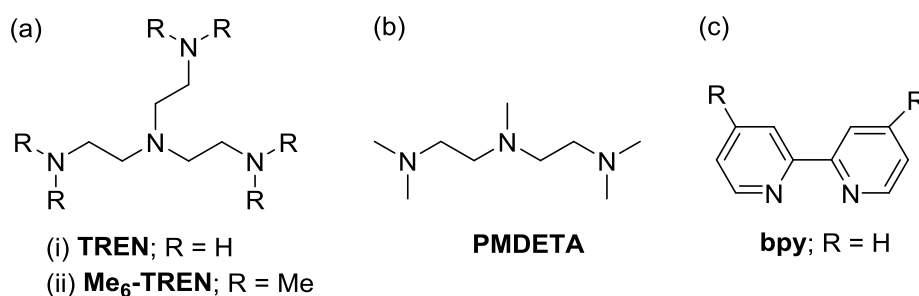


Figure 1.9: Assorted multidentate ligands used in RDRP (a) (i) Tris(2-aminoethyl)amine (ii) Tris[2-(dimethylamino)ethyl]amine (b) N,N,N',N'',N''-Pentamethyldiethylenetriamine (c) 2,2'-bipyridyl

The polymerisation is initiated by the catalyst abstracting a halide atom from the initiator leaving a propagating radical and an oxidised catalyst. The activated initiator is now capable of reacting with an activated monomer. An equilibrium is established between the active polymer chain and the halogen end capped dormant chain (Figure 1.10). The balance of the equilibrium controls the rate of reaction, if the rate of deactivation is increased it will decrease the rate of reaction and termination, hence increasing control over the polymer's properties but lower molecular weights may be achieved.³⁴

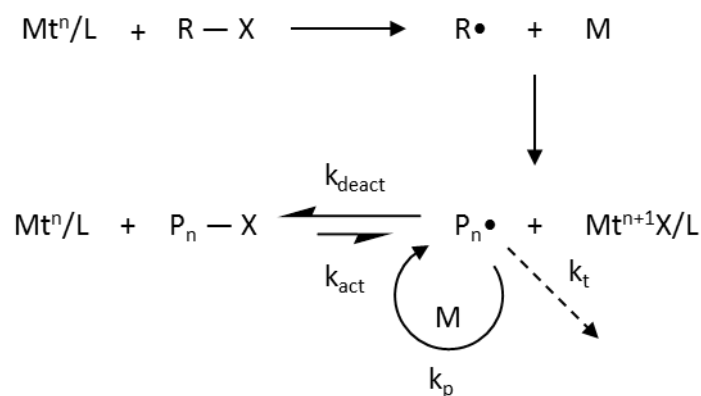


Figure 1.10: Mechanism of ATRP

Complex architectures are possible using this technique using multifunctional initiators. However, as the polymerisation proceeds *via* the persistent radical effect bimolecular termination cannot be avoided. This changes the morphology of the polymer as cyclic arms can be formed due to intramolecular recombination and cross-linked materials from intermolecular termination. The monomer conversion is therefore kept low to minimise these side reactions.⁴⁰

The disadvantages of ATRP are that it requires high catalyst content and is intolerant to impurities.⁴¹ Therefore, modified ATRP based techniques have been developed to reduce the catalyst by regenerating Cu(I), *e.g.* Initiators for continuous activator regeneration (ICAR) – ATRP;⁴² and handling the unstable Cu(I) catalyst by using Cu(II), *e.g.* reverse ATRP.⁴³

1.3.2.1.2. Single Electron Transfer - Living Radical Polymerisation

An alternative RDRP technique to ATRP is SET-LRP which commonly uses Cu(0) as a catalyst. The mechanism of SET-LRP (Figure 1.11) differs from conventional ATRP due to the use of a zero valent transition metal. It is claimed to be a living polymerisation technique as polymerisations have retained chain end functionalities $\geq 99\%$.⁴⁴

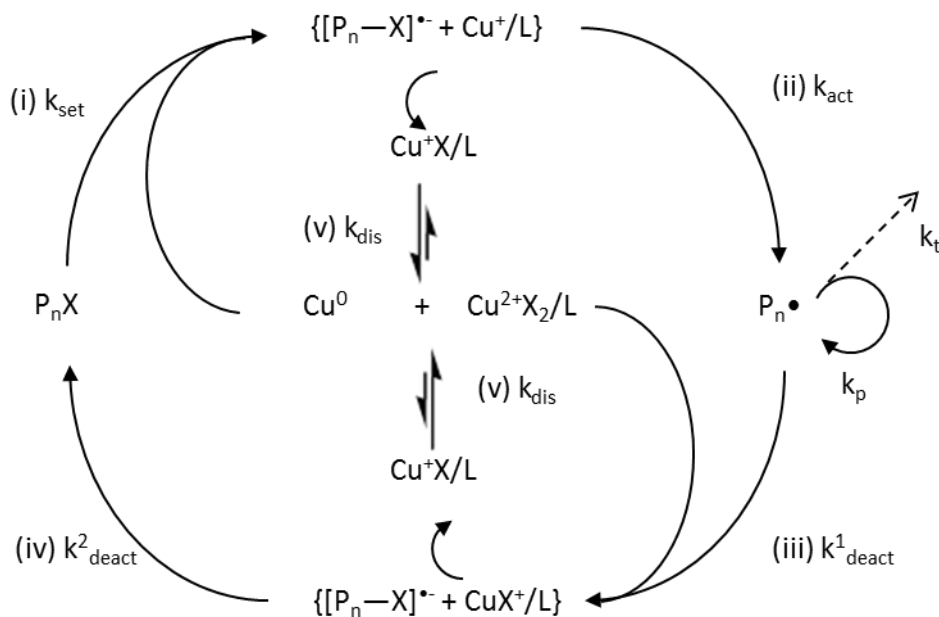


Figure 1.11: Mechanism of SET-LRP

Cu(0) heterogeneously activates the alkyl halide by an outer sphere electron transfer (OSET) process (Figure 1.11.i), the decomposition of the radical anion intermediate produces the propagating radical (Figure 1.11.ii). The propagating radical can now increase the chain length; as well as potentially terminate the polymer chain. The Cu(I) produced from the OSET process instantly disproportionates (Figure 1.11.v) producing Cu(0) and Cu(II). The propagating polymer chain is deactivated by Cu(II) (Figure 1.11.iii and 1.11.iv) to the dormant alkyl halide.⁴⁵

The reaction components for SET-LRP are selected to maximise disproportionation of Cu(I) and to facilitate the OSET process. DMSO is commonly used as a solvent, due to the high polarity promotes electron transfer and stabilises nascent Cu(0); water has also been used as a polymerisation solvent.^{35,46} (Me₆-)/TREN (Figure 1.9.a) are used as ligands as they promote disproportionation and favour the trigonal bipyramidal structure of Cu(II) over the (distorted) tetrahedral configuration of Cu(I).⁴⁷ The OSET process means that SET-LRP can be initiated heterogeneously. Cu(0) powder, with its larger surface offers faster rates than Cu(0) wire; however, the surface uniformity and ease of removal of Cu(0) wire makes its usage more popular.⁴⁸

The legitimacy of the SET-LRP mechanism proffered by Percec has been disputed by Matyjaszewski, who claims Cu(0) based RDRP polymerisations proceed *via* the supplemental activator and reducing agent (SARA)-ATRP pathway.⁴⁹ Where Cu(0) as well as Cu(I) act as

activators, and Cu(0) reduces Cu(II)Br₂ to the activator, Cu(I)Br. The differences between the two mechanisms are surmised in Figure 1.12.

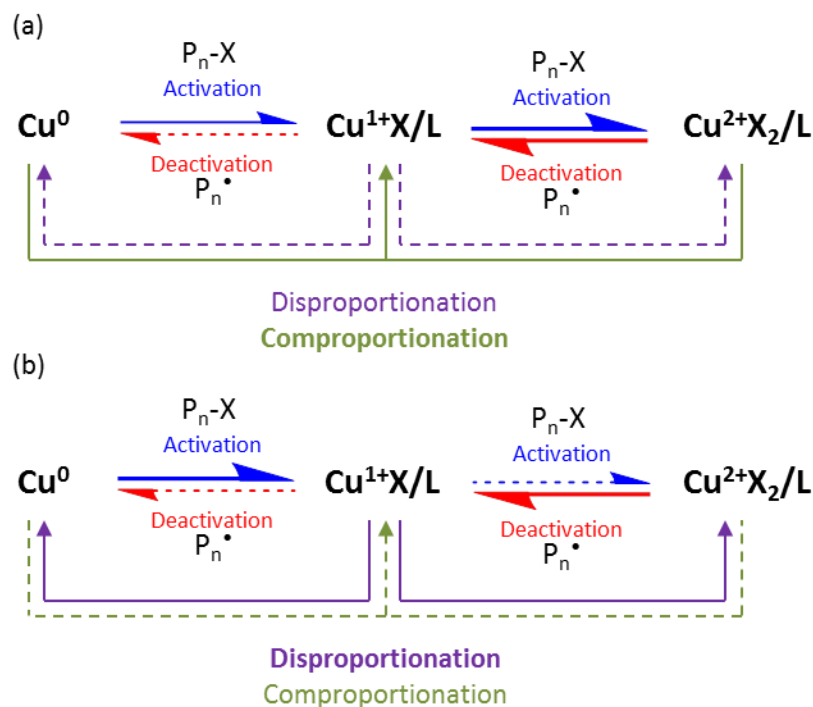


Figure 1.12: The mechanisms of (a) SARA-ATRP and (b) SET-LRP; where bold lines indicate major processes, solid lines indicate contributing processes and dashed lines indicate minor processes

The contested mechanistic steps between the two pathways is whether Cu(0) or Cu(I) is the predominant activator? If an OSET (SET-LRP) or inner sphere electron transfer (ISET) process (SARA-ATRP) is used to activate the alkyl halide? Which is more dominant disproportionation (SET-LRP) or comproportionation, the formation of Cu(I)Br from Cu(0) and Cu(II)Br₂ (SARA-ATRP)? Finally, whether the polymerisation can actually be classified as a ‘living’ polymerisation (SET-LRP)? Matyjaszewski *et al.* have produced a detailed review on why it is SARA-ATRP,⁴⁹ and Percec has produced literature supporting the SET-LRP mechanism.³⁵

Independent of what mechanism it proceeds through, Cu(0) based RDRP provides easy removal of the catalyst, tolerance to impurities (including radical inhibitors) and control over the polymer’s structure.

1.3.3. Graft Copolymerisation

The synthesis of graft copolymers can be achieved by three different pathways: ‘grafting from’, ‘grafting to’ and ‘grafting through’. The ‘grafting from’ approach entails using a polymeric

multi-initiator and a polymer chain is grown away from the backbone (Figure 1.13.a). The 'grafting to' method is where a polymer is synthesised using an initiator with another reactive functional group, that can subsequently be reacted with the polymer backbone (Figure 1.13.b). 'Grafting through' does not involve the modification of a preformed polymer, instead a macromonomer is formed which is then polymerised to form the backbone chain and the side chains simultaneously (Figure 1.13.c).⁵⁰

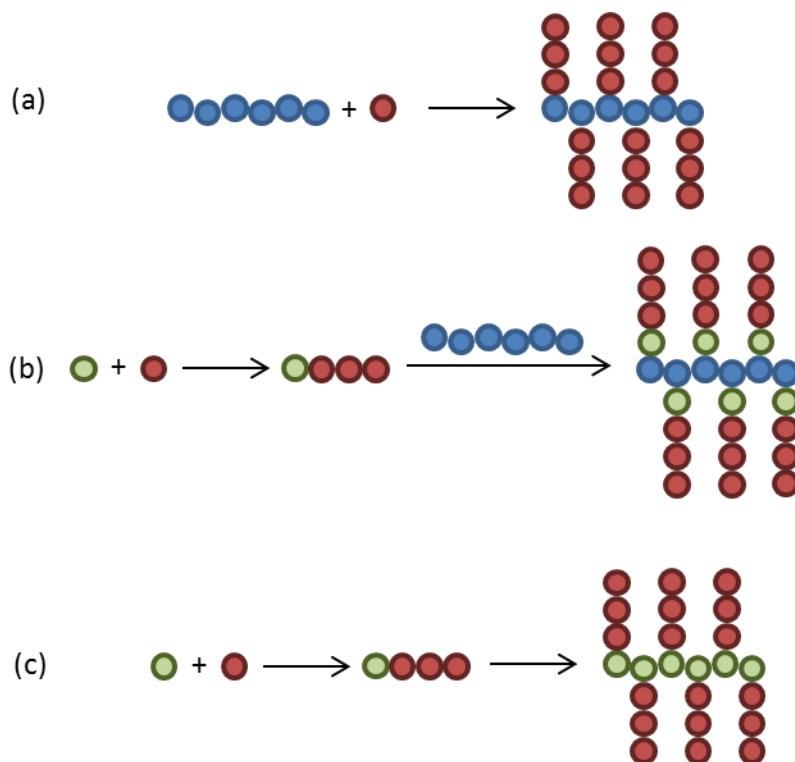


Figure 1.13: The different techniques for synthesising graft copolymers (a) 'grafting from' (b) 'grafting to' (c) 'grafting through'

The purification of synthesised polymers in 'grafting through' and 'grafting to' methods is difficult due to use of polymeric reagents which are chemically similar to the product so precipitation is not a reliable purification technique, unlike for 'grafting from' methodology. Hence, more labour intensive purification techniques to remove unreacted monomer are required, *i.e.* fractionation.⁵¹

All grafting methods have high tunability of the polymer chain, although each has its own deficiencies. Steric hindrance can affect the grafting density in 'grafting to' and 'grafting from', and the length of the polymer backbone in 'grafting through', respectively.^{52,53} In 'grafting to' the density is reduced due to the unavailability of the reactive functionalities on the backbone after the addition of polymeric side chains, meaning the synthesis of molecular brushes is

difficult. In 'grafting from' the initiator sites can become hindered if all the chains are not initiated simultaneously. Molecular brushes are readily made by 'grafting through' although the length of the macromonomer can reduce the degree of polymerisation (DP) of the desired backbone chain due to difficulties finding the single propagating end.⁵⁴

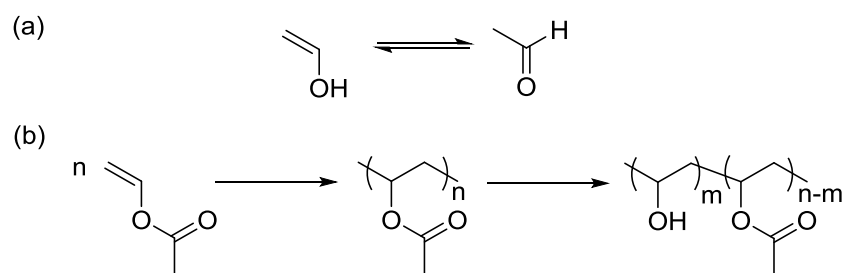
A disadvantage for the 'grafting from' method, which is not a factor in the other two processes, is combination termination. Due to the quantity of propagating chains per molecule, termination can result in the formation of polymeric loops (intramolecular) and cross-linked polymer networks (intermolecular).⁵³ Combination termination has been retarded by limiting the monomer conversion in ATRP, which requires a large monomer excess to achieve desired molecular weights.⁴⁰

1.4. Polymeric materials

1.4.1 Poly(vinyl alcohol)

Poly(vinyl alcohol) (PVA) is the only biodegradable vinyl polymer, it is also biocompatible, has good film forming properties and can form coacervates.^{1,55} Furthermore, it can be functionalised by reactions with the secondary hydroxyls along the polymer chain.^{55,56}

PVA cannot be synthesised using FRP like other vinyl polymers due to the tautomerisation of vinyl alcohol into acetaldehyde (Scheme 1.1.a); therefore it is synthesised by the saponification of PVAc (Scheme 1.1.b); PVAc is synthesised by radical polymerisation.⁵⁷



Scheme 1.1 (a) Tautomerisation of vinyl alcohol (b) Synthesis of PVA

This synthetic pathway results in PVA being commercially available as a copolymer, with differing degrees of acetylation. As PVA is water soluble and PVAc is not, the degree of acetylation determines the solubility characteristics, with increased acetylation increasing its affinity with organic solvents.

PVA is biodegradable under both aerobic and anaerobic conditions.^{55,58} Under both sets of conditions the presence of acclimatised microbes is required for the cleavage of polymer

chains. The total biodegradation of PVA (blown film and PVA98 (containing 2% acetate)) has been shown to be comparable with cellulose in the presence of sewage sludge, however the rate of biodegradation is slower, Figure 1.14. The extent of biodegradation when non-acclimatised microbes are used is negligible.⁵⁵

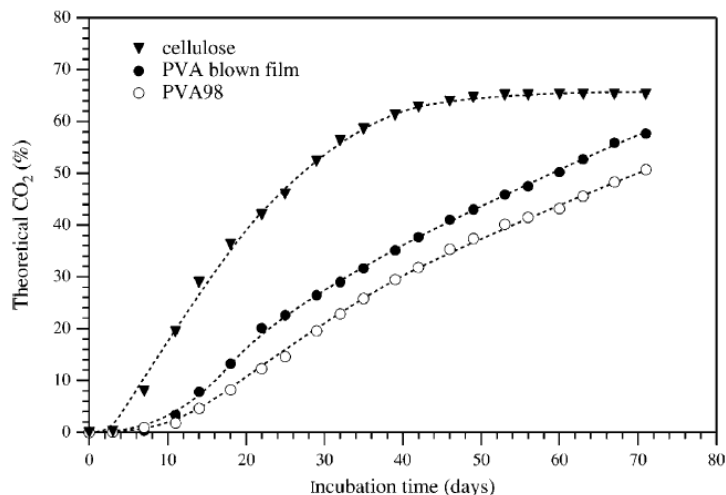
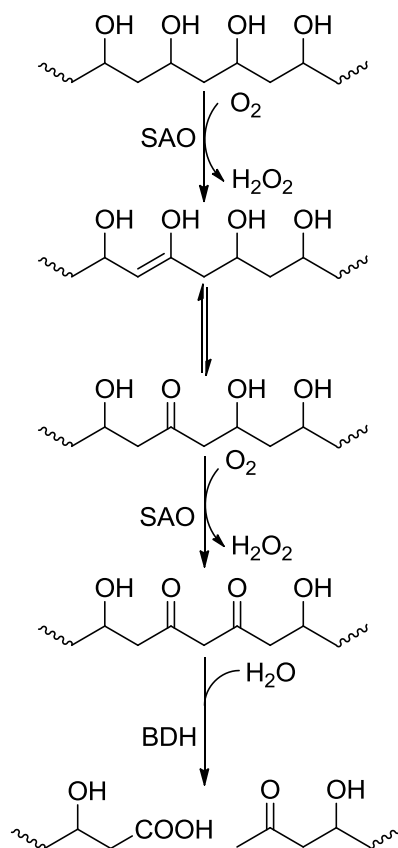


Figure 1.14: A graph comparing the biodegradation rates of cellulose and PVA films⁵⁵

The biodegradation of PVA under aerobic conditions can be achieved through different pathways. Bacterial strains have been shown to have an active role in the degradation of PVA, whether as a single strain or in a symbiotic partnership.^{59,60} It has also been shown that fungi and yeasts can take part in the degradation of PVA.⁶¹

Watanabe *et al.* found that an enzyme produced by a *Pseudomonas* species was a secondary alcohol oxidase (SAO) which can oxidise the alcohols on PVA to ketones forming β - hydroxyketones.⁶² The enzyme was shown to work in an extracellular fashion.⁶³ Therefore, there is no theoretical limit on the molecular weights of PVA that can be degraded by the enzyme. A second enzyme is also produced by the *Pseudomonas* species which has been shown to hydrolytically cleave the oxidised PVA, this is known as β -diketone hydrolase (BDH). The cleavage produces a methyl ketone and a carboxylic acid, with the methyl ketone forming on the longer polymer chain.⁶² The proposed biodegradation pathway is shown in Scheme 1.2.



Scheme 1.2: The aerobic biodegradation of PVA mediated by SAO and BDH.⁶²

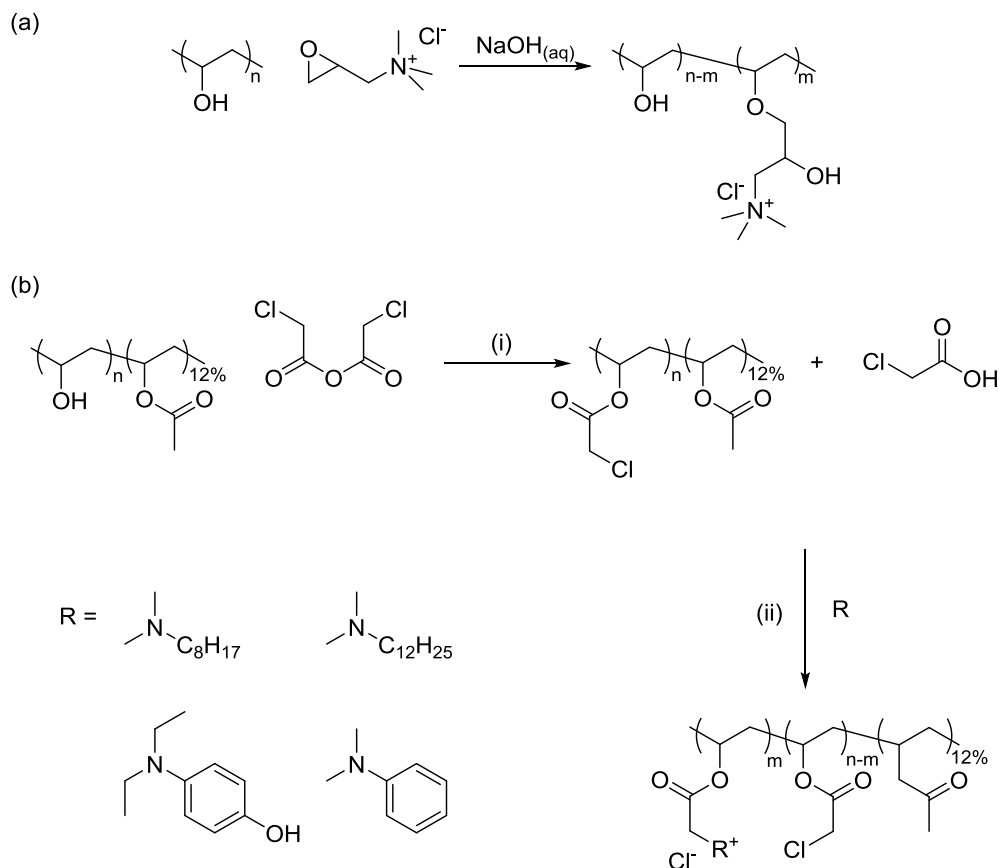
The degradation of PVA in anaerobic conditions was first identified by Matsumura *et al.* it was shown that PVA was degraded in a nitrogen atmosphere by both river sediment from an industrial area and anaerobically treated activated sludge. The tests showed that the higher molecular weight polymer chains took longer to degrade.⁵⁸

1.4.1.1. Synthesis of cationic Poly(vinyl alcohol)

Functionalisation of PVA through the secondary hydroxyls can provide pathways to cationic polymers amongst other interesting polymers. Different functional groups have been used to modify PVA, such as epoxides,⁶⁴ acyl chlorides,⁶⁵ isocyanates,⁶⁶ carboxylic acid,⁶⁷ and anhydrides.⁶⁸ PVA has also been partially tosylated, so that azide groups could be included in the polymer structure for 'click' reactions.⁶⁹

The reaction of PVA with glycidyltrimethylammonium chloride (GTMAC) has been used to synthesise poly[(vinyl alcohol)-*ran*-(vinyl, 2-hydroxypropyl ether trimethylammonium chloride)] (P[(VA)-*r*-(VETMAC)]), using base catalysis (Scheme 1.3.a). Due to the limited solubility of PVA finding appropriate solvents is difficult. This reaction is carried out in water,

although water will also react with GTMAC, thus complete substitution of PVA has not been claimed.²⁸ Research by Fatehi *et al.* has looked into using different solvents and changing other reaction conditions but the quaternary nitrogen content (%QNC) has never been claimed to be greater than 10%.⁷⁰



Scheme 1.3: (a) Synthesis of P[(VA)-*r*-(VETMAC)] (b) Synthesis of poly(vinyl chloroacetate) and quaternisation of resulting poly(vinyl chloroacetate) with tertiary amines

A two-step heterogeneous synthetic pathway has been used to prepare fully substituted cationic PVA. The modification of PVA with chloroacetic anhydride is carried out in butanone despite PVA's insolubility, as the reaction progresses the polymer becomes soluble and the reaction finishes as a homogenous mixture (Scheme 1.3.b.i).⁴ The homogeneity of the reaction is helped by using 12% acetylated PVA. Poly(vinyl chloroacetate) is then quaternised using tertiary amines with long alkyl chains in acetone for use in biocidal coatings (Scheme 1.3.b.ii).

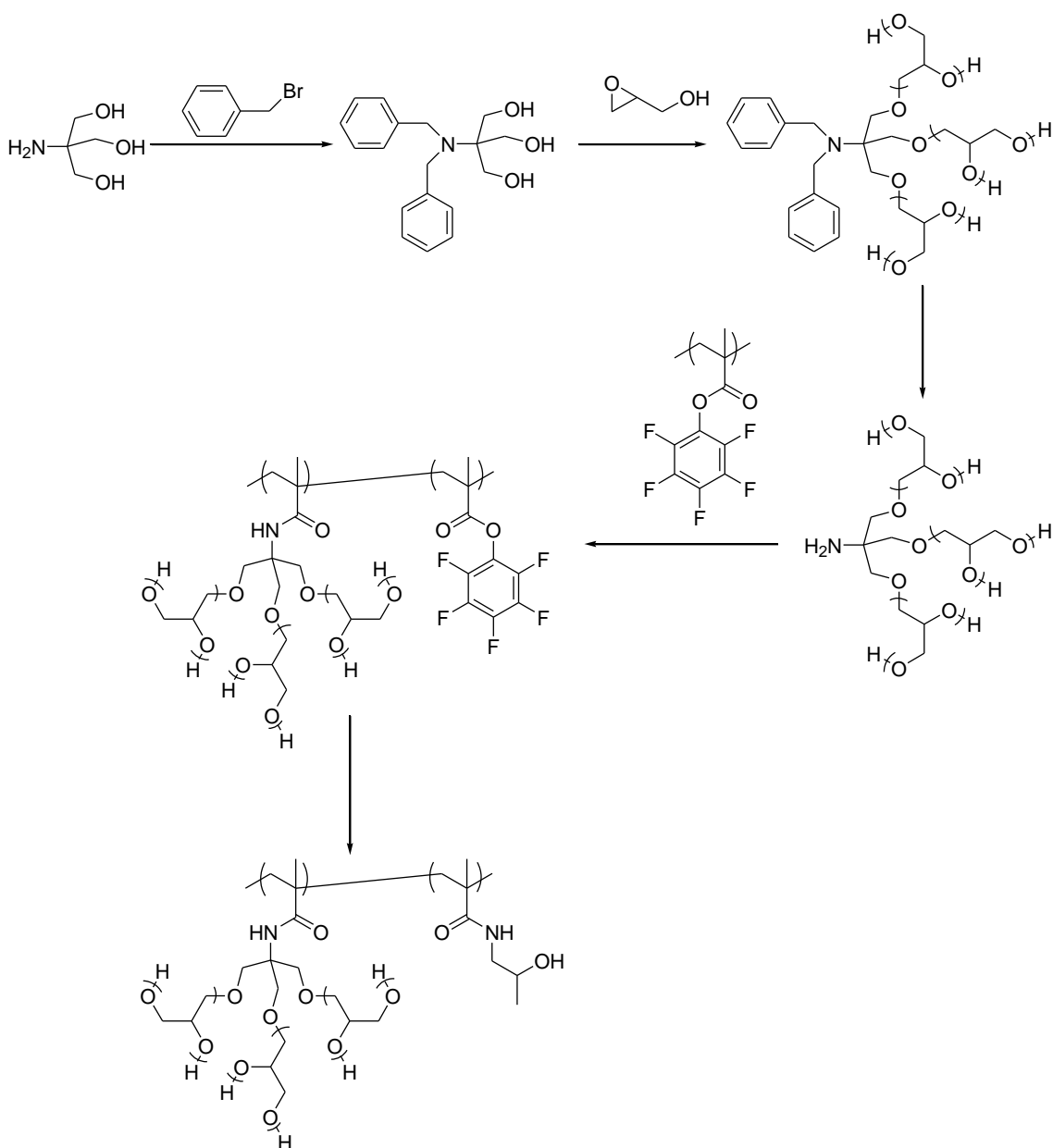
The charge density of PVCA was controlled by varying the molar quantity of the tertiary amine allowing for partial quaternisation and a range of charge densities. However, this method leaves none of the original PVA repeat units available for further modification.

The synthesis of hPG with controlled molecular weight and \bar{D} was first achieved by Sunder *et al.* via anionic ROP, using a partially deprotonated multifunctional initiator and slow monomer addition.⁷⁴ Cationic polymerisation of glycidol has also been carried out, however lower molecular weights were achieved.⁷⁷

Normally, the %DB of hPG increases with DP. However, control over the %DB has been achieved by Harth *et al.* using tin octoate as the catalyst, they showed that a reduction in the temperature reduced the %DB.^{74,78}

One of the problems during the polymerisation of AB₂ monomers is the decrease in concentration of active propagating sites as the reaction proceeds. To combat this, hPG has been used as a macroinitiator to further polymerise glycidol to achieve higher molecular weights.⁷⁹ Higher molecular weight polymers ($\geq 1 \times 10^5 \text{ g mol}^{-1}$) were also prepared using 1,4-dioxane as an emulsifying agent.⁸⁰

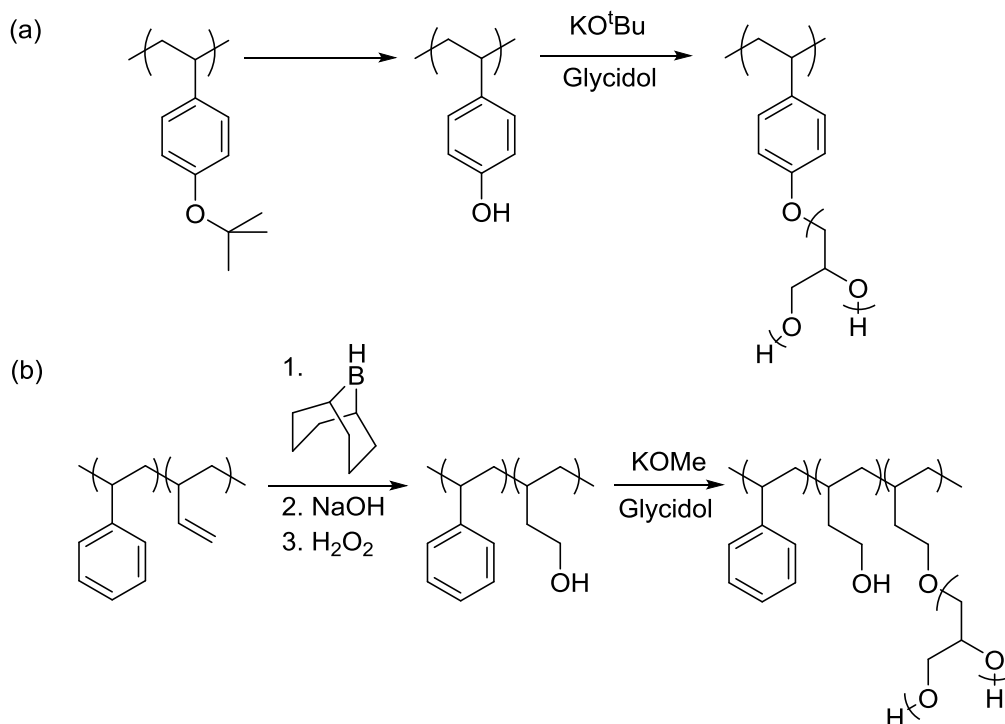
Graft copolymers with polyglycerol side chains have been synthesised. The 'grafting to' technique has been used by synthesising polyglycerol with a protected tris(hydroxymethyl) aminomethane initiator with a range of M_w from 500 g mol^{-1} to $1.5 \times 10^4 \text{ g mol}^{-1}$. After deprotection the amino functional group reacts with a reactive ester methyl methacrylate based polymer, to form the graft copolymer (Scheme 1.5). The mole fraction of hPG (x_{hPG}) in the graft copolymer was not determined. However, the number of substituted repeat units was measured, graft copolymers with degrees of substitution (%DS) between 11% and 32% were achieved.⁸¹



Scheme 1.5: 'Grafting to' method to produce hPG graft copolymer

The 'grafting from' method is most common and has been used with polymeric backbones with hydroxyl functionalities on the repeat unit, which can be used to initiate the polymerisation. Poly(hydroxystyrene) has been used as a macroinitiator for ROP of glycidol, Scheme 1.6.a.⁸¹ Complete substitution of the macroinitiator (%DS = 100%) was possible due to fast proton exchange, slow monomer addition and the higher acidity of the aromatic hydroxyl group in the macroinitiator compared to hPG. The graft copolymers had $x_{(\text{hPG})}$ of up to 94%; they also had %DB between 55 - 57%. The inclusion of the flexible side chains vastly decreased the glass transition temperature (T_g) of the product from 122 °C for 0% $x_{(\text{hPG})}$ to -36 °C for 94%

$x_{(\text{hPG})}$. Poly(4-hydroxystyrene-*graft*-glycerol) has also been quoted as having increased solubility in polar solvents, *e.g.* methanol (MeOH), in comparison with the PHOS.



Scheme 1.6: Synthesis of hPG graft copolymers using a 'grafting from' methodology

A hydroxylated butadiene copolymer, also containing a polystyrene block, has also been used as a macroinitiator for the ROP of glycidol (Scheme 1.6.b).⁸² The graft copolymers had a weight percentage between 5% and 52%. Complete substitution of the initiator was not possible. Furthermore, the %DS of hydroxyl groups on the macroinitiator was not calculated, as the difference in proton and carbon environments in the modified and unmodified initiator were not great enough to be detected by NMR spectroscopy. The grafting efficiency (%GE) of the reaction (60 - 76%) was determined from the ratio of added glycidol and the amount of hPG in the graft copolymer.

1.5. Aims and objectives

Cationic polymers play a crucial role in modern day shampoo formulations increasing the efficacy of silicon emulsion deposition and there by improve the feel of hair. A large range of polyquats are currently available, however none combine high levels of tunability and biodegradation.

The main aims of this thesis were to synthesise cationic polymers for potential use within conditioning shampoo formulations. The polymers were designed to couple the efficacy of synthetic polymers with the biodegradability of materials based on natural products. A range of polymers were produced with different charge densities and hydrophobicities, to be sent to Ashland Inc. for evaluation of its potential use in personal products.

This work details the modification of PVA for potential use in conditioning shampoo formulations, as it is a synthetic and biodegradable polymer. PVA will be modified with GTMAC, chloroacetic anhydride and subsequent quarternisation with trimethylamine to prepare cationic polymers with a range of charge densities. The synthesis of graft copolymers is also investigated to monitor the effects of polymer architecture on the cationic polymers physical properties. Furthermore, polymers containing hydrophobic long alkyl chains will be synthesised using epoxyoctane.

Additionally, PVA-based macroinitiators with varying compositions of RDRP initiator repeat units will be synthesised. SET-LRP will then be used to synthesise graft copolymers, to see the effect this method has on the materials produced. Various monomers will be polymerised to produce graft copolymers with different physical and chemical properties.

1.6. References

- (1) Goddard, E. D. *J. Soc. Cosmet. Chem.* **1990**, *41*, 23.
- (2) Moore, L. E.; Ledder, R. G.; Gilbert, P.; McBain, A. J. *Appl. Environ. Microbiol.* **2008**, *74*, 4825.
- (3) Bolto, B. A.; Dixon, D. R.; Eldridge, R. J.; King, S. J. In *Chemical Water and Wastewater Treatment V*; Hahn, H., Hoffmann, E., Ødegaard, H., Eds.; Springer Berlin Heidelberg, **1998**.
- (4) Baudrion, F.; Perichaud, A.; Coen, S. *J. Appl. Polym. Sci.* **1998**, *70*, 2657.
- (5) Fatehi, P.; Xiao, H. N. *Nord Pulp Pap Res J* **2008**, *23*, 285.
- (6) Lochhead, R. Y.; Huisinga, L. R. *Cosmetics & Toiletries Magazine* **2005**, *120*, 69
- (7) Evans, T.; Wickett, R. R. *Practical Modern Hair Science*; Wissenschaftliche, 2012.
- (8) Hossel, P.; Dieing, R.; Norenberg, R.; Pfau, A.; Sander, R. *Int. J. Cosmet. Sci.* **2000**, *22*, 1.
- (9) Gruber, J. V.; Lamoureux, B. R.; Joshi, N.; Moral, L. *Colloid Surf. B Biointerfaces* **2000**, *19*, 127.
- (10) Goddard, E. D.; Phillips, T. S.; Hannan, R. B. *J. Soc. Cosmet. Chem.* **1975**, *26*, 461.
- (11) Goddard, E. D. *J. Am. Oil Chem. Soc.* **1994**, *71*, 1.
- (12) Lynch, I.; Sjostrom, J.; Piculell, L. *J. Phys. Chem. B* **2005**, *109*, 4258.
- (13) Svensson, A. V.; Huang, L.; Johnson, E. S.; Nylander, T.; Piculell, L. *ACS Appl. Mater. Interfaces* **2009**, *1*, 2431.
- (14) Svensson, A. V.; Johnson, E. S.; Nylander, T.; Piculell, L. *ACS Appl. Mater. Interfaces* **2010**, *2*, 143.
- (15) Pfau, A.; Hössel, P.; Vogt, S.; Sander, R.; Schrepp, W. *Macromolecular Symposia* **1998**, *126*, 241.
- (16) Li, W.; Jordan, S. L. P. *Cosmetics and Toiletries Manufacture Worldwide* **2003**.
- (17) Goddard, E. D.; Braun, D. B. *Cosmet. Toiletries* **1985**, *100*, 41.
- (18) Personal Care Products, *International Buyer's Guide*, **2011**.
- (19) Personal Care Products, *International Buyer's Guide*, **2012**.
- (20) Wang, Y. L.; Kimura, K.; Dubin, P. L.; Jaeger, W. *Macromolecules* **2000**, *33*, 3324.
- (21) Pfau, A.; Hossel, P.; Vogt, S.; Sander, R.; Schrepp, W. *Macromolecular Symposia* **1998**, *126*, 241.
- (22) Johnson, E. S.; Zhang, J. J.; Picullel, L.; Santos, O.; Clauzel, M.; Svensson, A. V.; Nylander, T. *IFSCC magazine* **2010**, *13*, 177.
- (23) Santos, O.; Johnson, E. S.; Nylander, T.; Panandiker, R. K.; Sivik, M. R.; Piculell, L. *Langmuir* **2010**, *26*, 9357.

- (24) Jordan, S. L.; Zhang, X.; Amos, J.; Frank, D.; Menon, R.; Galley, R.; Davis, C.; Kalantar, T.; Ladika, M. J. *Cosmet. Sci.* **2009**, *60*, 239.
- (25) Horn, D. In *Polymeric Amines and Ammonium salts*; Goethals, E. J., Ed.; Pergamon Press: New York, **1980**.
- (26) Gummow, B. D.; Roberts, G. A. F. *Makromol Chem.* **1985**, *186*, 1245.
- (27) Kam, S. K.; Gregory, J. *Colloid Surface A* **1999**, *159*, 165.
- (28) Fatehi, P.; Singh, R.; Ziaee, Z.; Xiao, H.; Ni, Y. *Eur. Poly. J.* **2011**, *47*, 997.
- (29) Duda, A.; Kowalski, A. In *Handbook of Ring-Opening Polymerization*; Wiley-VCH Verlag GmbH & Co. KGaA, **2009**.
- (30) Brocas, A. L.; Mantzaridis, C.; Tunc, D.; Carlotti, S. *Prog. Polym. Sci.* **2013**, *38*, 845.
- (31) Penczek, S.; Cypriak, M.; Duda, A.; Kubisa, P.; Slomkowski, S. *Prog. Polym. Sci.* **2007**, *32*, 247.
- (32) Richards, D. H.; Szwarc, M. *Transactions of the Faraday Society* **1959**, *55*, 1644.
- (33) Cowie, J. M. G.; Arrighi, V. *Polymers: Chemistry and Physics of Modern Materials, Third Edition*; Taylor & Francis, **2007**.
- (34) Matyjaszewski, K.; Xia, J. H. *Chem. Rev.* **2001**, *101*, 2921.
- (35) Rosen, B. M.; Percec, V. *Chem. Rev.* **2009**, *109*, 5069.
- (36) Chiefari, J.; Chong, Y. K.; Ercole, F.; Krstina, J.; Jeffery, J.; Le, T. P. T.; Mayadunne, R. T. A.; Meijs, G. F.; Moad, C. L.; Moad, G.; Rizzardo, E.; Thang, S. H. *Macromolecules* **1998**, *31*, 5559.
- (37) Braunecker, W. A.; Matyjaszewski, K. *Prog. Polym. Sci.* **2007**, *32*, 93.
- (38) Wang, J. S.; Matyjaszewski, K. *J. Am. Chem. Soc.* **1995**, *117*, 5614.
- (39) Kamigaito, M.; Ando, T.; Sawamoto, M. *Chem. Rev.* **2001**, *101*, 3689.
- (40) Beers, K. L.; Gaynor, S. G.; Matyjaszewski, K.; Sheiko, S. S.; Moller, M. *Macromolecules* **1998**, *31*, 9413.
- (41) Pintauer, T.; Matyjaszewski, K. *Chem. Soc. Rev.* **2008**, *37*, 1087.
- (42) Matyjaszewski, K.; Jakubowski, W.; Min, K.; Tang, W.; Huang, J. Y.; Braunecker, W. A.; Tsarevsky, N. V. *Proc. Natl. Acad. Sci. U. S. A.* **2006**, *103*, 15309.
- (43) Wang, J. S.; Matyjaszewski, K. *Macromolecules* **1995**, *28*, 7572.
- (44) Lligadas, G.; Percec, V. *J Polym Sci Pol Chem* **2007**, *45*, 4684.
- (45) Guliashvili, T.; Percec, V. *J. Polym. Sci. Polym. Chem.* **2007**, *45*, 1607.
- (46) Zhang, Q.; Wilson, P.; Li, Z. D.; McHale, R.; Godfrey, J.; Anastasaki, A.; Waldron, C.; Haddleton, D. M. *J. Am. Chem. Soc.* **2013**, *135*, 7355.
- (47) Rosen, B. M.; Percec, V. *J. Polym. Sci. Polym. Chem.* **2007**, *45*, 4950.

- (48) Nguyen, N. H.; Rosen, B. M.; Lligadas, G.; Percec, V. *Macromolecules* **2009**, *42*, 2379.
- (49) Konkolewicz, D.; Wang, Y.; Krys, P.; Zhong, M.; Isse, A. A.; Gennaro, A.; Matyjaszewski, K. *Polym. Chem.* **2014**, *5*, 4396.
- (50) Shi, H. F.; Zhao, Y.; Dong, X.; Zhou, Y.; Wang, D. J. *Chem. Soc. Rev.* **2013**, *42*, 2075.
- (51) Sumerlin, B. S.; Neugebauer, D.; Matyjaszewski, K. *Macromolecules* **2005**, *38*, 702.
- (52) Neugebauer, D.; Sumerlin, B. S.; Matyjaszewski, K.; Goodhart, B.; Sheiko, S. S. *Polymer* **2004**, *45*, 8173.
- (53) Sheiko, S. S.; Sumerlin, B. S.; Matyjaszewski, K. *Prog. Polym. Sci.* **2008**, *33*, 759.
- (54) Yamada, K.; Miyazaki, M.; Ohno, K.; Fukuda, T.; Minoda, M. *Macromolecules* **1999**, *32*, 290.
- (55) Chiellini, E.; Corti, A.; D'Antone, S.; Solaro, R. *Prog. Polym. Sci.* **2003**, *28*, 963.
- (56) Aoi, K.; Aoi, H.; Okada, M. *Macromol. Chem. Physic* **2002**, *203*, 1018.
- (57) Wang, B.; Bao, X.; Jiang, M.; Ye, G.; Xu, J. *J. Appl. Polym. Sci.* **2012**, *125*, 2771.
- (58) Matsumura, S.; Kurita, H.; Shimokobe, H. *Biotechnol. Lett.* **1993**, *15*, 749.
- (59) Watanabe, Y.; Morita, M.; Hamada, N.; Tsujisaka, Y. *Biosci. Biotechnol. Biochem.* **1975**, *39*, 2447.
- (60) Sakazawa, C.; Shima, M.; Taniguchi, Y.; Kato, N. *Appl. Environ. Microbiol.* **1981**, *41*, 261.
- (61) Nord, F. *Naturwissenschaften* **1936**, *24*.
- (62) Sakai, K.; Hamada, N.; Watanabe, Y. *Biosci. Biotechnol. Biochem.* **1986**, *50*, 989.
- (63) Watanabe, Y.; Hamada, N.; Morita, M.; Tsujisaka, Y. *Arch. Biochem. Biophys.* **1976**, *174*, 575.
- (64) Reis, A. V.; Fajardo, A. R.; Schuquel, I. T. A.; Guilherme, M. R.; Vidotti, G. J.; Rubira, A. F.; Muniz, E. C. *J. Org. Chem.* **2009**, *74*, 3750.
- (65) Eastman, S. A.; Lesser, A. J.; McCarthy, T. J. *Macromolecules* **2010**, *43*, 4584.
- (66) Moreno, G.; de Paz, M. V.; Valencia, C.; Franco, J. M. *J Appl Polym Sci* **2012**, *125*, 3259.
- (67) Lejardi, A.; Etxeberria, A.; Meaurio, E.; Sarasua, J. R. *Polymer* **2012**, *53*, 50.
- (68) Ruiz, J.; Mantecon, A.; Cadiz, V. *J Appl Polym Sci* **2003**, *87*, 693.
- (69) Gacal, B. N.; Koz, B.; Gacal, B.; Kiskan, B.; Erdogan, M.; Yagci, Y. *J Polym Sci Pol Chem* **2009**, *47*, 1317.
- (70) Fatehi, P.; Xiao, H. N.; van de Ven, T. G. M. *Langmuir* **2011**, *27*, 13489.
- (71) Calderon, M.; Quadir, M. A.; Sharma, S. K.; Haag, R. *Adv. Mater.* **2010**, *22*, 190.
- (72) Wu, C. Z.; Strehmel, C.; Achazi, K.; Chiapisi, L.; Dervede, J.; Lensen, M. C.; Gradzielski, M.; Ansorge-Schumacher, M. B.; Haag, R. *Biomacromolecules* **2014**, *15*, 3881.

- (73) Kainthan, R. K.; Janzen, J.; Levin, E.; Devine, D. V.; Brooks, D. E. *Biomacromolecules* **2006**, *7*, 703.
- (74) Sunder, A.; Hanselmann, R.; Frey, H.; Mulhaupt, R. *Macromolecules* **1999**, *32*, 4240.
- (75) Stiriba, S. E.; Kautz, H.; Frey, H. *J. Am. Chem. Soc.* **2002**, *124*, 9698.
- (76) Gao, C.; Yan, D. *Prog. Polym. Sci.* **2004**, *29*, 183.
- (77) Dworak, A.; Walach, W.; Trzebicka, B. *Macromol Chem Phys* **1995**, *196*, 1963.
- (78) Spears, B. R.; Waksal, J.; McQuade, C.; Lanier, L.; Harth, E. *Chem. Commun.* **2013**, *49*, 2394.
- (79) Wilms, D.; Wurm, F.; Nieberle, J.; Bohm, P.; Kemmer-Jonas, U.; Frey, H. *Macromolecules* **2009**, *42*, 3230.
- (80) Kainthan, R. K.; Muliawan, E. B.; Hatzikiriakos, S. G.; Brooks, D. E. *Macromolecules* **2006**, *39*, 7708.
- (81) Schull, C.; Nuhn, L.; Mangold, C.; Christ, E.; Zentel, R.; Frey, H. *Macromolecules* **2012**, *45*, 5901.
- (82) Barriau, E.; García Marcos, A.; Kautz, H.; Frey, H. *Macromol. Rapid Comm.* **2005**, *26*, 862.
- (83) Hata, K. S., Takaya.; Nisshinbo Industries, Inc., **2003**; Vol. US 6,533,964 B1.

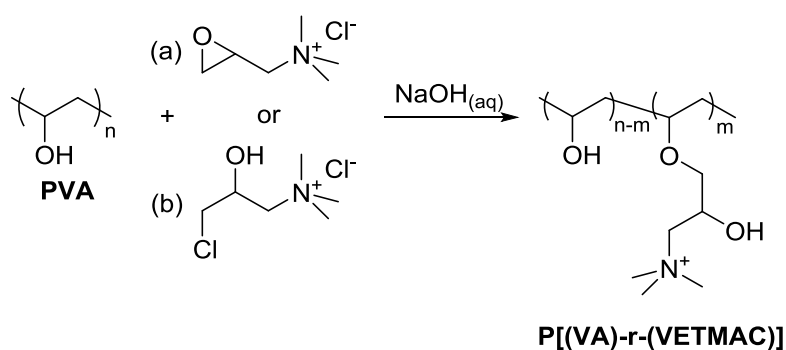
Chapter 2

Synthesis and characterisation of cationic poly(vinyl alcohol)

2.1. Introduction

Poly(vinyl alcohol) (PVA) is a neutral polymer and therefore modification is required to incorporate cationic charges into the polymer structure for it to be an effective conditioning agent in personal products.

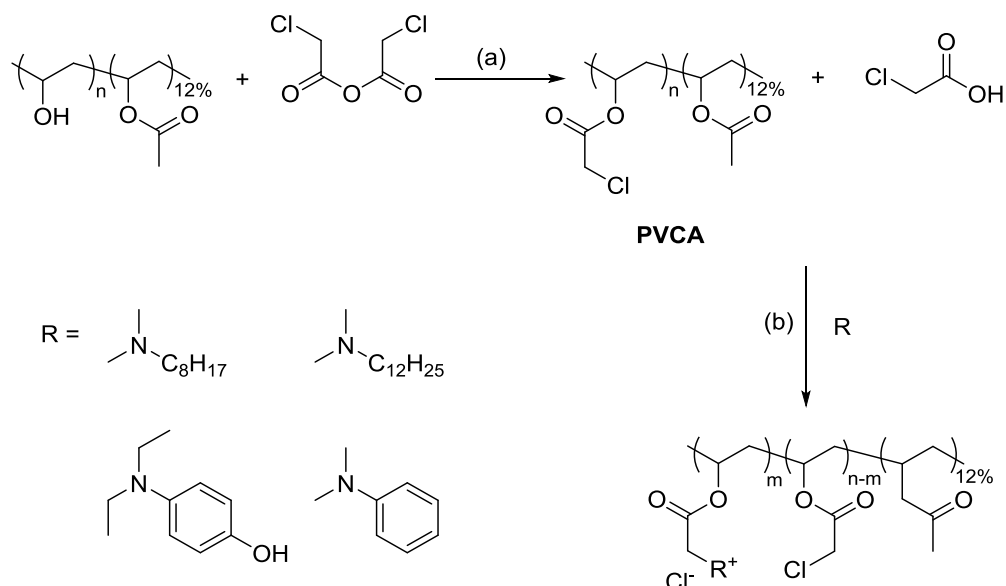
PVA has been reacted with glycidyltrimethylammonium chloride (GTMAC) on an industrial scale to synthesise poly[(vinyl alcohol)-*ran*-(vinyl, 2-hydroxypropyl ether trimethylammonium chloride)] (P[(VA)-*r*-(VETMAC)]) (Scheme 2.1.a).^{1,2} The effects of reaction solvent, time, temperature and the molar equivalences of catalyst (sodium hydroxide) or GTMAC on the charge density (CD) of P[(VA)-*r*-(VETMAC)] have been investigated.³ However, despite attempts to increase the CD of P[(VA)-*r*-(VETMAC)], the maximum recorded value has been reported to be 1.7 meq g⁻¹.⁴



Scheme 2.1: Synthesis of P[(VA)-*r*-(VETMAC)] using (a) GTMAC (b) CHPTMAC

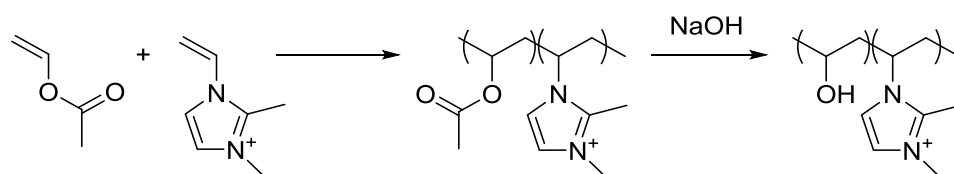
P[(VA)-*r*-(VETMAC)] has alternatively been synthesised using 1,2-chlorohydroxypropylammonium chloride (CHPTMAC) (Scheme 2.1.b). However, the reported quaternary nitrogen content (%QNC) has been shown to be marginally lower (2.2%) than when GTMAC was used instead (2.6%).¹

Quantitative modification of PVA has been achieved using chloroacetic anhydride (CAA).⁵ Subsequent quarternisation of the resulting poly(vinyl chloroacetate) (PVCA) with 4 different tertiary amines (*e.g.* N,N-dimethyloctylamine and dimethyldoceylamine) produced polymers with a %QNC between 10% and 80% (Scheme 2.2). The water soluble cationic polymers were synthesised for potential use in biocidal coating. Control over the CD of the polymer has been achieved by varying the molar equivalents of tertiary amine or reaction time during the quarternisation of PVCA.



Scheme 2.2: (a) Synthesis of PVCA from 88% hydrolysed PVA and CAA (b) Quarternisation of PVCA with tertiary amines to synthesise cationic polymers

Cationic PVA has been synthesised from the saponification of cationic poly(vinyl acetate) (PVAc) containing copolymers (Scheme 2.3). However, lower molecular weight polymers compared to the previously mentioned modification reactions were synthesised, which can negatively affect the deposition behaviour of the conditioning agent.^{6,7}



Scheme 2.3: Copolymerisation of vinyl acetate and vinyl-2,3-dimethylimidazoliniumchloride followed by saponification

In this chapter the synthesis of P[(VA)-*r*-(VETMAC)] with increased CDs and poly(vinyl betaine) (PVB) with controlled hydroxyl content and CD will be discussed.

2.2. Experimental

2.2.1. Materials

Low molecular weight (LMW) PVA ($M_w = 1.8 \times 10^4 \text{ g mol}^{-1}$, 1% acetylated), 88% hydrolysed LMW PVA ($M_w = 1.8 \times 10^4 \text{ g mol}^{-1}$, 12% acetylated), high molecular weight (HMW) ($M_w = 1.68 \times 10^5 \text{ g mol}^{-1}$, 1% acetylated), , 88% hydrolysed HMW PVA ($M_w = 1.68 \times 10^5 \text{ g mol}^{-1}$, 12% acetylated), GTMAC ($\geq 90\%$, based on dry substance; contains 20 - 25% H_2O), CHPTMAC

(60% wt. in H₂O), CAA (95%), trimethylamine (NMe₃) solution (25% H₂O), sodium bicarbonate (NaHCO₃), *o*-Toluidine blue (*o*-Tb) (~80%), potassium poly(vinyl sulphate) (KPVS) ($M_w = 1.70 \times 10^5 \text{ g mol}^{-1}$), hexadecyltrimethylammonium bromide (CTAB) ($\geq 99\%$), dimethyl sulfoxide (DMSO) ($\geq 99.9\%$) and dialysis tubing (molecular weight cut-off (MWCO) = $2 \times 10^3 \text{ g mol}^{-1}$) were purchased from Sigma Aldrich and used without further purification. Sodium hydroxide (NaOH) (98.5%), hydrochloric acid (HCl), methanol (MeOH), ethanol and acetone were purchased from Fisher Scientific and used without further purification. Deuterium oxide (D₂O) and deuterated DMSO (*d*₆-DMSO) were purchased from Goss Scientific and used with out purification.

2.2.2. Instrumentation

Dropwise additions were carried out using a KDS-100-CE syringe pump.

¹H Nuclear magnetic resonance (NMR) spectra were recorded using a Bruker Avance-400 operating at 400 MHz or VNMRS-700 operating at 700 MHz. ¹³C NMR spectra were recorded using a Bruker Avance-400 operating at 101 MHz or VNMRS-700 operating at 178 MHz respectively. Inverse gated ¹³C NMR were carried out using a VNMRS-700 at 176 MHz.

Fourier transform infra-red spectroscopy (FT-IR) was performed using a Perkin Elmer 1600 Series FT-IR.

UV-Vis spectra were recorded using a Cary 100 Bio UV-Vis Spectrophotometer; all measurements were conducted at 25°C.

Thermogravimetric analysis (TGA) measurements were collected using a Perkin Elmer Pyris 1 TGA, samples were heated in air or nitrogen (N₂) to 500 °C at a rate of 10 °C min⁻¹.

Differential scanning calorimetry (DSC) measurements were carried out using a TA Instruments DSC Q1000, over a temperature range of -50 and 300 °C at a rate of 10 °C min⁻¹.

2.2.3. Synthesis of poly[(vinyl alcohol)-*ran*-(vinyl, 2-hydroxypropyl ether trimethylammonium chloride)]

2.2.3.1. Using Glycidyltrimethylammonium chloride

LMW or HMW PVA (0.5 – 20.0 g, 11.4 - 454 mmol) was dissolved in water (4.0 – 160.0 mL) at 95 °C in a two necked round bottom flask (50.0 – 250.0 mL) equipped with a rubber septum, water cooled condenser and magnetic stirrer bar. NaOH_(aq) (0.2 - 4.6 mL, 5 M, 5

mol%, 0.6 - 22.7 mmol) was added to the reaction mixture. GTMAC (2.3 - 47.2 mL, 50 - 200 mol%, 11.4 - 272.0 mmol) was added at a rate of 0.16 - 0.99 mL h⁻¹ or as a single addition and the reaction mixture was stirred at 95 °C for 1 - 24 h. The reaction was quenched with HCl_(aq) (5 M) and then purified by dialysis (MWCO = 2 x 10³ g mol⁻¹) against water for 72 h, the water was changed every 24 h. The solvent was either removed under reduced pressure, or the mixture was added to acetone precipitating the polymer. The resulting P[(VA)-*r*-(VETMAC)] was dried under reduced pressure.

Yield = 9.92 g (50%). ¹H NMR (D₂O): δ (ppm): 1.67 (m, 2H, CH₂CH), 1.85 (m, 2H, CH₂CH), 3.24 (m, 9H, N⁺(CH₃)₃), 3.50 (m, 2H, NCH₂), 3.63 (m, 2H, OCH₂), 3.84 (m, 1H, CHCH₂), 4.04 (m, 1H, CHCH₂), 4.23 (m, 1H, CH₂CHCH₂), 4.41 (m, 1H, CH₂CHCH₂). ¹³C NMR (D₂O): δ (ppm): 41.1 (CH₂CH), 44.1 (CH₂CH), 54.1 (N⁺(CH₃)₃), 64.7 (CHCH₂), 65.2 (CH₂CHCH₂), 66.2 (CHCH₂), 67.6 (CHCH₂), 68.3 (NCH₂), 70.7 (CH₂O), 73.3 (CH₂CHCH₂), 75.0 (CHCH₂), 76.5 (CHCH₂). FT-IR ν (cm⁻¹): 3318 (ν_{-OH}), 2952 (ν_{C-H}), 1108 (ν_{-O-}). T_g = 84 °C, T_m = 186 - 200 °C

2.2.3.2. Using 1,2-Chlorohydroxypropyltrimethylammonium chloride

HMW PVA (1.0 g, 22.7 mmol) was dissolved in water (8.0 mL) at 95 °C in a round bottom flask (250 mL) equipped with a water cooled condenser and magnetic stirrer bar. NaOH_(aq) (0.4 mL, 5 M, 2.3 mmol) was added followed by CHPTMAC (3.7 mL, 13.6 mmol) and the reaction mixture and was stirred at 95 °C for 1 h. The reaction was quenched with HCl_(aq) (5 M) and purified by dialysis against water for 72 h (MWCO = 2 x 10³ g mol⁻¹); the water was changed every 24 h. The purified reaction mixture was added to acetone precipitating the polymer. The resulting P[(VA)-*r*-(VETMAC)] was dried under reduced pressure.

Yield = 0.64 g (58%). ¹H NMR (D₂O): δ (ppm): 1.53 (m, 2H, CH₂CH), 3.12 (m, 9H, N(CH₃)₃), 3.93 (m, 1H, CHCH₂). ¹³C NMR: δ (ppm): 43.9 (CH₂CH), 54.2 (N⁺(CH₃)₃), 64.7 (CH₂CH), 66.2 (CH₂CH), 67.7 (CH₂CH), 74.6 (CH₂CHCH₂). FT-IR ν (cm⁻¹): 3256 (ν_{-OH}), 2900 (ν_{C-H}). T_m = 223 °C.

2.2.4. Synthesis of Poly(vinyl chloroacetate)

88% HMW PVA (1.0 g, 20.0 mmol) and butanone (10.0 mL) were mixed and stirred at 80 °C in a round bottom flask (50 mL) equipped with a water cooled condenser and a magnetic stirrer bar. Chloroacetic anhydride (CAA) (3.4g, 20.0 mmol) was added and the mixture was stirred at 80 °C for 24 h. The initially heterogeneous mixture became a homogeneous viscous yellow liquid as the reaction proceeded. The reaction mixture was added to NaHCO₃ solution (5 %wt) and a yellow solid was formed. The solid was dissolved in acetone

and added to methanol to precipitate the polymer. The resulting PVCA was dried under reduced pressure for 16 h.

Yield = 1.5 g (63%). ^1H NMR (CDCl_3): δ (ppm): 0.85 (m, 3H, CH_3CH_2), 1.24 (m, 3H, CH_3CH_2), 1.53 (m, 2H, CH_2CH), 1.89 (m, 4H, CH_2CH), 1.96 (m, 3H, CH_3), 3.81 (m, 1H, CH_2CH), 4.06 (m, 2H, CH_2Cl), 4.91 (m, 1H, CH_2CH). ^{13}C NMR (CDCl_3): δ (ppm): 8.5 (CH_3CH_2), 17.3 (CH_3C), 21.08 (CH_3), 35.6 (CH_3CH_2), 38.9 (CH_2CH), 41.0 (CH_2Cl), 43.0 (CH_2CH), 62.0 (CH_2CH), 66.4 (CH_2CH), 68.9 (CH_2CH), 100.3 (C), 167.2 (CO), 170.5 (COCH_3). FT-IR ν (cm^{-1}): FT-IR ν (cm^{-1}): 2958 ($\nu_{\text{C-H}}$), 1730 ($\nu_{\text{C=O}}$). $T_g = 47^\circ\text{C}$.

2.2.5. Synthesis of Poly(vinyl betaine)

PVCA (1.4 g, 11.67 mmol) was dissolved in DMSO (10.0 mL) at ambient temperature in a round bottom flask (50 mL). NMe_3 (1.1 mL, 14.0 mmol) was added and the reaction was stirred for 3 h at ambient temperature. The reaction mixture was added to acetone precipitating the polymer product. The polymer was further purified by dissolving in MeOH and precipitating in acetone. The resulting PVB was dried under reduced pressure at 40°C for 16 h.

Yield = 1.83 g (88%). ^1H NMR (d_6 -DMSO): 0.81 (m, 3H, CH_2CH_3), 1.12 (m, 3H, CH_3C), 1.45 (m, 2H, CH_2CH_3), 1.92 (m, 2H, CHCH_2), 3.64 (m, 9H, $\text{N}(\text{CH}_3)_3$), 4.37 (m, 2H, CH_2N), 4.92 (m, 1H, CHCH_2). δ (ppm): ^{13}C NMR (D_2O): δ (ppm): 20.6 (CH_3), 38.4 (CH_2CH), 54.1 $\text{N}^+(\text{CH}_3)_3$, 63.4 (CH_2N^+), 69.8 (CH_2CH), 165.0 (CO), 173.7 (COCH_3). FT-IR ν (cm^{-1}): 3376 ($\nu_{\text{O-H}}$), 2944 ($\nu_{\text{C-H}}$), 1736 ($\nu_{\text{C=O}}$).

2.2.7. Synthesis of Poly[(vinyl alcohol)-*ran*-(vinyl betaine)]

PVB (0.1 g, 0.5 mmol) was dissolved in MeOH (8.2 mL) and water (2.7 mL) in a round bottom flask (50 mL). $\text{NaOH}_{(\text{aq})}$ (0.1 mL, 5 M, 0.5 mmol) was added and the reaction mixture was stirred for 0.13 h. $\text{HCl}_{(\text{aq})}$ (0.6 mL, 0.4 M, 0.6 mmol) was added to quench the reaction and the solvent was removed under reduced pressure. The reaction mixture was dialysed against water ($\text{MWCO} = 2 \times 10^3 \text{ g mol}^{-1}$) for 72 h, the water was changed every 24 h. The solvent was removed under reduced pressure. The resulting polymer was dried under reduced pressure for 16 h.

Yield = 0.016 g (65%). ^1H NMR (d_6 -DMSO): δ (ppm): 0.84 (m, 3H, CH_3CH_2), 0.99 (m, 3H, CH_3CH_2), 1.16 (m, 3H, CH_3C), 1.37 (m, 2H, CHCH_2), 3.82 (m, 1H, CHCH_2), 4.02 (CH_2CH), 4.21 (m, 1H, OH), 4.46 (m, 1H, OH), 4.66 (m, 1H, OH).

2.2.8. Colloid titration monitored by UV-Vis spectroscopy

The titration was carried out following the method outlined by Kam *et al.*⁸ A quartz cuvette containing a magnetic stirrer was charged with a 1.5 mL solution containing *o*-Tb (few drops, 0.077 mg mL⁻¹), deionised water (0 - 1.5 mL) and either CTAB (40.0 – 100.0 μL, 0.9955 meq mL⁻¹) or P[(VA)-*r*-(VETMAC)] (0.4 - 1.5 mL, 0.114 mg mL⁻¹). Aliquots of KPVS (20 μL, 0.400 mg mL⁻¹) were added to the solution at 25 °C. The absorbance of the solution was recorded at λ = 643 nm by UV-Vis spectroscopy after every aliquot addition.

2.3. Results and Discussion

2.3.1. Synthesis of poly[(vinyl alcohol)-*ran*-(vinyl, 2-hydroxypropyl ether trimethylammonium chloride)]

2.3.1.1. Synthesis of P[(VA)-*r*-(VETMAC)] with GTMAC

P[(VA)-*r*-(VETMAC)] was synthesised using GTMAC as a reagent and PVA as a macroinitiator (Scheme 2.1.a). The reaction was catalysed with NaOH_(aq), and the residual GTMAC was removed by dialysis.

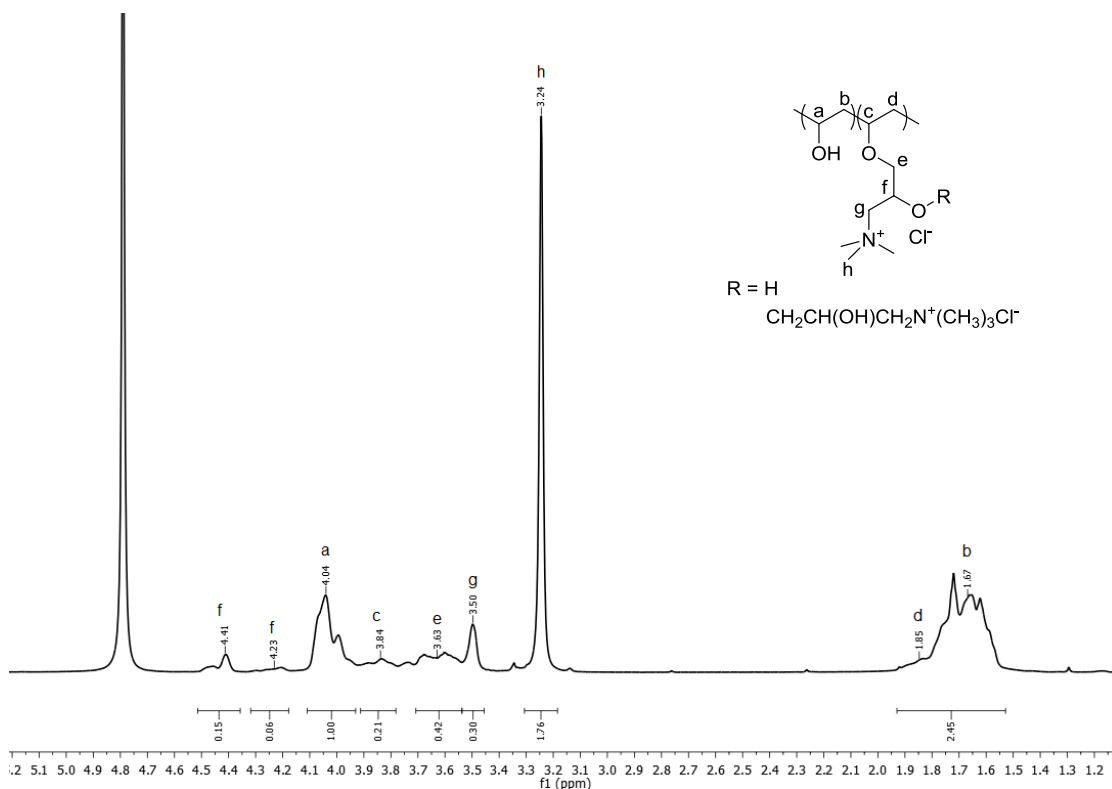


Figure 2.1: 700 MHz ¹H NMR spectrum of P[(VA)-*r*-(VETMAC)] in D₂O

In the ^1H NMR spectrum of P[(VA)-*r*-(VETMAC)], shown in Figure 2.1, the methylene protons on the polymer backbone (b, d) are assigned to the broad resonance at 1.55 - 1.95 ppm. The methyl protons attached to the quaternary nitrogen (h) are attributed to the resonance at 3.24 ppm. The methylene proton adjacent to the quaternary nitrogen (g) corresponds to the resonance at 3.50 ppm. The methylene protons neighbouring the ether linkage (e) are assigned to the resonance at 3.63 ppm. The methine protons on the polymer backbone (c) and (a) were assigned to 3.84 ppm and 3.95 - 4.10 ppm, respectively. The correlation between the protons on the polymer backbone can be seen in the ^1H - ^1H correlation spectroscopy (COSY) spectrum (Figure 2.2). The methine proton neighbouring the hydroxyl group in the side chain (f) corresponds to the resonances at 4.23 ppm and 4.41 ppm, both resonances correspond to the two methylene proton environments in the side chain of PVETMAC (e and g) in the ^1H - ^1H COSY spectrum (Figure 2.2).

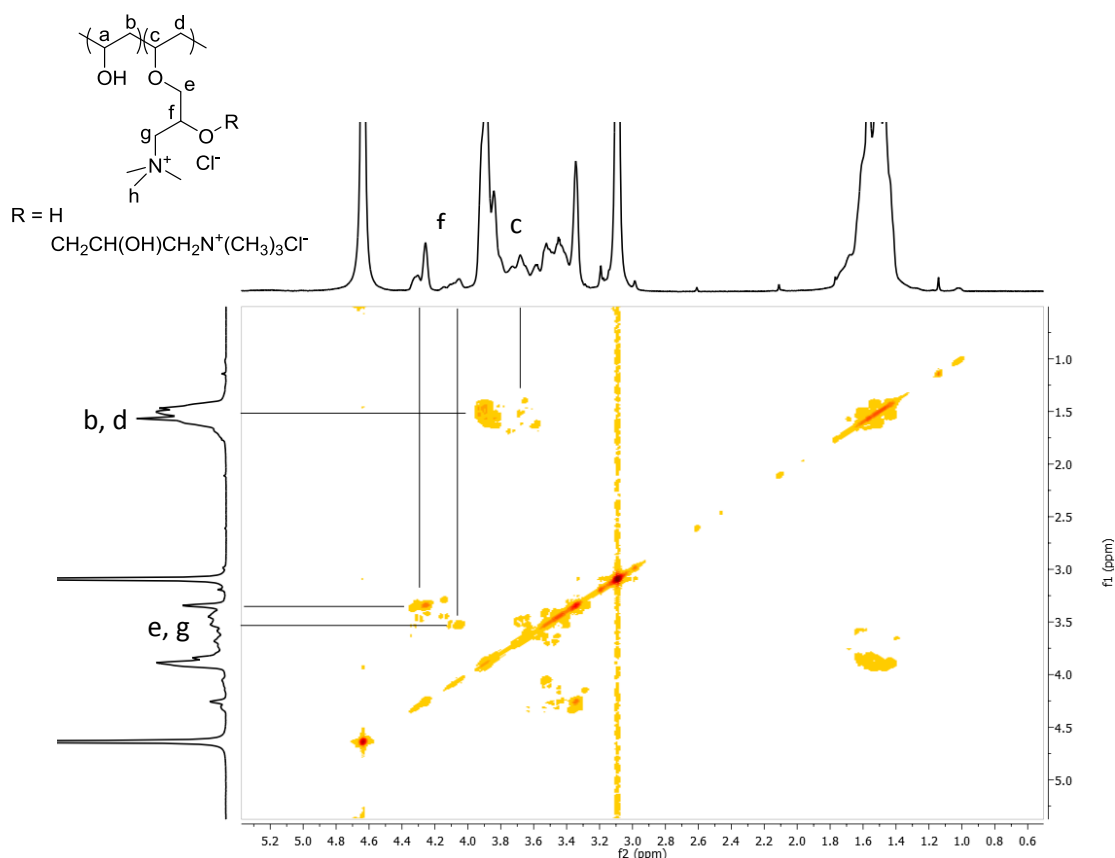


Figure 2.2: 700 MHz ^1H - ^1H COSY spectrum of P[(VA)-*r*-(VETMAC)] in D_2O

The ratio between the methyl protons attached to the quaternary nitrogen (h) and the methine protons (a) in PVA is used to determine the %QNC, using Equation 2.1.

$$\%QNC = \frac{\int h}{\int a \times n} \quad \text{Equation 2.1}$$

Where $\int a$ and $\int h$ are the integrals of the resonances at 4.04 ppm and 3.24 ppm in Figure 2.1, respectively, and n is the number of methyl protons attached to the quaternary nitrogen atom (*i.e.* $n = 9$). The %QNC was determined to be 20% for P[(VA)-*r*-(VETMAC)] shown in Figure 2.1.

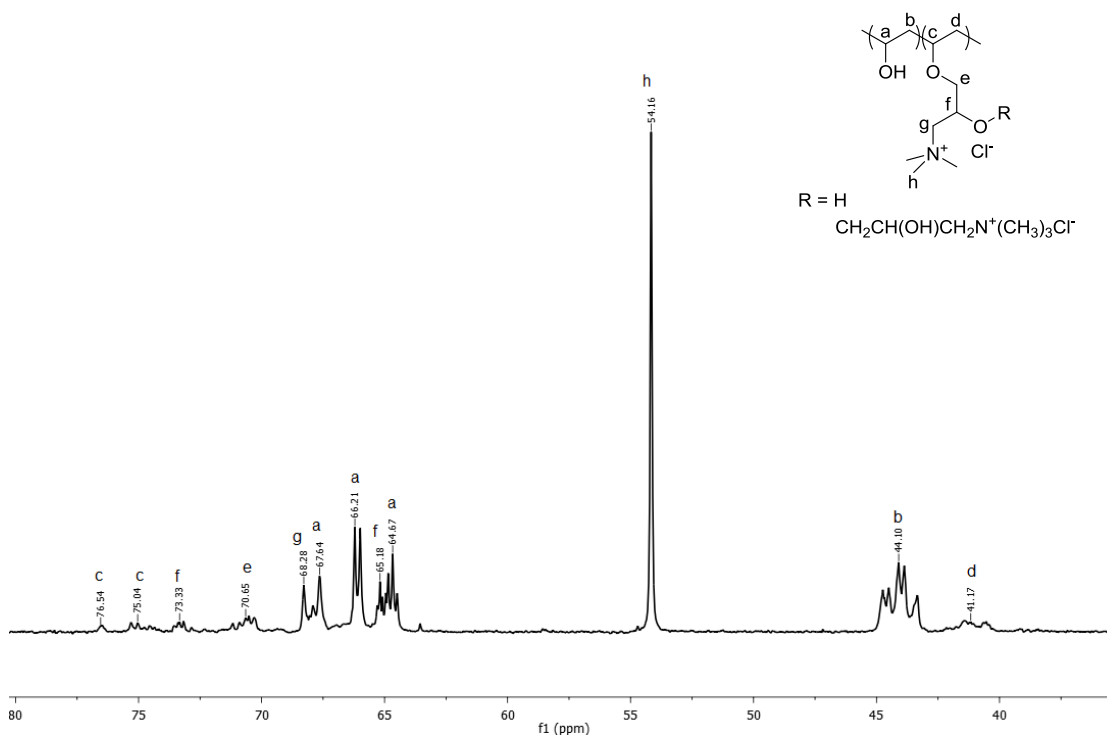


Figure 2.3: 176 MHz ^{13}C NMR spectrum of P[(VA)-*r*-(VETMAC)] in D_2O

The ^{13}C NMR spectrum of P[(VA)-*r*-(VETMAC)] is shown in Figure 2.3. The resonances at 41.2 ppm and 44.1 ppm correspond to the methylene carbon atoms on the polymer backbone (d) and (b), respectively. The $^1\text{H} - ^{13}\text{C}$ heteronuclear single quantum coherence (HSQC) spectrum (Figure 2.4) supports this assignment, as the resonance at 41.2 ppm correlates to the resonance at 1.9 ppm in the ^1H NMR spectrum assigned to (d) in Figure 2.1. The resonances at 64.7 ppm, 66.2 ppm and 67.6 ppm are attributed to methine carbon atoms on the polymer backbone (a). The resonances at 75.0 ppm and 76.5 ppm are attributed to the methine carbon atoms on the substituted polymer backbone (c). The resonance at 54.2 ppm is assigned to the methyl proton attached to the quaternary nitrogen atom (h); this resonances correlates in the $^1\text{H} - ^{13}\text{C}$ heteronuclear multiple-bond correlation (HMBC) spectrum (Figure 2.5) with the signal attributed to the methylene proton (g) in the ^1H NMR spectrum (Figure 2.1). The resonance at 68.3 ppm is assigned to

the methylene proton neighbouring the quaternary nitrogen atom (g). The resonances at 65.2 ppm and 73.3 ppm correspond to the methine carbon atoms adjacent to the hydroxyl group in PVETMAC (f, if R = H). The assignment of two resonances for the methine protons is supported by the $^1\text{H} - ^{13}\text{C}$ HMBC spectrum (Figure 2.5) as they correlate to the methylene groups in the side chain.

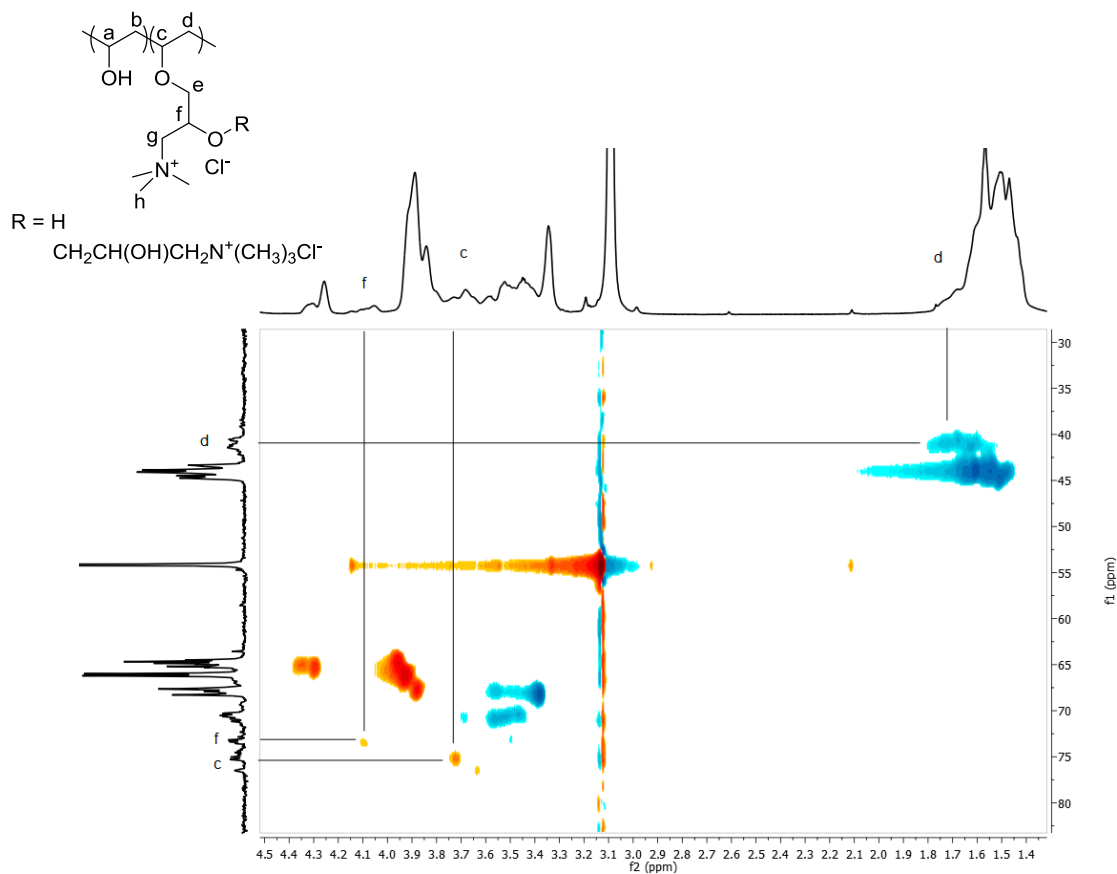


Figure 2.4: 178 MHz $^1\text{H} - ^{13}\text{C}$ HSQC NMR spectrum of P[(VA)-*r*-(VETMAC)] in D_2O

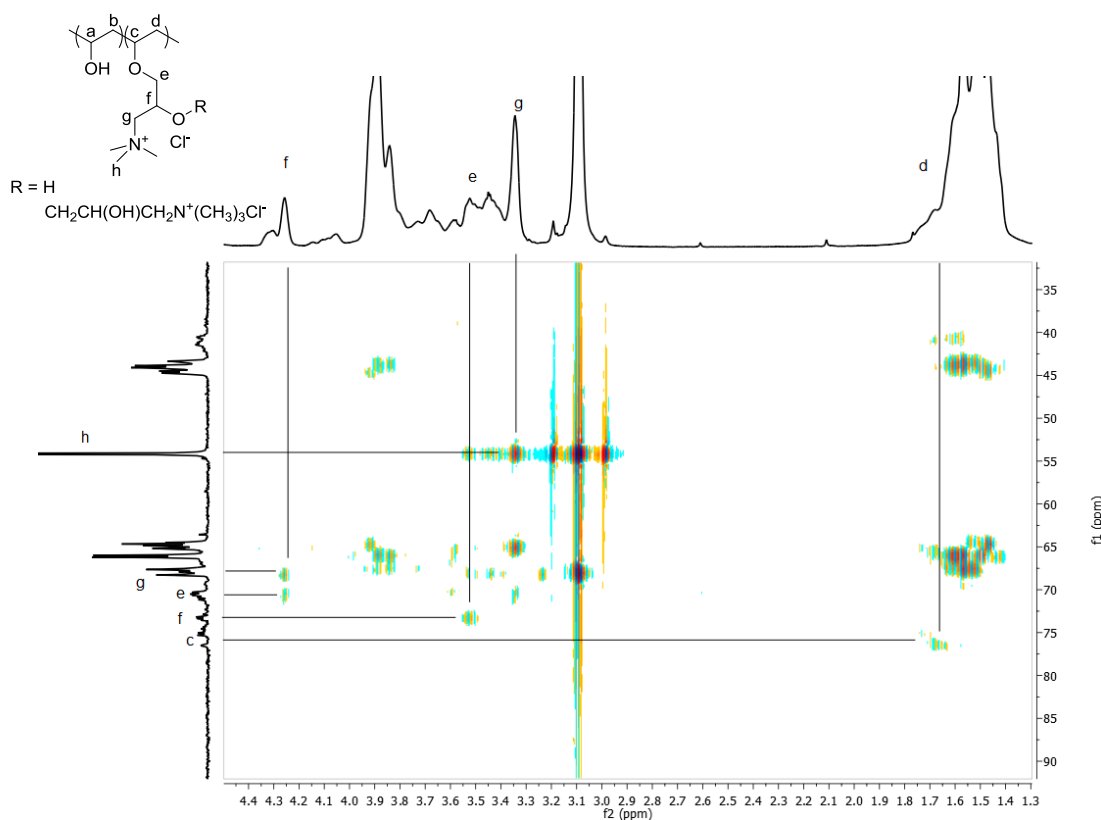


Figure 2.5: 178 MHz ^1H - ^{13}C HMBC spectrum of P[(VA)-*r*-(VETMAC)] in D_2O

The degree of substitution (%DS) of the polymer backbone was determined from the ratio between the two methylene carbon environments on the polymer backbone using Equation 2.2.

$$\%DS = \frac{\int d}{\int b + \int d} \quad \text{Equation 2.2}$$

Where $\int d$ is the integral at the resonance at 41.2 ppm and $\int b$ is the integral of the resonance at 44.1 ppm, in the ^{13}C NMR spectrum.

The %DS was determined to be 17%, however this is less than the %QNC determined by Equation 1 (20%), this suggests the formation of oligomeric chains by GTMAC reacting with already attached GTMAC pendant chains. This is supported by the two different resonances attributed to the methine proton and carbon atoms in the NMR spectra (Figure 2.1 and Figure 2.3).

In the DSC thermogram of semicrystalline PVA (Figure 2.6.a) the glass transition temperature (T_g) is observed at 79 °C as well as a large melting endotherm at 219 °C with a enthalpy of fusion (ΔH_f) of 44.06 J g $^{-1}$, which is in good agreement with the literature values.⁹ However, after PVA was reacted with GTMAC to synthesise P[(VA)-*r*-(VETMAC)],

the DSC thermogram (Figure 2.6.b) displays a more defined T_g at 83 °C and no melting endotherm. This shows that semicrystalline PVA has been successfully modified to form amorphous P[(VA)-*r*-(VETMAC)].

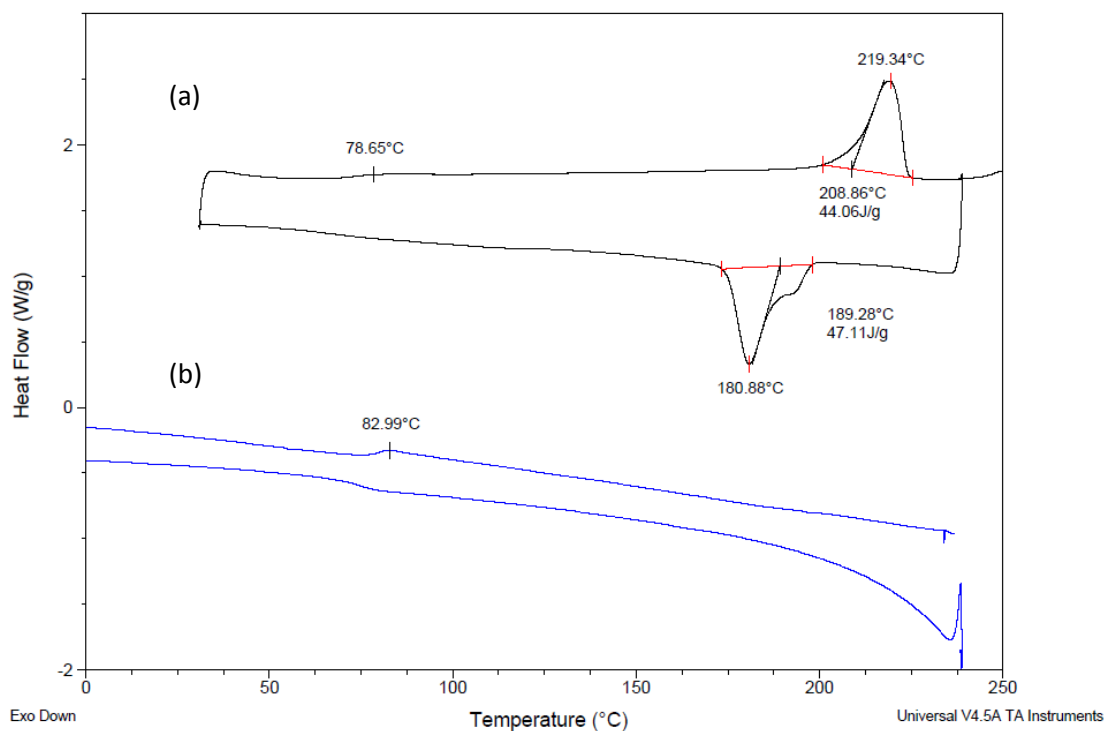
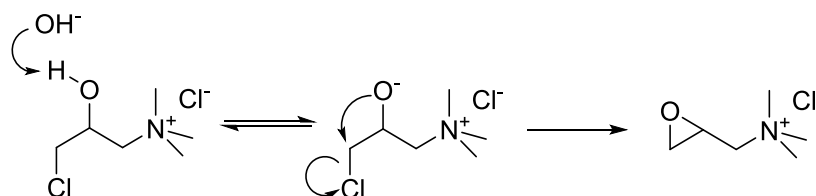


Figure 2.6: DSC thermograms (a) PVA (b) P[(VA)-*r*-(VETMAC)]

2.3.1.2. Synthesis of P[(VA)-*r*-(VETMAC)] with CHPTMAC

P[(VA)-*r*-(VETMAC)] was synthesised by reaction of PVA with CHPTMAC following the procedure outlined in the patent discussed in the previous section.² It is claimed that an increased molar quantity of base catalyst ($\text{NaOH}_{(\text{aq})}$) is required compared with that for GTMAC. It is claimed in the same patent that the reaction proceeds *via* the *in situ* formation of GTMAC, which we propose to happen *via* the mechanism shown in Scheme 2.4.



Scheme 2.4: Mechanism for the formation of GTMAC from CHPTMAC

P[(VA)-*r*-(VETMAC)] was analysed by ^1H NMR spectroscopy (Figure 2.7), in a similar manner to that used for the same polymer synthesised by GTMAC (Figure 2.1).

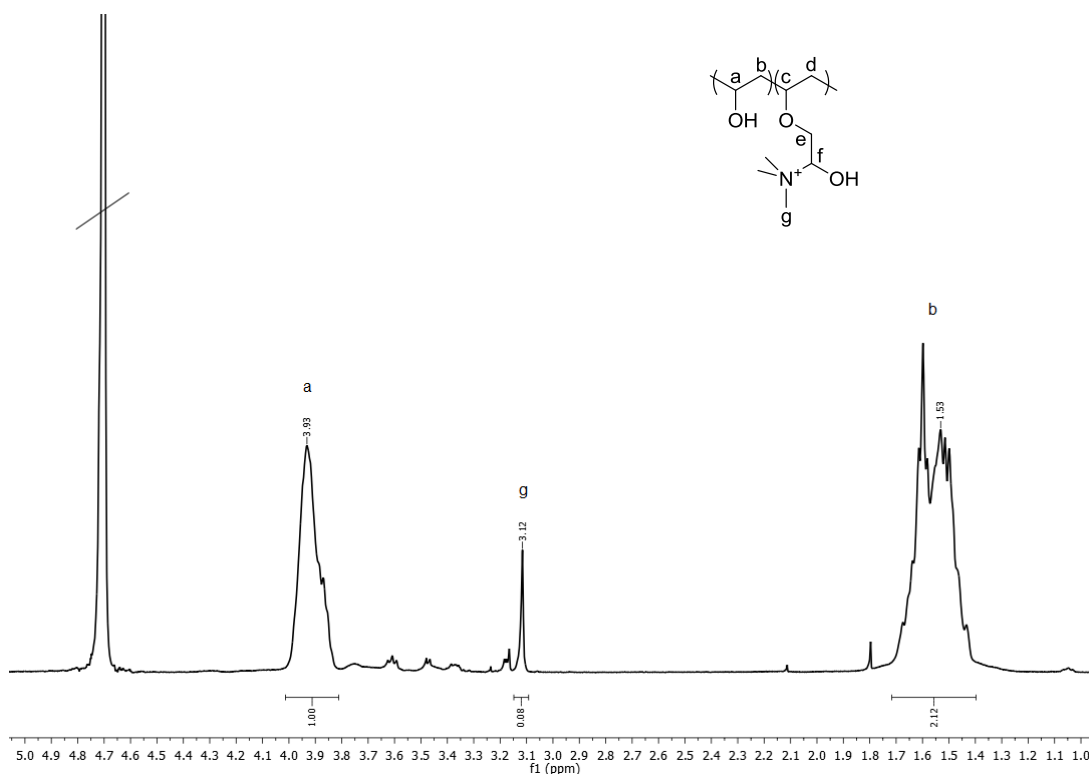


Figure 2.7: 400 MHz ^1H NMR spectrum of P[(VA)-*r*-(VETMAC)] in D_2O

The %QNC of P[(VA)-*r*-(VETMAC)] was determined to be 0.11% when CHPTMAC was used as a reagent, this is less than when GTMAC was used (1.11%) (Section 2.3.1.1.). Therefore, P[(VA)-*r*-(VETMAC)] was synthesised using GTMAC as the reagent.

2.3.1.3. Determining charge density of P[(VA)-*r*-(VETMAC)]

2.3.1.3.1. Colloid titration of P[(VA)-*r*-(VETMAC)]

The CD of P[(VA)-*r*-(VETMAC)] was determined by colloid titration against an anionic polymer, KPVS. Initially, the CD of KPVS was determined by titration against CTAB solutions of defined CDs made from an initial stock solution of $0.9955 \text{ meq mL}^{-1}$ (Figure 2.8). The end points of the titrations were marked by a change in the gradient of the titration curve. The upper break point is observed, when the indicator starts binding with KPVS (Figure 2.8, blue trace), at $180 \mu\text{L}$ of KPVS for 0.07 meq mL^{-1} CTAB solution (Table 2.1, Entry 1). The upper break point is not observed for 0.03 meq mL^{-1} (Figure 2.8, red trace) and 0.02 meq mL^{-1} (Figure 2.8, green trace) because the concentration of CTAB is too low and the indicator begins to bind with KPVS immediately. The lower break point was observed at different volumes depending when the indicator finished binding with KPVS, (Table 2.1).

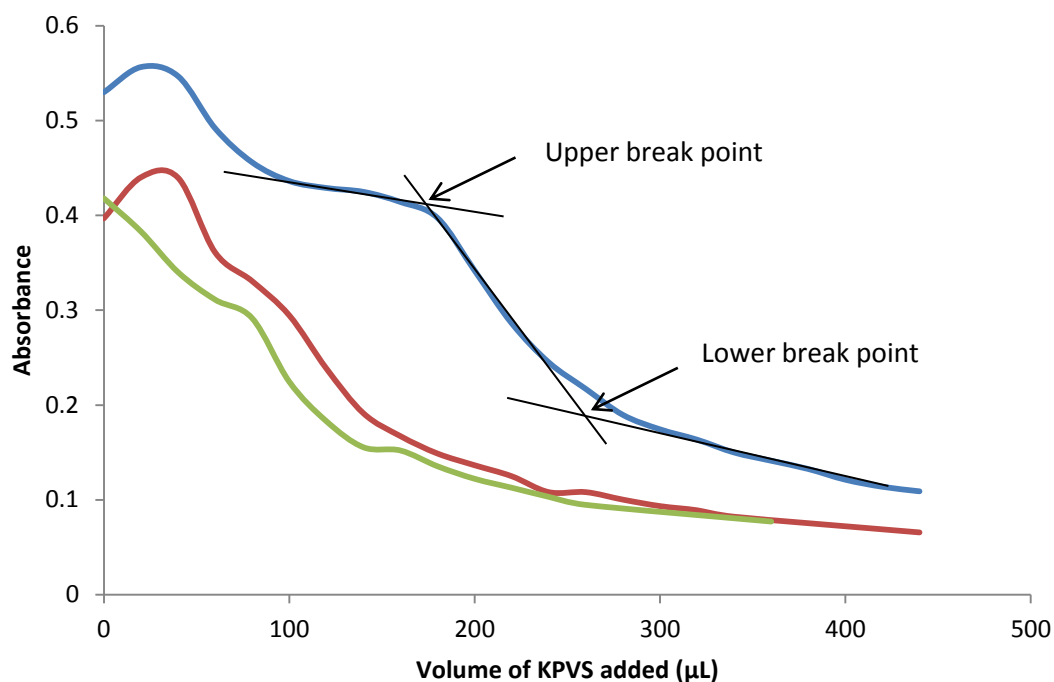


Figure 2.8: The decrease in absorbance with addition of KPVS to solutions of CTAB; 0.07 meq mL⁻¹ (—), 0.03 meq mL⁻¹ (—), 0.02 meq mL⁻¹ (—)

Table 2.1: The upper and lower break points from the titration of different CTAB solutions with KPVS

Entry	Concentration of CTAB (meq mL ⁻¹)	Upper Break point (μL)	Lower Break point (μL)
1	0.07	180	260
2	0.03	N/a	160
3	0.02	N/a	140

The CD was determined from the average of the lower break points of these three solutions using Equation 2.3; Where CD is the charge density of KPVS (meq mL⁻¹), v_{KPVS} is the volume of KPVS at the break point (mL).

$$CD = \frac{n}{v_{KPVS}} \quad \text{Equation 2.3}$$

The n in Equation 2.3 is the number of moles of CTAB (mol), which is determined from Equation 2.4; where c is the concentration of CTAB solution (meq mL⁻¹) (*i.e.* 0.9955 meq mL⁻¹) and v_{CTAB} is the volume of CTAB solution in the titrand (*i.e.* 100 μL for 0.07 meq

mL^{-1} , $50 \mu\text{L}$ for 0.03 meq mL^{-1} and $40 \mu\text{L}$ for 0.02 meq mL^{-1}). Therefore, the CD of KPVS was determined to be $0.5368 \text{ meq mL}^{-1}$.

$$n = c \cdot v_{CTAB} \quad \text{Equation 2.4}$$

A range of solutions containing different concentrations of P[(VA)-*r*-(VETMAC)] ($0.03 - 0.11 \text{ mg mL}^{-1}$) were then titrated against KPVS of now known CD ($0.5368 \text{ meq mL}^{-1}$), Figure 2.9. The break points (marked on the 0.08 mg mL^{-1} titration curve, purple trace) vary depending on the concentration of the titrand used, Table 2.2. The abruptness of the end points decreases with decreasing CD (Chapter 1, Section 1.2.1), as determination of break points is difficult for this P[(VA)-*r*-(VETMAC)] sample is difficult, it can be assumed that a low CD will be determined.

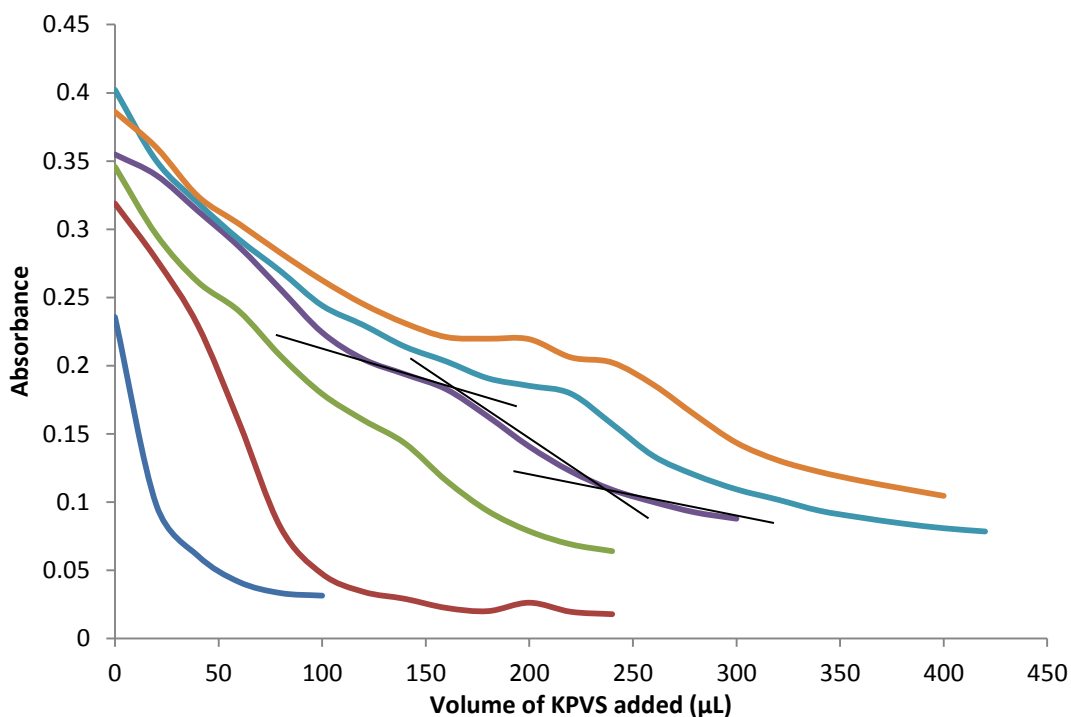


Figure 2.9: The change of absorbance of different concentrations of P[(VA)-*r*-(VETMAC)] solution with the addition of KPVS. 0 mg mL^{-1} (—), 0.03 mg mL^{-1} (—), 0.06 mg mL^{-1} (—), 0.08 mg mL^{-1} (—), 0.10 mg mL^{-1} (—), 0.11 mg mL^{-1} (—).

Table 2.2: The upper and lower break points from the titration of different P[(VA)-*r*-(VETMAC)] solutions with KPVS

Entry	Concentration of P[(VA)-<i>r</i>-(VETMAC)] (mg mL⁻¹)	Upper break point (μL)	Lower break point (μL)
1	0	N/a	22
2	0.03	36	94
3	0.06	142	177
4	0.08	161	227
5	0.10	223	272
6	0.11	252	302

A plot of the concentration of P[(VA)-*r*-(VETMAC)] against the break point volume of KPVS was plotted (Figure 2.10). The CD can then be determined from the gradient of the straight lines; this is a more reliable method than calculating the CD from a single break point.⁸

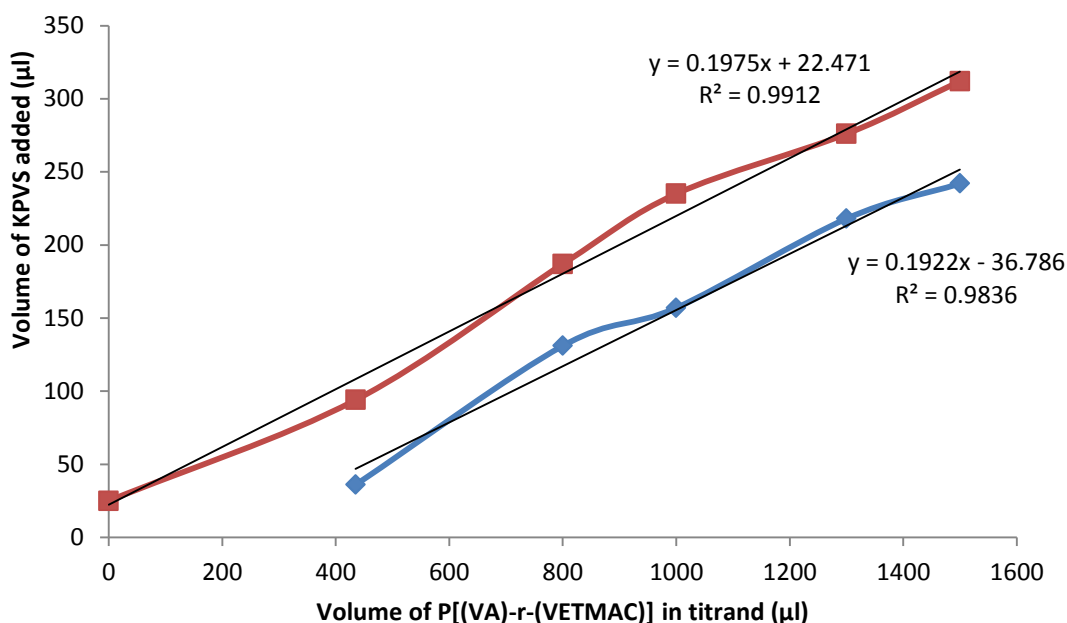


Figure 2.10: The volume of KPVS ($0.5368 \text{ meq mL}^{-1}$) added at the end point of titrations of different concentrations of P[(VA)-r-(VETMAC)] solution. Upper break point (—), Lower break point (—)

The gradient of the straight line is used to determine the CD of the polymer using Equation 2.5.

$$CD = Gradient \times \frac{c_a}{c_c} \quad \text{Equation 2.5}$$

Where c_a is the concentration of anionic polymer solution (meq L^{-1}) (*i.e.* $0.5368 \text{ meq mL}^{-1}$) and c_c is the concentration of cationic polymer solution (g L^{-1}) (*i.e.* 0.1114 g L^{-1}). A CD of 0.94 meq g^{-1} was determined from the average of the two gradients.

Despite the lack of clarity in break point determination the precision in the correlation coefficients, which approach unity (average $r^2 = 0.9874$) in Figure 2.10, highlights the reliability of the method.

2.3.1.3.2. ^1H NMR spectroscopy

The %QNC of P[(VA)-r-(VETMAC)] has previously been used to determine the CD of cationic polymers, without indicating the relevant equation.³ Therefore, Equation 2.4 was derived using literature values for %QNC and the resulting CD.

$$CD = 1000 \left(\frac{Q_c \times n_{poly} \times \%QNC}{m_{initial} + (MW_{added} \times (n_{poly} \times \%QNC))} \right) \quad \text{Equation 2.6}$$

Where CD is the charge density (meq g⁻¹), Q_c is the charge of the cationic subunit, n_{poly} is the moles of polymer (mol), %QNC is the quaternary nitrogen content, m_{initial} is the initial mass of polymer used (g) and MW_{added} is the molecular weight of substituent (g mol⁻¹).

The CD of P[(VA)-*r*-(VETMAC)] discussed in Section 2.3.1.3.1 was correctly predicted to be 0.94 meq g⁻¹ using Equation 2.6. This method accurately predicts the CD of the cationic polymer and is less time consuming than the spectrophotometric titrations. Therefore, all further quoted CDs are determined using ¹H NMR spectroscopy and Equation 2.6.

2.3.1.4. Effects of reaction conditions on charge density of P[(VA)-*r*-(VETMAC)]

2.3.1.4.1. Molar equivalents of GTMAC

It has been shown that a maximum CD of P[(VA)-*r*-(VETMAC)] was achieved at 50% molar equivalences of GTMAC (relative to hydroxyl groups in PVA), before a subsequent decrease at 100% molar equivalences.³ No explanation has been offered for the presence of the maximum. Therefore, in our work here the molar equivalence of GTMAC was varied between the two values (50% - 100%), Figure 2.11.

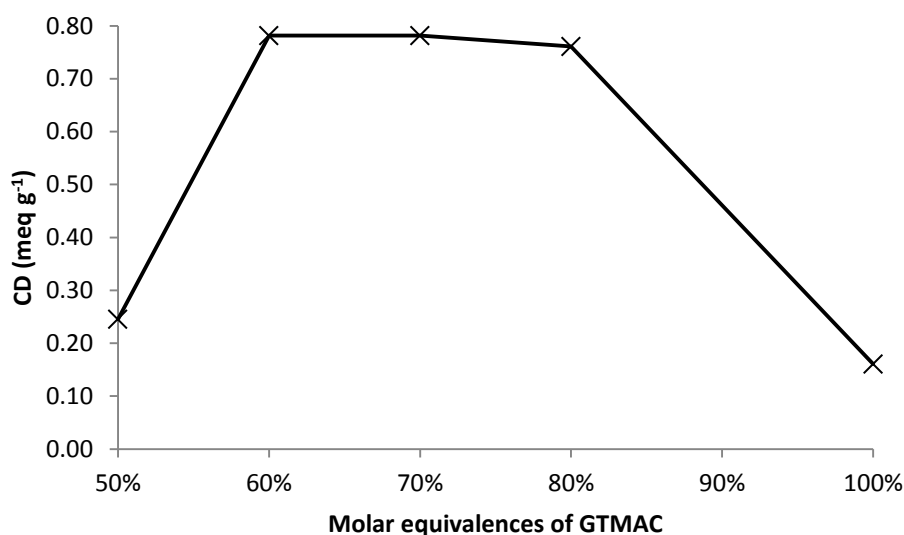
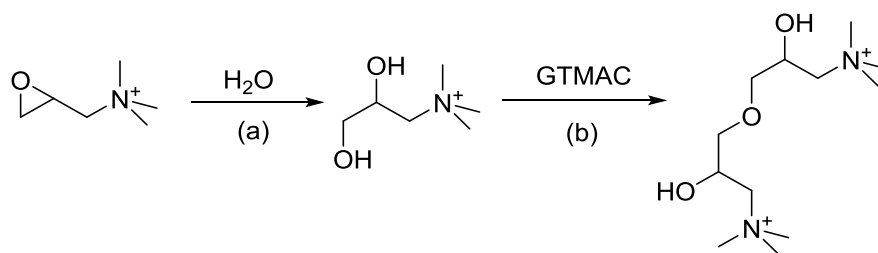


Figure 2.11: The effect of molar equivalents of GTMAC on the CD of P[(VA)-*r*-(VETMAC)]

The recorded CDs of ≈ 0.78 meq g⁻¹ for 60% - 80% molar equivalents are greater than the recorded value of 0.25 meq g⁻¹ for 50% molar equivalents, before the decrease in CD at 100% molar equivalents (0.16 meq g⁻¹). We propose that the observed maximum is because

initially more molar equivalents results in more GTMAC available for the reaction, but the subsequent decrease is potentially caused by increased potential side reactions, proposed in Scheme 2.5.



Scheme 2.5: (a) Formation of 1,2-dihydroxypropyltrimethylammonium chloride (b) Propagation with GTMAC

2.3.1.4.2. Addition of inert diluent

Water reacts with GTMAC and can terminate the grafted chain which limits the CD of P[(VA)-*r*-(VETMAC)]. Therefore, the minimum amount of water was used; this resulted in a very viscous reaction mixture. Therefore, an inert diluent was added to the reaction mixture for greater mixing and hence possibly improving the reaction. The addition of toluene (8 mL) after dissolution of PVA was found to have no effect, as the same CD was obtained (1.18 meq g⁻¹) when no diluent was used.

2.3.1.4.3. Addition time of GTMAC

The addition of GTMAC in aliquots increased the CD from 1.18 meq g⁻¹ from an instant addition to 1.55 meq g⁻¹ for the addition of 0.5 mL every 0.5 h (Figure 2.12.A). To decrease the addition time, the aliquot volume and addition rate were increased (2 mL/0.5h, Figure 2.12.B) but the CD decreased (1.20 meq g⁻¹). The rate of addition was kept constant but the aliquot volume was increased (1 mL/1 h, Figure 2.12.C) and the CD decreased (1.08 meq g⁻¹). Therefore, it was concluded that decreasing the concentration of GTMAC in the reaction mixture increased the CD of P[(VA)-*r*-(VETMAC)].

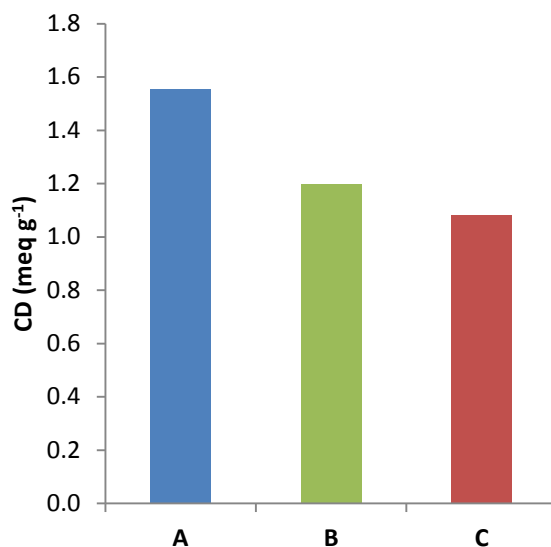


Figure 2.12: The effect that aliquot quantity and frequency of addition has on the CD of P[(VA)-*r*-(VETMAC)] (A) 0.5 mL/0.5 h (B) 2 mL/0.5 h (C) 1 mL/1 h

The concentration of GTMAC in the reaction mixture was decreased by controlled dropwise addition of GTMAC using a syringe pump (Figure 2.13). The CD initially increased from 1.14 meq g⁻¹ to 2.42 meq g⁻¹ over an 8 h addition time, before reaching a plateau. When the concentration of GTMAC in the reaction is kept low, the rate of the side reactions (Scheme 2.5) is decreased. A plateau is observed between 8 h and 24 h addition time, probably as an equilibrium is reached between the formation of P[(VA)-*r*-(VETMAC)] and the side products.

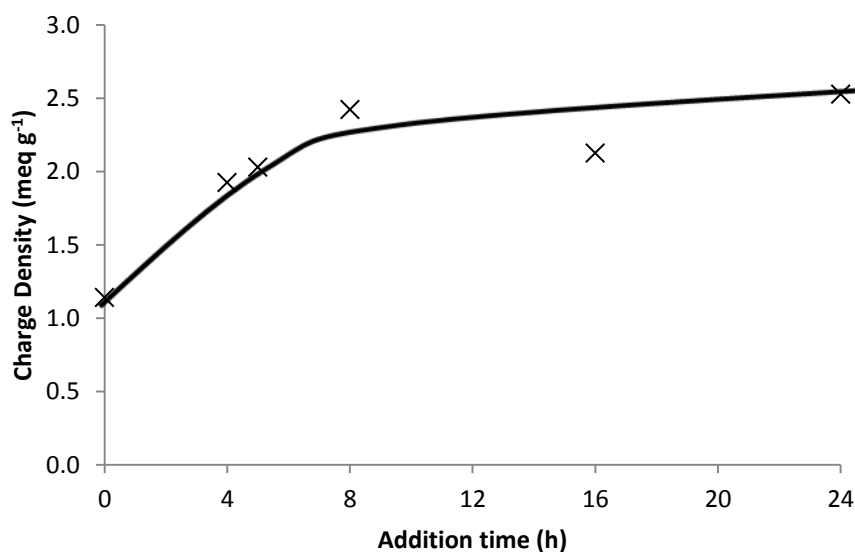


Figure 2.13: The effect on the rate of dropwise addition on the CD of P[(VA)-*r*-(VETMAC)]

2.3.1.4.5. Reproducibility

The reproducibility of the reaction was monitored over several months as GTMAC supplied by Sigma Aldrich is claimed to be hydrolysed at a rate of 3.5%/month at 20 °C.¹⁰ Therefore, in order to investigate the effect of degradation of GTMAC on CD, the same batch of GTMAC was used for the reaction with PVA over an extended period of time.

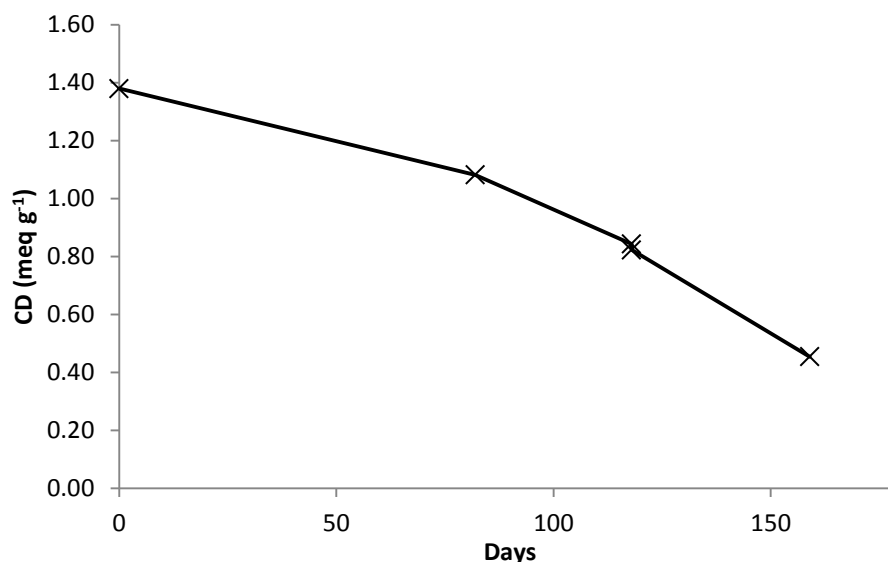


Figure 2.14: The change in CD of P[(VA)-r-(VETMAC)] with change in date

Figure 2.14, clearly shows that the efficacy of the reaction decreases with time, as the CD decreases by 67% over after 159 days from 1.38 meq g⁻¹ to 0.45 meq g⁻¹. This decrease is greater than the previously mentioned rate of hydrolysis at 20 °C (\approx 18%) even though GTMAC was stored at 0 °C. However, two parallel reactions carried out simultaneously only differed by 2% after 118 days. Unfortunately, an effective and applicable method to purify GTMAC of the hydrolysed contaminant (1,2-dihydroxypropyltrimethylammonium chloride) was not found.

2.3.3. Synthesis of poly(vinyl chloroacetate)

Poly(vinyl chloroacetate) (PVCA) was synthesised by reacting 88% hydrolysed PVA with CAA, following the procedure outlined by Baudrion *et al.* (Scheme 2.2.a).⁵ The initially heterogeneous reaction became a homogeneous mixture as the reaction proceeds. The resulting PVCA was insoluble in water and was fully characterised by FT-IR and NMR spectroscopy in CDCl₃.

The stretching frequency attributed to a hydroxyl group at 3200 - 3600 cm⁻¹ is not observed in the FT-IR spectrum of PVCA (Appendix 2.1, blue trace), unlike for 88% hydrolysed PVA

(Figure Appendix 2.1, red trace). This suggests that most likely quantitative conversion of the hydroxyl group was achieved. The stretching band at 1730 cm^{-1} is attributed to the ester linkage in PVCA. Despite the poor quality of the FT-IR spectrum greater intensity is observed when compared with the signal in 88% hydrolysed PVA.

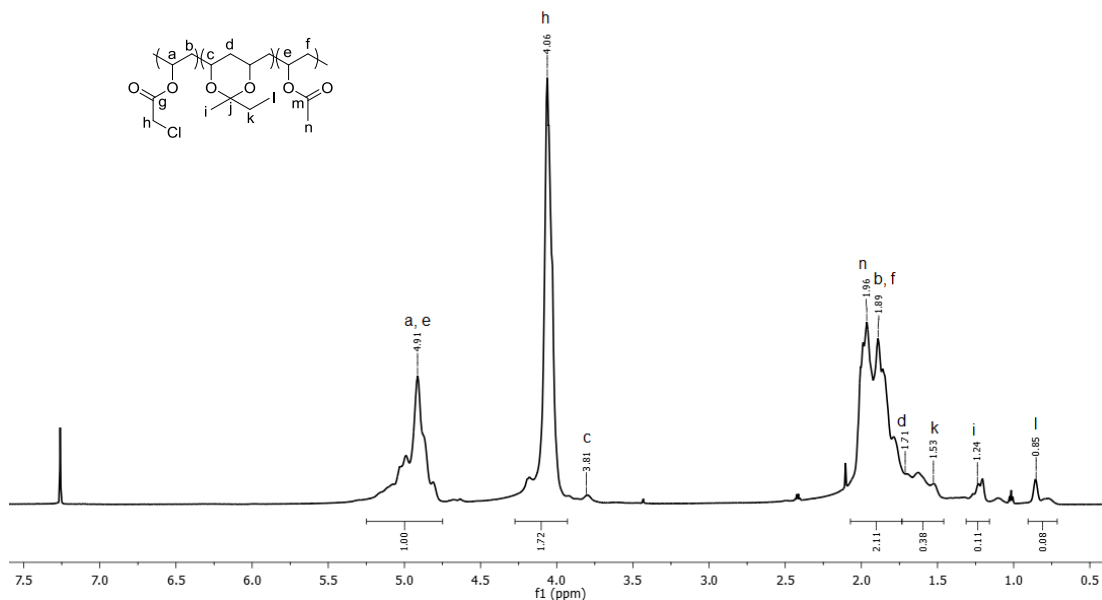


Figure 2.15: 700 MHz ^1H NMR spectrum of PVCA in CDCl_3

PVCA was analysed by ^1H NMR spectroscopy, Figure 2.15. For the PVCA segment the resonances at 1.89 ppm is assigned to the methylene protons on the polymer backbone (b, f), 4.06 ppm to the methylene proton adjacent to the chlorine atom (h) and 4.91 ppm for the methine protons on the polymer backbone (a, e). The resonance at 1.96 ppm is assigned to the methyl proton in PVAc (n). Quantitative conversion of PVA to PVCA is not evident as poly(vinyl 2-butyral) (PVByl) is also formed during the reaction. This is indicated by resonances at 0.85 ppm for the methyl proton (l) and at 1.53 ppm for the methylene proton (k). These assignments are corroborated by the $^1\text{H} - ^1\text{H}$ COSY (Figure 2.16). The resonance at 1.24 ppm is attributed to the methyl protons neighbouring the quaternary carbon atom (i), 1.71 ppm to the methylene protons on the polymer backbone (d) and 3.81 ppm to the methine proton on the polymer backbone (c).

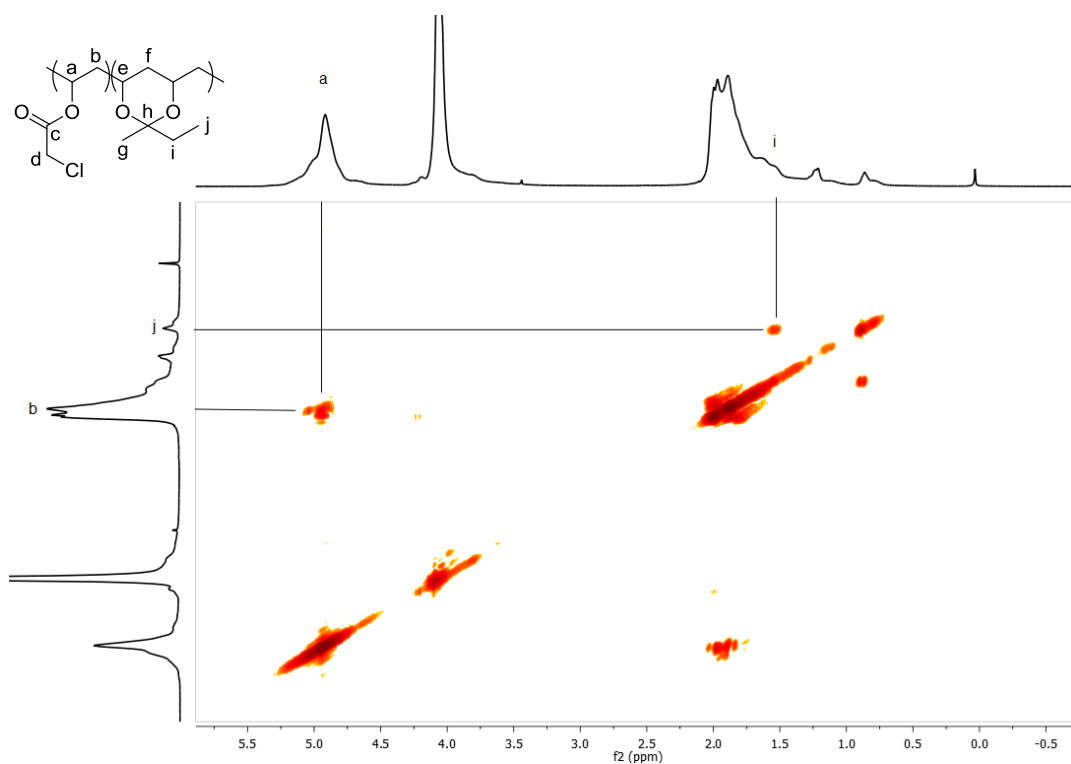
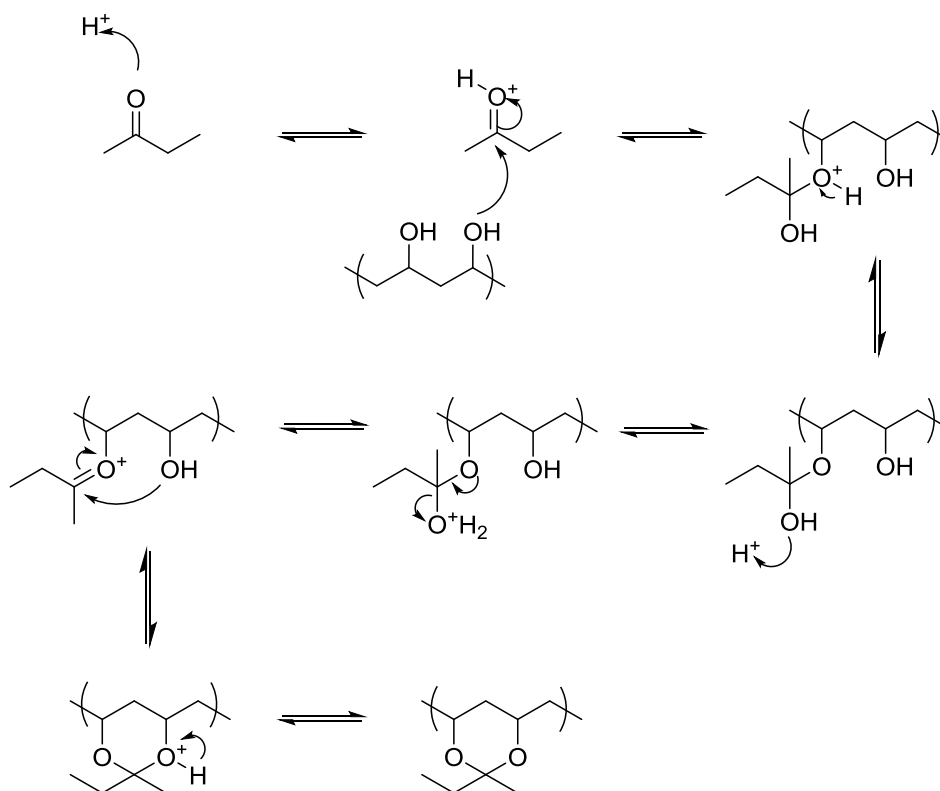


Figure 2.16: 176MHz ^1H - ^1H COSY spectrum of PVCA in CDCl_3 , highlighting the correlations in PVCA and PVByl

PVByl is believed to be formed from the chloroacetic acid catalysed reaction between PVA and butanone (reaction solvent). The possible mechanism for the reaction is proposed in Scheme 2.6.



Scheme 2.6: Mechanism for the formation of PVByl from PVA and butanone

The composition of the PVCA copolymer was determined by Equation 2.7.

$$\%RU = 0.88 \left(\frac{x_{RU}}{x_{PVCA} + x_{PVByl}} \right) \quad \text{Equation 2.7}$$

Where %RU is the percentage of a selected repeat unit and x_i is a generic term for the integral of the resonance normalised to a single proton (*i.e.* i is 'RU', 'PVCA' or 'PVByl'), which is determined from Equation 2.8. The ratio is multiplied by 0.88 to factor in the degree of hydrolysis of PVA.

$$x_i = \frac{\int i}{n} \quad \text{Equation 2.8}$$

Where $\int i$ is the integral of a resonance (ppm) and n is the number of protons in the proton environment attributed to the resonance. For PVCA, $i = 4.06$ ppm and $n = 2$; and for PVByl, $i = 0.85$ ppm and $n = 3$. From the ^1H NMR spectrum (Figure 2.16), the composition of PVCA was determined to be 85%:3%:12% (PVCA:PVByl:PVAc).

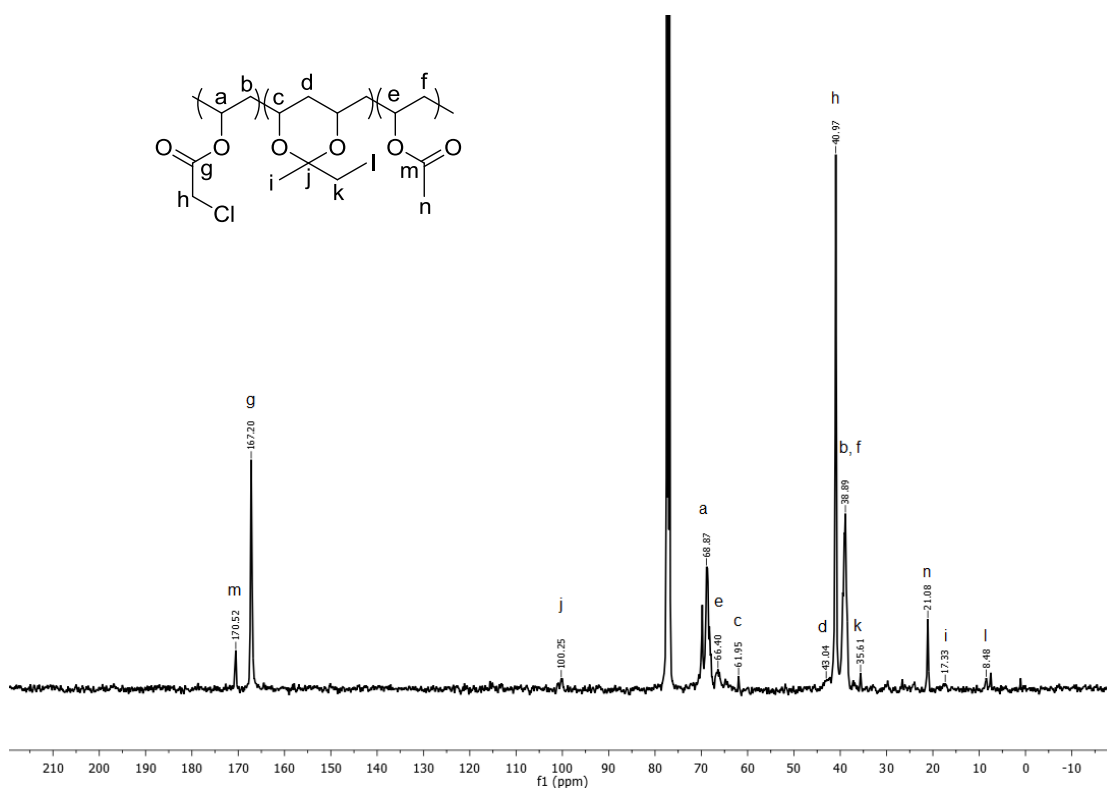


Figure 2.17: 176 MHz ^{13}C NMR spectrum of PVCA in CDCl_3

In the ^{13}C NMR spectrum of PVCA, Figure 2.17, the resonances relating to PVCA are the resonances at 38.99 ppm for the methylene carbon atom on the polymer backbone (b), at 41.0 ppm for the methylene carbon atom neighbouring the chlorine atom (h), at 68.7 ppm for the methine carbon atom on the polymer backbone (a), and at 167.2 ppm for the carbonyl carbon atom (g). The resonances that correspond to the PVAc are the resonances at 21.08 ppm for the methyl carbon atom (n), at 38.9 ppm for the methylene carbon atom on the polymer backbone (f), at 66.4 ppm for the methine carbon atom on the polymer backbone (e) and at 170.5 ppm for the carbonyl carbon atom (m). The assignments of the resonances attributed to the carbonyl carbon atoms (g and m) are supported by the $^1\text{H} - ^{13}\text{C}$ HMBC spectrum (Figure 2.18).

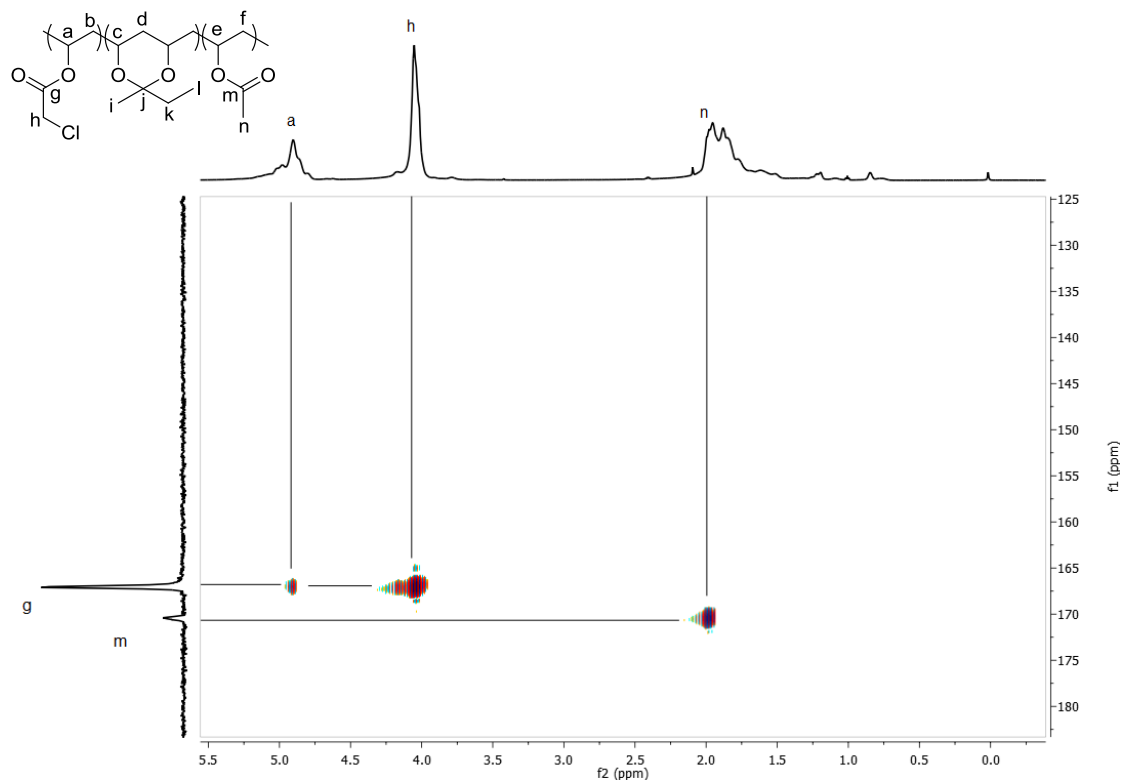


Figure 2.18: 176 MHz ^1H - ^{13}C HMBC spectrum in CDCl_3 , showing the correlations of the carbonyl carbon environments

The peaks in Figure 2.18, that correlate to PVByl are the resonances at 8.5 ppm for the methyl carbon atom (l), at 35.6 ppm for the methylene carbon atom at (k), at 17.3 ppm for the methyl carbon neighbouring the quaternary carbon atom (i), at 43.0 ppm for the methylene carbon atom on the polymer backbone (d), at 62.0 ppm for the methine carbon atom on the polymer backbone (c), and at 100.3 ppm for to the quaternary carbon atom (j). Evidence for the quaternary carbon atom is seen in the distortionless enhancement by polarization transfer-135 (DEPT-135) spectrum due to the disappearance of the resonance at 100.3 ppm, Figure 2.19.

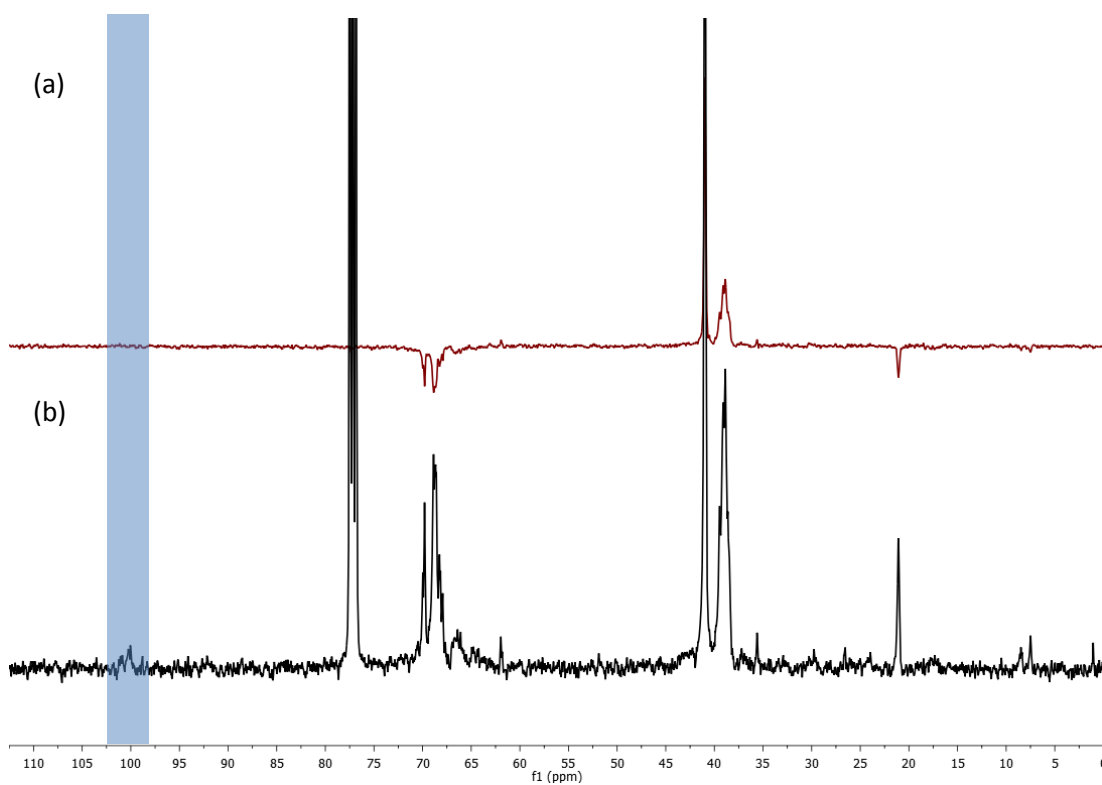


Figure 2.19: 176 MHz NMR in CDCl₃ (a) DEPT-135 (b) ¹³C NMR spectrum

Moreover, the ¹H - ¹³C HMBC spectrum (Figure 2.20) indicates that this quaternary carbon atom is incorporated into PVByl as it correlates to the methyl proton (i and l) and methylene proton (k) environments.

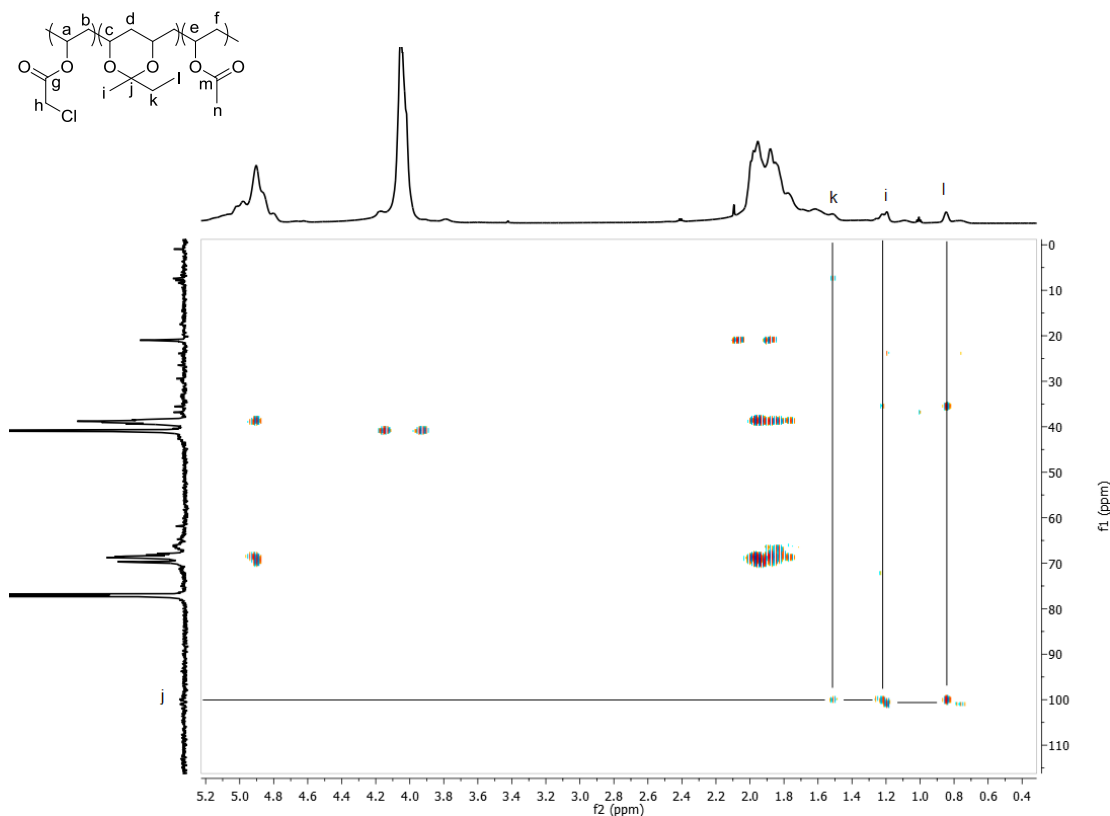
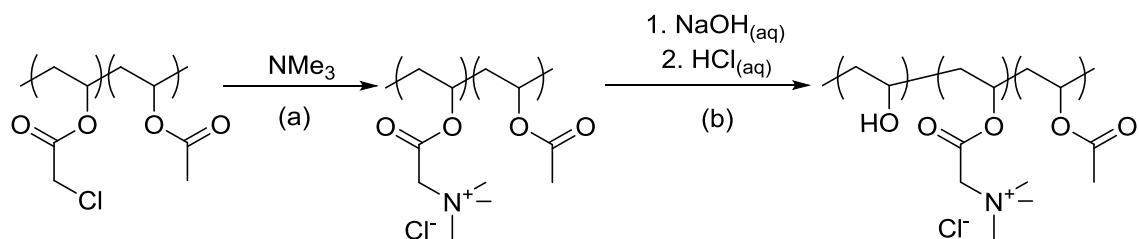


Figure 2.20: 176 MHz ^1H - ^{13}C HMBC spectrum of PVCA in CDCl_3

2.3.5. Synthesis of Poly(vinyl betaine)

Baudrion *et al.* quarternised PVCA with four different amines to synthesise cationic PVA (Scheme 2.2.b) with %QNC between 10 - 80%, for use in biocidal coatings.⁵ However, smaller quaternary nitrogen atoms are used in cationic polymers for conditioning shampoos, therefore we have selected NMe_3 for the quarternisation of PVCA to synthesise PVB (Scheme 2.7.a). DMSO was used as the reaction solvent as this affords increased %QNC ($\geq 80\%$) for PVB, instead of using acetone as PVB precipitates at approximately 33% %QNC.



Scheme 2.7: (a) Quarternisation of PVCA (b) Saponification of PVB to synthesise $\text{P}[(\text{VB})\text{-}r\text{-}(\text{VA})]$

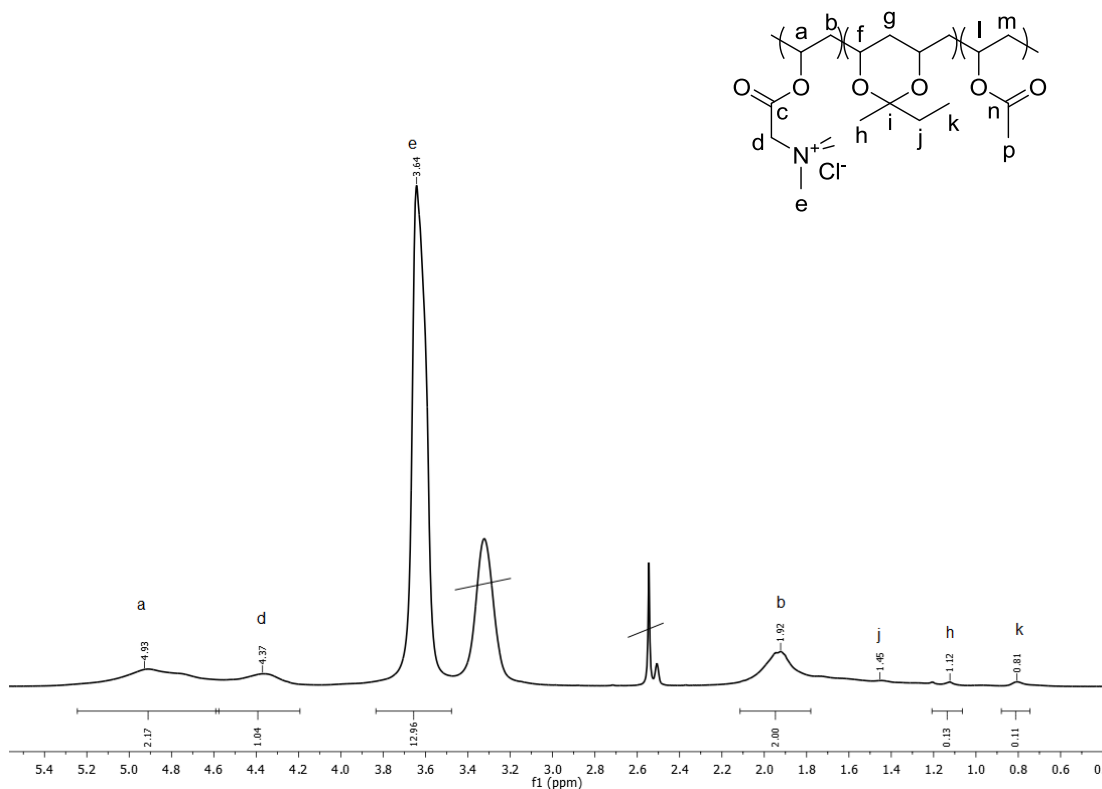


Figure 2.21: 400 MHz ^1H NMR spectrum of PVB in d_6 -DMSO

The ^1H NMR spectrum of PVB is shown in Figure 2.21. The resonances corresponding to PVB are assigned to 1.92 ppm for the methylene protons on the polymer backbone (b), at 4.93 ppm for the methine protons on the polymer backbone (a), which are both supported by $^1\text{H} - ^1\text{H}$ COSY spectrum (Figure 2.22). The resonance at 3.64 ppm and 4.37 ppm are attributed to the protons associated with the quaternary nitrogen atom (e) and the methylene protons neighbouring the carbonyl carbon (d), respectively.

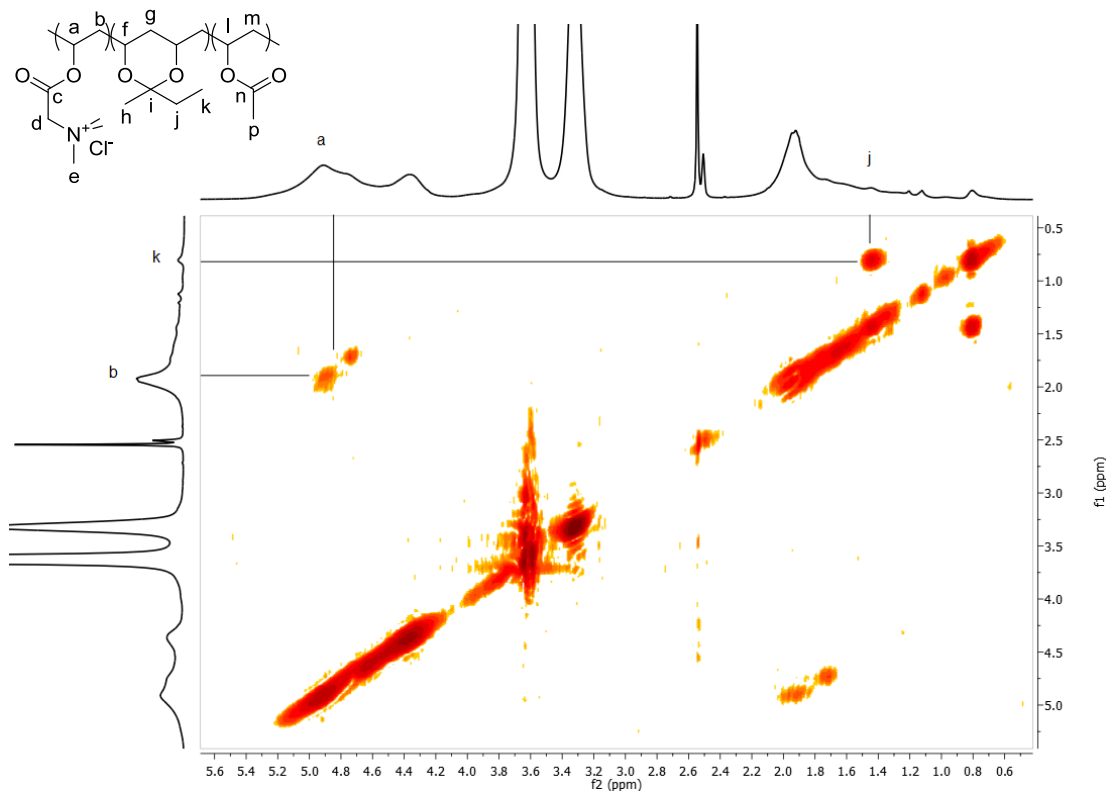


Figure 2.22: 400 MHz $^1\text{H} - ^1\text{H}$ COSY spectrum of PVB in d_6 -DMSO highlighting the correlations along the polymer backbone and in PVByl

The resonances of PVByl repeat unit are observed at 0.81 ppm for the methyl protons (k), and at 1.45 ppm for the methylene protons (j), both of which correlate together in the $^1\text{H} - ^1\text{H}$ COSY spectrum, Figure 2.22. Furthermore, resonances due to the methyl protons next to the quaternary carbon (h) are seen at 1.12 ppm.

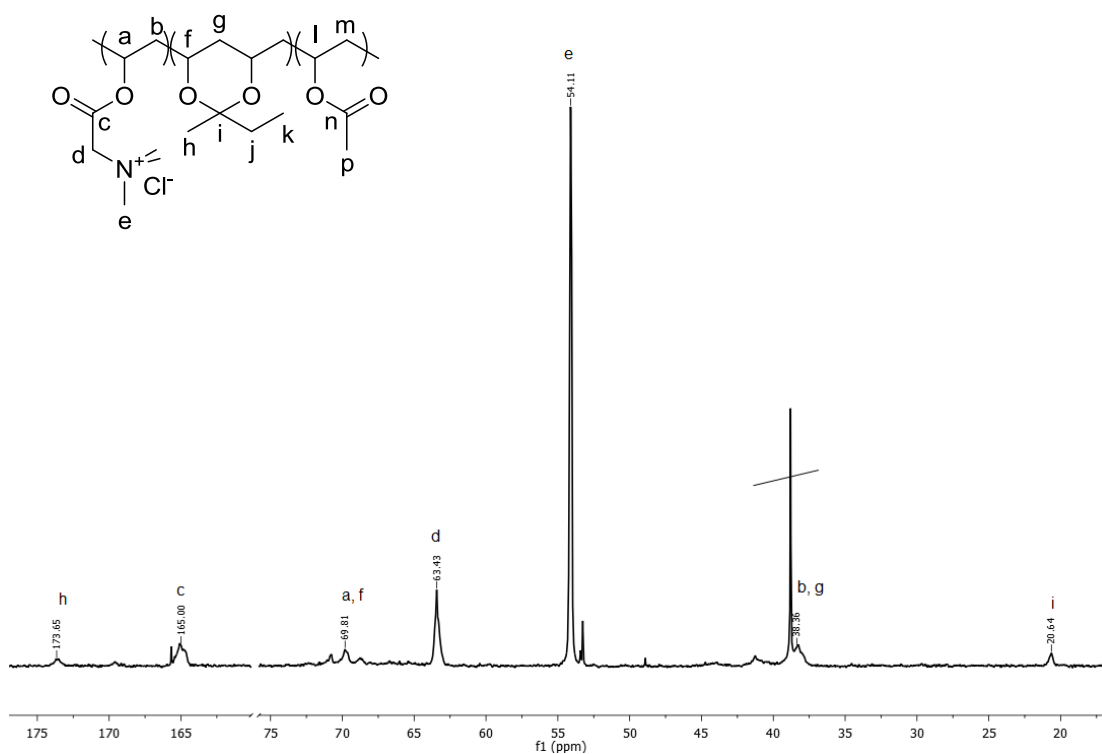


Figure 2.23: 176 MHz ¹³C NMR spectrum of PVB in *d*₆-DMSO

The polymer was further analysed using ¹³C NMR spectroscopy, Figure 2.23. The resonances relating to PVB polymer backbone are attributed to 38.4 ppm for the methylene carbon atom on the polymer backbone (b) and to 69.8 ppm for the methine carbon atom on the polymer backbone (a). Furthermore, the resonance at 63.4 ppm is attributed to the methylene carbon atom neighbouring the quaternary nitrogen atom (d), and at 54.1 ppm to the methyl carbon atom adjacent to the quaternary nitrogen atom (e). The carbonyl carbon atom is assigned to the resonance at 165.0 ppm (c). The assignments of the carbon environments are supported by the ¹H - ¹³C HSQC spectrum (Figure 2.24).

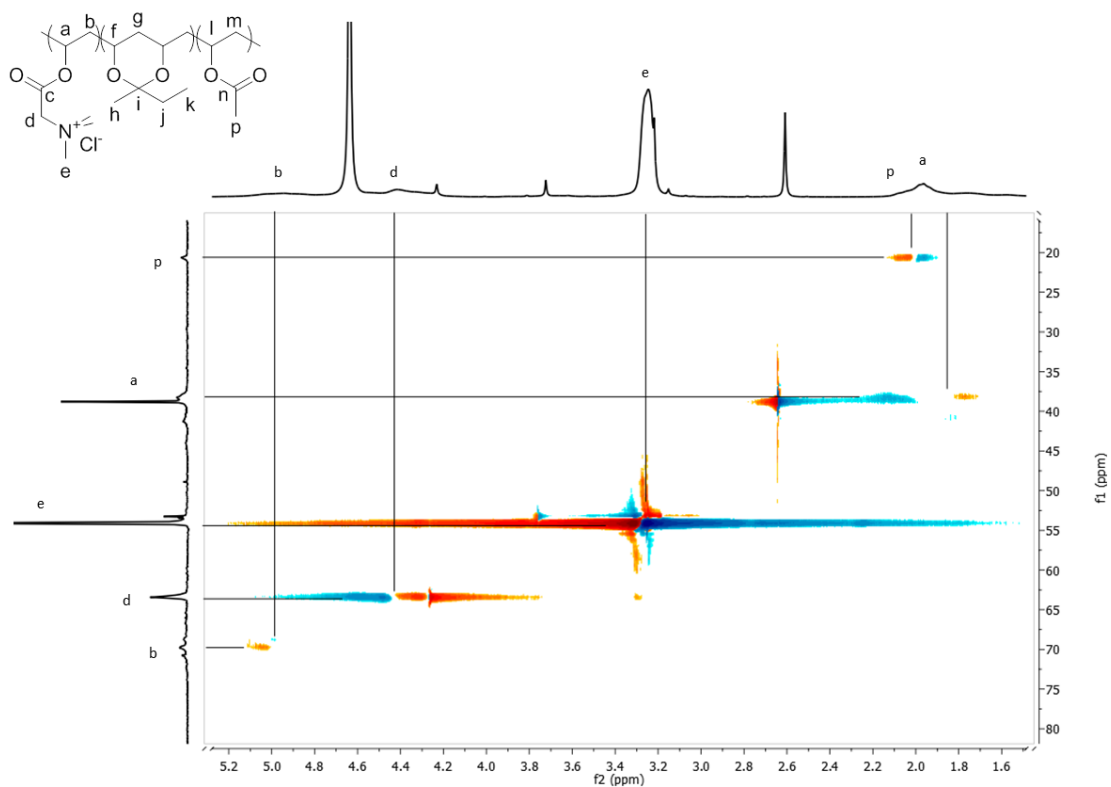


Figure 2.24: 176 MHz ^1H - ^{13}C HSQC spectrum of PVB in d_6 -DMSO

In Figure 2.23, peaks that correspond to the PVAc backbone are assigned to the resonances at 38.36 ppm for the methylene carbon atoms (d) and 69.8 ppm for the methine carbon atom (c). The resonance at 20.6 ppm is assigned to the methyl carbon atom (i), and at 173.7 ppm to the carbonyl carbon atom (h), this is confirmed by the correlation with the methyl protons (i) in the ^1H - ^{13}C HMBC spectrum, Figure 2.25. A negligible resonance at 169.6 ppm is observed which is attributed to the carbonyl carbon in unreacted PVCA.

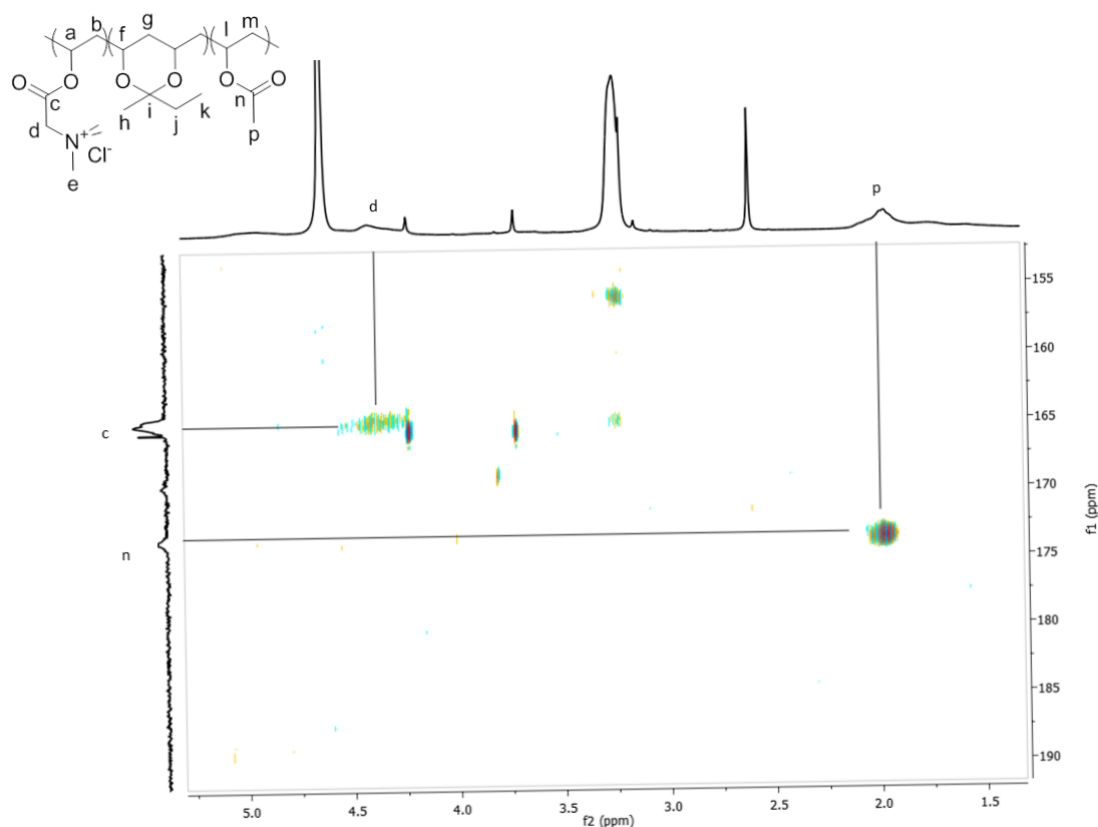
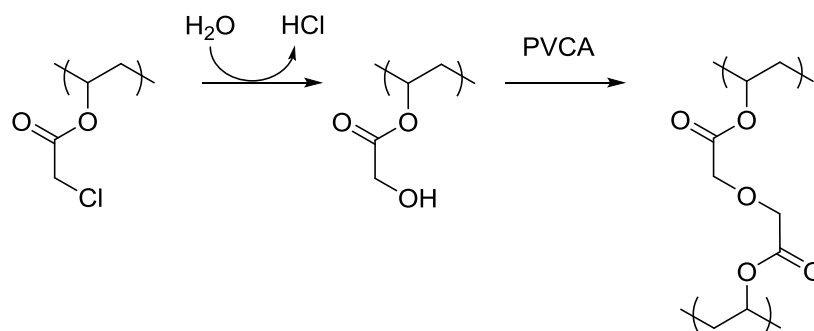


Figure 2.25: 176 MHz ^1H - ^{13}C HMBC spectrum in d_6 -DMSO, highlighting the correlations of the carbonyl carbons in PVB

The composition of PVB was assumed to be 85:3:12 (PVB:PVByl:PVAc) based on the previously determined composition of PVCA (Section 2.3.3). As quantitative conversion of PVCA to PVB was achieved as only a negligible carbonyl carbon for PVCA was observed in the ^{13}C NMR spectrum (Figure 2.23). The CD of the polymer was therefore determined to be 5.3 meq g^{-1} , using Equation 2.6.

Baudrion *et al.* controlled the CD of cationic PVA by the molar quantity of tertiary amine or reaction time used in the quarternisation reaction.⁵ However, when their method was applied to control the CD of poly[(vinyl betaine)-*ran*-(vinyl chloroacetate)], the formation of cross-linked materials was observed. The formation of cross-linked materials was not reported in their publication. We propose that the crosslinking reaction is most likely caused by Williamson etherification as the result of hydroxyl groups, reacting with PVCA, Scheme 2.8.



Scheme 2.8: Proposed possible formation for the formation of cross-linked PVCA

2.3.6. Synthesis of Poly[(vinyl betaine)-*ran*-(vinyl alcohol)]

The determined CD for PVB of 5.3 meq g⁻¹ is too great for use in conditioning shampoos. This is because high CD polymers accumulate on the hair surface making hair appear lank as the cationic polymers do not desorb sufficiently from the hair surface.¹¹ Hence, it was decided to control the CD *via* a hydrolysis reaction to synthesise poly[(vinyl betaine)-*ran*-(vinyl alcohol)] (P[(VB)-*r*-(VA)]) (Scheme 2.7.b).

Therefore, PVB was subjected to hydrolysis to synthesise P[(VB)-*r*-(VA)] with a 50:50 composition of PVB:PVA. The ¹H NMR spectrum of the reaction product is shown in Figure 2.26.b.

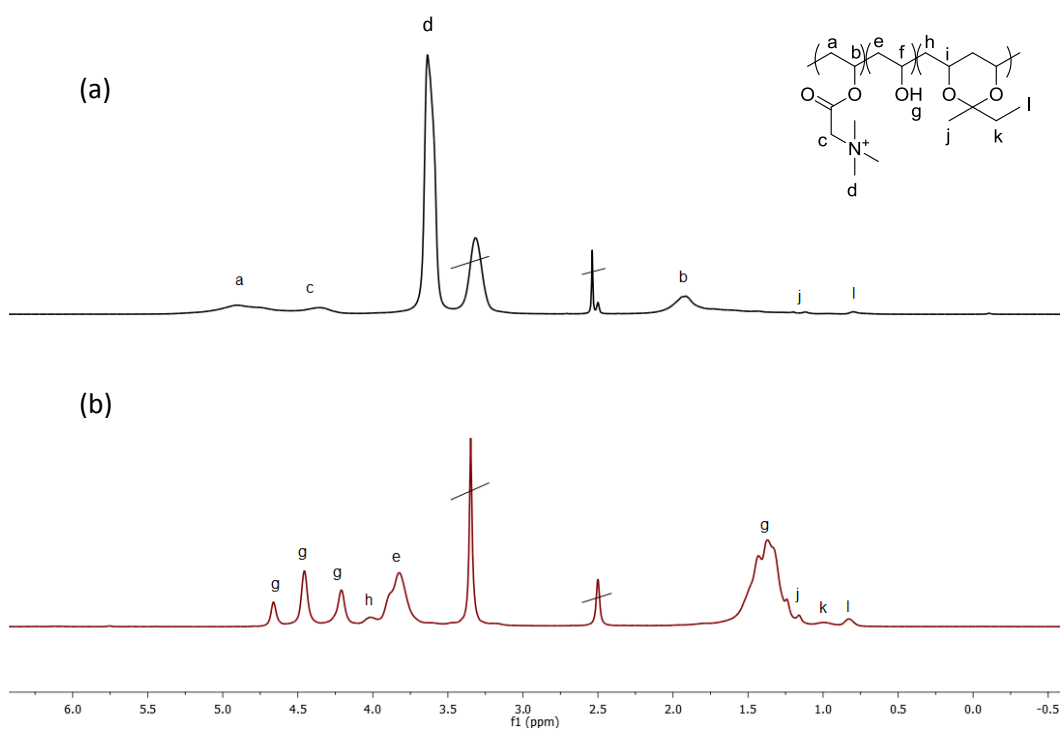


Figure 2.26: 400 MHz ¹H NMR spectra in d₆-DMSO (a) PVB (b) hydrolysed PVB

None of the expected resonances relating to the PVB repeat unit (Figure 2.26.a) are observed for “P[(VB)-*r*-(VA)]” in Figure 2.26.b. For the PVA segment the resonance at 1.86 ppm is attributed to the methylene protons on the polymer backbone (b), and at 3.83 ppm to the methine protons on the polymer backbone (e). Furthermore, the resonances at 4.22 ppm, 4.46 ppm and 4.67 ppm are attributed to the hydroxyl group protons (g). For the PVByl repeat units the resonance at 0.84 ppm is attributed to the methyl protons (l) and at 0.99 ppm to the methylene protons (k). The resonance at 1.16 ppm is attributed to the methyl protons neighbouring the quaternary carbon atom (j) and at 4.02 ppm to the methine protons on the polymer backbone (h). Therefore, the analysis confirms that complete saponification is achieved resulting in the formation of PVA.

Further attempts to control the saponification process were unsuccessful, including neutralisation using acidic resins or using a pH meter to ensure accurate quenching of the reaction. The inability to control the saponification process may be due to protic reaction solvent or counterion exchange between the initially present chloride ion and the added hydroxide ion. If counterion exchange occurred the new hydroxide counterion could potentially continue to catalyse the hydrolysis of the ester bond.

2.4. Conclusion

P[(VA)-*r*-(VETMAC)] was synthesised using either GTMAC or CHPTMAC. P[(VA)-*r*-(VETMAC)] synthesised using GTMAC produced greater CDs than when CHPTMAC was used. The molar equivalents of GTMAC and the addition of an inert diluent were investigated resulting in either small or no effect on the CD, respectively. Greater CDs than claimed in publications (1.7 meq g^{-1})⁴ were achieved by slowing the rate of addition of the reagent with a maximum CD of 2.5 meq g^{-1} being recorded

PVCA was successfully synthesised from the reaction of 88% hydrolysed PVA with CAA. However, the formation of PVByl was also observed due to the side reaction of PVA with butanone, used as solvent. PVB was then synthesised by the subsequent reaction of PVCA with trimethylamine, to synthesise a copolymer with a composition of 85:3:12 for PVB:PVByl:PVAc with a CD of 5.3 meq g^{-1} . Controlling the CD of PVB by adjusting the molar equivalents of NMe₃ resulted in the formation of cross-linked materials by Williamson etherification between hydroxyl groups in PVA and chlorine atoms in PVCA. Therefore, an alternative route to control CD was attempted via the hydrolysis of PVB to synthesise P[(VB)-*r*-(VA)]. However, the reaction was unsuccessful as this resulted in complete hydrolysis of PVB producing PVA.

2.5. Reference

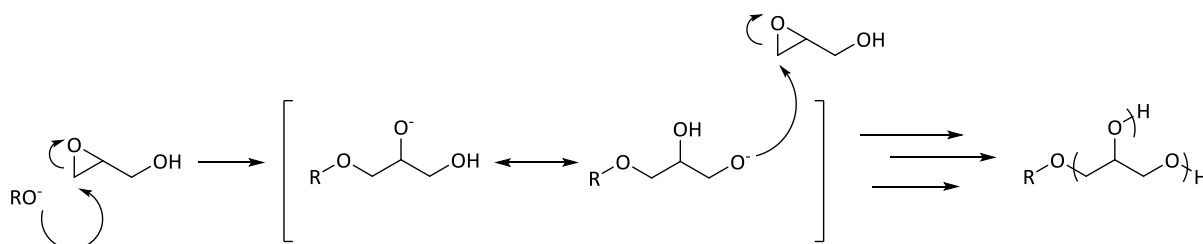
- (1) Davis, R. I.; Phalangas, C. J.; Titus, G. R.; US 4690817 A, 1987.
- (2) Phalangas, C. J.; US 5112886, 1992.
- (3) Fatehi, P.; Singh, R.; Ziaee, Z.; Xiao, H.; Ni, Y. *Eur. Polym. J.* **2011**, *47*, 997.
- (4) Fatehi, P.; Xiao, H. N.; van de Ven, T. G. M. *Langmuir* **2011**, *27*, 13489.
- (5) Baudrion, F.; Perichaud, A.; Coen, S. *J. Appl. Polym. Sci.* **1998**, *70*, 2657.
- (6) Moritani, T.; Yamauchi, J. *Polymer* **1998**, *39*, 559.
- (7) Wang, Y. L.; Kimura, K.; Dubin, P. L.; Jaeger, W. *Macromolecules* **2000**, *33*, 3324.
- (8) Kam, S. K.; Gregory, J. *Colloids Surf., A* **1999**, *159*, 165.
- (9) Mark, J. E. *Polymer Data Handbook*; Oxford University Press, **1999**.
- (10) <http://www.sigmaaldrich.com/catalog/product/aldrich/50053>; Vol. Accessed - 29/04/15.
- (11) Pfau, A.; Hössel, P.; Vogt, S.; Sander, R.; Schrepp, W. *Macromolecular Symposia* **1998**, *126*, 241.

Chapter 3

**Synthesis and characterisation of
poly[(vinyl alcohol)-*graft*-(hyperbranched
polyglycerol)]**

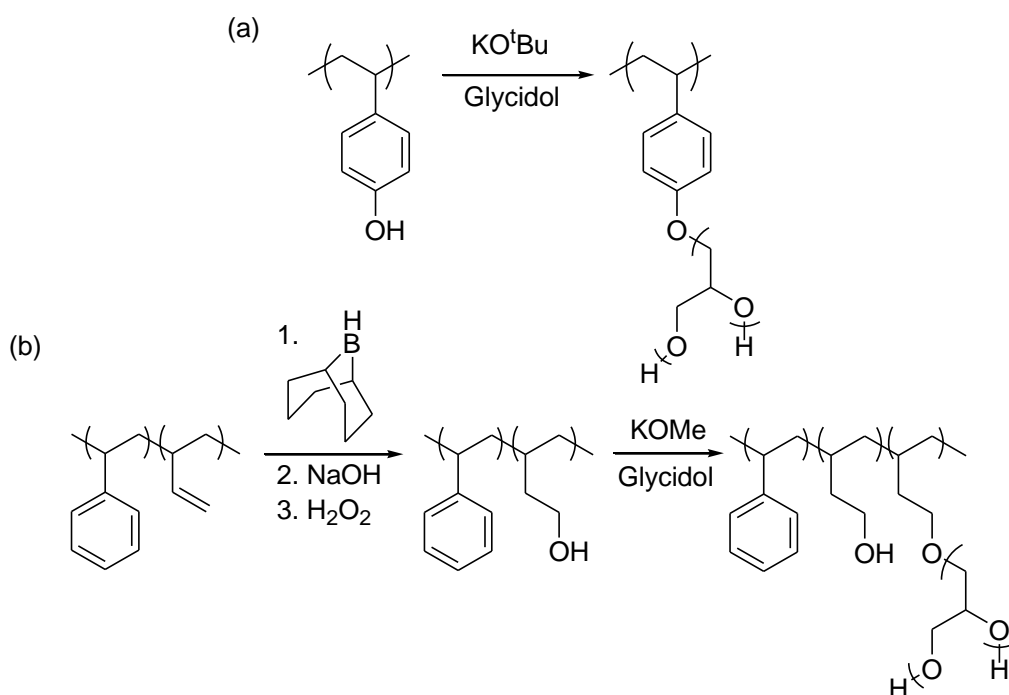
3.1. Introduction

The anionic ring-opening polymerisation (ROP) of glycidol produces hyperbranched polyglycerol (hPG) which contains primary and secondary hydroxyl groups (Scheme 3.1).



Scheme 3.1: Mechanism for the ROP of glycidol to synthesise hPG

A range of hydroxyl group containing polymers has been used as macroinitiators for the 'grafting from' polymerisation of glycidol. Frey *et al.* grafted glycidol onto poly(4-hydroxystyrene) (PHOS) (Scheme 3.2.a).¹ Complete substitution of the initiator was possible due to fast proton exchange, slow monomer addition and the higher acidity of the aromatic hydroxyl group in the macroinitiator compared to hPG. The degree of branching (%DB) of the synthesised polymers has been reported to be between 55 - 57% and the inclusion of the side chains vastly decreased the glass transition temperature (T_g) of the product. Poly[(4-hydroxystyrene)-*graft*-(hPG)] (P[(HOS)-*g*-(hPG)]) has also been quoted as having increased solubility in polar solvents, *e.g.* methanol (MeOH), in comparison with the PHOS.



Scheme 3.2: (a) The synthesis of P[(HOS)-*g*-(hPG)] (b) Formation of hydroxylated butadiene followed by the reaction with glycidol to form Poly[(styrene)-*block*-(butadiene)-*g*-(hPG)]

A hydroxylated butadiene copolymer, containing a polystyrene block, has also been used as a macroinitiator for the ROP of glycidol (Scheme 3.2.b).² Complete substitution of the initiator was not possible. Furthermore, the degree of substitution (%DS) of hydroxyl groups on the macroinitiator was not calculated, as the difference in proton and carbon environments in the modified and unmodified initiator were not great enough to be detected by nuclear magnetic resonance (NMR) spectroscopy. The grafting efficiency (%GE) of the reaction (60 - 76%) was determined from the ratio of added glycidol and the amount of hPG in the graft copolymer.

The functionalisation of poly(vinyl alcohol) (PVA) has been limited as it comprises secondary hydroxyl groups. Therefore, in this chapter the incorporation of primary hydroxyl groups into PVA *via* the reaction with glycidol will be discussed.

There are no peer-reviewed publications on the polymerisation of glycidol using PVA as an initiator. However, a patent has claimed to synthesise poly[(vinyl alcohol)-*graft*-(hyperbranched polyglycerol)] (P[(VA)-*g*-(hPG)]) for use as a binder in batteries. However, use of acetone (common non-solvent for PVA) as the solvent for the homogeneous reactions casts doubt over the legitimacy of these claims.³

3.2. Experimental

3.2.1. Materials

Low molecular weight (LMW) PVA ($M_w = 1.3 \times 10^4 \text{ g mol}^{-1}$ (DP \approx 295), 99% hydrolysed), high molecular weight (HMW) PVA ($1.86 \times 10^5 \text{ g mol}^{-1}$ (DP \approx 4227), 99% hydrolysed) 1,1,1-tris(hydroxymethyl)propane (THMP) ($\geq 98.0\%$), DOWEX[®] MARATHON MR-3 mixed bed ion-exchange (DOWEX) resin, dimethyl sulfoxide (DMSO), 1,3-Dimethyl-3,4,5,6-tetrahydro-2(1H)-pyrimidinone (DMPU), 4-Dimethylaminopyridine (DMAP) and sodium methoxide solution (NaOMe) (25 %wt in MeOH) were purchased from Sigma Aldrich and used without further purification. Glycidol was purchased from Sigma Aldrich and was purified by vacuum distillation and stored at 0 °C under N₂. Acetone, MeOH, isopropanol, hydrochloric acid (HCl) and sodium hydroxide (NaOH) were purchased from Fischer Scientific and used without further purification. Deuterium oxide (D₂O) was purchased from Goss Scientific and used without purification.

3.2.2. Instrumentation

Dropwise additions were carried out using a KDS-100-CE syringe pump.

¹H NMR spectra were all recorded on a Bruker Avance-400 operating at 400 MHz or VNMR-700 at 700 MHz. ¹³C NMR and Inverse gated ¹³C NMR spectra were carried out on a VNMR-700 at 176 MHz.

Fourier transform infra-red (FT-IR) spectroscopy was performed using a Perkin Elmer 1600 Series FT-IR.

Thermogravimetric analysis (TGA) measurements were collected using a Perkin Elmer Pyris 1 in a nitrogen (N₂) atmosphere. Samples were heated at a rate of 10 °C min⁻¹ to 500 °C.

Differential scanning calorimetry (DSC) measurements were carried out using a TA Instruments DSC Q1000. Samples were heated at a rate of 10 °C min⁻¹ between -50 °C and 300 °C.

3.2.3. Synthesis of hyperbranched polyglycerol

hPG was synthesised following the method outlined by Sunder *et al.*⁴ A three-necked round bottom flask (250 mL) equipped with a dropping funnel, mechanical stirrer and distillation set was charged with THMP (1 g, 7.5 mmol) and NaOMe (0.8 mL, 0.8 mmol). MeOH was then removed by distillation under reduced pressure and the reaction flask was placed under a N₂ atmosphere. Glycidol (19.8 mL, 29.8 mol) was added dropwise at a rate of 5.6 mL h⁻¹ and the reaction mixture was stirred at 95 °C for 24 h. The reaction mixture was diluted with MeOH

and stirred over DOWEX resin. The reaction mixture was filtered to remove the DOWEX resin and then added to acetone producing a viscous liquid. The supernatant was decanted off. The viscous liquid was dissolved in MeOH and added to acetone to again produce a viscous liquid. The viscous liquid was dried under reduced pressure for 16 h, to afford hPG.

Yield = 12.8 g (55%). ^1H NMR (700MHz, D_2O): δ (ppm): 0.87 (s, 3H, CH_3), 1.36 (s, 2H, CH_2CH_3), 3.44 (m, 2H, CCH_2O), 3.57 (m, 4H, $\text{CH}_2\text{CH}(\text{OH})\text{CH}_2$), 3.64 (m, 7H, $\text{CH}_2\text{CH}(\text{OH})\text{CH}_2$), 3.73 (m, 4H, $\text{CH}_2\text{CH}(\text{OH})\text{CH}_2$), 3.80 (m, 3H, $\text{CH}_2\text{CH}(\text{OH})\text{CH}_2$), 3.89 (m, 1H, $\text{CH}_2\text{CH}(\text{OH})\text{CH}_2$), 4.02 (m, 1H, $\text{CH}_2\text{CH}(\text{OH})\text{CH}_2$). ^{13}C NMR (176 MHz, D_2O): δ (ppm): 0.3 (CH_3), 22.58 (CH_2CH_3), 43.7 (C), 61.4 ($\text{CH}_2\text{CH}(\text{OH})\text{CH}_2$), 63.2 ($\text{CH}_2\text{CH}(\text{OH})\text{CH}_2$), 69.5 ($\text{CH}_2\text{CH}(\text{OH})\text{CH}_2$), 71.0 ($\text{CH}_2\text{CH}(\text{OH})\text{CH}_2$), 72.3 (CCH_2O), 72.8 ($\text{CH}_2\text{CH}(\text{OH})\text{CH}_2$), 78.5 ($\text{CH}_2\text{CH}(\text{OH})\text{CH}_2$), 80.1 ($\text{CH}_2\text{CH}(\text{OH})\text{CH}_2$).

3.2.4. Synthesis of poly[(vinyl alcohol)-graft-(hyperbranched glycerol)] in water

PVA (1.0 – 20.0 g, 22.7×10^{-3} - 45.4 mol) was dissolved in water (8.0 – 160.0 mL) at 80 °C in a two necked round bottom flask (50 - 500 mL) equipped with a rubber septum, magnetic stirrer bar and a water cooled condenser. The reaction mixture was then acclimatised to the reaction temperature (0 - 100 °C). $\text{NaOH}_{(\text{aq})}$ (0 - 2.3 mL, 0 - 50 mol%, 5 M, 0.0 – 22.0 mmol) was added followed by glycidol (0.8 - 68.7 mL, 50 - 350 mol%) at an addition rate of 6 - 0.075 mL h^{-1} and stirred for 4 - 44 h. The reaction mixture was then neutralised with $\text{HCl}_{(\text{aq})}$ (5 M) and was added into acetone. The resulting white solid was purified by Soxhlet extraction using isopropanol to remove the hPG contaminant. The purified solid was reprecipitated from water into acetone and dried under reduced pressure for 16 h at 40 °C, to afford P[(VA)-g-(hPG)].

Yield = 22.8 g (89%). ^1H NMR (700 MHz, D_2O): δ (ppm): 1.66 (m, 2H, CH_2), 3.62 (m, 5H, $\text{CH}_2\text{CH}(\text{OH})\text{CH}_2$), 4.04 (m, 1H, CH). ^{13}C NMR (176 MHz, D_2O): δ (ppm): 41.3 (CH_2), 44.2 (CH_2), 61.0 ($\text{CH}_2\text{CH}(\text{OH})\text{CH}_2$), 62.8 ($\text{CH}_2\text{CH}(\text{OH})\text{CH}_2$), 64.9 (CH), 66.4 (CH), 68.0 (CH), 69.3 ($\text{CH}_2\text{CH}(\text{OH})\text{CH}_2$), 70.7 ($\text{CH}_2\text{CH}(\text{OH})\text{CH}_2$), 72.3 ($\text{CH}_2\text{CH}(\text{OH})\text{CH}_2$), 75.2 (CH), 76.8 ($\text{CH}_2\text{CH}(\text{OH})\text{CH}_2$), 79.7 ($\text{CH}_2\text{CH}(\text{OH})\text{CH}_2$). FT-IR ν (cm^{-1}): 3290 ($\nu_{-\text{OH}}$), 2902($\nu_{\text{C-H}}$), 1052 ($\nu_{-\text{O}}$). $T_m = 219 - 200$ °C; $T_g = 43 - 49$ °C.

3.2.5. Synthesis of Poly[(vinyl alcohol)-graft-(hyperbranched glycerol)] in organic solvents

PVA (1.0 g, 22.7 mmol) was dissolved in DMSO (16.0 mL) or DMPU (10.0 mL) at 80 - 130 °C in a two necked round bottom flask (50 mL) equipped with a rubber septum, magnetic stirrer bar and a water cooled condenser. DMAP in DMSO or DMPU (0.5 mL, 5 mol%, 2.5 M, 1.1 mmol) was added followed by glycidol (3.0 mL, 200 mol%, 45.4 mmol) and was stirred for 24 h at

130 °C. The reaction mixture was neutralised with HCl_(aq) (5 M) and was added into acetone. The resulting dark brown solid was then purified by Soxhlet extraction using isopropanol to remove the hPG contaminant. The purified solid was then reprecipitated from water into acetone and dried under reduced pressure for 16 h at 40 °C, to afford P[(VA)-*g*-(hPG)].

Yield = 1.1 g (79%). ¹H NMR (D₂O): δ (ppm): 1.72 (m, 2H, CH₂), 3.64 (m, 5H, CH₂CH(OH)CH₂), 4.04 (m, 1H, CH), 5.41. ¹³C NMR (D₂O): δ (ppm): 41.7 (CH₂), 44.12 (CH₂), 60.7 (CH₂CH(OH)CH₂), 62.5 (CH₂CH(OH)CH₂), 64.6 (CH), 66.0 (CH), 67.6 (CH), 69.3 (CH₂CH(OH)CH₂), 70.4 (CH₂CH(OH)CH₂), 72.1 (CH₂CH(OH)CH₂), 75.0 (CH), 76.5 (CH₂CH(OH)CH₂), 79.7 (CH₂CH(OH)CH₂). FT-IR ν (cm⁻¹): 3290 (ν_{-OH}), 2902(ν_{C-H}), 1052 (ν_{-O-}).

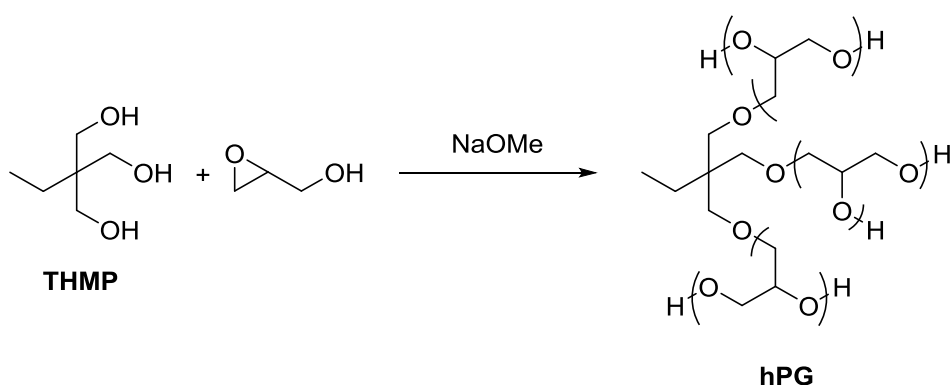
3.2.6. Preparation of Poly(vinyl alcohol)/hyperbranched polyglycerol blends

hPG (0.04 g, 5.7 mmol) was stirred with LMW PVA (0.1 g, 2.2 mmol) (either as a solid or in an aqueous solution (2.2 mol L⁻¹)), in 8 mL vials to prepare a heterogeneous or homogenous blend, respectively. The solvent was then removed under reduced pressure to prepare the homogenous blend of PVA/hPG.

3.3. Results and Discussion

3.3.1. Synthesis of hyperbranched polyglycerol

Hyperbranched polyglycerol (hPG) was synthesised using glycidol and THMP, as an initiator, Scheme 3.3.



Scheme 3.3: Synthesis of hPG using THMP as an initiator

The reaction was carried out in bulk conditions and at 95 °C above the melting point (T_m) of the initiator ($T_m = 56 - 58$ °C). To ensure THMP solely acts as the initiator, MeOH was removed under reduced pressure before the start of the polymerisation reaction. The slow addition of

glycidol was adopted as it has been claimed to decrease the dispersity (\mathcal{D}) of the resulting polymer.⁴

There are four separate structural units that can be formed in the structure of hPG (Figure 3.1): terminal (T) (Figure 3.1.e), dendritic (D) (Figure 3.1.c), linear 1,3 ($L_{1,3}$) (Figure 3.1.b) and linear 1,4 ($L_{1,4}$) (Figure 3.1.d).

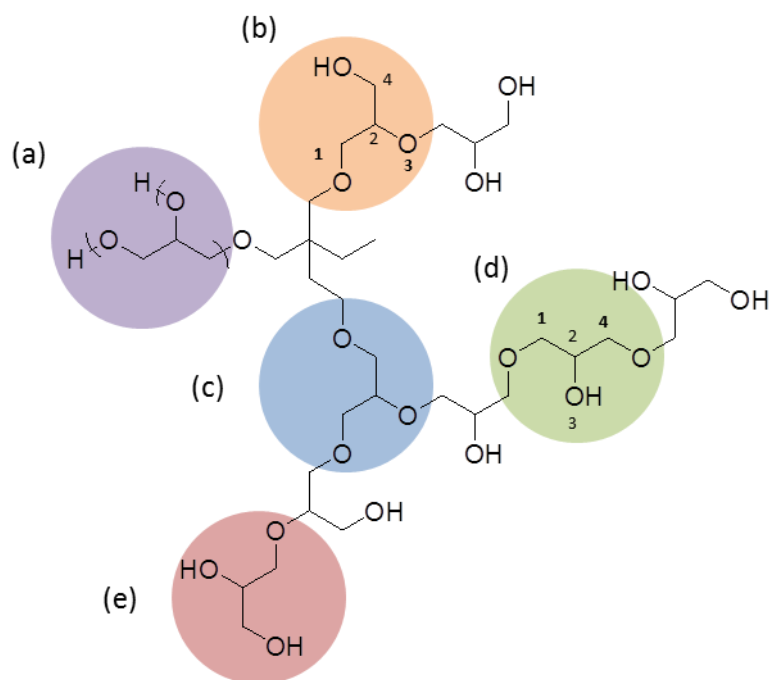


Figure 3.1: Structure of hPG (a) repeat unit (b) $L_{1,3}$ unit (c) D unit (d) $L_{1,4}$ unit (e) T unit

The ratio of the individual structural units can be distinguished by ^{13}C NMR spectroscopy as each structural unit has characteristic resonances allowing for detailed interpretation of the structure. The ^{13}C NMR spectrum of hPG is shown in Figure 3.2.

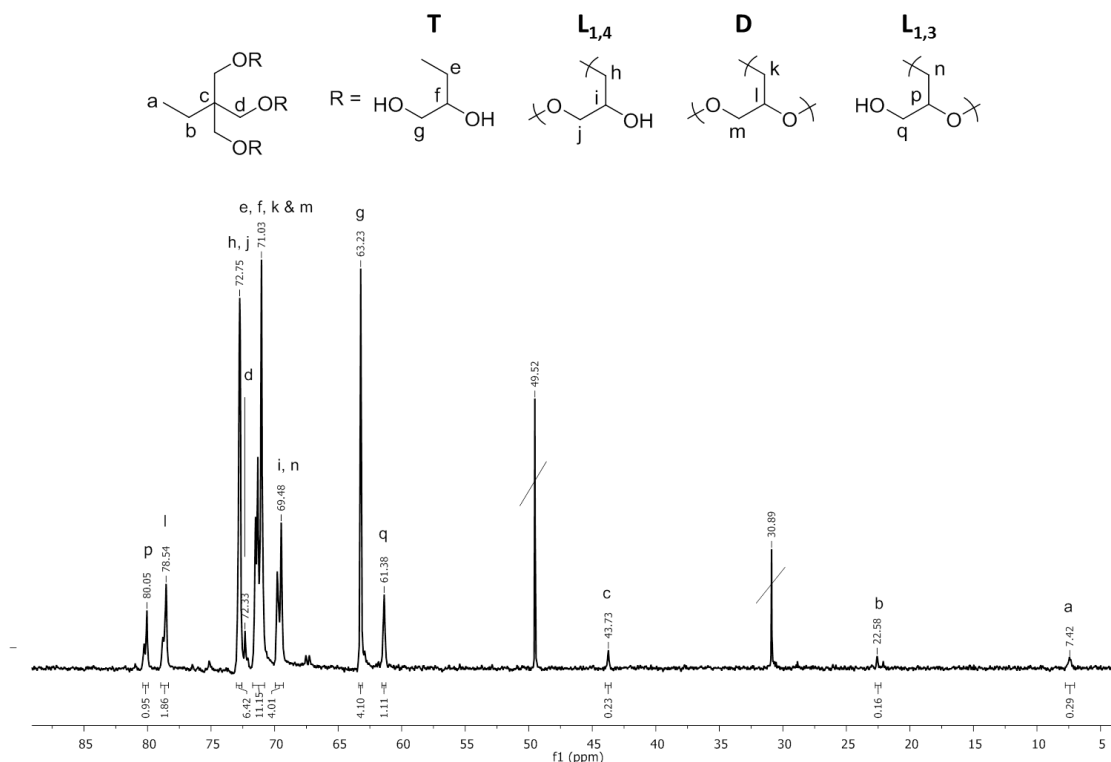


Figure 3.2: 176 MHz ¹³C NMR spectrum of hPG in D₂O

The methylene carbon atoms adjacent to the primary oxygen atom can be seen at 61.4 ppm (q, **L_{1,3}**), 63.2 ppm (g, **T**), 71.0 ppm (m, **D**) and 72.8 ppm (j, **L_{1,4}**). The methylene carbon atoms neighbouring the ether linkage are observed at 69.5 ppm (n, **L_{1,3}**), 71.0 ppm (e, **T**; k, **D**) and 72.8 ppm (h, **L_{1,4}**). The methine carbon atoms of hPG were attributed to resonances at 69.5 ppm (i, **L_{1,4}**), 71.0 ppm (f, **T**), 78.5 ppm (l, **D**) and 80.0 ppm (p, **L_{1,3}**). The resonance at 43.7 ppm was assigned to the quaternary carbon atom of THMP (c) using distortionless enhancement by polarization transfer-135 (DEPT-135) spectroscopy (Figure 3.3). The carbon atoms in the ethyl chain of THMP correspond to the resonances at 7.4 ppm (a) and 22.6 ppm (b) for the methyl and methylene carbon atoms, respectively. The carbon atoms neighbouring the ether linkage in THMP relates to the resonance at 72.3 ppm (d). The assignments are in good agreement with those reported by Sunder *et al.*⁴

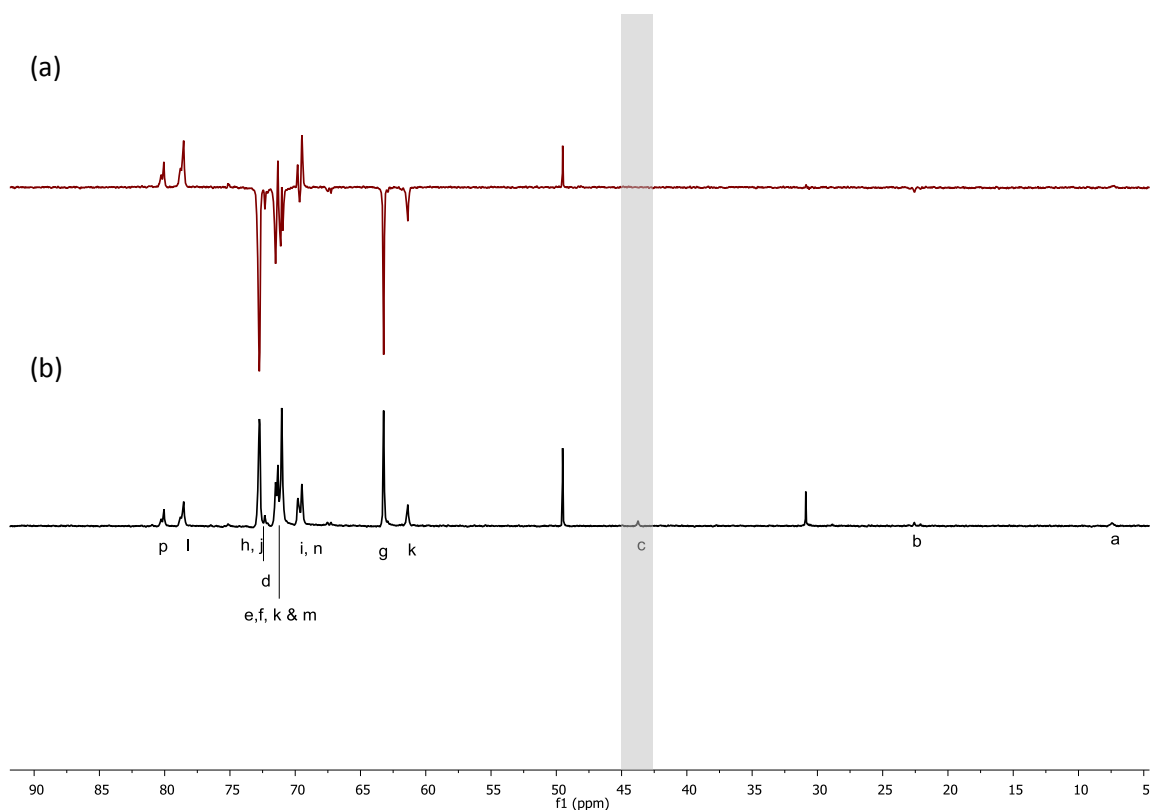


Figure 3.3: 176 MHz ^{13}C NMR (a) DEPT-135 and (b) spectrum of hPG highlighting the disappearance of the quaternary carbon in THMP

Further evaluation of the hPG structure was carried out using ^1H NMR spectroscopy (Figure 3.4).

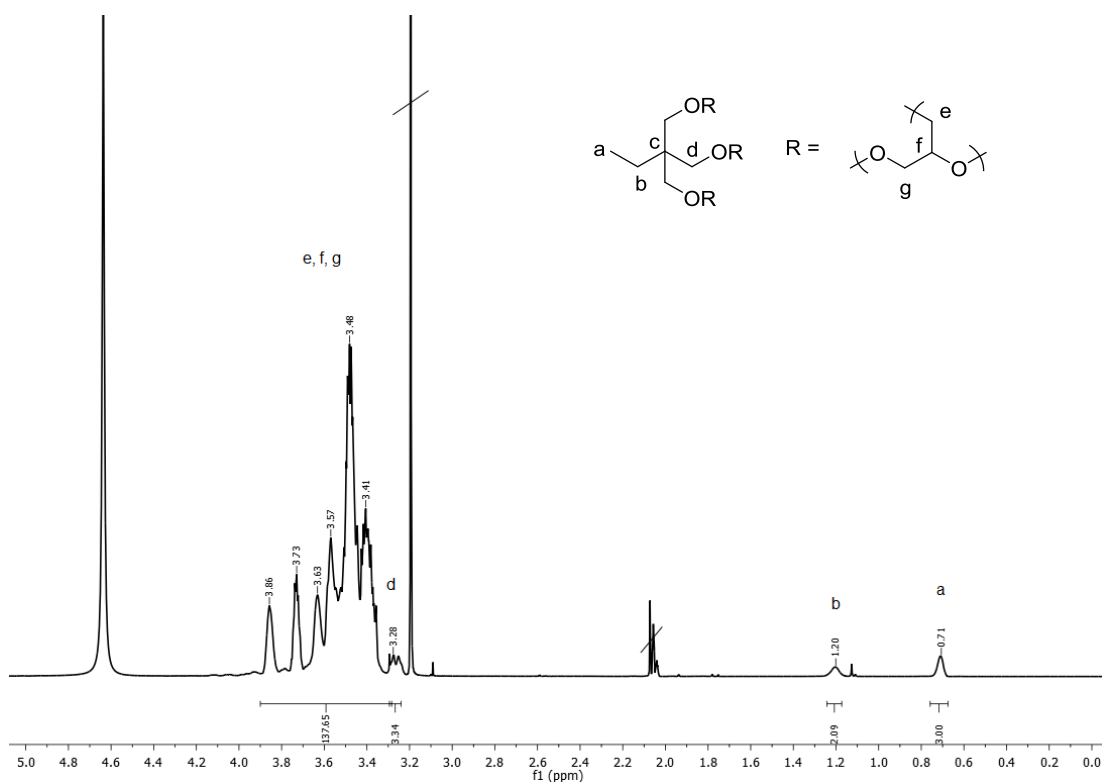


Figure 3.4: 700 MHz ^1H NMR spectrum of hPG

The resonances at 0.71 ppm and 1.20 ppm are assigned to the methyl protons of the THMP initiator (a), and the methylene group adjacent to methyl proton (b), respectively. This is supported by $^1\text{H} - ^1\text{H}$ correlation spectroscopy (COSY) spectrum (Figure 3.5) and the 3:2 ratio between the two resonance ratios. The resonance at 3.28 ppm relates to the methylene protons neighbouring the ether linkage on THMP (d), identified using $^1\text{H} - ^{13}\text{C}$ heteronuclear multiple-bond correlation (HMBC) spectroscopy (Figure 3.6) as it correlates to the methylene protons (b) as well as the quaternary carbon atom. The resonances from 3.41 - 3.86 ppm correspond to all the protons in the structural units of hPG. The labile hydroxyl protons are not observed as they are subject to hydrogen/deuterium exchange with D_2O .

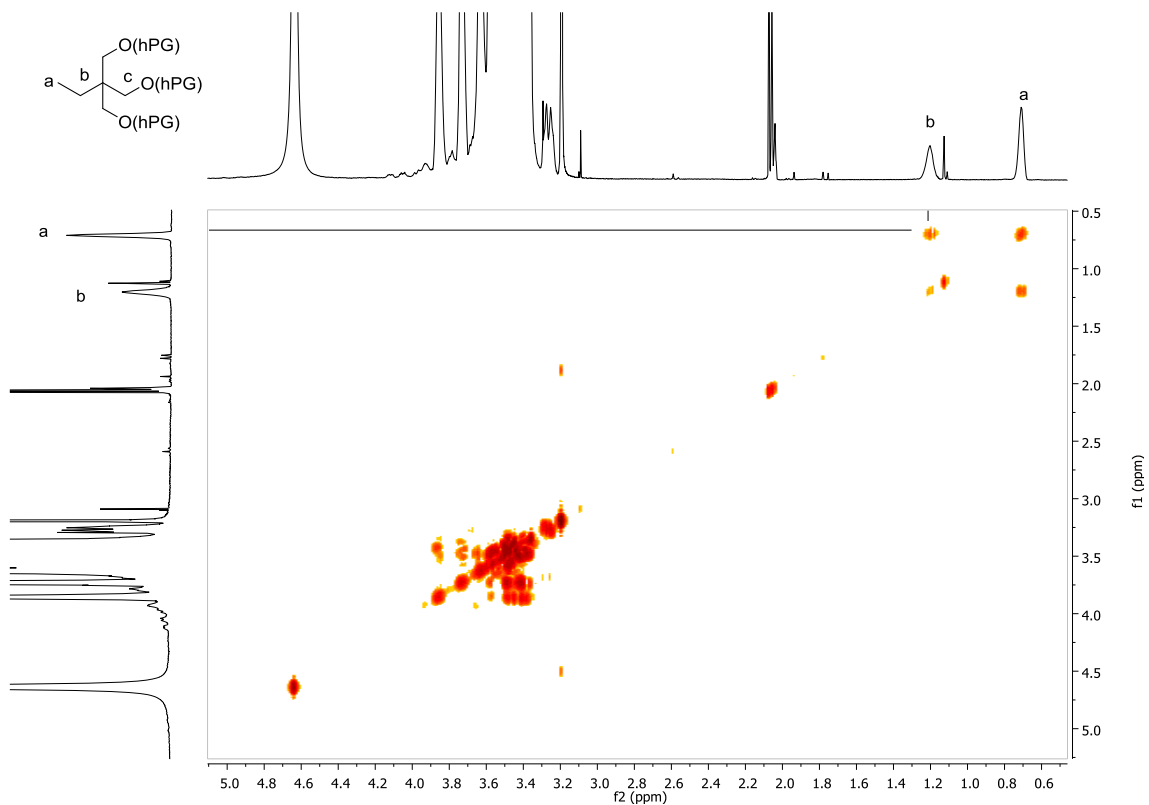


Figure 3.5: $^1\text{H} - ^1\text{H}$ COSY of hPG highlighting the correlation between the resonances corresponding to the ethyl chain in THMP

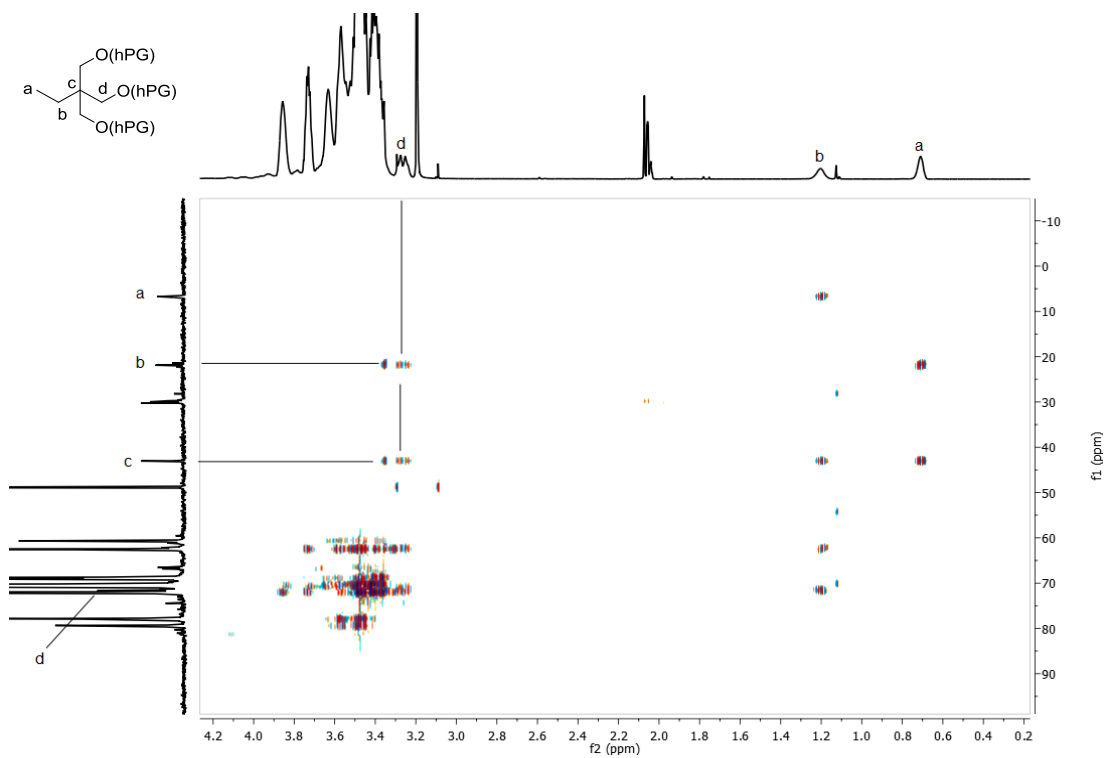


Figure 3.6: $^1\text{H} - ^{13}\text{C}$ HMBC of hPG highlighting that methylene proton (d) is incorporated within THMP

The %DB is determined, using quantitative ^{13}C NMR spectroscopy, by the ratio between the linear and dendritic structural units (Equation 3.1).⁴

$$\%DB = \frac{2 \cdot \%D}{2 \cdot \%D + \%L_{1,3} + \%L_{1,4}} \quad \text{Equation 3.1}$$

Where %D is the abundance of D units and %L_{1,3} and %L_{1,4} is the abundance of the two linear units. The abundances of the structural units were determined from Equation 3.2.

$$\%RU = \frac{\int RU}{\int D + \int L_{1,3} + \left(\frac{\int 2 \cdot L_{1,4}}{2}\right) + \int T} \quad \text{Equation 3.2}$$

Where %RU is the relative abundance of a structural unit, $\int RU$ is the integral of the resonance corresponding to the structural unit being considered in the ^{13}C NMR spectrum, $\int D$ is the integral of the resonance at 78.5 ppm, $\int L_{1,3}$ is the integral of the resonance at 80.0 ppm, $\int 2 \cdot L_{1,4}$ is the integral of the resonances at 72.9 ppm (which consists of two L_{1,4} carbon environments, therefore it is halved) and $\int T$ is the integral of the resonance at 63.2 ppm.

The %DB was therefore determined to be 46%, in comparison with 53% claimed by Sunder *et al.* under the same reaction conditions.⁴

The degree of polymerisation (DP) was also calculated using quantitative ^{13}C NMR spectroscopy using Equation 3.3.⁴

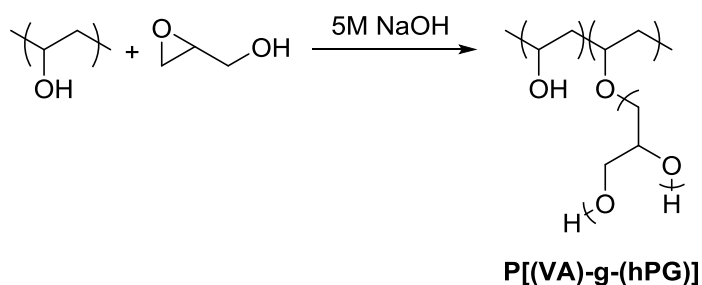
$$DP = \frac{\%T + \%L_{1,3} + \%L_{1,4} + \%D}{\%T - \%D} \times f_c \quad \text{Equation 3.3}$$

Where DP is the degree of polymerisation, %D is the relative abundance of D units, %L_{1,3} is the relative abundance of L_{1,3} units, %L_{1,4} is the relative abundance of L_{1,4} units and f_c is functionality of the core. The DP was 13 in comparison with 15 claimed by Sunder *et al.*; who observed an increase in %DB with increasing DP which might account for the decreased %DB in our product.⁴

3.3.2. Synthesis of Poly[(vinyl alcohol)-graft-(hyperbranched glycerol)] in water

P[(VA)-*g*-(hPG)] was successfully synthesised at high yield using PVA and glycidol (Scheme 3.4). Bulk conditions, previously used for the synthesis of hPG (Section 3.1), were not used as the T_m of PVA is too close to its degradation temperature; therefore water was used as a solvent. $\text{NaOH}_{(\text{aq})}$ was used to catalyse the reaction instead of NaOMe, as removal of MeOH would be

unnecessary in the water solvated reaction. P[(VA)-*g*-(hPG)] was purified by Soxhlet extraction in isopropanol.



Scheme 3.4: Synthesis of P[(VA)-*g*-(hPG)]

FT-IR spectrum of pure P[(VA)-*g*-(hPG)] in comparison with PVA (Figure 3.7) shows the stretching frequency that correlates to a hydroxyl functional group ($\nu = 3290 \text{ cm}^{-1}$) and more importantly the appearance of a signal that corresponds to an ether linkage ($\nu = 1052 \text{ cm}^{-1}$).

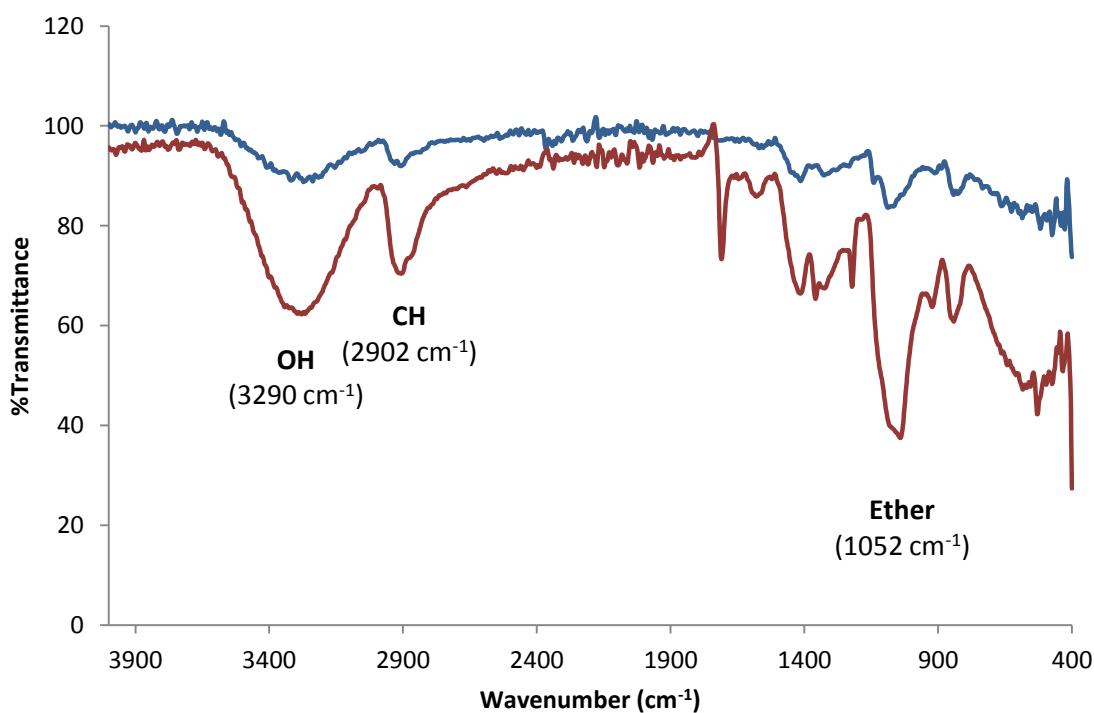


Figure 3.7: The FT-IR spectrum of PVA (—) and P[(VA)-*g*-(hPG)] (—)

The ^1H NMR spectrum of P[(VA)-*g*-(hPG)] is shown in Figure 3.8.

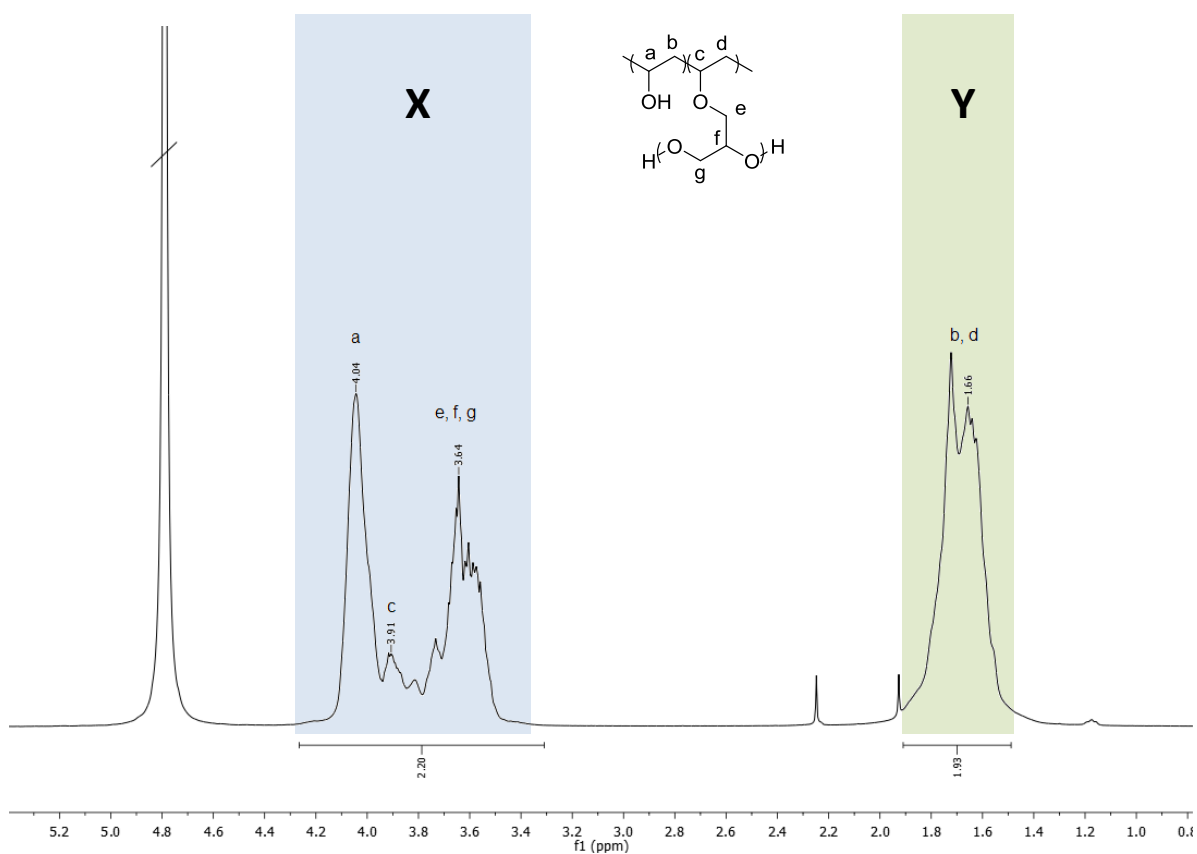


Figure 3.8: 400 MHz ^1H NMR of $\text{P}[(\text{VA})\text{-}g\text{-(hPG)}]$ carried out in D_2O

The resonance at 1.66 ppm is attributed to the methylene protons on the backbone of PVA and $\text{P}[(\text{VA})\text{-}g\text{-(hPG)}]$ (b and d) and 4.04 ppm to the methine protons on the backbone of PVA (a). Their assignments are based on their correlation in the ^1H - ^1H COSY spectrum (Figure 3.9). The resonance at 3.91 ppm corresponds to the proton by the ether linkage (c) on the polymer backbone. The coalesced resonances for all three proton environments in hPG are assigned to 3.63 ppm (e, f and g).

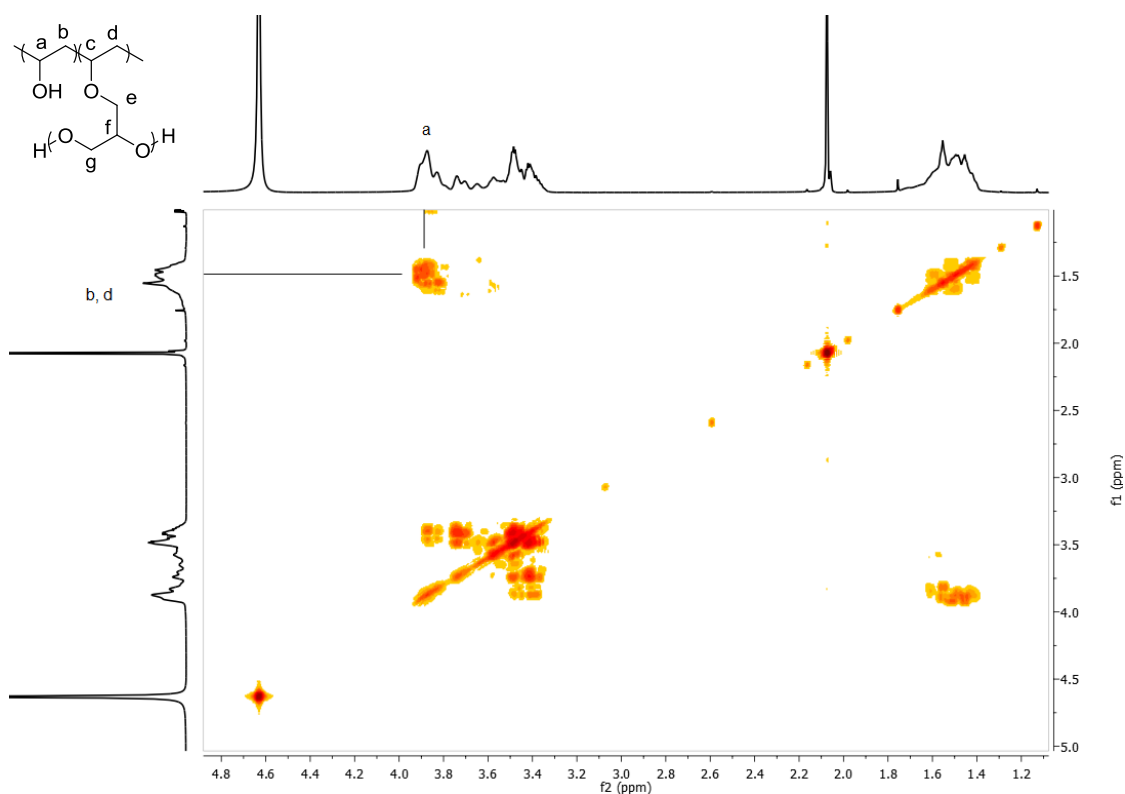


Figure 3.9: 400 MHz $^1\text{H} - ^1\text{H}$ COSY spectrum of P[(VA)-*g*-(hPG)] in D_2O

The ratio between the resonances of PVA and hPG can be used to determine the mole fraction of hPG ($x_{(\text{hPG})}$) in P[(VA)-*g*-(hPG)], using Equation 3.4.

$$x_{(\text{hPG})} = \frac{\int X - 0.5 \int Y}{\int X + \int Y} \quad \text{Equation 3.4}$$

Where $\int X$ is the integral of the signals between 3.5 ppm and 4.2 ppm (a, c; e, f and g) and $\int Y$ is the integral of the signal at 1.9 ppm (b and d). In Figure 3.8, the signals labelled 'X' attributed to the methine proton of PVA and hPG protons coalesce; therefore the contribution of hPG is determined by subtracting half the integral of the methylene proton resonance (simulating the integral of the methine proton) from the integral of 'X'.

The ^{13}C NMR spectrum (Figure 3.10) allows for evaluation of the %DB and %DS of the hyperbranched structure of the hPG grafted chains.

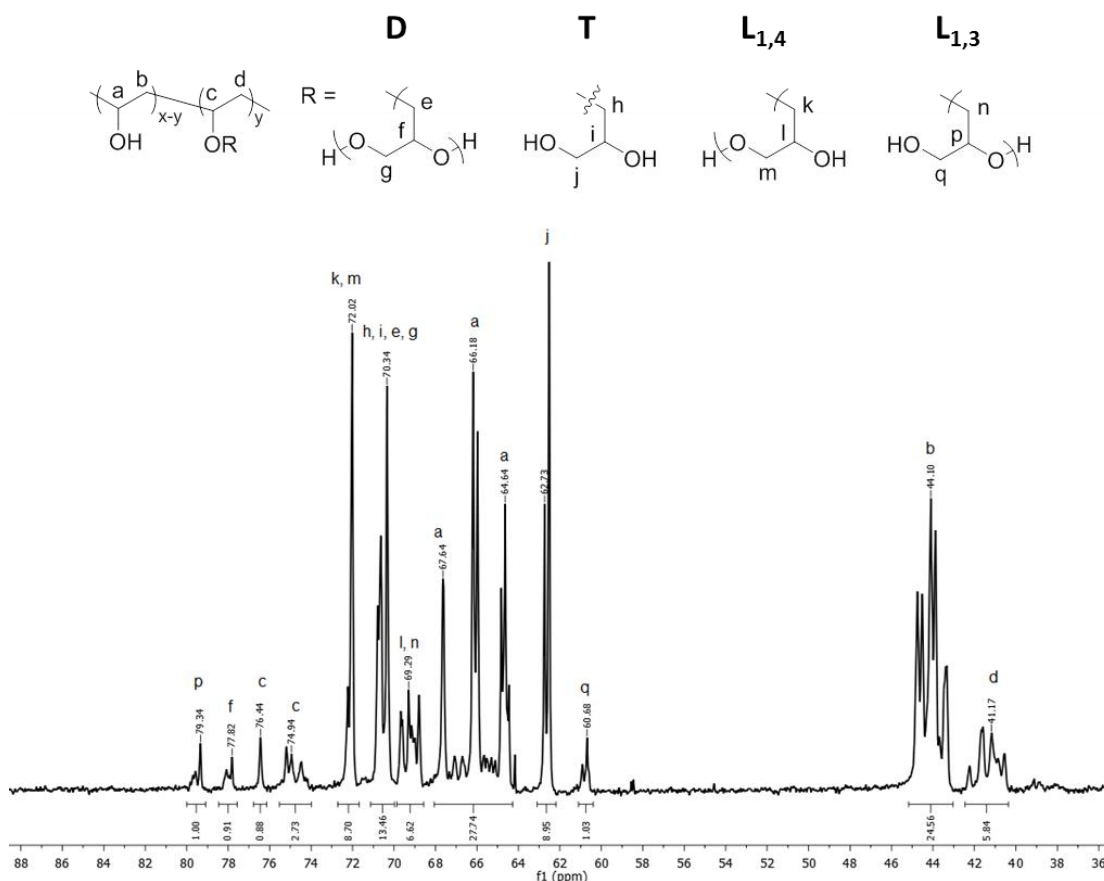


Figure 3.10: 176 MHz ^{13}C NMR spectrum of P[(VA)-g-(hPG)]

The carbon environments of the hPG side chains were assigned using the previously characterised ^{13}C NMR spectrum of hPG. The multiple resonances corresponding to the carbon atom neighbouring the secondary hydroxyl/ether group in each structural unit are observed at 77.8 ppm (f, **D**), 70.3 ppm (i, **T**), 69.3 ppm (l, **L_{1,4}**) and 79.3 ppm (p, **L_{1,3}**). The carbon atom neighbouring the primary hydroxyl/ether group in each structural unit are seen at 70.3 ppm (g, **D**), 62.7 ppm (j, **T**), 72.0 ppm (m, **L_{1,4}**) and 60.7 ppm (q, **L_{1,3}**). The remaining carbon atom environments in the hPG chains, by the ether linkage of each structural unit are at 70.3 ppm (e, **D**; h, **T**), 72.0 ppm (k, **L_{1,4}**) and 69.3 ppm (n, **L_{1,3}**). Along the polymer's backbone, the resonance at 44.1 ppm corresponds to the methylene carbon atom of PVA (b) and the resonance at 41.2 ppm is attributed to the methylene carbon atom of P[(VA)-g-(hPG)] (d). The three resonances at 67.6 ppm, 66.2 ppm and 64.6 ppm correspond to the methine carbon atom of PVA (a). The resonances at 74.9 ppm and 76.4 ppm are attributed to the methine carbon atom of P[(VA)-g-(hPG)] (c). The resonances due to carbon atoms on the backbone are verified using $^1\text{H} - ^{13}\text{C}$ heteronuclear single quantum coherence (HSQC) spectroscopy (Figure 3.11) and $^1\text{H} - ^{13}\text{C}$ HMBC spectroscopy (Figure 3.12).

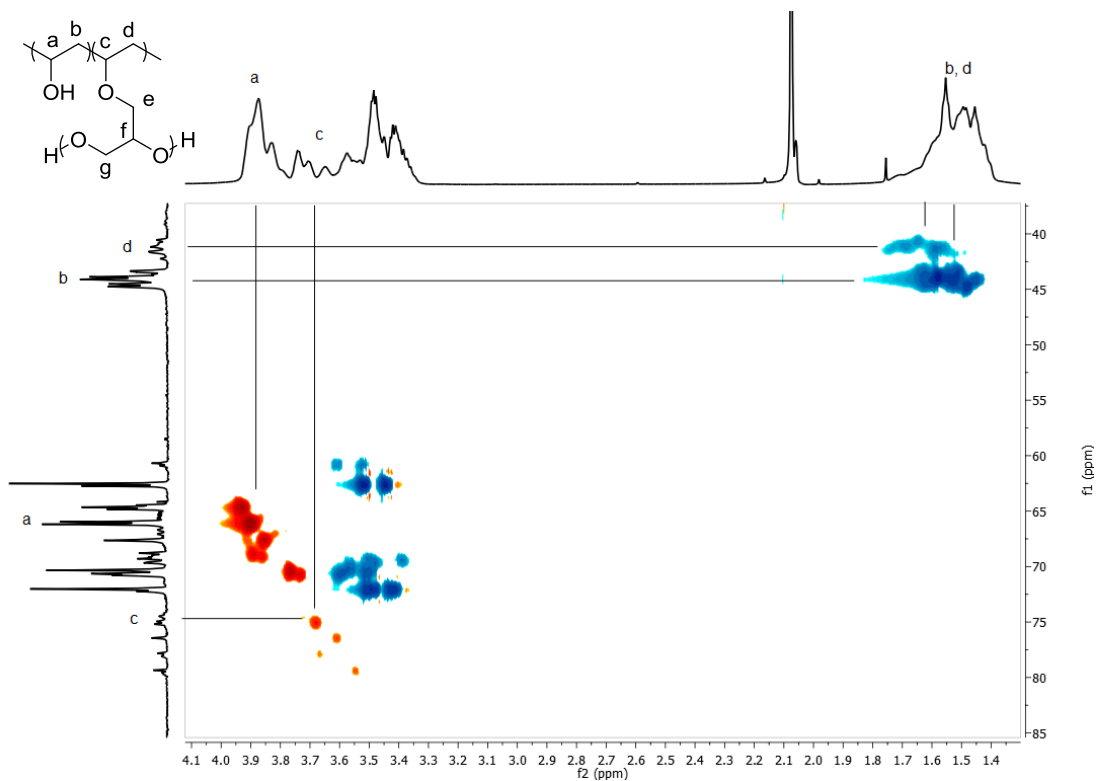


Figure 3.11: 176 MHz ^1H - ^{13}C HSQC of P[(VA)-*g*-(hPG)], showing assignments on the polymer backbone

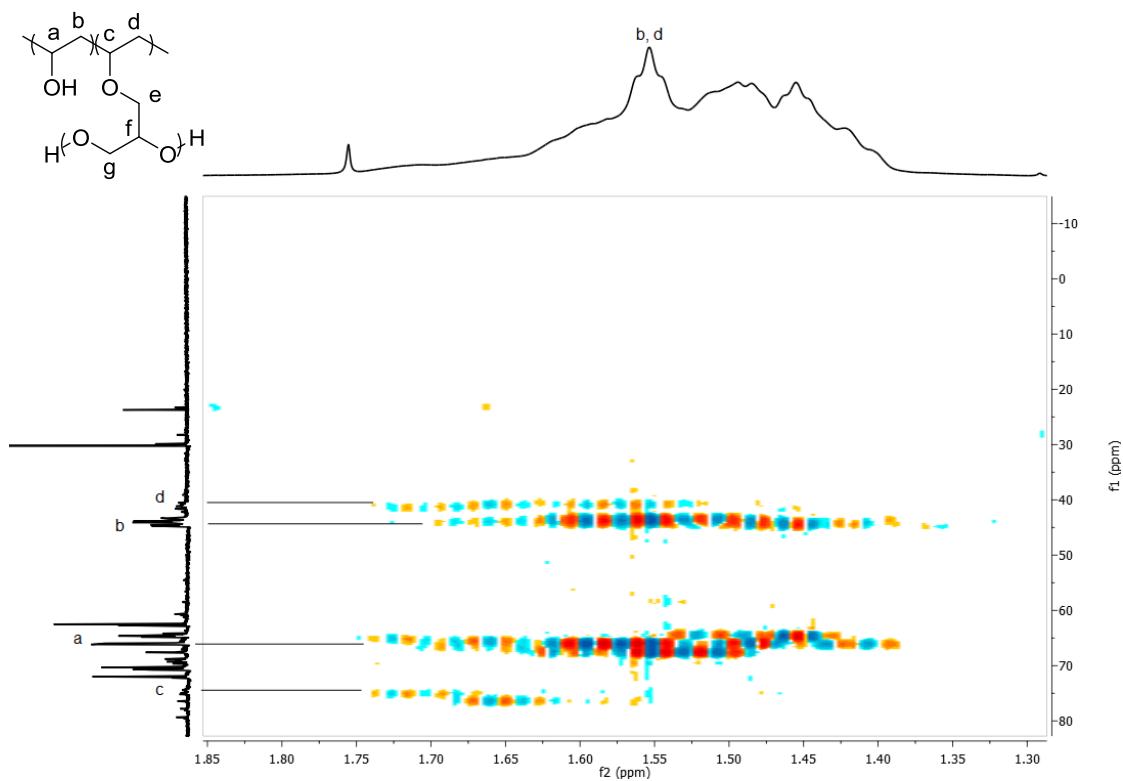


Figure 3.12: ^1H - ^{13}C HMBC of P[(VA)-*g*-(hPG)], showing assignments on the polymer backbone

Comparisons between the ^{13}C NMR spectrum of P[(VA)-*g*-(hPG)] synthesised here (Figure 3.13.a) and the spectrum supplied in the patent (Figure 3.13.b) clearly show the absence of the resonances corresponding to the carbon atoms of the poly(vinyl ether) polymer backbone at 41.3 ppm and 73.0 ppm. This indicates a physical blend of hPG and PVA is formed not P[(VA)-*g*-(hPG)].

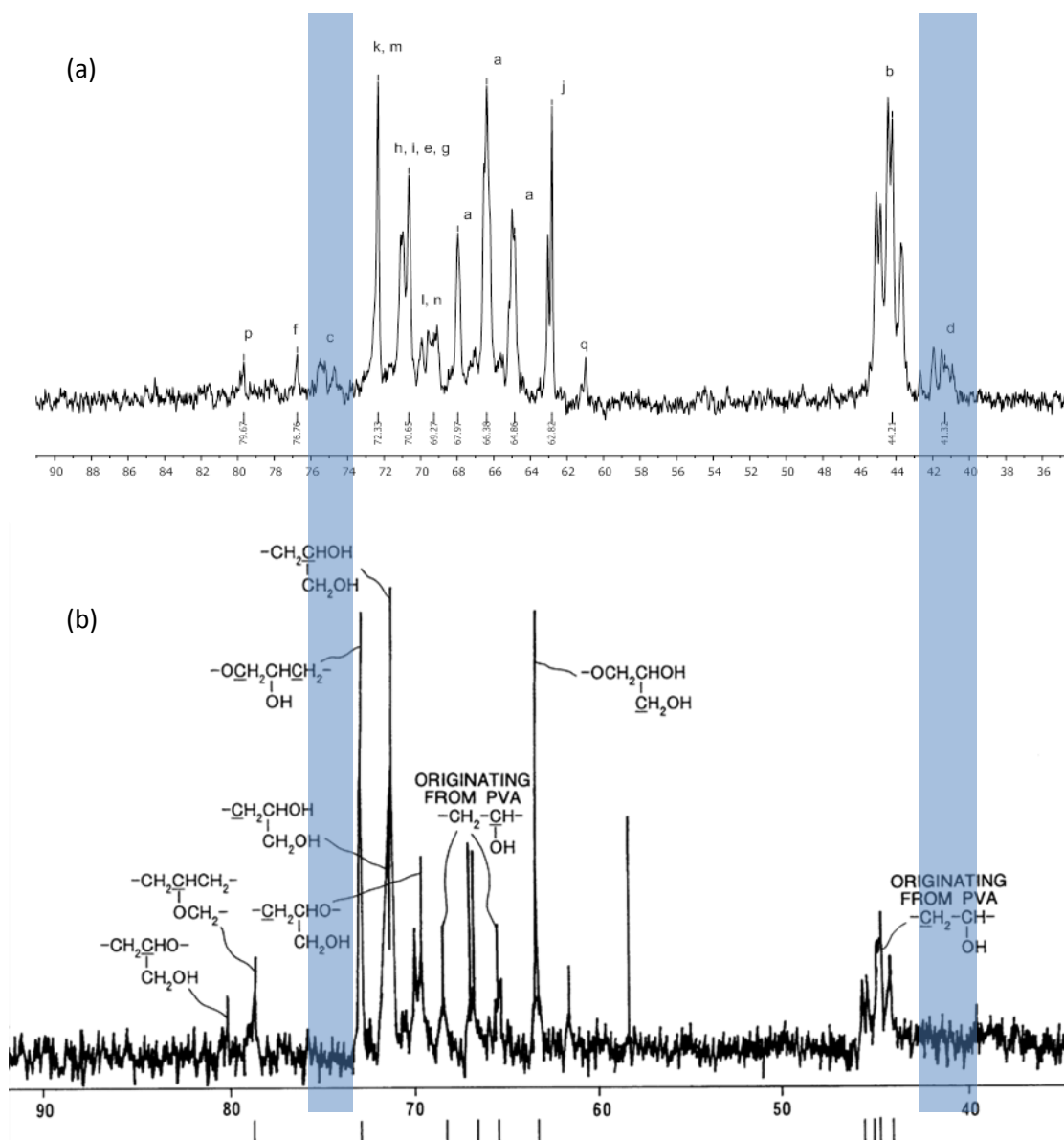


Figure 3.13: ^{13}C NMR spectra (a) P[(VA)-*g*-(hPG)] (700 MHz) and (b) “P[(VA)-*g*-(hPG)]” claimed in patent

The existence of different carbon resonances on the polymer backbone, due to the successful grafting reaction, means that the %DS of P[(VA)-*g*-(hPG)] can be determined using quantitative ^{13}C NMR spectroscopy. This is achieved by using the ratio of the integral of the resonance

assigned to methylene adjacent to the substituted alcohol and the sum of the integrals of the resonances corresponding to all the methylene carbon atoms on the polymer backbone (Equation 3.5).

$$\%DS = \frac{\int d}{\int b + \int d} \quad \text{Equation 3.5}$$

Where $\int d$ is the resonance due to the methylene carbon atom of P[(VA)-*g*-(hPG)] at 41.3ppm and $\int b$ is the resonance of the methylene carbon of PVA at 44.2 ppm.

The signal to noise ratio results in semi-quantitative data for %DB of these samples and the %DB could only be determined for samples with $x_{(hPG)} > 15\%$, using Equation 3.1.

The DP of the grafted chains can be determined using Equation 3.6. Due to limited substitution of the initiator, f_c is determined from Equation 3.6.

$$f_c = DP \times \%DS \quad \text{Equation 3.6}$$

Where DP is the degree of polymerisation of the initiator (Section 3.2.1) and %DS is the degree of substitution of P[(VA)-*g*-(hPG)].

In Chapter 2, reactions of PVA with GTMAC suffered from reproducibility due to the purity of the reagent. Therefore, the reproducibility of the reaction was investigated by synthesising three different samples of P[(VA)-*g*-(hPG)] on different days using the same reaction conditions (Table 3.1).

Table 3.1: The synthesis of P[(VA)-*g*-(hPG)] using the same reaction conditions on different dates

Entry	Date	$x_{(hPG)}$	%DS	%DB	DP	%T	%L _{1,3}	%L _{1,4}	%D
1	10/01/14	26.3%	12.8	19.6	112	45.8	4.7	42.7	6.8
2	17/03/14	23.8%	8.7	22.6	72	54.7	3.4	36.1	5.7
3	24/03/14	26.9%	10.8	17.0	92	51.9	6.1	37.5	4.5
Average		25.57%	10.77	19.73	92	50.8	4.7	38.8	5.7
		± 1.6	± 2.1	± 2.8	±20	± 4.6	± 1.4	± 3.5	± 1.2

The purification of glycidol by vacuum distillation and subsequent storage under N_2 at $0\text{ }^\circ\text{C}$ gave comparable results.

3.3.2.1. Effects of reaction conditions

As the addition of glycidol to PVA is not quantitative, the effects of the reaction conditions were investigated to attempt to maximise $x_{(\text{hPG})}$. Therefore, the effect of varying the concentration of PVA in water, and the molecular weight of the initiator were investigated (Figure 3.14).

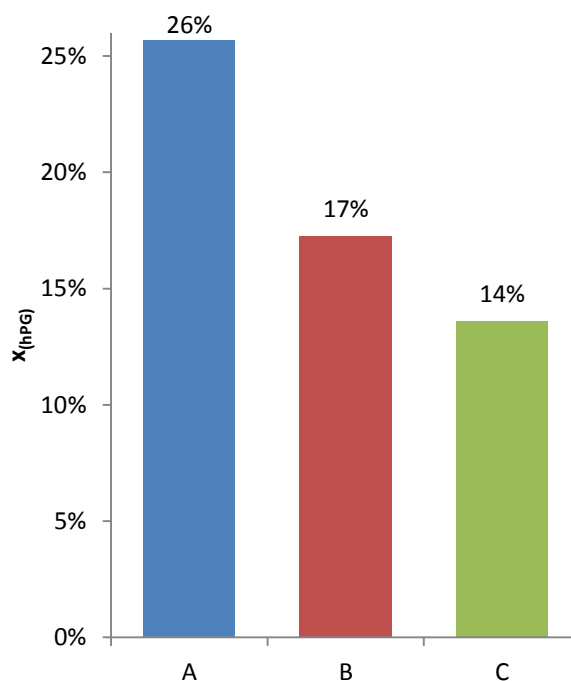


Figure 3.14: The effect of molecular weight and concentration of PVA on $x_{(\text{hPG})}$ of P[(VA)-g-(hPG)] (A) LMW PVA at 5.68 mol L^{-1} , (B) LMW PVA at 2.84 mol L^{-1} , (C) HMW PVA at 2.84 mol L^{-1} .

When the concentration of LMW PVA was halved the $x_{(\text{hPG})}$ decreased from 26% to 17% (Figure 1.A and B), as the likelihood of the side reaction to form glycerol and the rate of termination increased. The $x_{(\text{hPG})}$ for P[(VA)-g-(hPG)] synthesised from HMW PVA was lower (14%, Figure 14.C) compared to that of LMW PVA (17%, Figure 14.B) at the same concentration, due to the decreased solubility of HMW PVA in water.

Furthermore, the M_w of PVA appears to have an effect on the %DS in relation to the $x_{(\text{hPG})}$. A LMW sample with a $x_{(\text{hPG})} = 21\%$ and a HMW sample with a $x_{(\text{hPG})} = 19\%$ showed %DS of 14% and 9%, respectively. The decrease may be caused by the lower solubility of HMW PVA in

water which results in greater steric hindrance, therefore limiting the reaction with the polymer backbone.

3.3.2.1.1. Reaction time

The effect of reaction time on $x_{(\text{hPG})}$ of P[(VA)-*g*-(hPG)] was investigated using parallel reactions, Figure 3.15. The polymerisation of glycidol appears to proceed rapidly to a $x_{(\text{hPG})}$ of 23% after 4 h, and then slightly increases to 26% after 24 h. This polymerisation behaviour, despite fast initial monomer consumption, is possibly due to poor mixing in the highly viscous reaction mixture, as the minimum amount of solvent (water) is used.

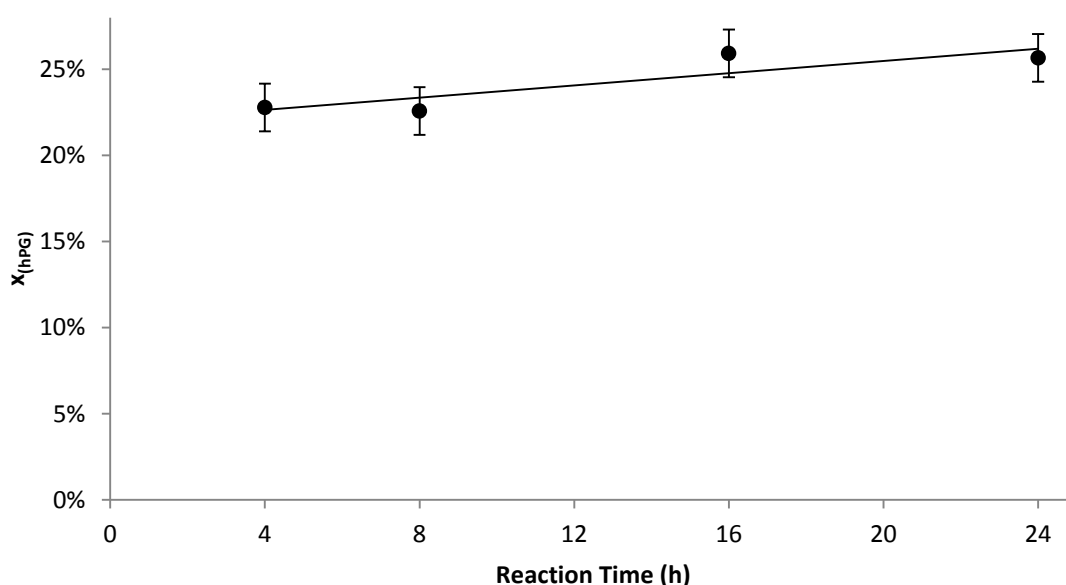


Figure 3.15: The effect of reaction time on $x_{(\text{hPG})}$ of P[(VA)-*g*-(hPG)], when mol% NaOH (5 M) = 5%, mol% glycidol = 200%, addition time = 0 h, [PVA] = 5.68 mol L⁻¹ and temperature = 50 °C.

3.3.2.1.2. Molar equivalence of NaOH

The effect of varying molar equivalence of base catalyst on $x_{(\text{hPG})}$ was investigated (Figure 3.16). Low catalyst (NaOMe) content has previously been used in the synthesis of hPG to control the \bar{M}_n .⁴ However, increased catalyst amounts could also increase the molecular weight as more initiating sites will be available. Increasing the amount of catalyst resulted in a decrease in $x_{(\text{hPG})}$; from 26% to 18% for 5% and 50% molar equivalences of NaOH, respectively. This may be caused by a slight increase in water content, as a constant concentration (5 M) of NaOH_(aq) was added diluting the reaction mixture.

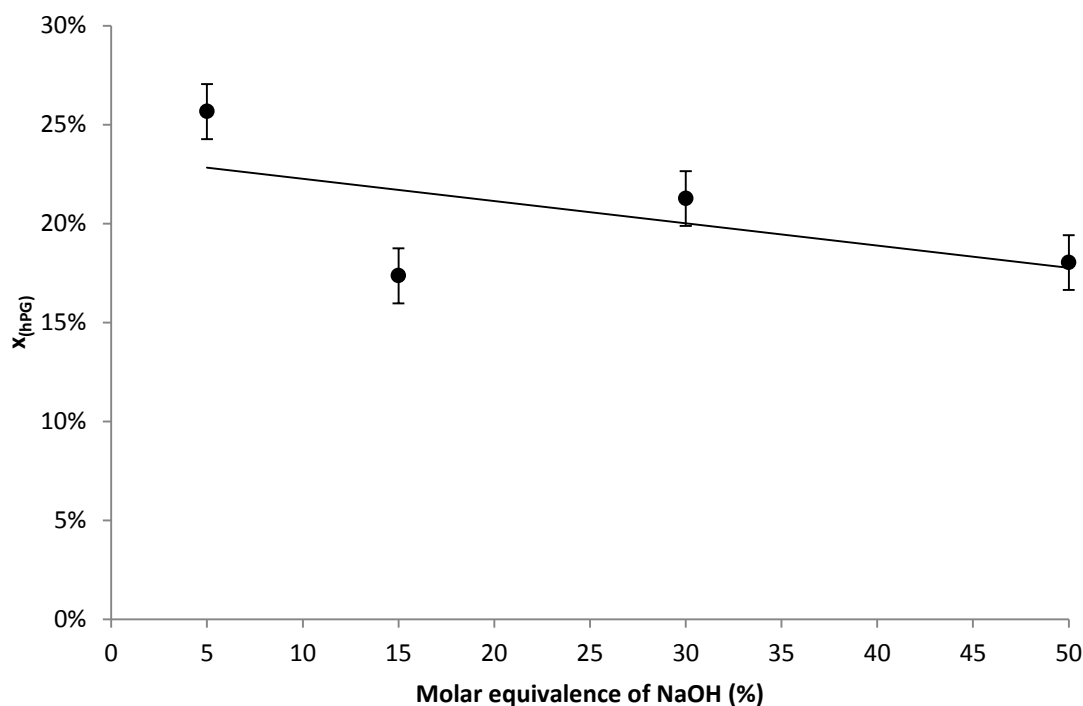


Figure 3.16: The effect of molar equivalence of 5M NaOH_(aq) on $x_{(hPG)}$ of P[(VA)-g-(hPG)], when reaction time = 24 h, mol% glycidol = 200%, addition time = 0 h, [PVA] = 5.68 mol L⁻¹ and temperature = 50 °C.

In order to further investigate the effect of catalyst on the synthesis of P[(VA)-g-(hPG)], PVA and glycidol were reacted together without the use of a catalyst. P[(VA)-g-(hPG)] was synthesised with a $x_{(hPG)}$ of 2%, showing that the use of catalyst vastly increases the $x_{(hPG)}$.

3.3.2.1.3. Molar equivalence of glycidol

An increase in molar quantity of glycidol resulted in an increase in $x_{(hPG)}$ (Figure 3.17,●) and %DS (Figure 3.17,▲); this is expected as more glycidol will be available for the reaction. However, a maximum is only observed for the $x_{(hPG)}$ at 225% molar equivalences, but not for the %DS. This suggests that the %DS depends on the amount of glycidol added, whereas the $x_{(hPG)}$ is also affected by the randomly branched structure of the grafted chains.

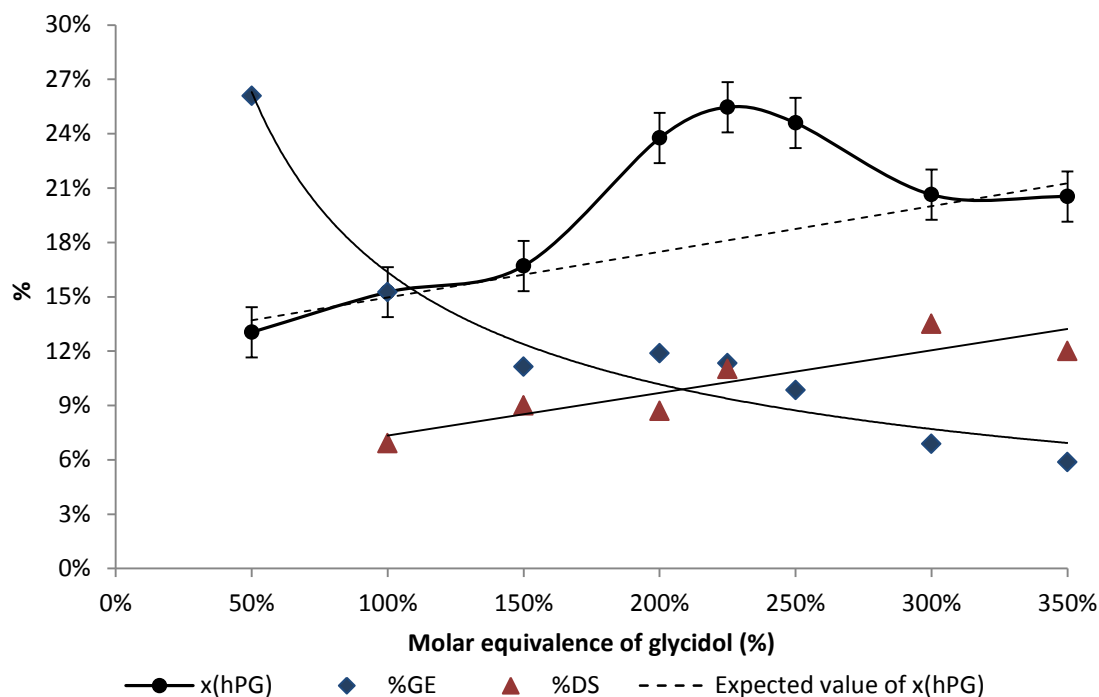


Figure 3.17: The effect on $x_{(hPG)}$ of P[(VA)-g-(hPG)] with varying amounts of glycidol when reaction time = 24 h, mol% NaOH (5 M) = 5%; addition time = 0 h and [PVA] = 5.68 mol L⁻¹.

The %GE of the reaction is determined by comparing the $x_{(hPG)}$ with the molar quantity of glycidol used (Equation 3.7); where n_{gly} is the moles of added glycidol.

$$\%GE = \frac{x_{hPG}}{n_{gly}} \quad \text{Equation 3.7}$$

It is expected that %GE will remain constant and independent of the molar equivalence of glycidol. However, the %GE decreases with increasing molar equivalents of glycidol from 26% to 6% for 50% and 350% molar equivalences, respectively (Figure 3.17, ♦). As the rates of side product formation (*e.g.* hPG and thermally ring-opened glycidol) is greater than the rate of P[(VA)-g-(hPG)] formation, the yield of the side products is anticipated to increase disproportionately compared to the yield of P[(VA)-g-(hPG)] with added molar equivalents of glycidol.

3.3.2.1.4. Reaction temperature

Increases in $x_{(hPG)}$ (Figure 3.18, ●) and %DS (Figure 3.18, ▲) were both observed with an increasing reaction temperature; may be due to the improved solubility of PVA at higher temperatures.

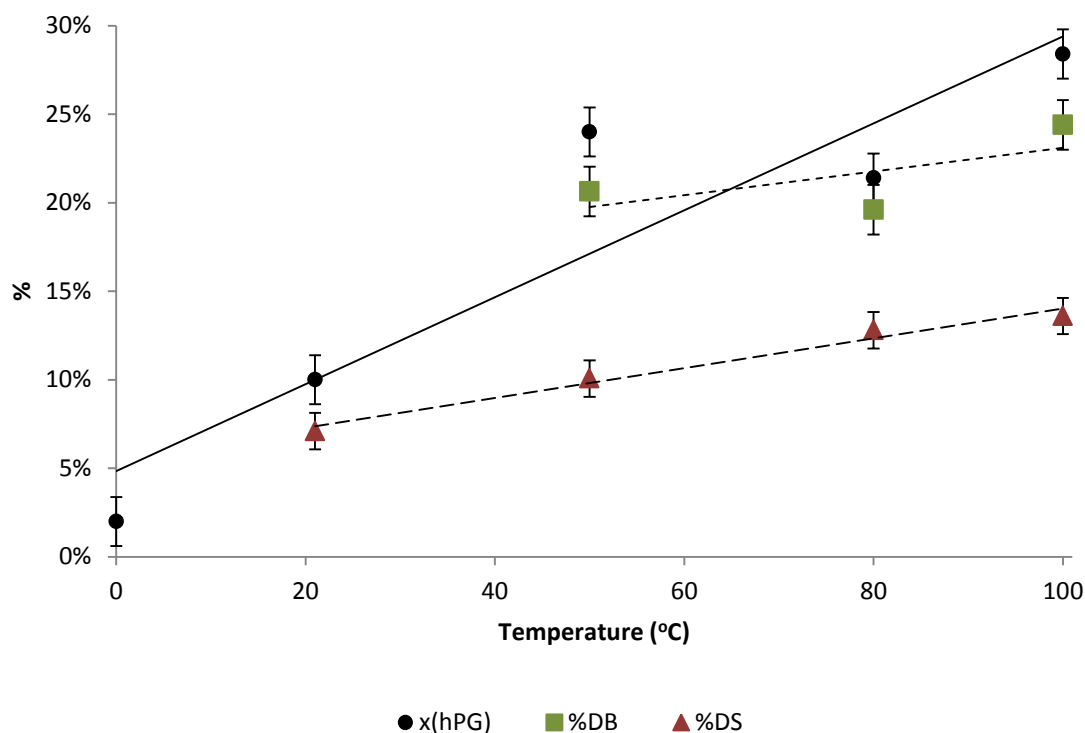


Figure 3.18: The effect of reaction temperature on structure of P[(VA)-g-(hPG)], when reaction time = 24 h, mol% NaOH (5 M) = 5%; mol% glycidol = 200%; addition time = 0 h and [PVA] = 5.68 mol L⁻¹.

No distinct increase in the %DB (Figure 3.18, ■) with temperature was observed for P[(VA)-g-(hPG)], in contrast to the work on the synthesis of hPG carried out by Harth *et al.*⁵ This could be attributed to their smaller initiator (isoamyl alcohol), different catalyst (tin[II] trifluoromethanesulfonate), or the short chain lengths of the grafted hPG chains in P[(VA)-g-(hPG)] prepared here. The data points in Figure 3.18 as well as the ratios of the structural units used to calculate %DB are shown in Table 3.2.

Table 3.2: The effect on structure of P[(VA)-*g*-(hPG)] with change in temperature when reaction time = 24 h, mol% NaOH (5 M) = 5%; mol% glycidol = 200%; addition time = 0 h and [PVA] = 5.68 mol L⁻¹.

Entry	Temperature	$x_{(\text{hPG})}$	%DS	%DB	DP	%T	%L _{1,3}	%L _{1,4}	%D
1	0	3%	N/a	N/a	N/a	N/a	N/a	N/a	N/a
2	21	14%	4	N/a	N/a	N/a	N/a	N/a	N/a
3	50	29	11	22	112	45.8	42.7	4.7	6.8
4	80	26	13	20	101	56.5	33.5	5.3	4.7
5	100	32	14	22	125	50.6	37.4	6	7.1

Furthermore, when HMW PVA was used as an initiator and the temperature was increased from 50 °C to 100 °C, an increase in $x_{(\text{hPG})}$ from 14% to 19% was observed, respectively.

3.3.2.1.5. Glycidol addition time

Reducing the rate of glycidol addition to the reaction from instant to 0.08 mL h⁻¹ resulted in an increase in $x_{(\text{hPG})}$ from 26% to 42% (Figure 3.19,●) and %DS from 10% to 20% (Figure 3.19,▲). This could be explained by a decreased concentration of glycidol in the reaction mixture retarding the homopolymerisation reaction producing hPG homopolymer.

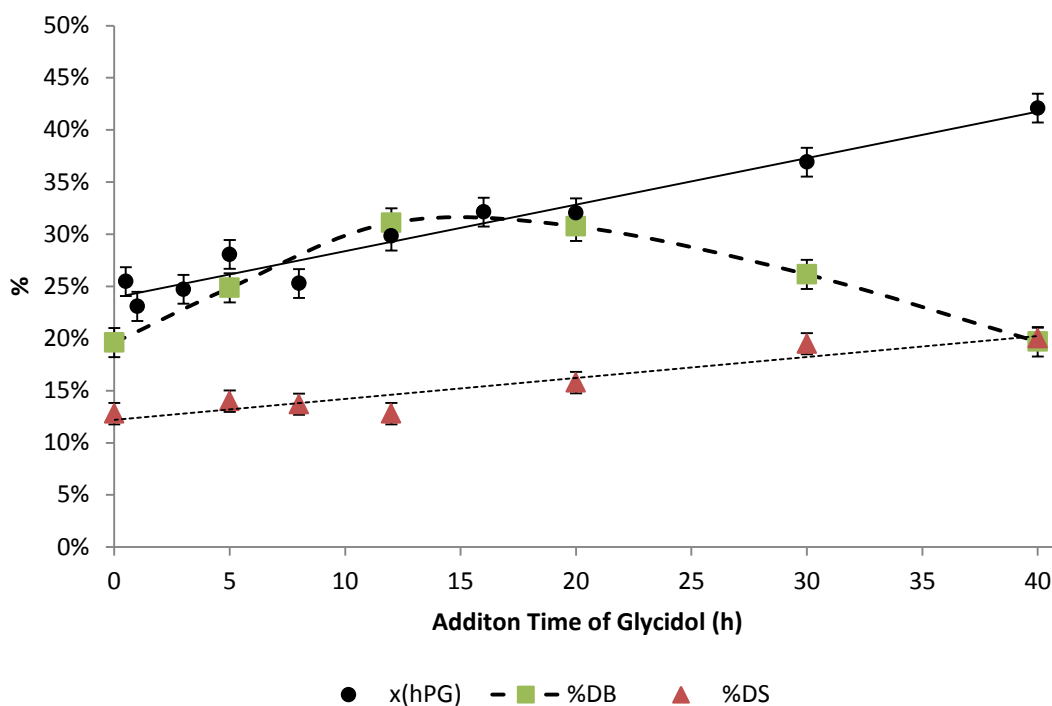


Figure 3.19: The effect of addition time of glycidol (45.5 mmol) on the structure of P[(VA)-g-(hPG)], when reaction time = 24 h, mol% NaOH (5M) = 5%; mol% glycidol = 200%; [PVA] = 5.68 mol L⁻¹ and temperature = 50 °C.

Initially, an increase in %DB (Figure 3.19, ■) was observed with an increase in $x_{(hPG)}$. However, at higher $x_{(hPG)}$ (30%), %DB begins to decrease. A hypothesis for this occurrence could be linked to the probability of forming dendritic sub units from a linear sub unit (Figure 3.1). Dendritic units (Figure 3.1.c) are more likely to form from the more reactive primary alcohol in L_{1,3} units (Figure 3.1.b), compared to the secondary alcohol in L_{1,4} units (Figure 3.1.d). When the polymer chains begin to grow, hydrogen bonding between grafted hPG and PVA backbone may result in more comparable probabilities of forming either of the two linear units, from a T unit (Figure 3.1.e). Therefore, with increased L_{1,3} units there will be more possibilities for the formation of dendritic units. When longer graft chains are formed at the later stages in the polymerisation, the formation of more favourable L_{1,4} units over L_{1,3} units is resumed. This reduces the likelihood of forming dendritic units and therefore decreasing the %DB. However, it should be taken into account that the data is only semi-quantitative due to the large signal to noise ratio in the quantitative ¹³C NMR spectrum and therefore accurate conclusions may not be drawn. The data points in Figure 3.19 as well as the ratios of the structural units used to calculate the %DB are shown in Table 3.3.

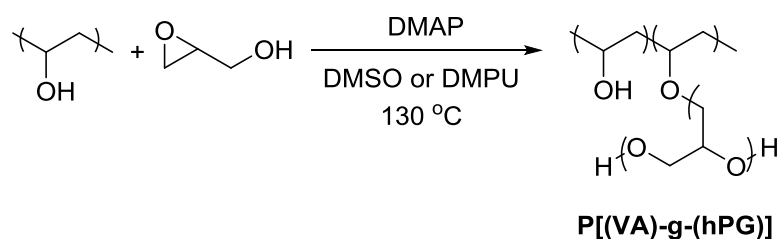
Table 3.3: The effect on structure of P[(VA)-g-(hPG)] with change in glycidol (45.5 mmol) addition time of when reaction time = 24 h, mol% NaOH (5 M) = 5%; mol% glycidol = 200%; [PVA] = 5.68 mol L⁻¹ and temperature = 50 °C.

Entry	Addition								
	rate (mL h ⁻¹)	x _(hPG)	%DS	%DB	DP	%T	%L _{1,3}	%L _{1,4}	%D
1	Instant	26	10	20	89	54.4%	5%	35.7%	5%
2	6.00	26	N/a	N/a	N/a	N/a	N/a	N/a	N/a
3	3.00	23	N/a	N/a	N/a	N/a	N/a	N/a	N/a
4	1.00	25	N/a	N/a	N/a	N/a	N/a	N/a	N/a
5	0.6	28	14	25	112	57.1	7.03	29.8	6.1
6	0.38	25	14	23	104	59.5	10.1	25.0	5.3
7	0.25	30	13	31	111	55.3	4.0	32.4	8.2
8	0.19	32	N/a	N/a	N/a	N/a	N/a	N/a	N/a
9	0.15	32	16	31	134	56.1	5.1	30.9	8.0
10	0.10	37	20	26	161	56.1	7.5	29.8	6.6
11	0.08	42	20	20	161	55.5	6.2	33.4	4.9

Frey *et al.* have used hPG as an initiator for the polymerisation of glycidol to further increase the M_w of hPG, because a maximum in M_w is reached during the initial polymerisation. This maximum is due to the percentage of alkoxide moieties decreasing during the multibranching polymerisation in comparison to hydroxyl groups.⁶ Therefore, as the $x_{(hPG)}$ of P[(VA)-g-(hPG)] synthesised from HMW PVA is lower than from LMW PVA, HMW P[(VA)-g-(hPG)] was used as a macroinitiator for the polymerisation of glycidol. The $x_{(hPG)}$ of P[(VA)-g-(hPG)] was successfully increased from 19% to 30%; the increase is less than anticipated (< 19%) and is potentially due to increased steric hindrance in the macroinitiator compared to PVA.

3.3.3. Synthesis of Poly[(vinyl alcohol)-*graft*-(hyperbranched glycerol)] in organic solvents

As water initiates the polymerisation of glycidol to form the hPG side product and which can terminate the growing hPG grafts in P[(VA)-*g*-(hPG)], the use of alternative solvents was investigated. P[(VA)-*g*-(hPG)] was synthesised from the polymerisation of glycidol using HMW PVA as an initiator in organic solvents DMSO or DMPU. DMAP was chosen as a catalyst due to limited solubility of NaOH in DMSO and DMPU, Scheme 3.5.



Scheme 3.5: The synthesis of P[(VA)-*g*-(hPG)] in organic solvents using DMAP as a catalyst

The reaction in DMSO produced a greater $x_{(\text{hPG})}$ of 45%, compared to water solvated reactions (19%). A %DS of 40% and a %DB of 19% was also determined for P[(VA)-*g*-(hPG)]. However, the graft copolymer produced had a dark brown colour when compared to the colourless graft copolymers synthesised in the water solvated reactions. To investigate the cause of the discolouration, glycidol was heated in DMSO at the reaction temperature (130 °C), upon which the solution turned black overnight. It is therefore concluded that the discolouration is the consequence of a side reaction between glycidol and DMSO. The nature of the side reaction was not investigated.

The polymerisation of glycidol using HMW PVA as an initiator in DMPU as the solvent produced P[(VA)-*g*-(hPG)] with a $x_{(\text{hPG})}$ of 17%, which is slightly lower than the $x_{(\text{hPG})}$ produced when water was used as a solvent (19%). The polymer also had a slight yellow discolouration.

3.3.4. Physical Properties of Poly[(vinyl alcohol)-*graft*-(hyperbranched glycerol)]

The thermal stability of P[(VA)-*g*-(hPG)] in comparison with PVA was monitored using TGA by measuring the onset of degradation for LMW PVA ($x_{(\text{hPG})} = 0\%$) and corresponding P[(VA)-*g*-(hPG)], Figure 3.20. The thermal stability of LMW PVA and P[(VA)-*g*-(hPG)] was found to be the same within the experimental error.

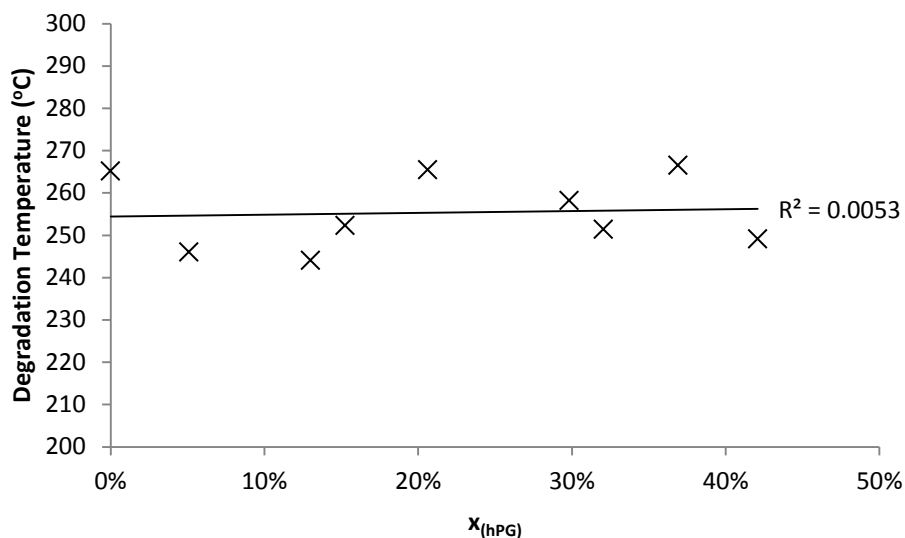


Figure 3.20: The degradation temperature of P[(VA)-g-(hPG)] with different $x_{(hPG)}$

DSC thermograms were also recorded for LMW PVA and corresponding P[(VA)-g-(hPG)], Figure 3.21. Upon heating, P[(VA)-g-(hPG)] shows a T_m at 209 °C (Figure 3.21.b) which is lower than the T_m of PVA at 219 °C (Figure 3.21.a). The T_g of P[(VA)-g-(hPG)] at 49 °C is lower than the T_g of PVA at 79 °C, due to the addition of flexible hPG side chains. However, PVA and P[(VA)-g-(hPG)] both display a crystallisation temperature (T_c) of 180 °C.

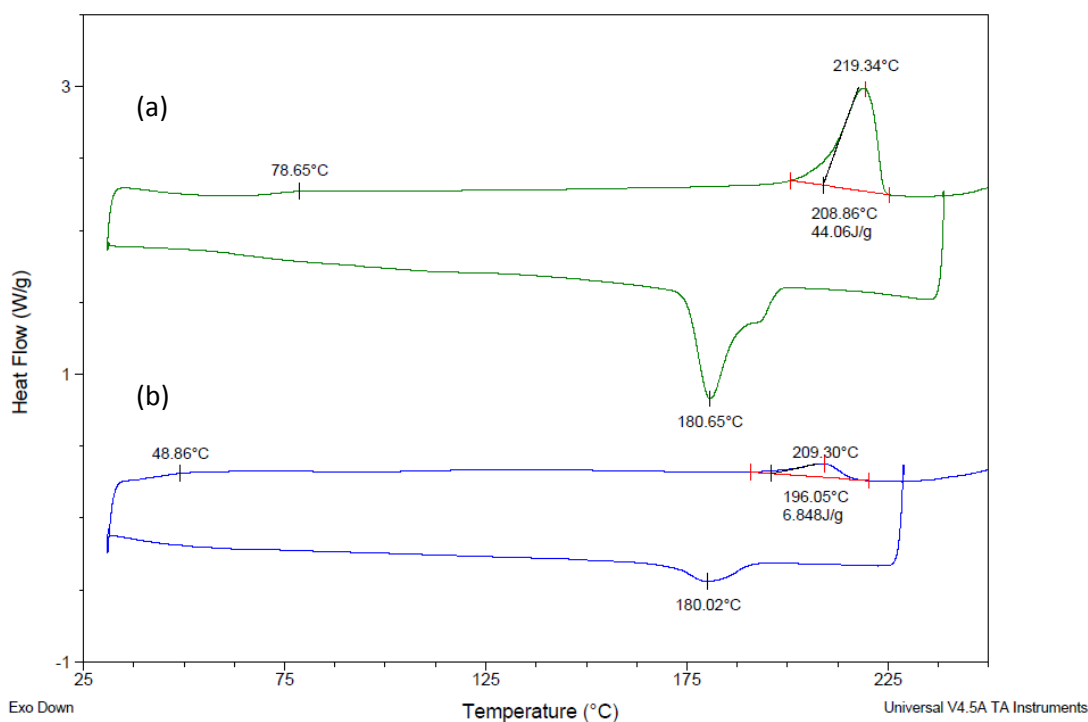


Figure 3.21: DSC thermograms showing T_m , T_g and T_c ; (a) PVA (b) P[(VA)-g-(hPG)]

The degree of crystallinity (χ_c) was determined from Equation 3.8, where ΔH_f is the measured enthalpy of fusion and ΔH_{f^*} is the enthalpy of fusion for a perfectly crystalline sample, Table 3.4. All samples were compared to perfectly crystalline PVA where $\Delta H_{f^*} = 138.6 \text{ J g}^{-1}$.

$$\chi_c = \frac{\Delta H_f}{\Delta H_{f^*}} \quad \text{Equation 3.8}$$

A large decrease in χ_c of PVA was observed with the introduction of hPG side chains. The χ_c reduced from 40.8% in LMW PVA (Table 3.4, Entry 1) to 2.5% for LMW P[(VA)-*g*-(hPG)] with a $x_{(\text{hPG})}$ of 9% (Table 3.4, Entry 2). This is due to the disruption to the packing of polymeric chains from the addition of hPG.

Table 3.4: The thermal properties of P[(VA)-*g*-(hPG)] with varying $x_{(\text{hPG})}$

Entry	$x_{(\text{hPG})}$	T_m (°C)	ΔH_f (J g ⁻¹)	χ_c
1	0%	222	56.5	40.8%
2	9%	219	3.4	2.5%
3	15%	214	4.5	3.2%
4	21%	216	8.6	6.2%
5	26%	206	0.2	0.1%
6	30%	206	13.3	9.6%
7	32%	206	2.9	2.1%
8	37%	203	0.8	0.6%
9	42%	200	3.7	2.7%

Furthermore, the T_m of P[(VA)-*g*-(hPG)] decreased with an increasing $x_{(\text{hPG})}$, this is due to the decrease in the χ_c (Figure 3.22).

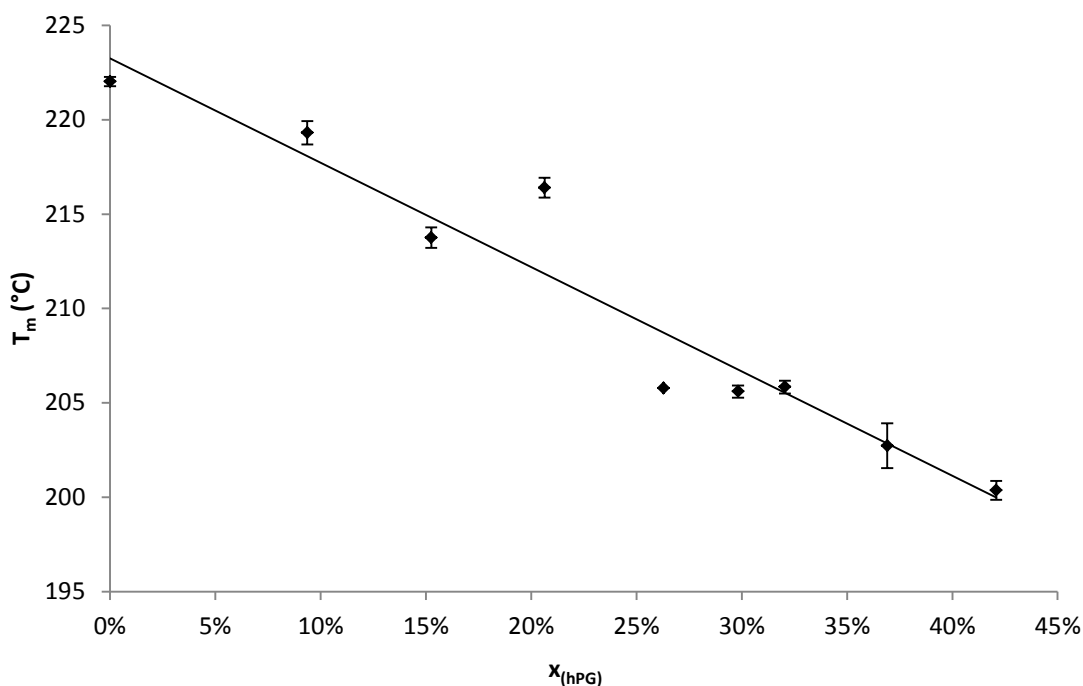


Figure 3.22: A graph showing a decrease in T_m with increasing $x_{(\text{hPG})}$ of P[(VA)-g-(hPG)].

3.3.5. Poly(vinyl alcohol)/hyperbranched polyglycerol blends

The physical properties of polymer blends were investigated to compare the influence of physically trapped hPG to that of chemically bound. Glycerol is commonly used as a plasticizer in PVA as it is known to increase the degradation temperature and the melting point by disrupting the packing of semicrystalline PVA.⁸ However, as far as we are aware no blends comprising of hPG and PVA have been prepared and studied.

Two blends which were prepared using homogeneous and heterogeneous methods (Section 2.6) were investigated. Although, PVA requires heating for complete dissolution in water, P[(VA)-g-(hPG)] readily dissolves in water at room temperature. Neither of the prepared blends displayed complete dissolution at room temperature.

The thermal properties of the two blends were monitored by DSC analysis, Table 3.5. The T_m of PVA at 222 °C (Table 3.5, Entry 1) is similar to those for both blends, at 218 °C (Table 3.5, Entry 3) and 219 °C (Table 3.5, Entry 4). A lower T_m is observed at 210 °C when hPG is chemically bound in P[(VA)-g-(hPG)] (Table 3.5, Entry 2), when compared with blends containing the same $x_{(\text{hPG})}$. Furthermore, the χ_c decreases from 40.7% in PVA to 17.4% in the homogenous blend and to 25.1% in the heterogeneous blend. Similarly, a significantly lower χ_c is observed for P[(VA)-g-(hPG)] (3.2%) than for the blends.

Table 3.5: Thermal properties of PVA, P[(VA)-*g*-(hPG)], PVA/hPG homogeneous blend and PVA/hPG heterogeneous blend

Entry	Polymer	T _m (°C)	ΔH _f (J g ⁻¹)	χ _c
1	PVA	222	56.5	40.7%
2	P[(VA)- <i>g</i> -(hPG)]	210	4.5	3.2%
3	Homogenous blend	218	24.1	17.4%
4	Heterogeneous Blend	219	34.8	25.1%

3.4. Conclusion

PVA of different molecular weights were successfully used as macroinitiators for ROP of glycidol to synthesise the novel polymer P[(VA)-*g*-(hPG)] with varying $x_{(hPG)}$. P[(VA)-*g*-(hPG)] is soluble in water at room temperature unlike PVA.

P[(VA)-*g*-(hPG)] was synthesised using water as a solvent with a maximum $x_{(hPG)}$ of 42%, %DS of 20% and %DB of 20%. The $x_{(hPG)}$ of P[(VA)-*g*-(hPG)] was increased by increasing the reaction temperature from 0 °C to 100 °C and the reaction time from 4 h to 24 h. Furthermore, an increase was observed for increasing molar equivalents of glycidol from 50% to 225% and addition time of glycidol from single addition to over a 40 h time period. The increase in $x_{(hPG)}$ could also be achieved by increasing the concentration of PVA up to 5.68 mol L⁻¹ for LMW PVA or by using P[(VA)-*g*-(hPG)] as a macroinitiator for the ROP of glycidol.

An increase in %DS coincided with an increase in the $x_{(hPG)}$. A small increase in %DB was observed with increasing temperature. A maximum in %DB was observed with increasing reagent addition time (31% after 12 h). The average %DB of P[(VA)-*g*-(hPG)] was 25%, indicating a slightly branched structure.

P[(VA)-*g*-(hPG)] was also synthesised in organic solvents with a $x_{(hPG)}$ of 45%, %DS of 19% and %DB of 19%. However, a discoloured product was recovered due to the side reaction between the solvent (DMSO) and glycidol.

The χ_c of P[(VA)-*g*-(hPG)] decreased greatly in comparison with PVA, this is due to the disruption to the packing of polymeric chains from the addition of hPG. The T_m of P[(VA)-*g*-(hPG)] decreased with increasing $x_{(hPG)}$, this is due to the decrease in the χ_c . Furthermore, the change in degradation temperature of P[(VA)-*g*-(hPG)] compared with PVA was negligible.

PVA/hPG blends were also produced; however the blends did not show the improved solubility, the change in T_m or the magnitude of change in χ_c .

3.5. References

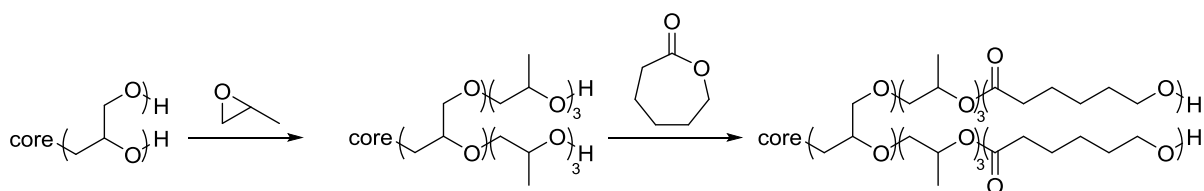
- (1) Schull, C.; Frey, H. *ACS Macro. Lett.* **2012**, *1*, 461.
- (2) Barriau, E.; García Marcos, A.; Kautz, H.; Frey, H. *Macromol. Rapid Comm.* **2005**, *26*, 862.
- (3) Hata, K. S., Takaya.; US 6,533,964 B1, **2003**.
- (4) Sunder, A.; Hanselmann, R.; Frey, H.; Mulhaupt, R. *Macromolecules* **1999**, *32*, 4240.
- (5) Spears, B. R.; Waksal, J.; McQuade, C.; Lanier, L.; Harth, E. *Chem. Commun.* **2013**, *49*, 2394.
- (6) Wilms, D.; Wurm, F.; Nieberle, J.; Bohm, P.; Kemmer-Jonas, U.; Frey, H. *Macromolecules* **2009**, *42*, 3230.
- (7) Peppas, N. A.; Merrill, E. W. *J. Appl. Polym. Sci.* **1976**, *20*, 1457.
- (8) Mohsin, M.; Hossin, A.; Haik, Y. *J. Appl. Polym. Sci.* **2011**, *122*, 3102.

Chapter 4

**Synthesis and characterisation of
cationic poly[(vinyl alcohol)-*graft*-
(hyperbranched polyglycerol)]**

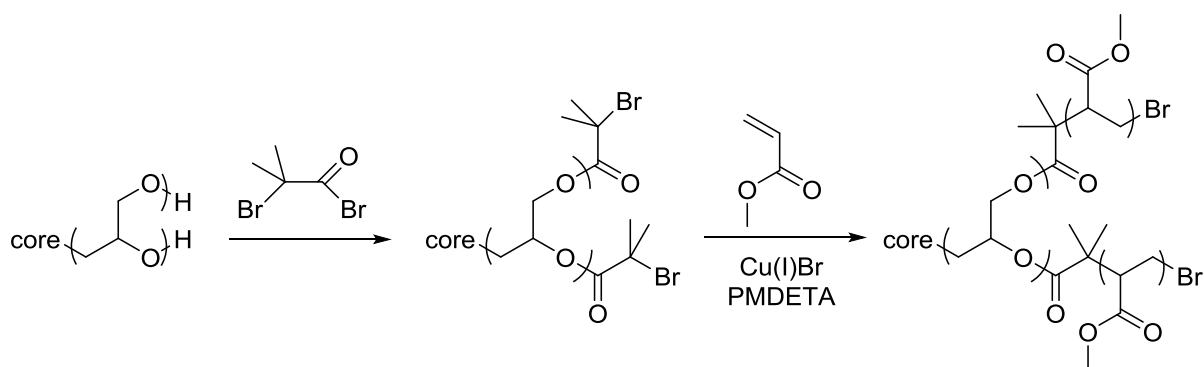
4.1. Introduction

The hydroxyl content of hyperbranched polyglycerol (hPG) has previously been exploited to produce multi-armed copolymers. The ring-opening polymerisation of ϵ -caprolactone on propoxylated hPG in bulk conditions has been carried out (Scheme 4.1).¹ hPG was quantitatively propoxylated so the polymer structure only contains secondary hydroxyl groups to ensure simultaneous propagation.² However, quantitative conversion of propoxylated hPG was not observed.¹



Scheme 4.1: Synthesis of hPG-*block*-propylene oxide-*block*-poly(ϵ -caprolactone)]

The incorporation of 2-bromoisobutyryl bromide in hPG has allowed for controlled radical polymerisation of methyl acrylate (Scheme 4.2). The conversion of the polymerisation was limited (< 35%) to prevent gelation.³ Various vinyl monomers have since been used to synthesise different copolymers, *i.e.* *tert*-butyl acrylate and hydroxethyl methacrylate.^{4,5}



Scheme 4.2: Synthesis of hPG-*graft*-poly(methyl acrylate)

Modifications with small molecules (*e.g.* sulphates and amines) to synthesise ionic polymers or amphiphilic polymers (*e.g.* fatty acids) for drug delivery have also been carried out.^{6,7}

However, no articles discussing the modification of graft copolymers containing grafted hyperbranched polyglycerol (hPG) chains have been published, as far as we are aware.

Poly[(vinyl alcohol)-*graft*-(hyperbranched polyglycerol)] (P[(VA)-*g*-(hPG)]), synthesised in Chapter 3, is predicted to have an increased hydroxyl group content compared to poly(vinyl alcohol) (PVA). Hence, higher quaternary nitrogen content (%QNC) are anticipated and cationic polymers with higher charge density could therefore be synthesised.

In this chapter, poly[(vinyl alcohol)-*ran*-(vinyl, 2-hydroxypropyl ether trimethylammonium chloride)] (P[(VA)-*r*-(VETMAC)]) and poly(vinyl betaine) (PVB) analogues will be synthesised using P[(VA)-*g*-(hPG)] as a macroinitiator instead of PVA, to synthesise Poly[(vinyl alcohol)-*ran*-(vinyl, 2-hydroxypropyl ether trimethylammonium chloride)-*graft*-(hyperbranched polyglycerol-2-hydroxypropyl ether trimethylammonium chloride)] (P[(VA)-*r*-(VETMAC)-*g*-(hPG)-PETMAC]) and Poly[(vinyl betaine)-*graft*-(hyperbranched polyglycerol betaine)] (P[(VB)-*g*-(hPG)-B]).

4.2. Experimental

4.2.1 Materials

Glycidyltrimethylammonium chloride (GTMAC) ($\geq 90\%$), chloroacetic anhydride (CAA) (95%), butanone ($\geq 99.0\%$), sodium bicarbonate (NaHCO_3) ($\geq 99.0\%$), dimethylsulfoxide (DMSO), trimethylamine (NMe_3) solution (25 %wt in methanol) and dialysis tubing (molecular weight cut-off (MWCO) = $2 \times 10^3 \text{ g mol}^{-1}$) were purchased from Sigma Aldrich and used without further purification. Acetone, methanol (MeOH), sodium hydroxide (NaOH) and hydrochloric acid (HCl) were purchased from Fisher Scientific and used without further purification. Deuterium oxide and deuterated DMSO (d_6 -DMSO) were purchased from Goss Scientific and used without purification.

4.2.2 Instrumentation

Dropwise additions were carried out using a KDS-100-CE syringe pump.

^1H nuclear magnetic resonance (NMR) spectra were recorded on a Bruker Avance-400 operating at 400 MHz or VNMRS-700 at 700 MHz. ^{13}C NMR and Inverse gated ^{13}C NMR spectra were carried out on a VNMRS-700 at 176 MHz.

Fourier transform infra-red (FT-IR) spectroscopy was performed using a Perkin Elmer 1600 Series FT-IR.

Thermogravimetric analysis (TGA) measurements were collected using a Perkin Elmer Pyris 1 TGA samples were heated in a nitrogen (N_2) atmosphere to $500 \text{ }^\circ\text{C}$ at a rate of $10 \text{ }^\circ\text{C min}^{-1}$.

Differential scanning calorimetry (DSC) measurements were carried out using a TA Instruments DSC Q1000 at rate of $10\text{ }^{\circ}\text{C min}^{-1}$ between $-50\text{ }^{\circ}\text{C}$ and $300\text{ }^{\circ}\text{C}$.

4.2.3. Synthesis of Poly[(vinyl alcohol)-*ran*-(vinyl,2-hydroxypropyl ether trimethylammonium chloride)-graft-(hyperbranched polyglycerol-2-hydroxypropyl ether trimethylammonium chloride)]

P[(VA)-*g*-(hPG)] with varying $x_{(\text{hPG})}$ (0.5 g, 11.6 - 13.9 mmol) was dissolved in water at $95\text{ }^{\circ}\text{C}$ in a two necked 50 mL round bottom flask equipped with a rubber septum, magnetic stirrer bar and a water cooled condenser. $\text{NaOH}_{(\text{aq})}$ (0.1 mL, 5% mol, 5 M, 0.6 - 0.7 mmol) was added followed by addition of GTMAC (3.2 - 4.8 mL, 200% mol, 23.2 - 27.8 mmol) at a rate of 1 mL h^{-1} . The reaction mixture was stirred at 95°C for 1 h. The reaction was quenched by neutralisation with $\text{HCl}_{(\text{aq})}$ (5 M). The mixture was purified by dialysis against water ($\text{MWCO} = 2 \times 10^3\text{ g mol}^{-1}$), the water was changed every 24 h for a duration of 72 h. The solvent was then removed leaving a transparent film. The product was then dried under reduced pressure for 16 h, to obtain P[(VA)-*r*-(VETMAC)-*g*-(hPG-PETMAC)].

Yield = 7.25 g (29%). $^1\text{H NMR}$ (D_2O): δ (ppm): 1.69 (m, 2H, CH_2), 3.22 (s, 9H, CH_3), 3.49 (m, 8H, $\text{CH}_2\text{CH}(\text{OH})\text{CH}_2\text{N}(\text{CH}_3)_3$), 3.64 (m, 5H, $\text{CH}_2\text{CH}(\text{OH})\text{CH}_2$), 4.02 (m, 1H, CH), 4.22 (s, 1H, $\text{CH}_2\text{CH}(\text{OH})\text{CH}_2$), 4.43 (s, 1H, $\text{CH}_2\text{CH}(\text{OH})\text{CH}_2$). $^{13}\text{C NMR}$ (D_2O): δ (ppm): 41.4 (CH_2), 44.2 (CH_2), 54.2 (CH_3), 60.8 ($\text{CH}_2\text{CH}(\text{OH})\text{CH}_2$), 62.8 ($\text{CH}_2\text{CH}(\text{OH})\text{CH}_2$), 64.9 (CH), 66.2 (CH), 67.9 (CH), 68.2 ($\text{CH}_2\text{CH}(\text{OH})\text{CH}_2\text{N}^+(\text{CH}_3)_3$), 69.2 ($\text{CH}_2\text{CH}(\text{OH})\text{CH}_2$), 70.6 ($\text{CH}_2\text{CH}(\text{OH})\text{CH}_2\text{N}^+(\text{CH}_3)_3$), 70.7 ($\text{CH}_2\text{CH}(\text{OH})\text{CH}_2$), 72.1 ($\text{CH}_2\text{CH}(\text{OH})\text{CH}_2$), 73.2 ($\text{CH}_2\text{CH}(\text{OH})\text{CH}_2\text{N}^+(\text{CH}_3)_3$), 74.8 (CH), 76.6 ($\text{CH}_2\text{CH}(\text{OH})\text{CH}_2$), 79.5 ($\text{CH}_2\text{CH}(\text{OH})\text{CH}_2$). FT-IR ν (cm^{-1}): 3304 ($\nu_{\text{-OH}}$), 2952 ($\nu_{\text{C-H}}$), 1110 ($\nu_{\text{-O-}}$). $T_g = 88\text{ }^{\circ}\text{C}$, $T_m = 221\text{ }^{\circ}\text{C}$.

4.2.4. Synthesis of Poly[(vinyl chloroacetate)-graft-(hyperbranched polyglycerol 2-chloroacetate)]

P[(VA)-*g*-(hPG)] (1.0 g, 27.2 mmol) was stirred in butanone (10.0 mL) at $80\text{ }^{\circ}\text{C}$ in a 50 mL round bottom flask equipped with a magnetic stirrer bar and water cooled condenser. CAA (5.4g, 31.8 mmol) was added. The reaction was stirred at $80\text{ }^{\circ}\text{C}$ for 24 h. The reaction mixture was precipitated into water and neutralised with NaHCO_3 . The precipitate was collected by filtration under vacuum. The yellow solid was purified by successive additions from acetone in MeOH to precipitate the polymer. The solid was then dried under vacuum at $40\text{ }^{\circ}\text{C}$ for 16 h, to give Poly[(vinyl chloroacetate)-*graft*-(hyperbranched polyglycerol 2-chloroacetate)] (P[(VCA)-*g*-(hPG-CA)])

Yield = 1.42 g (52%). ^1H NMR (D_2O): δ (ppm): 0.82 (m, 3H, CH_2CH_3), 1.14 (m, 3H, CH_3C), 1.34 (m, 2H, CHCH_2), 1.46 (m, 2H, CH_2CH_3), 1.63 (m, CH_2), 1.89 (m, 2H, CHCH_2), 3.59 (m, 5H, CH_2CHCH_2), 3.97 (m, 1H, CHCH_2), 4.30 (m, 4H, CH_2Cl), 4.60 (s, 1H, OH), 4.90 (m, 1H, CHCH_2), 5.07 (m, 5H, CH_2CHCH_2). ^{13}C NMR (D_2O): δ (ppm): 7.7 (CH_3CH_2), 23.5 (CH_3C), 26.3 (CH_3C), 35.1 (CH_2CH_3), 38.1 (CHCH_2), 41.1 (CH_2), 45.7 (CHCH_2), 59.6 (CHCH_2), 63.5 (CH_2Cl), 65.4 (CH_2CHCH_2), 69.2 (CH_2CHCH_2), 71.5 (CHCH_2), 72.9 (CH_2CHCH_2), 99.3 (C), 166.8 (CO). FT-IR ν (cm^{-1}): 2970 ($\nu_{\text{C-H}}$), 1736 ($\nu_{\text{C=O}}$), 1140 ($\nu_{\text{-O-}}$). $T_g = 40^\circ\text{C}$

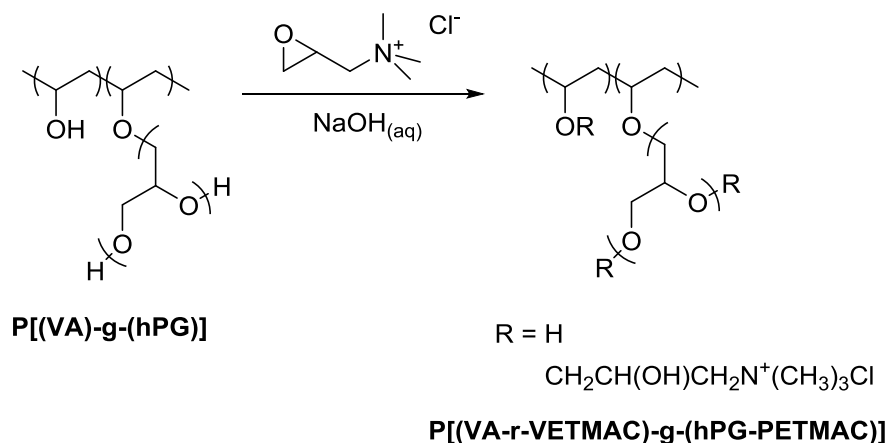
4.2.5. Synthesis of Poly[(vinyl betaine)-*graft*-(hyperbranched polyglycerol betaine)]

P[(VCA)-*g*-(hPG-CA)] (1.0 g, 10.0 mmol) was dissolved in DMSO (10.0 mL) at room temperature in a stoppered 50 mL round bottom flask. NMe_3 solution (8.5 mL, 10.8 mmol) was added and the reaction mixture was stirred for 3 h. The mixture was added dropwise into acetone producing a yellow solid. The polymer was purified by repeated precipitations from MeOH into acetone. The purified yellow solid was dried under reduced pressure at 50°C for 40 h, affording P[(VB)-*g*-(hPG-B)].

Yield = 1.12 g (78%). ^1H NMR (D_2O): δ (ppm): 0.82 (m, 3H, CH_3CH_2), 1.14 (m, 3H, CH_3C), 1.30 (m, 2H, CHCH_2), 1.46 (m, 2H, CH_2CH_3), 1.64 (m, 2H, CH_2), 1.95 (m, 2H, CHCH_2), 3.18 (m, 9H, NCH_3), 3.55 (m, 6H, CH_2CHCH_2 , CHCH_2), 3.69 (m, 2H, CH_2N), 3.86 (m, 2H, CH_2N), 4.72 (m, 1H, CHCH_2), 5.20 (m, 5H, CH_2CHCH_2). ^{13}C NMR (D_2O): δ (ppm): 8.5 (CH_3CH_2), 17.7 (CH_3C), 26.6 (CH_3CH_2), 35.2 (CH_3CH_2), 37.8 (CHCH_2), 45.8 (CHCH_2), 52.1 (CH_3N), 57.1 (CHCH_2), 62.4 (CH_2CHCH_2), 65.8 (CH_2N), 68.5 (CHCH_2), 70.8 (CH_2CHCH_2), 72.9 (CH_2CHCH_2), 99.2 (C), 165.0 (CO). FT-IR ν (cm^{-1}): 3284 ($\nu_{\text{-OH}}$), 2918 ($\nu_{\text{C-H}}$), 1620 ($\nu_{\text{C=O}}$), 1094 ($\nu_{\text{-O-}}$).

4.3. Results and Discussion

4.3.1. Synthesis Poly[(vinyl alcohol)-*ran*-(vinyl,2-hydroxypropyl ether trimethylammonium chloride)-*graft*-(hyperbranched polyglycerol-2-hydroxypropyl ether trimethylammonium chloride)]



Scheme 4.3: The synthesis of P[(VA)-*r*-(VETMAC)-*g*-(hPG-PETMAC)]

A novel high charge density cationic polymer was synthesised using GTMAC and P[(VA)-*g*-(hPG)] ,as an initiator, to synthesise Poly[(vinyl alcohol)-*ran*-(vinyl,2-hydroxypropyl ether trimethylammonium chloride)-*graft*-(hyperbranched polyglycerol-2-hydroxypropyl ether trimethylammonium chloride)] (P[(VA)-*r*-(VETMAC)-*g*-(hPG-PETMAC)]), Scheme 4.3.

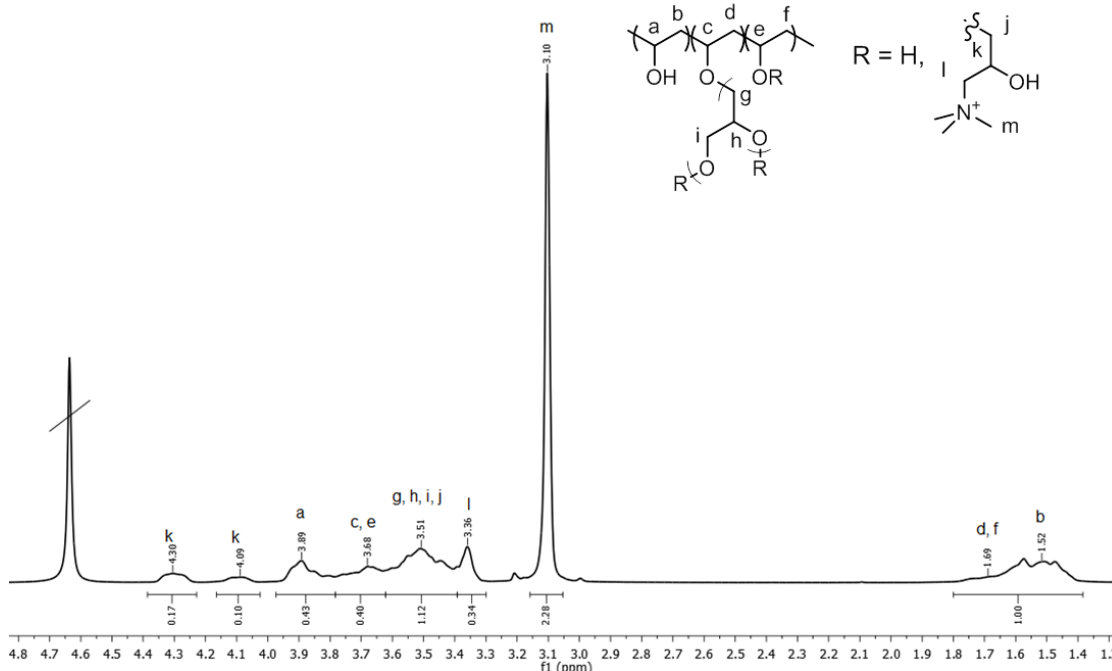


Figure 4.1: 700 MHz ^1H NMR spectrum of P[(VA)-*r*-(VETMAC)-*g*-(hPG-PETMAC)]in D_2O

The ^1H NMR spectrum (Figure 4.1) shows resonances due to the methylene protons on the PVA backbone (b) at 1.40 – 1.65 ppm and the methylene protons on the vinyl ether backbone (d, f) at 1.65 – 1.70 ppm. The resonance at 3.10 ppm is attributed to the methyl

protons associated with the quaternary nitrogen atom (m) and at 3.36 ppm to the methylene protons adjacent to the nitrogen atom (l). The broad multiplet at 3.51 ppm is assigned to all the proton environments of hPG (g, h and i) as well as the methylene protons neighbouring the ether linkage in 2-hydroxypropyl ether trimethylammonium chloride (PETMAC) (j). The resonance at 3.68 ppm relates to the methine protons along the polymeric backbone attached to the vinyl ether repeat unit (c, e). The resonance at 3.89 ppm is attributed to the methine proton attached to the hydroxyl group on the PVA backbone (a). The resonances at 4.09 ppm and 4.30 ppm are assigned to the methine proton adjacent to the hydroxyl group in PETMAC (k).

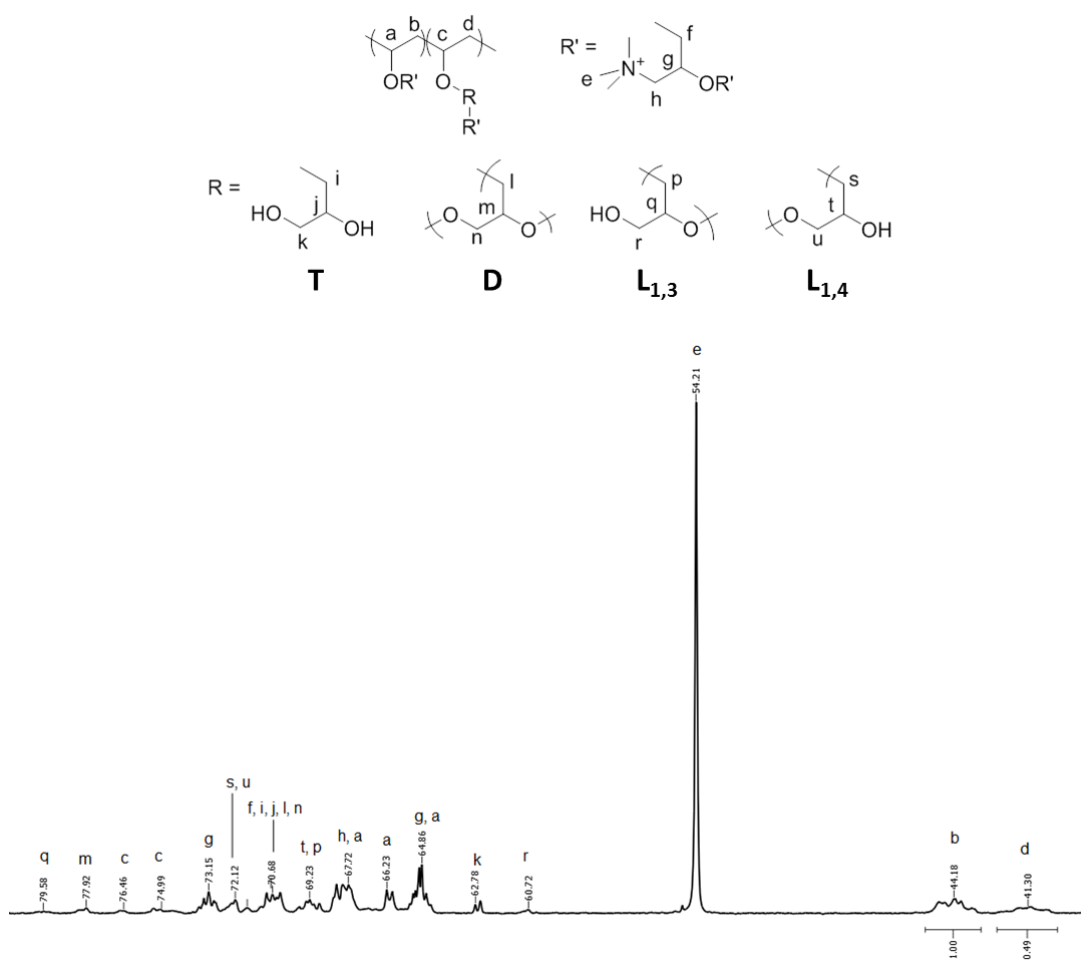


Figure 4.2: 176 MHz ¹³C NMR spectrum of P[(VA)-*r*-(VETMAC)-*g*-(hPG-PETMAC)] in D₂O

The ¹³C NMR spectrum of P[(VA)-*r*-(VETMAC)-*g*-(hPG-PETMAC)] is shown in Figure 4.2. The resonances at 41.3 ppm and 44.2 ppm are assigned to the methylene carbon atoms of the graft copolymer backbone (d) and (b), respectively. The methyl protons attached to the quaternary nitrogen (e) are attributed to the resonance at 54.2 ppm. The resonances at 60.7 ppm and 62.8 ppm are assigned to the methylene protons neighbouring the primary

hydroxyl group (r, $L_{1,3}$) and (k, T), respectively. The resonance at 64.9 ppm is assigned to the methine proton on the polymer backbone (a) and the methine proton in PETMAC (g). The resonances at 66.2 ppm and 67.7 ppm are attributed to the polymer backbone (a), 67.7 ppm to the methylene proton adjacent to the quaternary nitrogen atom (h). The resonance at 69.2 ppm is assigned to the methine proton (t, $L_{1,4}$) and a methylene proton (p, $L_{1,3}$) in the hPG chain. The resonance at 70.7 ppm is assigned to the methylene proton neighbouring the ether linkage in PETMAC (f) and all the proton environments in hPG (i, T ; j, T ; l, D ; n, D). The resonance at 72.1 ppm is attributed to the methylene protons in hPG (s, $L_{1,4}$; u, $L_{1,4}$). The resonance at 73.2 ppm is due to the methine proton in PETMAC (g). The resonances at 75.0 ppm and 76.5 ppm are assigned to the substituted methine protons on the polymer backbone (c). The resonance at 77.9 ppm is assigned to the methine proton in hPG (m, D) and 79.6 ppm is attributed to the methine proton in hPG (q, $L_{1,3}$).

The quaternary nitrogen content (%QNC) is determined from the 1H NMR spectrum (Figure 4.1) using Equation 4.1.

$$\%QNC = \frac{\int m \times \left(\frac{\int b + \int d + \int f}{n_b} \right)}{n_m} \quad \text{Equation 4.1}$$

Where $\int m$ is the integral of the resonance at 3.1 ppm, $\int b + \int d + \int f$ is the integral of the resonances at 1.52 ppm and 1.69 ppm, and n_i is the number of protons attributed to the resonance ($n = 2$, when $i = b$; $n = 9$, when $i = m$)

The degree of substitution (%DS) of the polymer can be determined from the ^{13}C NMR spectrum (Figure 4.2) using Equation 4.2.

$$\%DS = \frac{\int d}{\int b + \int d} \quad \text{Equation 4.2}$$

Where $\int d$ is the integral of the resonance at 41.3 ppm and $\int b$ is the integral of the resonance at 44.2 ppm.

The %DS of P[(VA)-*g*-(hPG)] (20%, synthesised in Chapter 3) increased to 33% when reacted with GTMAC to form P[(VA)-*r*-(VETMAC)-*g*-(hPG-PETMAC)] with a %QNC of 52%. As the %QNC is much greater than the 13% increase in %DS from the initiator, it is predicted that the majority of GTMAC (39%) attaches to the grafted hPG chains instead of the polymer backbone.

The %QNC of the polymer is then used to determine the charge density from Equation 4.3.

$$CD = 1000 \left(\frac{Q_c \times n_{OH} \times \%QNC}{m_{init} + (MW_{added} \times \%QNC)} \right) \quad \text{Equation 4.3}$$

Where CD = Charge density (meq g⁻¹), Q_c = Charge of the cationic sub unit, n_{OH} = Moles of hydroxyls on polymer (mol), %QNC = Quaternary nitrogen content, m_{init} = Initial mass of polymer (g) and MW_{added} = Molecular weight of substituent (g mol⁻¹).

Samples of P[(VA)-*g*-(hPG)] of varying x_(hPG) were reacted with GTMAC to monitor the effect on the charge density of P[(VA)-*r*-(VETMAC)-*g*-(hPG)-PETMAC]], Figure 4.3.

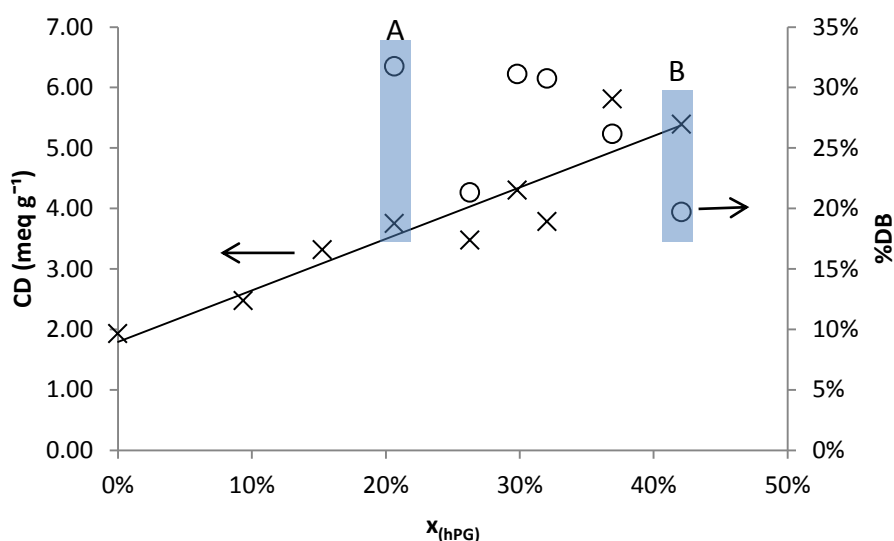


Figure 4.3: A graph showing the effect on charge density of P[(VA)-*r*-(VETMAC)-*g*-(hPG)-PETMAC]] dependent on the x_(hPG) and %DB of P[(VA)-*g*-(hPG)] initiator

An increase in the CD of P[(VA)-*r*-(VETMAC)-*g*-(hPG)-PETMAC]] is observed with increasing x_(hPG). This is due to the increase in primary alcohols in the polymer structure and as previously stated the majority of GTMAC attaches to the hPG chains. However, Figure 4.3 shows that CD increases despite decreasing degree of branching (%DB), although the hydroxyl content is expected to increase with increasing %DB. For example, the CD (3.8 meq g⁻¹) of P[(VA)-*g*-(hPG)] with a %DB of 32% (Figure 4.3, box A) is lower than the CD (5.4 meq g⁻¹) of P[(VA)-*g*-(hPG)] (Figure 4.3, box B) with a %DB of 20%. This indicates that x_(hPG) is more influential in increasing the CD of P[(VA)-*r*-(VETMAC)-*g*-(hPG)-PETMAC]] than the %DB.

The FT-IR traces of P[(VA)-*r*-(VETMAC)-*g*-(hPG)-PETMAC]], poly(vinyl alcohol-*ran*-vinyl[2-hydroxypropyl ether]trimethylammonium chloride) (P[(VA)-*r*-(VETMAC)]) and P[(VA)-*g*-(hPG)] are very similar as expected (Figure 4.4).

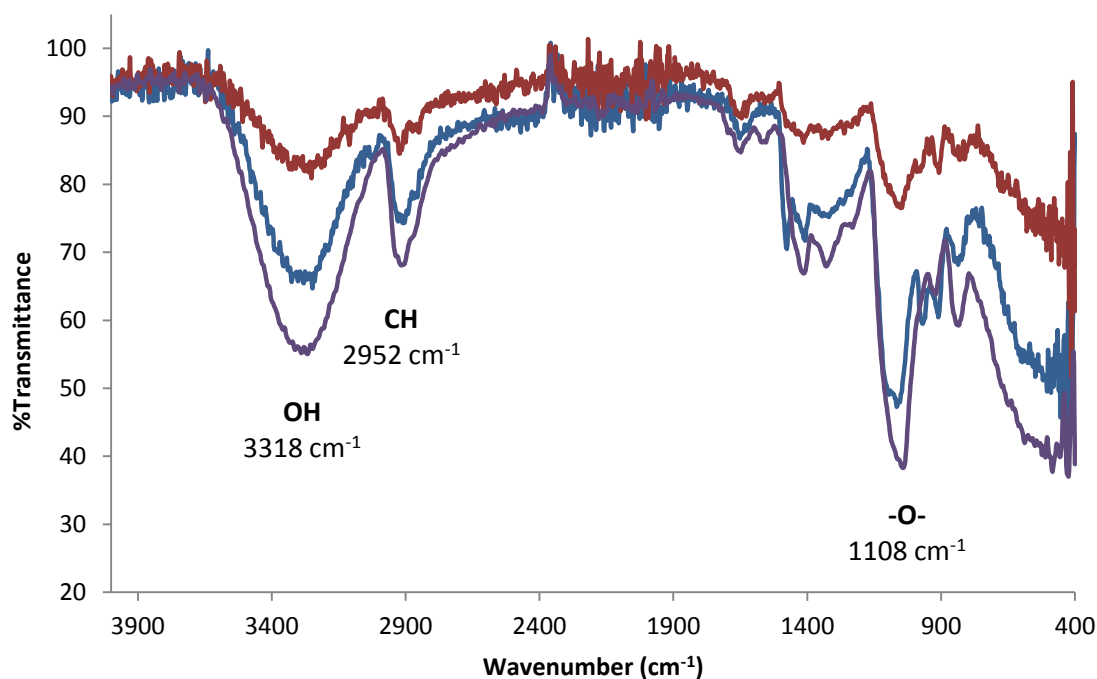
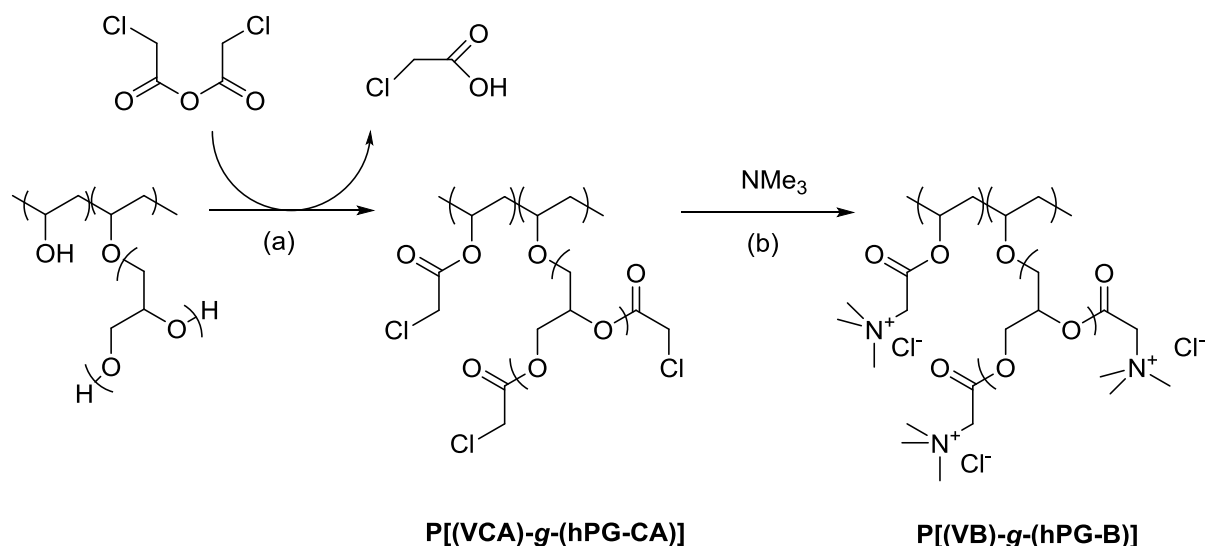


Figure 4.4: The FT-IR traces of P[(VA)-*r*-(VETMAC)-*g*-(hPG-PETMAC)] (—), P[(VA)-*r*-(VETMAC)] (—) and P[(VA)-*g*-(hPG)] (—)

All three traces show the expected OH ($\nu = 3318 \text{ cm}^{-1}$), CH ($\nu = 2952 \text{ cm}^{-1}$) and ether ($\nu = 1108 \text{ cm}^{-1}$) stretches.

4.3.2. Synthesis of Poly[(vinyl betaine)-*graft*-(hyperbranched polyglycerol betaine)]

A possible pathway to increase the CD of poly(vinyl betaine) (PVB) is to use P[(VA)-*g*-(hPG)] instead of PVA as the starting reagent, due to the predicted hydroxyl content increase in P[(VA)-*g*-(hPG)]. The synthesis of poly[(vinyl betaine)-*graft*-(hyperbranched polyglycerol betaine)] (P[(VB)-*g*-(hPG-B)]) *via* Poly[(vinyl chloroacetate)-*graft*-(hyperbranched polyglycerol 2-chloroacetate)] (P[(VCA)-*g*-(hPG-CA)]) is outlined in Scheme 4.4.



Scheme 4.4: Proposed synthesis of P[(VB)-g-(hPG-B)] via P[(VCA)-g-(hPG-CA)]

4.3.2.1. Synthesis of Poly[(vinyl chloroacetate)-*graft*-(hyperbranched polyglycerol 2-chloroacetate)]

P[(VCA)-g-(hPG-CA)] was synthesised by using P[(VA)-g-(hPG)] ($x_{(\text{hPG})} = 19\%$; %DS = 9%) as a macroinitiator and chloroacetic anhydride (CAA), Scheme 4.4.a. The initially heterogeneous reaction in butanone led to a completely homogeneous mixture as the reaction proceeded. The polymer was precipitated on addition to water highlighting the modification of the hydrophilic starting material.

P[(VCA)-g-(hPG-CA)] was successfully synthesised as shown by the ¹H NMR spectrum, Figure 4.5. Although the polymer was reprecipitated several times and dried thoroughly resonances relating to butanone are still observed in the spectrum.

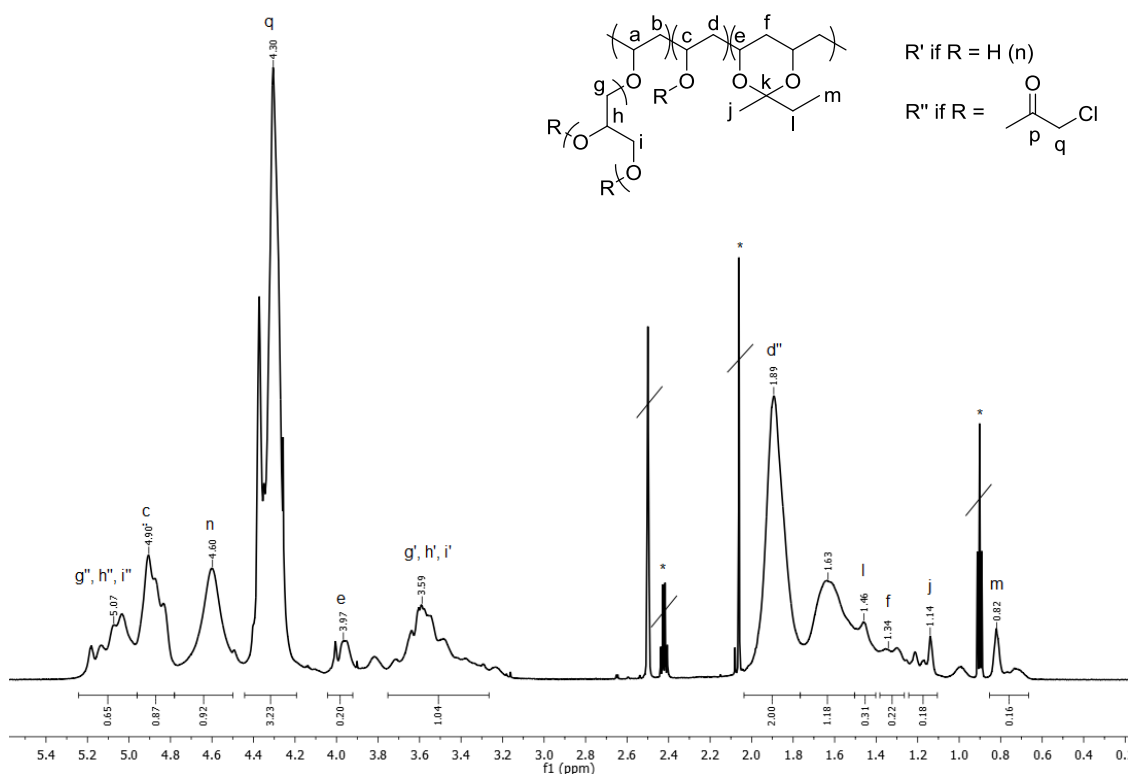


Figure 4.5: 700 MHz ^1H NMR spectrum of P[(VCA)-g-(hPG-CA)] in d_6 -DMSO

The resonances relating to PVCA are evident at 1.89 ppm corresponding to the methylene protons on the polymer backbone (d'' , *i.e.* $R = R''$), 4.90 ppm due to the methine proton on the polymer backbone (c''), and 4.30 ppm attributed to the methylene proton adjacent to the chlorine atom (q). The magnitude of the resonance at 4.30 ppm (q) is greater than the resonance at 1.89 ppm (d'') indicating that chloroacetate groups have attached to hPG chains as well as the polymer backbone; the magnitude of the two resonances would be equal if CAA had only reacted with the polymer backbone. The resonances that correspond to hPG are attributed to the large multiplet around 3.59 ppm (g' , h' , i') and 5.07 ppm (g'' , h'' , i''), depending on if the structural unit has reacted with CAA. This is supported by the ^1H - ^1H correlation spectroscopy (COSY) spectrum (Figure 4.6), as coupling exists between both hPG proton environments and the methylene proton adjacent to the chlorine atom in PVCA (q).

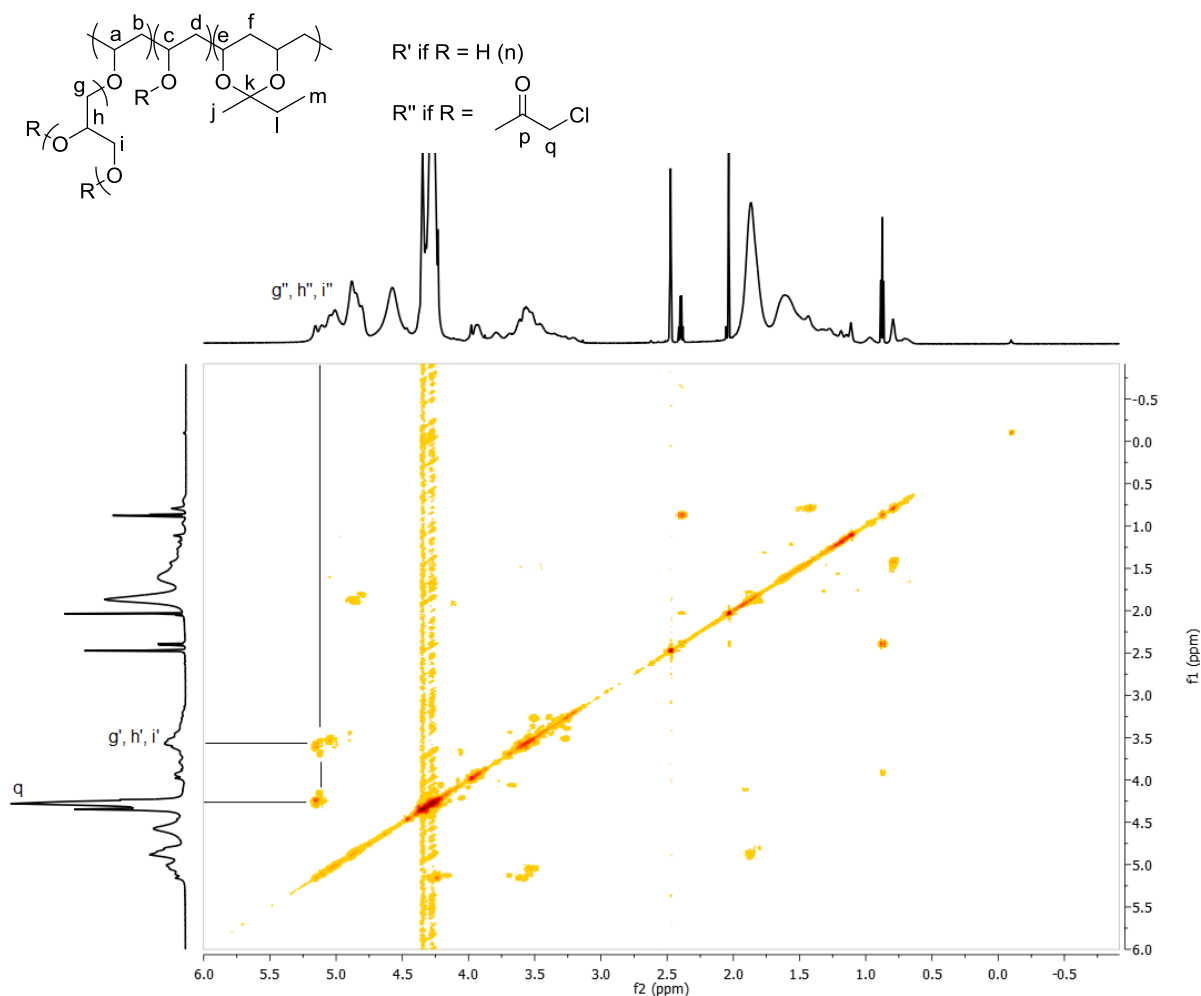


Figure 4.6: 700 MHz ^1H - ^1H COSY NMR of $P[(VCA)-g-(hPG-CA)]$ in d_6 -DMSO

The resonance at 4.60 ppm, Figure 4.5, is due to unreacted hydroxyl groups (n). This is highlighted by adding D_2O to the NMR sample to exploit deuterium/hydrogen exchange of labile protons (*e.g.* hydroxyl protons). The shift upfield of the resonance at 4.60 ppm to 3.95 ppm in Figure 4.7, indicates that hydroxyl groups are still present and quantitative conversion was not achieved.

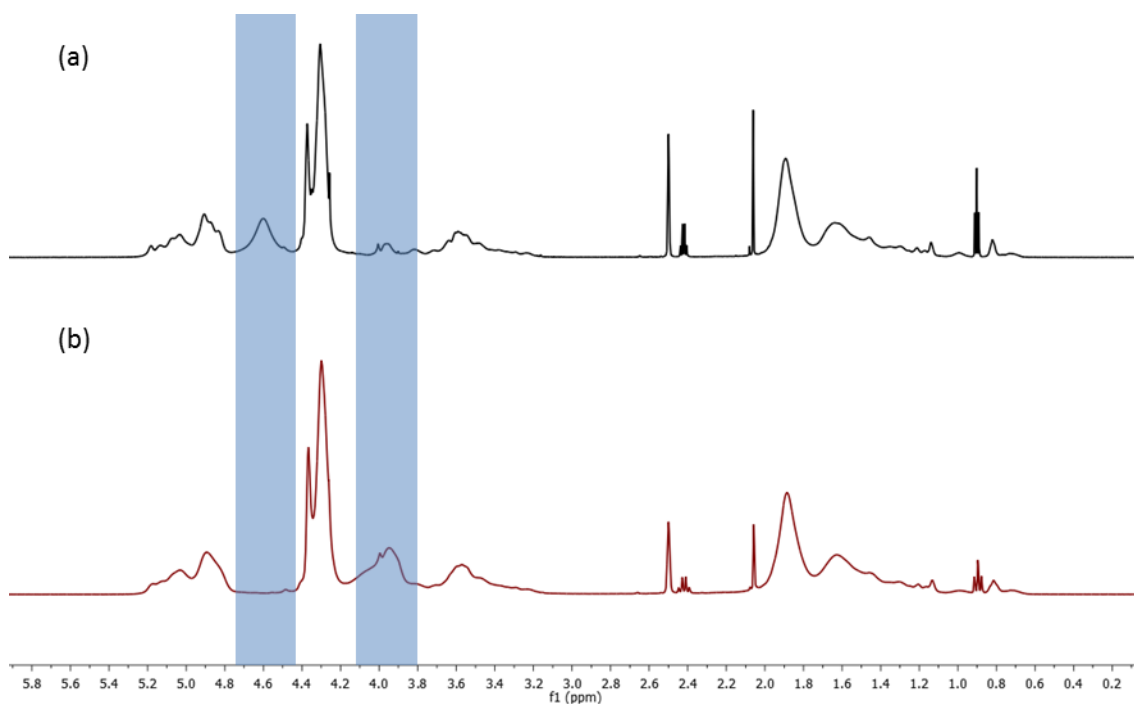


Figure 4.7: 400 MHz ^1H NMR spectrum (a) P[(VCA)-g-(hPG-CA)] in d_6 -DMSO (b) P[(VCA)-g-(hPG-CA)] in d_6 -DMSO and D_2O

The reaction between butanone and PVA to form poly(2-butyral) (PVByl) that was discussed in Chapter 2 (Section 2.3.3) for the synthesis of PVCA is still evident in Figure 4.5. The resonances at 0.82 ppm are assigned to the methyl proton (m); 1.46 ppm to the methylene protons (l), and 1.14 ppm to methyl proton neighbouring the quaternary carbon (j).

P[(VCA)-g-(hPG-CA)] was further characterised using ^{13}C NMR spectroscopy, Figure 4.8.

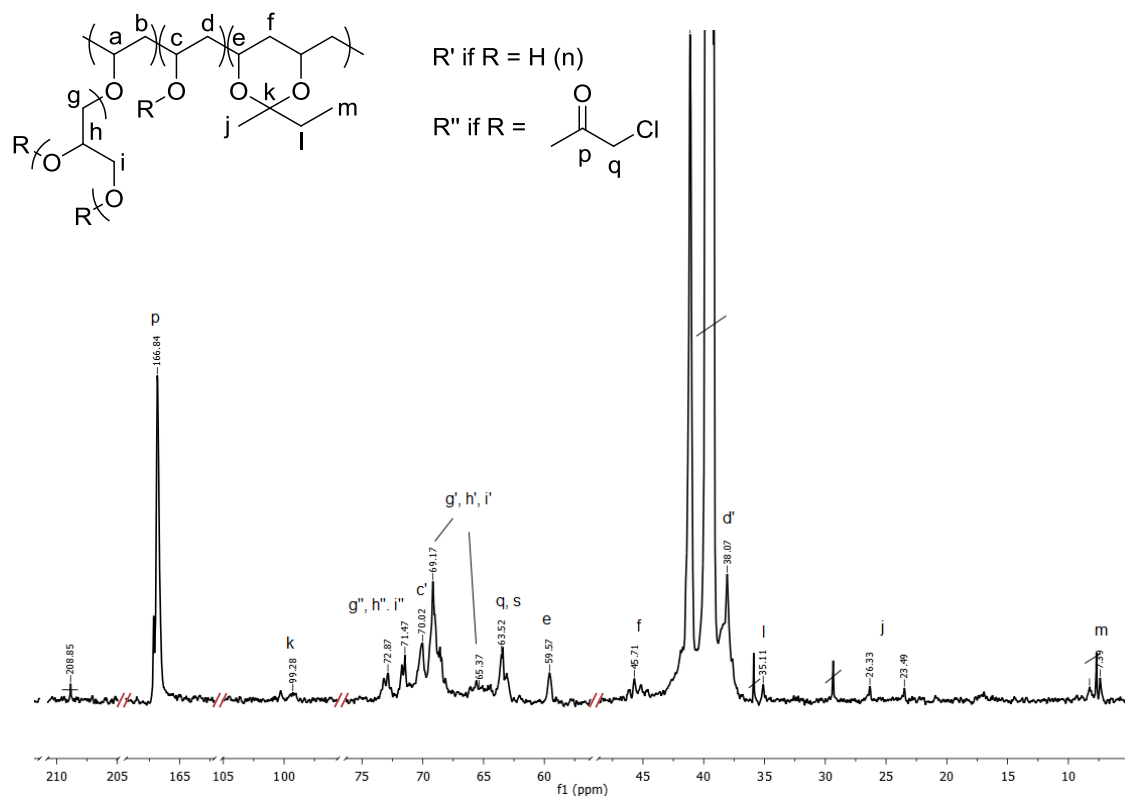


Figure 4.8: 176 MHz ^{13}C NMR spectrum of partially cross-linked P[(VCA)-g-(hPG-CA)] in d_6 -DMSO

The resonances corresponding to PVCA are at 38.1 ppm for the methylene carbon atom on the polymer backbone (d), 70.0 ppm for the methine proton on the polymer backbone (c), 63.5 ppm for the carbon atom adjacent to the chlorine atom (q) and 166.8 ppm for the carbonyl carbon (p). The resonances relating to unreacted hPG are seen at 65.4 ppm and 69.2 ppm (g' , h' , i'). The resonance at 72.9 ppm is assigned to hPG that has reacted with CAA (g'' , h'' , i''). The resonances corresponding to poly(vinyl, 2-butryal) (PVByl) are assigned at 7.7 ppm for the methyl carbon atom (m), 35.1 ppm for the methylene carbon (l), 26.3 ppm and 23.5 ppm for the methyl carbon atom (j) and 99.3 ppm for the quaternary carbon atom (k). The lack of correlation of the resonance at 99.3 ppm to any proton environment in the $^1\text{H} - ^{13}\text{C}$ heteronuclear single quantum coherence (HSQC) spectrum (Figure 4.9) provides further evidence of the formation of quaternary carbon atoms in PVByl.

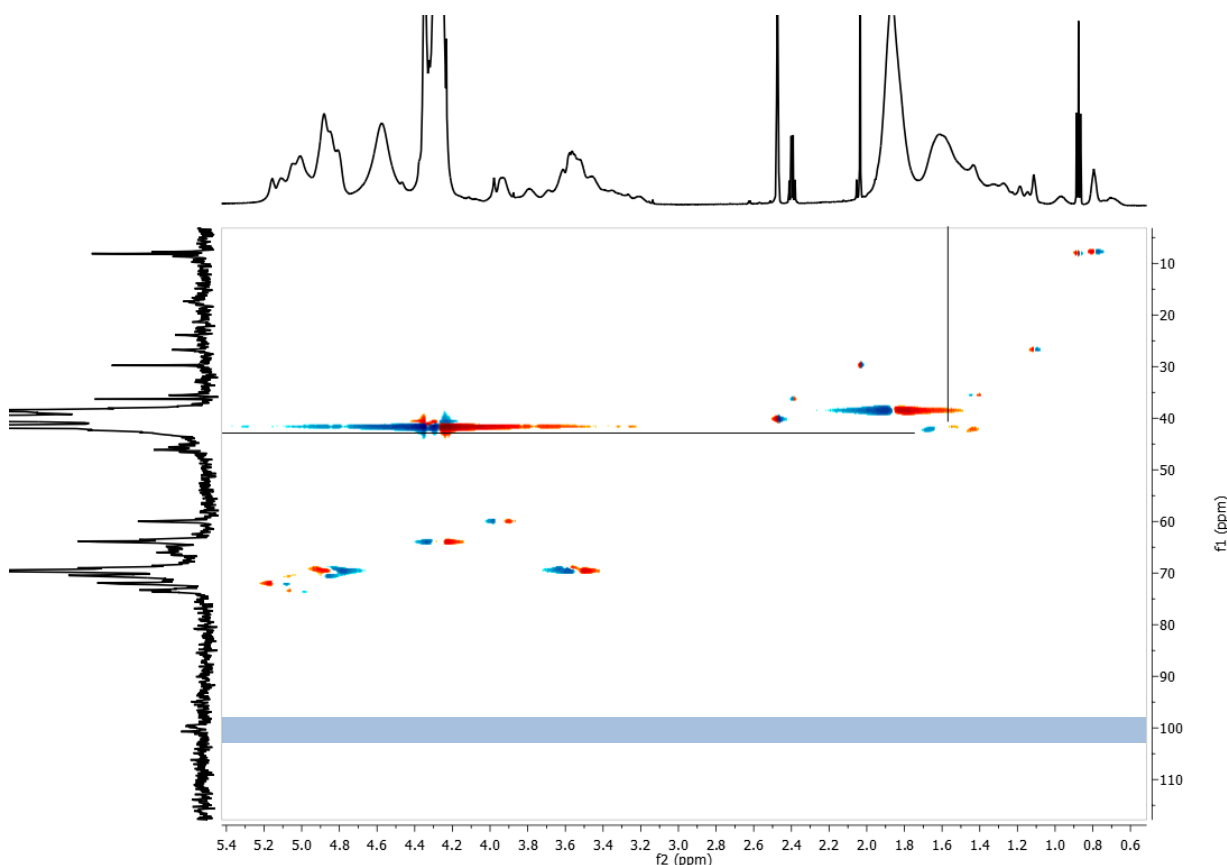


Figure 4.9: ^1H - ^{13}C HSQC spectrum showing the quaternary carbon in PVByl in d_6 -DMSO

Unfortunately, the resonance at 1.63 ppm in the ^1H NMR spectrum (Figure 4.5) and 41.4 ppm in the ^{13}C NMR spectrum (Figure 4.8) cannot be accurately assigned. Furthermore, the two resonances correspond to each other in the ^1H - ^{13}C HSQC (Figure 4.9), but no coupling is detected in the other 2D NMR spectra (*e.g.* ^1H - ^1H COSY spectrum, ^1H - ^{13}C heteronuclear multiple-bond correlation (HMBC) spectrum). As a consequence the composition of the product cannot be accurately determined.

The thermal transitions of P[(VCA)-*g*-(hPG-CA)] were measured by DSC analysis and the glass transition temperature (T_g) is observed at a lower temperature (41 °C) compared to PVCA (47.18 °C). This reduction in T_g is similar to what is observed for P[(VA)-*g*-(hPG)] compared to PVA.

4.3.2.2. Quarternisation of poly[(vinyl chloroacetate)-*graft*-(hyperbranched polyglycerol 2-chloroacetate)]

P[(VCA)-*g*-(hPG-CA)] was quarternised in a homogenous solution with NMe_3 producing P[(VB)-*g*-(hPG-B)] (Scheme 4.b). The ^1H NMR spectrum of P[(VB)-*g*-(hPG-B)] is shown in Figure 4.10.

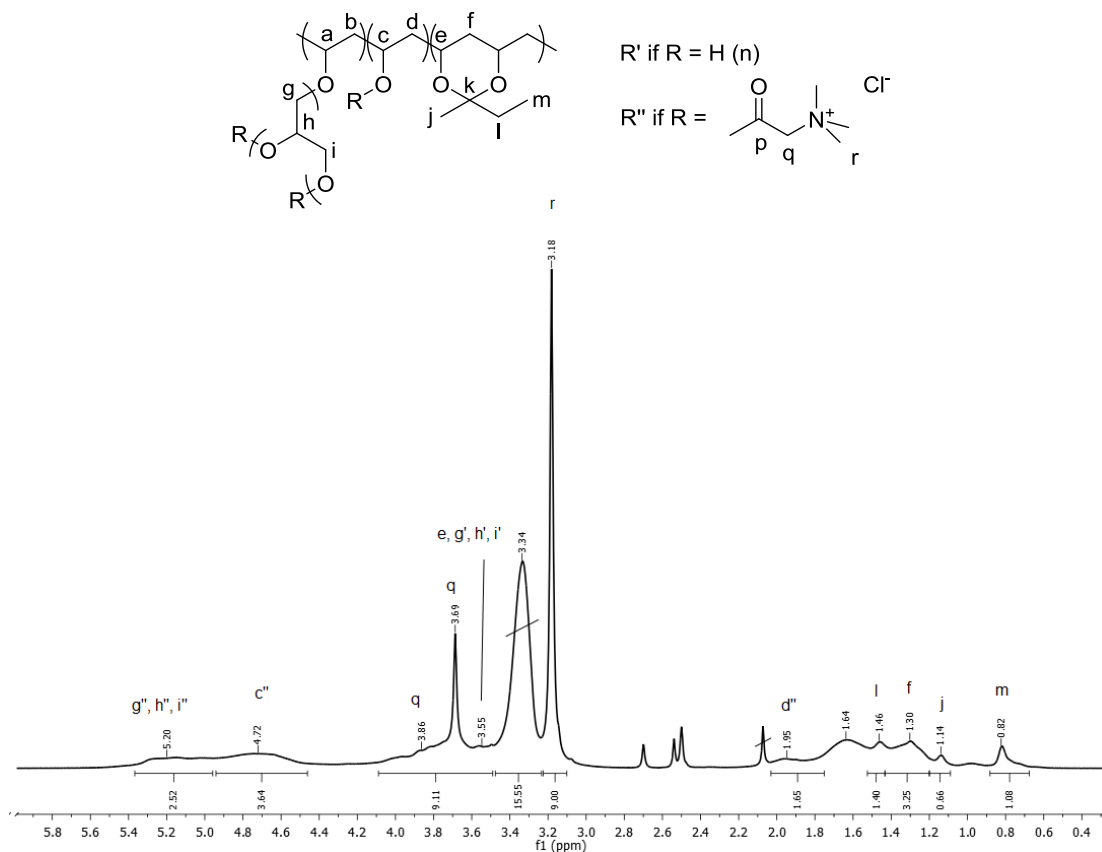


Figure 4.10: 700MHz ^1H NMR spectrum of P[(VB)-g-(hPG-B)] in d_6 -DMSO

The resonances corresponding to the PVB repeat unit are assigned to 1.95 ppm for the methylene protons on the polymer backbone (d''), 3.69 ppm and 3.86 ppm for the methylene protons neighbouring the quaternary nitrogen atom (q), 4.72 ppm for the methine proton on the polymer backbone (c''), and 3.18 ppm for the methyl protons next to the quaternary nitrogen atom (r). The resonances at 3.55 ppm and 5.20 ppm are attributed to the hPG side chains (g' , h' , i' and g'' , h'' , i'').

The resonances attributed to PVByl are assigned to 0.82 ppm for the methyl proton (m), 1.14 ppm for the methyl protons (j) neighbouring the quaternary carbon atom, the methylene protons (l) and 1.30 ppm for the methylene protons on the polymer backbone (f).

The resonance at 3.34 ppm is attributed to the reagent NMe_3 physically trapped in the cross-linked material, despite numerous reprecipitations and drying the material above the volatile material's boiling point under reduced pressure.

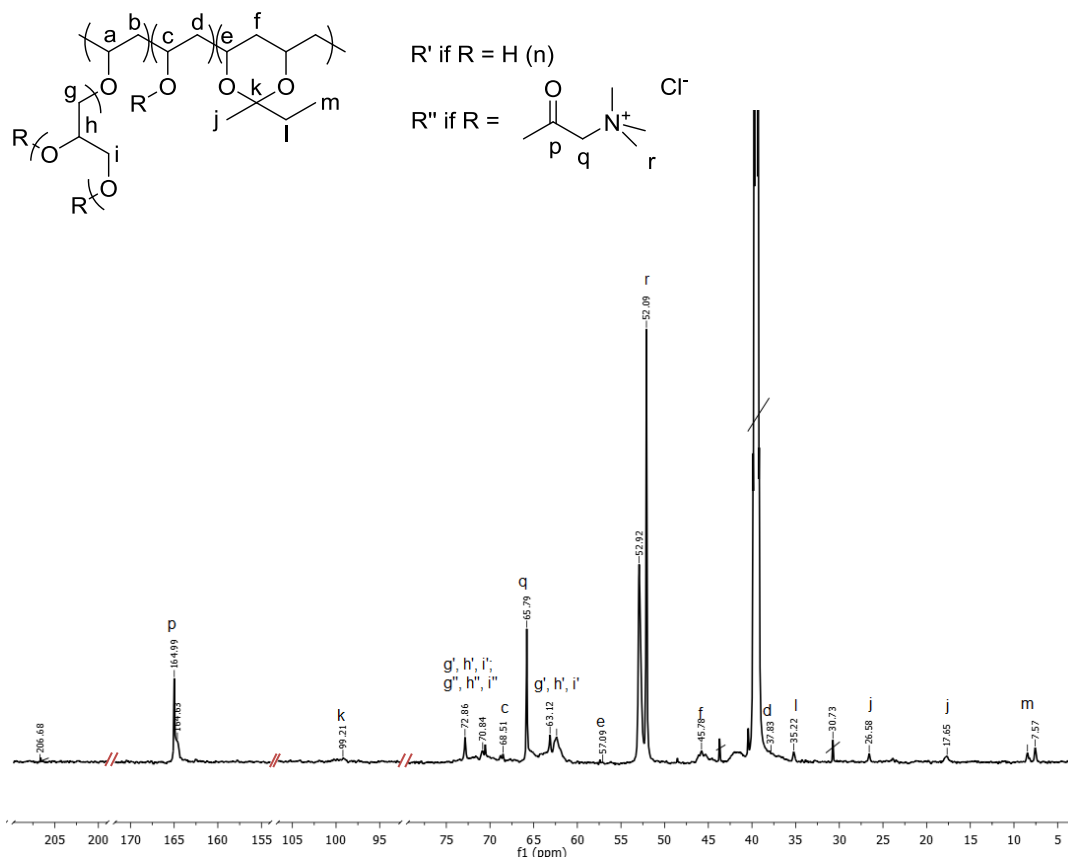


Figure 4.11: 176 MHz ^{13}C NMR spectrum of P[(VB)-g-(hPG-B)] in d_6 -DMSO

P[(VB)-g-(hPG-B)] was further characterised by ^{13}C NMR spectroscopy, Figure 4.11. The PVB repeat unit is attributed to the resonances at 37.8 ppm for the methylene carbon atom polymer backbone (d), 52.1 ppm for the methyl carbon atoms attached to the quaternary nitrogen atom (r), 65.8 ppm for the methylene proton neighbouring the nitrogen atom (q), 68.51 ppm for the methine proton on the polymer backbone (c) and 165.0 ppm to the carbonyl carbon (p). The resonance at 63.1 ppm is attributed to the unreacted hPG carbon atoms (g' , h' , i'). The resonances at 70.8 ppm and 72.9 ppm are attributed to all the hPG carbon atoms (g , h , i). The resonances corresponding to PVByl are at 8.5 ppm for the methyl carbon atom (m), 35.2 ppm for the methylene proton (l), 26.6 ppm for the methyl carbon atom (j) neighbouring the quaternary carbon atom, 45.8 ppm corresponds to the methylene carbon atom on the polymer back (f), 57.1 ppm is attributed to the methine carbon atom on the polymer backbone and 99.2 ppm to the quaternary carbon atom (k).

DSC analysis showed no T_g for P[(VB)-g-(hPG-B)] using DSC, similarly to PVB. The FT-IR traces, of the P[(VA)-g-(hPG)], P[(VCA)-g-(hPG-CA)] and P[(VB)-g-(hPG-B)] are shown in Figure 4.12. The appearance of the carbonyl stretching frequencies at 1736 cm^{-1} for P[(VCA)-g-(hPG-CA)] (red trace), which shifts to 1620 cm^{-1} in P[(VB)-g-(hPG-B)] (blue trace).

Despite the appearance of a resonance corresponding to an alcohol group in the ^1H NMR spectrum of P[(VCA)-*g*-(hPG-CA)] (Figure 4.5), no hydroxyl group stretching frequency is observed. This may be due to the magnitude of the recorded stretching bands, as the hydroxyl group stretching band can be observed for P[(VB)-*g*-(hPG-B)] (blue trace).

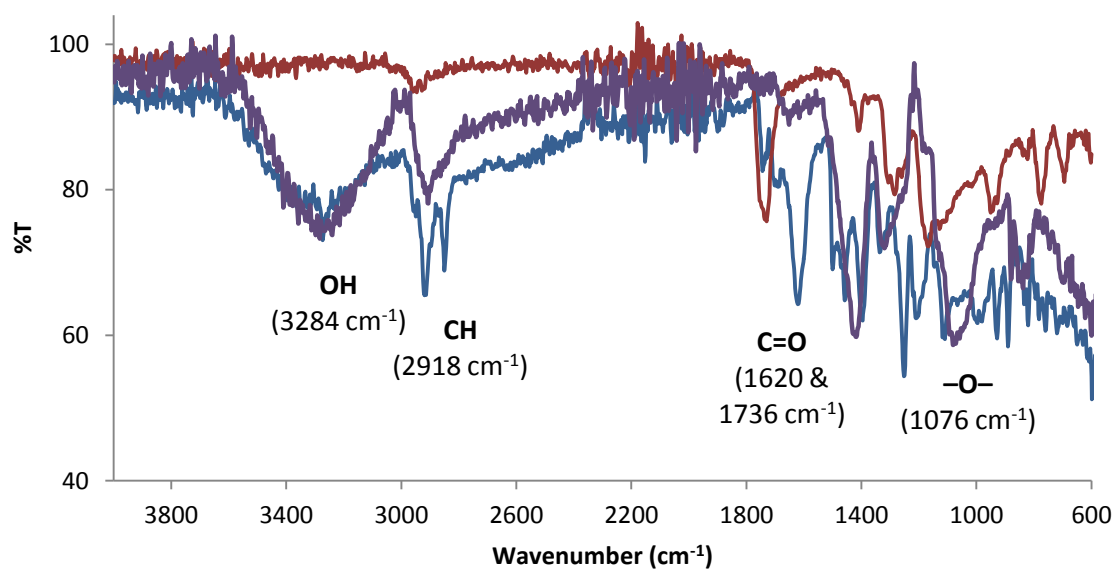


Figure 4.12: FT-IR spectrum of P[(VB)-*g*-(hPG-B)] (—), P[(VCA)-*g*-(hPG-CA)] (—) and P[(VA)-*g*-(hPG)] (—).

4.4. Conclusion

P[(VA)-*r*-(VETMAC)-*g*-(hPG-PETMAC)] was successfully synthesised and CDs greater than P[(VA)-*r*-(VETMAC)] (2.5 meq g^{-1}) were observed because of the increased availability of reactive alcohol moieties. The CD of these polymers increased with $x_{(\text{hPG})}$ of the P[(VA)-*g*-(hPG)] initiator. The highest CD achieved was 5.81 meq g^{-1} .

P[(VCA)-*g*-(hPG-CA)] was successfully synthesised, however, complete conversion of the hydroxyl groups was not achieved. P[(VCA)-*g*-(hPG-CA)] was quarternised to synthesise P[(VB)-*g*-(hPG-B)]. The composition of the polymer could not be determined, due to the coalesced resonances in the NMR spectra.

4.5. References

- (1) Burgath, A.; Sunder, A.; Neuner, I.; Mulhaupt, R.; Frey, H. *Macromol. Chem. Physic* **2000**, *201*, 792.
- (2) Sunder, A.; Mulhaupt, R.; Frey, H. *Macromolecules* **2000**, *33*, 309.
- (3) Maier, S.; Sunder, A.; Frey, H.; Mulhaupt, R. *Macromol. Rapid Commun.* **2000**, *21*, 226.
- (4) Shen, Z.; Chen, Y.; Barriau, E.; Frey, H. *Macromol. Chem. Physic* **2006**, *207*, 57.
- (5) Wilms, D.; Stiriba, S. E.; Frey, H. *Accounts Chem. Res.* **2010**, *43*, 129.
- (6) Khandare, J.; Mohr, A.; Calderon, M.; Welker, P.; Licha, K.; Haag, R. *Biomaterials* **2010**, *31*, 4268.
- (7) Sunder, A.; Krämer, M.; Hanselmann, R.; Mülhaupt, R.; Frey, H. *Angew. Chem. Int. Ed.* **1999**, *38*, 3552.

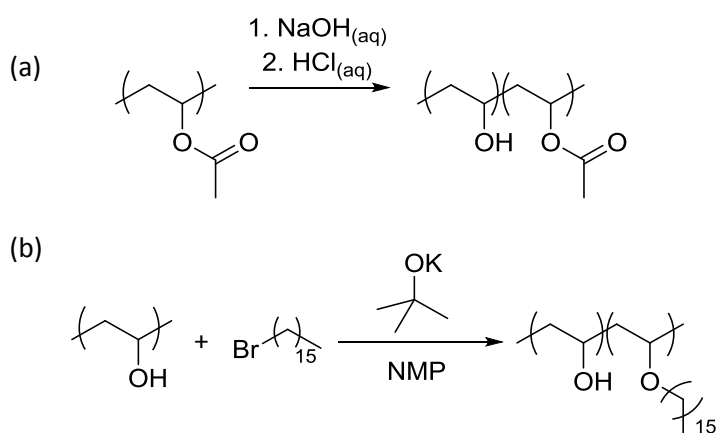
Chapter 5

Synthesis and Characterisation of hydrophobic poly(vinyl alcohol) derivatives

5.1. Introduction

The formation of polymer/surfactant complexes (*i.e.* coacervates) is integral to the conditioning effect by helping deposit silicone emulsion onto hair. Cationic polymers have previously been shown to have superior deposition when the second critical aggregation concentration is slightly greater than the surfactant concentration present in the shampoo formulation.¹ Although poly(vinyl alcohol) (PVA) has been reported to form coacervates, the deposition could be potentially increased by increasing the hydrophobicity of the polymer.²

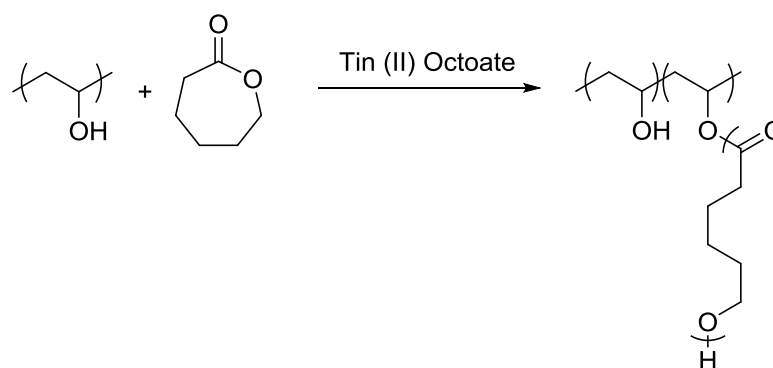
The hydrophobicity of PVA can be controlled during the hydrolysis of hydrophobic poly(vinyl acetate) (PVAc) (Scheme 5.1.a). Therefore, the hydrophobicity can be controlled by partial hydrolysis of PVAc to obtain poly[(vinyl acetate)-*ran*-(vinyl alcohol)] with different compositions.³ An alternative method to produce hydrophobic PVA is the addition of long alkyl chains. Marstokk *et al.*⁴ grafted on hexadecyl alkyl chains using a potassium *tert*-butoxide catalysed Williamson etherification reaction in N-methyl-2-pyrrolidone (NMP) to form a water insoluble material, Scheme 5.1.b. It should be noted that all the determined degrees of substitution were lower than the theoretical values.



Scheme 5.1: Synthesis of hydrophobic PVA (a) poly[(vinyl acetate)-*ran*-(vinyl alcohol)] (b) poly[(vinyl alcohol)-*ran*-(vinyl ether hexadecane)]

PVA has also been used as a macroinitiator for the ring opening polymerisation of ϵ -caprolactone using a tin (II) octoate catalyst, to synthesise a hydrophobic graft copolymer Scheme 5.2.⁵ The graft copolymers contained mole fractions between 11-97% of poly(ϵ -caprolactone), and a degree of substitution of PVA repeat units between 4 - 54%. The

water insoluble graft copolymers became soluble in organic solvents, *e.g.* toluene, a common solvent for poly(ϵ -caprolactone) but a non-solvent for PVA.



Scheme 5.2: Synthesis of poly[(vinyl alcohol)-graft-(ϵ -caprolactone)]

In this chapter a novel method to increase the hydrophobicity of PVA will be discussed. Epoxyoctane and PVA are reacted together to synthesise the novel hydrophobic poly[(vinyl alcohol)-*ran*-(vinyl, 2-hydroxy octyl ether)] (P[(VA)-*r*-(VOE)]). The reaction with epoxyoctane will also be carried out with the previously synthesised PVA derivatives discussed in Chapters 2, 3 and 4 to synthesise poly[(vinyl alcohol)-*ran*-(vinyl, 2-hydroxy octyl ether)-*ran*-(vinyl,2-hydroxypropyl ether trimethylammonium chloride)] (P[(VA)-*r*-(VOE)-*r*-(VETMAC)]), Poly[(vinyl alcohol)-*ran*-(vinyl, 2-hydroxy octyl ether)-*graft*-(hyperbranched polyglycerol-2-hydroxyoctyl ether)] (P[(VA)-*r*-(VOE)-*g*-(hPG-OE)]), and Poly[(vinyl, 2-hydroxy octyl ether)-*ran*-(vinyl, 2-hydroxypropyl ether trimethylammonium chloride)-*ran*-(vinyl alcohol)-*graft*-(hyperbranched polyglycerol)-(2-hydroxypropyl ether trimethylammonium chloride)/(2-hydroxy octyl ether)] (P[(VOE)-*r*-(VETMAC)-*r*-(VA)-*g*-(hPG-PETMAC/OE)]). A low degree of substitution is targetted to maintain the essential water solubility of the polymer for its potential application in conditioning shampoo formulations.

5.2. Experimental

5.2.1. Materials

High molecular weight (HMW) PVA ($M_w = 1.86 \times 10^5 \text{ g mol}^{-1}$, 1% acetylated) and epoxyoctane (96%) were purchased from Sigma Aldrich and used without further purification. Acetone and sodium hydroxide were purchased from Fisher Scientific and used

without further purification. Deuterium oxide (D₂O) and deuterated dimethyl sulfoxide (d₆-DMSO) were purchased from Goss Scientific and used without further purification.

Poly[(vinyl alcohol)-*ran*-(vinyl, 2-hydroxypropyl ether trimethylammonium chloride)] (P[(VA)-*r*-(VETMAC)]), Poly[(vinyl alcohol)-*graft*-(hyperbranched polyglycerol)] (P[(VA)-*g*-(hPG)]) and Poly[(vinyl alcohol)-*ran*-(vinyl, 2-hydroxypropyl ether trimethylammonium chloride)-*graft*-(hyperbranched polyglycerol-2-hydroxypropyl ether trimethylammonium chloride)] (P[(VA)-*r*-(VETMAC)-*g*-(hPG-PETMAC)]) were prepared following methods outlined in Chapter 2, Chapter 3 and Chapter 4, respectively.

5.2.2. Instrumentation

¹H Nuclear magnetic resonance (NMR) spectra were recorded on a Bruker Avance-400 operating at 400 MHz or VNMRS-700 at 700 MHz. ¹³C NMR were carried out in D₂O or d₆-DMSO on a VNMRS-700 at 176 MHz.

Solid state NMR spectra were recorded on samples swollen with d₆-DMSO with a Bruker Avance III with a 4 mL high-res magic angle spinning probe (8 kHz spin speed) at 20 °C. ¹H NMR spectra were collected at 400 MHz and ¹³C NMR spectra were recorded at 100 MHz.

Fourier transform infra-red (FT-IR) spectroscopy was performed using a Perkin Elmer 1600 Series FT-IR.

Thermogravimetric analysis (TGA) measurements were collected using a Perkin Elmer Pyris 1 in a nitrogen (N₂) atmosphere. Samples were heated at a rate of 10 °C min⁻¹ to 500 °C.

Differential scanning calorimetry (DSC) measurements were carried out using a TA Instruments DSC Q1000. Samples were heated at a rate of 10 °C min⁻¹ between -50 °C and 300 °C.

Contact Angle measurements were recorded on solvent casted polymer films prepared on washed glass sides. A FTÅ200 instrument was used over a 30 s time period. 1 - 4 measurements were taken for each sample and an average of the right and left contact angle were recorded.

5.2.4. Synthesis of Poly[(vinyl alcohol)-*ran*-(vinyl, 2-hydroxy octyl ether)]

HMW PVA (1.0 g, 22.7 mmol) was dissolved in water (8.0 mL) at 100 °C in a 50 mL round bottom flask equipped with a water cooled condenser and a magnetic stirrer bar. NaOH_(aq) (0.2 mL, 5 M, 1.1 mmol) was added followed by epoxyoctane (3.5 mL, 22.9 mmol). The reaction mixture was stirred for 24 h at 100 °C. A precipitate formed during the reaction stopping the stirring action. The reaction mixture was diluted with water and filtered under reduced pressure. The filtrate was added to acetone and a white solid, P[(VA)-*r*-(VOE)], was obtained which was dried under reduced pressure.

Yield = 0.98 g (96%). ¹H NMR (400 MHz, *d*₆-DMSO): δ (ppm): 1.08 (m, 3H, CH₃), 1.46 (m, 10H, CH₂), 1.59 (m, 4H, CHCH₂), 4.05 (m, 2H, CHCH₂), 4.52 (m, 1H, OH), 4.75 (m, 1H, OH), 4.91 (m, 1H, OH). DEPT-135 (100 MHz, *d*₆-DMSO): δ (ppm): 15.0 (CH₃), 22.6 (CH₂), 25.5 (CH₂), 29.4 (CH₂), 31.8 (CH₂), 34.2 (CH₂), 45.7 (CHCH₂), 64.3 (CHCH₂), 66.3 (CHCH₂), 68.3 (CHCH₂). FT-IR ν (cm⁻¹): 3268 (ν_{OH}), 2920 (ν_{C-H}), 1088 (ν_{-O-}). T_m = 182 °C; T_g = 104 °C. T_d = 235 °C. Contact Angle = 58.6° (0 s); 30.9° (10 s)

5.2.5. Synthesis of Poly[(vinyl alcohol)-*ran*-(vinyl, 2-hydroxy octyl ether)-*ran*-(vinyl,2-hydroxypropyl ether trimethylammonium chloride)]

HMW P[(VA)-*r*-(VETMAC)] (1.0 g, 22.7 mmol) was dissolved in water (8.0 mL) at 100 °C in a 50 mL round bottom flask equipped with a water cooled condenser and a magnetic stirrer bar. NaOH_(aq) (0.2 mL, 5 M, 1.1 mmol) was added followed by epoxyoctane (3.5 mL, 22.9 mmol). The reaction mixture was stirred for 24 h at 100 °C. A precipitate formed during the reaction stopping the stirring action. The reaction mixture was diluted with water and filtered under reduced pressure. The filtrate was added to acetone and a white solid, P[(VA)-*r*-(VOE)-*r*-(VETMAC)], was obtained which was dried under reduced pressure.

Yield = 0.84 g (83%). ¹H NMR (400 MHz, *d*₆-DMSO): δ (ppm): 1.07 (m, 3H, CH₃), 1.45 (m, 10H, CH₂), 1.59 (m, 2H, CHCH₂), 3.37 (m, 9H, CH₃), 3.60 (m, 2H, CH₂), 3.81 (m, 4H, CH₂), 4.05 (m, 2H, CHCH₂), 4.29 (m, 1H, CH₂), 4.52 (m, 1H, OH), 4.74 (m, 1H, OH), 4.90 (m, 1H, OH). DEPT-135 (100 MHz, *d*₆-DMSO): δ (ppm): 14.5 (CH₃), 22.5 (CH₂), 22.6 (CH₂), 29.4 (CH₂), 31.2 (CH₃), 31.8 (CH₂), 34.2 (CH₂), 45.7 (CHCH₂), 54.0 (CH₃), 64.3 (CHCH₂), 66.3 (CHCH₂), 68.2 (CHCH₂), 68.2 (CH₂), 70.9 (CH₂). FT-IR ν (cm⁻¹): 3280 (ν_{-OH}), 2924 (ν_{C-H}), 1052 (ν_{-O-}). T_g = 86 °C, T_m = 148 °C, T_d = 312 °C. Contact Angle = 73.3° (0 s); 43° (10 s)

5.2.6. Synthesis of Poly[(vinyl alcohol)-*ran*-(vinyl, 2-hydroxy octyl ether)-*graft*-(hyperbranched polyglycerol-2-hydroxyoctyl ether)]

HMW P[(VA)-*g*-(hPG)] (1 g, 24.3 mmol) was dissolved in water (8 mL) at 100 °C in a 50 mL round bottom flask equipped with a water cooled condenser and a magnetic stirrer bar. NaOH_(aq) (0.24 mL, 5 M, 1.2 mmol) was added followed by epoxyoctane (3.7 mL, 24.3 mmol). The reaction mixture was stirred for 24 h at 100 °C. A precipitate formed during the reaction stopping the stirring action. The reaction mixture was diluted with water and filtered under reduced pressure. The filtrate was added to acetone and a white solid, P[(VA)-*r*-(VOE)-*g*-(hPG-OE)], was obtained which was dried under reduced pressure.

Yield = 0.90 g (87%). ¹H NMR (400 MHz, *d*₆-DMSO): δ (ppm): 1.07 (m, 3H, CH₃), 1.46 (m, 1H, CH₂), 1.59 (m, 4H, CHCH₂), 3.54 (m, 5H, CH₂CHCH₂) 4.05 (m, 1H, CH), 4.51 (m, 1H, OH), 4.73 (m, 1H, OH), 4.90 (m, 1H, OH). DEPT-135 (100 MHz, *d*₆-DMSO): δ (ppm): 14.5 (CH₃), 22.6 (CH₂), 25.5 (CH₂), 29.4 (CH₂), 31.8 (CH₂), 34.2 (CH₂), 42.8 (CHCH₂), 46.2 (CHCH₂), 61.4 (CH₂CHCH₂), 63.7 (CH₂CHCH₂), 64.3 (CHCH₂), 66.3 (CHCH₂), 68.3 (CHCH₂), 70.6 (CH₂CHCH₂), 70.9 (CH₂CHCH₂), 71.1 (CHCH₂), 73.3 (CH₂CHCH₂), 74.8 (CH₂CHCH₂), 76.5 (CH₂CHCH₂). FT-IR ν (cm⁻¹): 3274 (ν -OH), 2908 (ν C-H), 1078 (ν -O-). T_g = 74 °C, T_m = 156 °C, T_d = 254 °C. Contact Angle = 79.4° (0 s); 32.2° (10 s)

5.2.7. Synthesis of Poly[(vinyl, 2-hydroxy octyl ether)-*ran*-(vinyl, 2-hydroxypropyl ether trimethylammonium chloride)-*ran*-(vinyl alcohol)-*graft*-(hyperbranched polyglycerol)-(2-hydroxypropyl ether trimethylammonium chloride)/(2-hydroxy octyl ether)]

HMW P[(VA)-*r*-(VETMAC)-*g*-(hPG-PETMAC)](1.0 g, 24.3 mmol) was dissolved in water (8.0 mL) at 100 °C in a 50 mL round bottom flask equipped with a water cooled condenser and a magnetic stirrer bar. NaOH_(aq) (0.2 mL, 5 M, 1.2 mmol) was added followed by epoxyoctane (3.7 mL, 24.3 mmol). The reaction mixture was stirred for 24 h at 100 °C. A precipitate formed during the reaction stopping the stirring action. The reaction mixture was diluted with water and filtered under reduced pressure. The filtrate was added to acetone and a pale yellow solid, P[(VOE)-*r*-(VETMAC)-*r*-(VA)-*g*-(hPG-PETMAC/OE)], was obtained which was dried under reduced pressure.

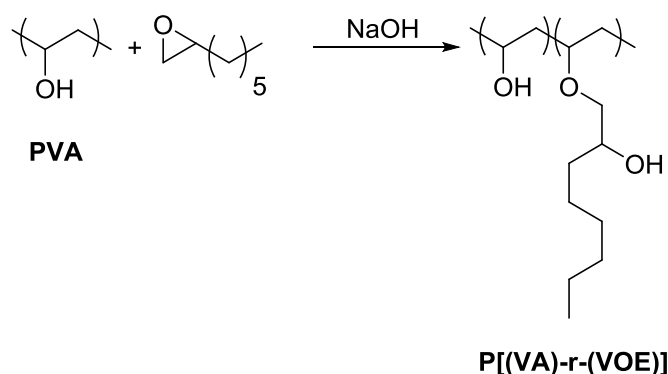
Yield = 0.94 g (90%). ¹H NMR (700 MHz, D₂O): δ (ppm): 0.90 (m, 3H, CH₃), 1.32 (m, 8H, CH₂), 1.45 (m, 2H, CH₂), 1.73 (m, 2H, CHCH₂), 1.87 (m, 2H, CHCH₂), 3.25 (m, 9H, CH₃), 3.52 (m, 2H,

CH₂), 3.66 (m, 9H, CH₂CHCH₂), 3.88 (m, 1H, CHCH₂), 4.05 (m, 1H, CHCH₂), 4.02 (m, 1H, CH).
¹³C NMR (176 MHz, D₂O): δ (ppm): 13.9 (CH₃), 22.34 (CH₂), 25.1 (CH₂), 28.8 (CH₂), 31.4 (CH₂),
 33.1 (CH₂), 41.5 (CHCH₂), 44.4 (CHCH₂), 54.5 (CH₃), 61.3 (m, 2H, CH₂), 63.1 (CH₂), 65.0
 (CHCH₂), 65.6 (CH), 66.6 (CHCH₂), 68.0 (CHCH₂), 68.5 (CH₂CHCH₂), 69.6 (CH₂CHCH₂), 70.7
 (CH₂CHCH₂), 72.4 (CH₂CHCH₂), 75.5 (CHCH₂), 76.8 (CH), 78.5 (CH), 80.1 (CH). FT-IR ν (cm⁻¹):
 3300 (ν_{-OH}), 2902 (ν_{C-H}), 1078 (ν_{-O-}). T_g = 71 °C, T_d = 317 °C. Contact Angle = 83° (0 s); 83.8°
 (10 s)

5.3. Results and Discussion

5.3.1. Synthesis of Poly[(vinyl alcohol)-*ran*-(vinyl, 2-hydroxy octyl ether)]

PVA was reacted with epoxyoctane in water using a base catalyst (NaOH_(aq)) to synthesise P[(VA)-*r*-(VOE)], Scheme 5.3. A solid precipitate was formed during the reaction, due to the increased hydrophobicity.



Scheme 5.3: Synthesis of P[(VA)-*r*-(VOE)]

P[(VA)-*r*-(VOE)] was found to be insoluble in a range of tested solvents (*i.e.* methanol, diethyl ether, ethyl acetate, hexane and dichloromethane), and partially soluble in water. Therefore, for comprehensive analysis P[(VA)-*r*-(VOE)] was analysed as a swollen gel in *d*₆-DMSO, by solid state NMR spectroscopy.

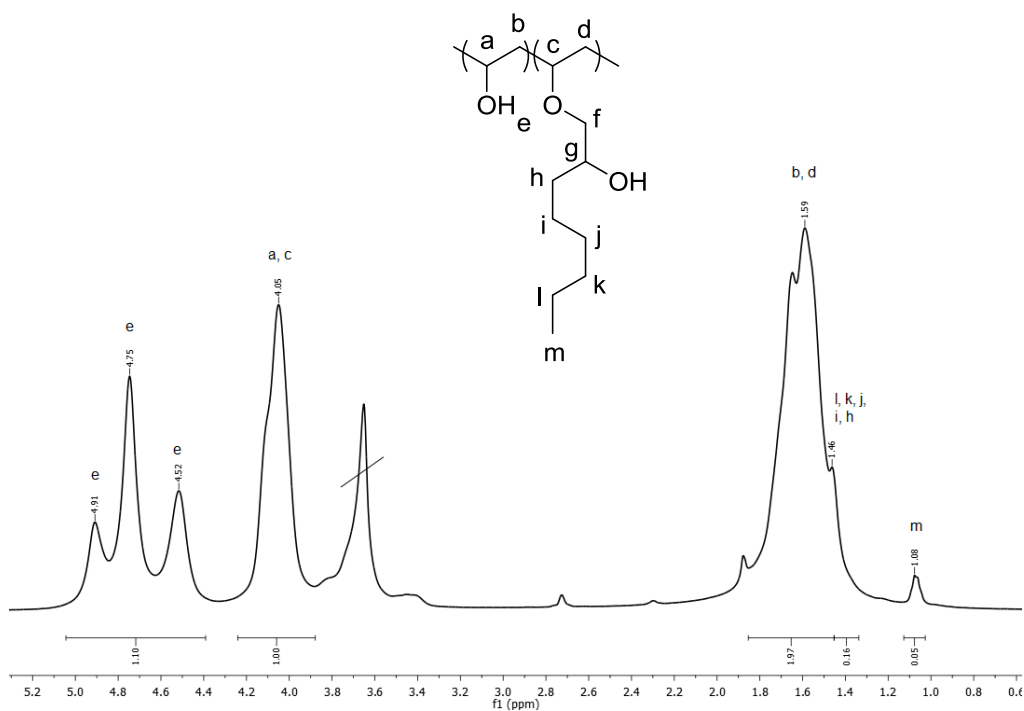


Figure 5.1: 400 MHz ^1H NMR spectrum of P[(VA)-*r*-(VOE)] swollen gel in d_6 -DMSO

The solid state ^1H NMR spectrum of P[(VA)-*r*-(VOE)] is shown in Figure 5.1. The broad resonance at 1.45 - 1.80 ppm is assigned to the methylene protons (b and d), and the broad resonance at 3.90 - 4.23 ppm to the methine protons on the polymer backbone (a, c). The triad of resonances at 4.52 ppm, 4.75 ppm and 4.91 ppm assigned to the hydroxyl protons attached to the polymer backbone (e). The resonances at 1.08 ppm is assigned to the methyl proton in the alkyl chain (m) and at 1.46 ppm to methylene protons (l) neighbouring the methyl protons, as confirmed by the ^1H - ^1H correlation spectroscopy (COSY) spectrum, Figure 5.2. Furthermore the resonance at 1.46 ppm is also attributed to other methylene protons in the alkyl chain (h, i, j, k), as confirmed by the ^1H - ^{13}C heteronuclear single quantum coherence (HSQC spectrum), Figure 5.4, see later.

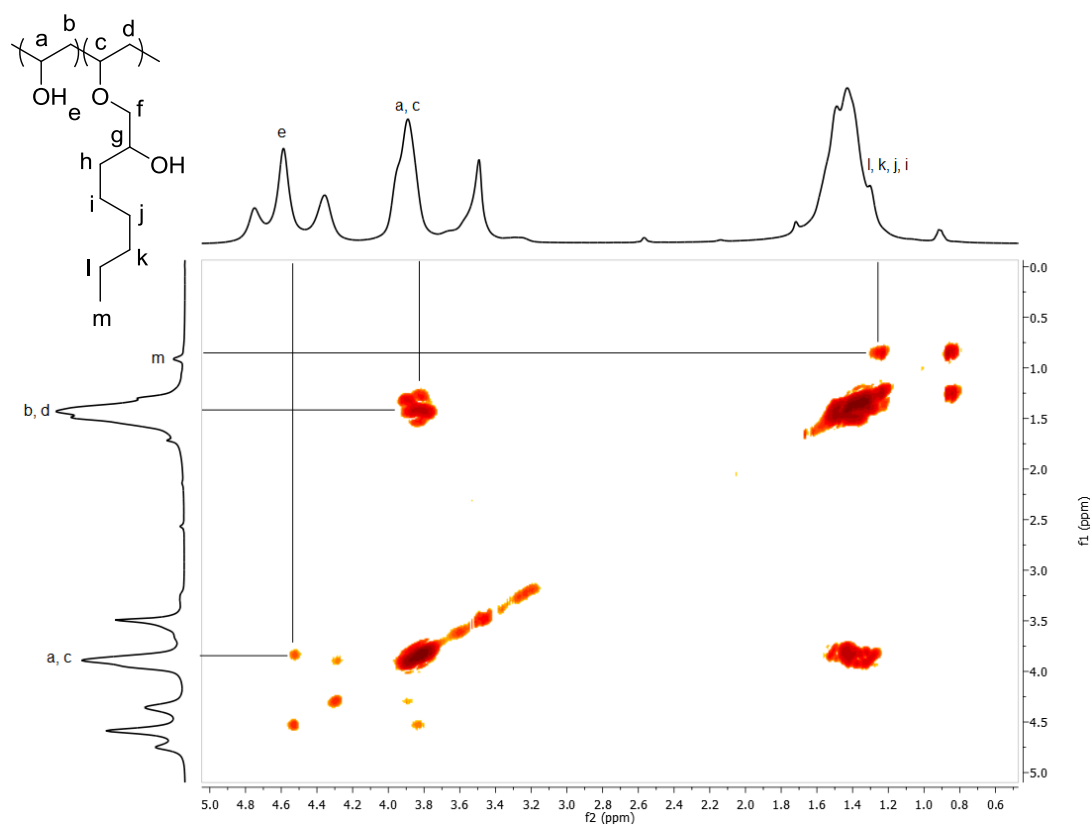


Figure 5.2: 400 MHz ¹H - ¹H COSY spectrum of P[(VA)-r-(VOE)] in d₆-DMSO

The degree of hydrophobic substitution (%HS) was determined from the ratio between the methine protons on the polymer backbone (a) and the methyl protons at the end of the alkyl chain (m), Equation 5.1. Where $\int a$ and $\int m$ are the integrals of the resonances at 4.05 ppm and 1.08 ppm respectively; and the integrals are normalised to a single proton. The %HS of P[(VA)-r-(VOE)] was determined to be 1.7%.

$$\%HS = \frac{\int m}{\int a \times 3} \quad \text{Equation 5.1}$$

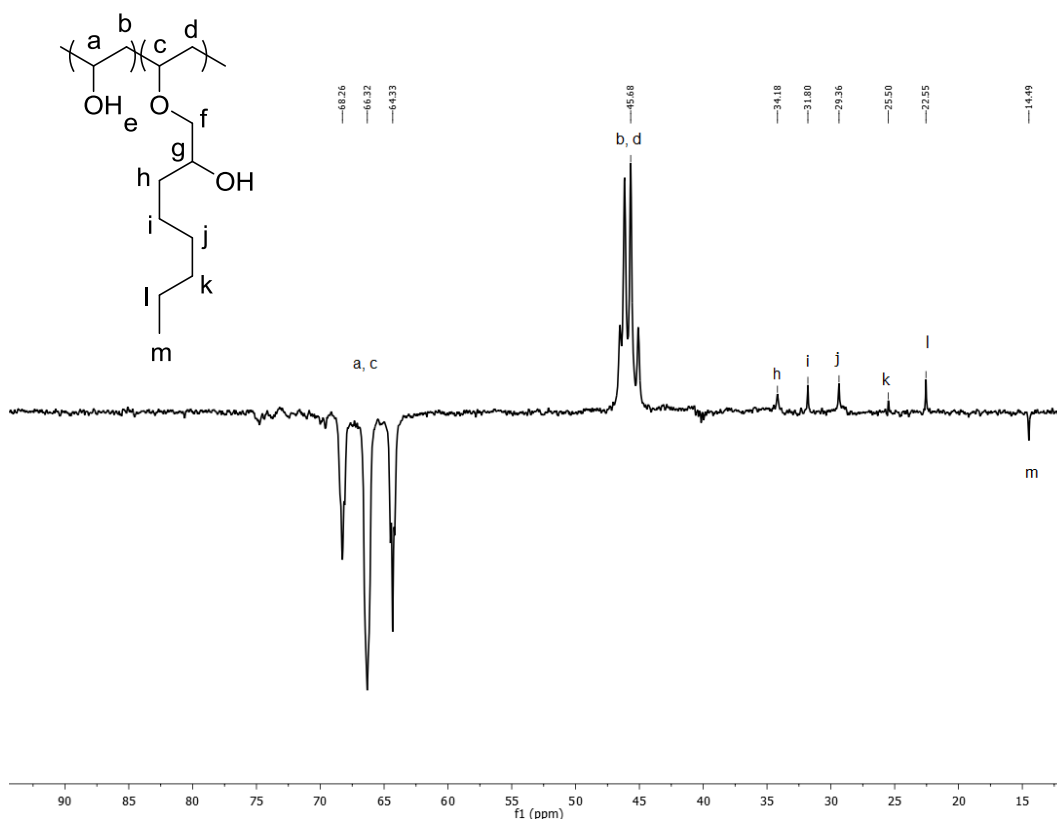


Figure 5.3: 100 MHz DEPT-135 NMR spectrum of P[(VA)-*r*-(VOE)] swollen in d_6 -DMSO

P[(VA)-*r*-(VOE)] was analysed by solid state distortionless enhancement by polarization transfer-135 (DEPT-135) NMR spectroscopy (Figure 5.3), as it provides a more resolved spectrum in comparison with a standard solid state ^{13}C NMR spectrum. The resonance at 14.49 ppm is attributed to the methyl proton (m), as confirmed by the $^1\text{H} - ^{13}\text{C}$ NMR spectrum, Figure 5.4.a. The resonances at 22.6 ppm, 25.5 ppm, 29.4 ppm, 31.8 ppm, 34.2 ppm are attributed to the methylene protons in the alkyl chain (l), (k), (j), (i) and (h), respectively. The assignments are collaborated by the $^1\text{H} - ^{13}\text{C}$ HSQC spectrum (Figure 5.4.b). The resonance at 45.7 ppm is attributed to the methylene protons on the polymer backbone (b, d), the resonances at 64.3 ppm, 66.3 ppm and 68.3 ppm correspond to the methine protons on the polymer backbone (a, c). The resonances attributed to the substituted polymer backbone in previously synthesised PVA derivatives (*e.g.* Chapter 3, Figure 3.10) differ to those of unreacted PVA. However, no new resonances are observed in Figure 5.3, this is likely due to the low resolution of the NMR experiment as well as the low %HS of the sample.

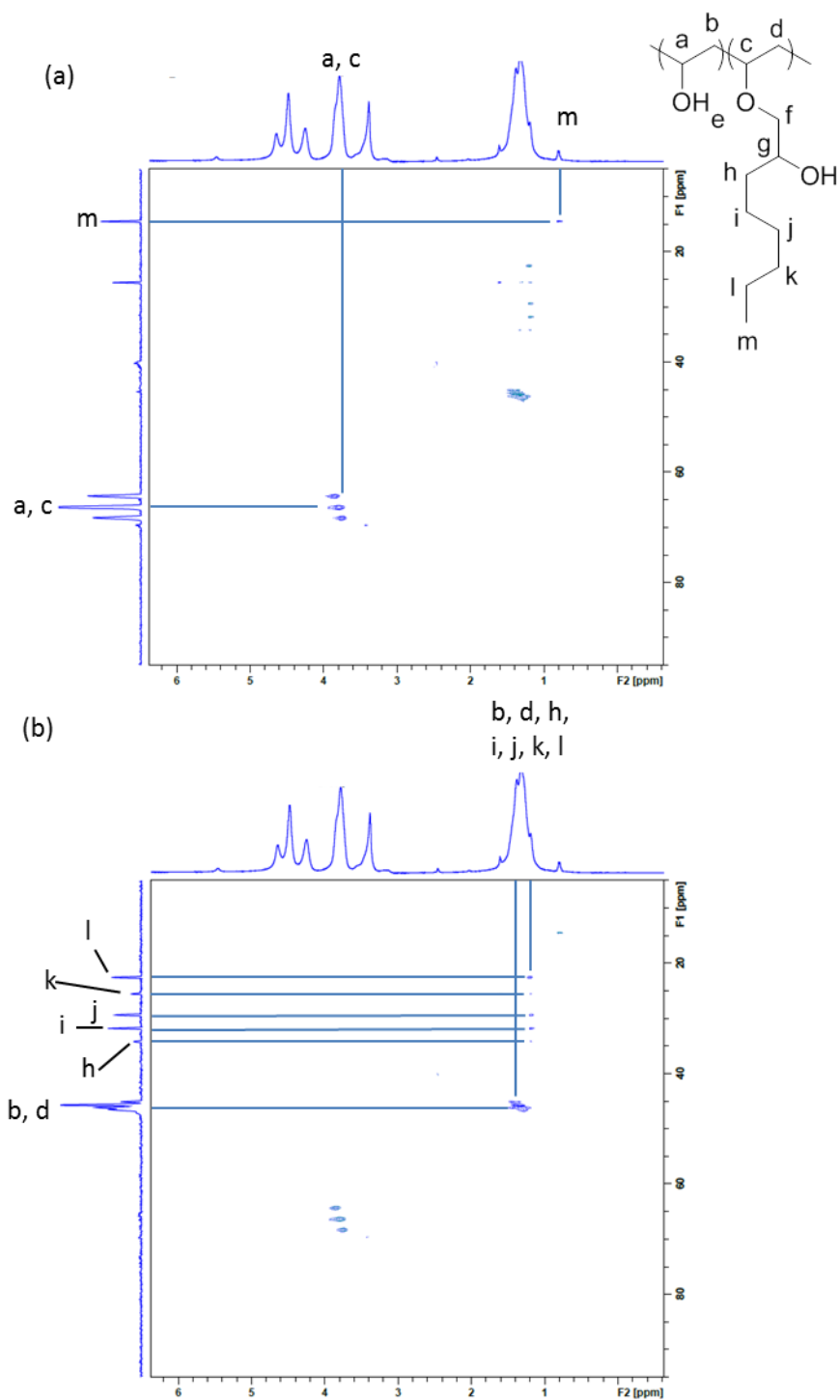


Figure 5.4: 100 MHz ^1H - ^{13}C HSQC of P[(VA)-*r*-(VOE)] swollen gel in d_6 -DMSO showing (a) methyl and methine carbon atoms (b) methylene carbon atoms

Furthermore, the water soluble fraction of P[(VA)-*r*-(VOE)] was analysed in D_2O by solution based ^1H NMR spectroscopy. A comparison of the solid state and solution based ^1H NMR spectra can be seen in Figure 5.5.

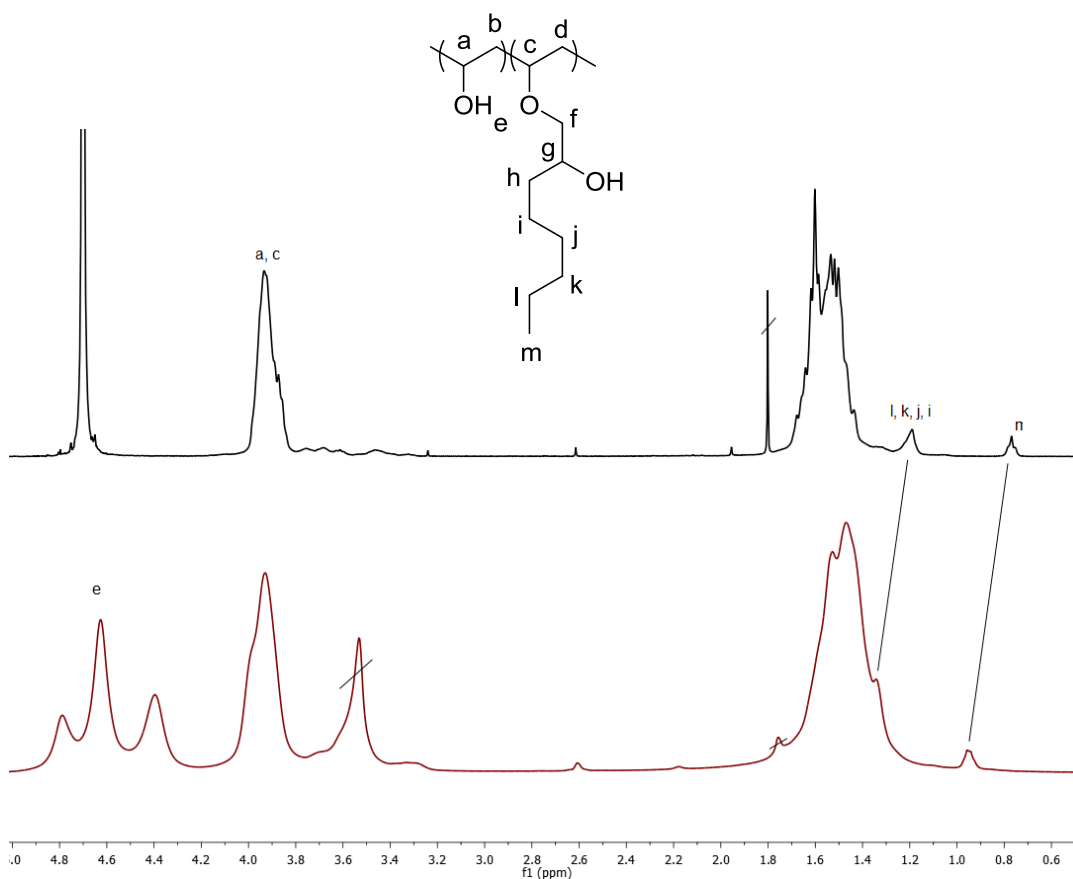


Figure 5.5: 400 MHz ¹H NMR spectra of P[(VA)-r-(VOE)] (a) in D₂O (b) swollen in d₆-DMSO

Despite slight changes in chemical shifts of the proton environments in the solution based ¹H NMR spectrum (Figure 5.5.a) due to the change in deuterated solvent, P[(VA)-r-(VOE)] can be analysed in the same way as the solid state ¹H NMR spectrum (Figure 5.5.b) once the chemical shifts are taken into account. Furthermore, the %HS was determined to be unchanged using Equation 5.1.

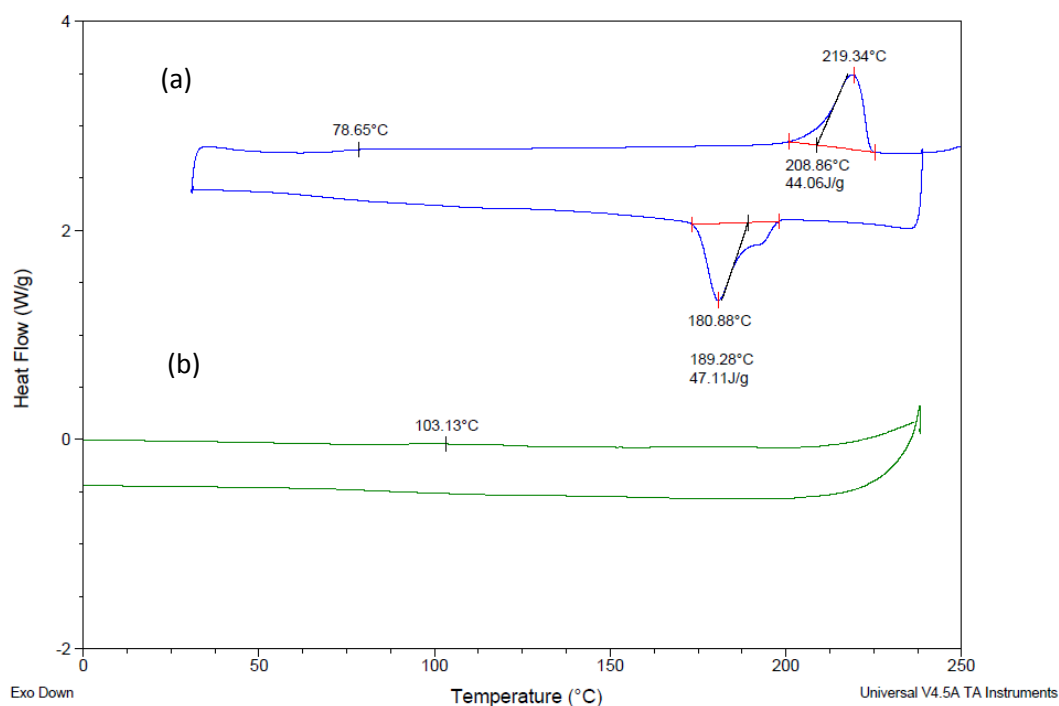


Figure 5.6: DSC thermograms of (a) PVA and (b) P[(VA)-r-(VOE)]

The DSC thermograms of P[(VA)-r-(VOE)] and PVA are shown in Figure 5.6. PVA (Figure 5.6.a) is a semi-crystalline material and as expected a glass transition (T_g) is observed at 79 °C, a melting point (T_m) at 219 °C and a crystallisation temperature (T_c) at 181 °C. For P[(VA)-r-(VOE)] (Figure 5.6.b), a T_g is observed at 103.13 °C, the increase in T_g from 79 °C in PVA is due to increased chain stiffness with the addition of the long alkyl chain. Furthermore, the disappearance of the T_m and T_c is due the addition of alkyl chains to semi-crystalline PVA has produced the amorphous P[(VA)-r-(VOE)].

5.3.2. Synthesis of Poly[(vinyl alcohol)-*ran*-(vinyl, 2-hydroxy octyl ether)-*ran*-(vinyl, 2-hydroxypropyl ether trimethylammonium chloride)]

P[(VA)-*r*-(VETMAC)], with a charge density (CD) of 0.88 meq g⁻¹, was reacted with epoxyoctane to synthesise Poly[(vinyl alcohol)-*ran*-(vinyl, 2-hydroxy octyl ether)-*ran*-(vinyl, 2-hydroxypropyl ether trimethylammonium chloride)] (P[(VA)-*r*-(VOE)-*r*-(VETMAC)]) (Scheme 5.4), to investigate whether the hygroscopic quaternary nitrogen atoms would increase the water solubility of the resulting hydrophobic polymer.

protons in poly(vinyl, 2-hydroxypropyl ether trimethylammonium chloride) segments (PVETMAC) (f). The broad resonance at 1.46 - 1.98 ppm are attributed to methylene protons on the polymer backbone (b, d), and the broad resonances at 3.92 - 4.14 ppm correspond to the methine protons on the polymer backbone (a, c). The resonance at 3.37 ppm is assigned to the methyl protons attached to the quaternary nitrogen atom (i). The resonance at 3.60 ppm is attributed to the methylene protons in PVETMAC segments (h) and the resonance at 4.29 ppm for the methine proton in PVETMAC segments (g). The triad of resonances at 4.90 ppm, 4.74 ppm and 4.52 ppm is assigned to the hydroxyl protons attached to the polymer backbone (e).

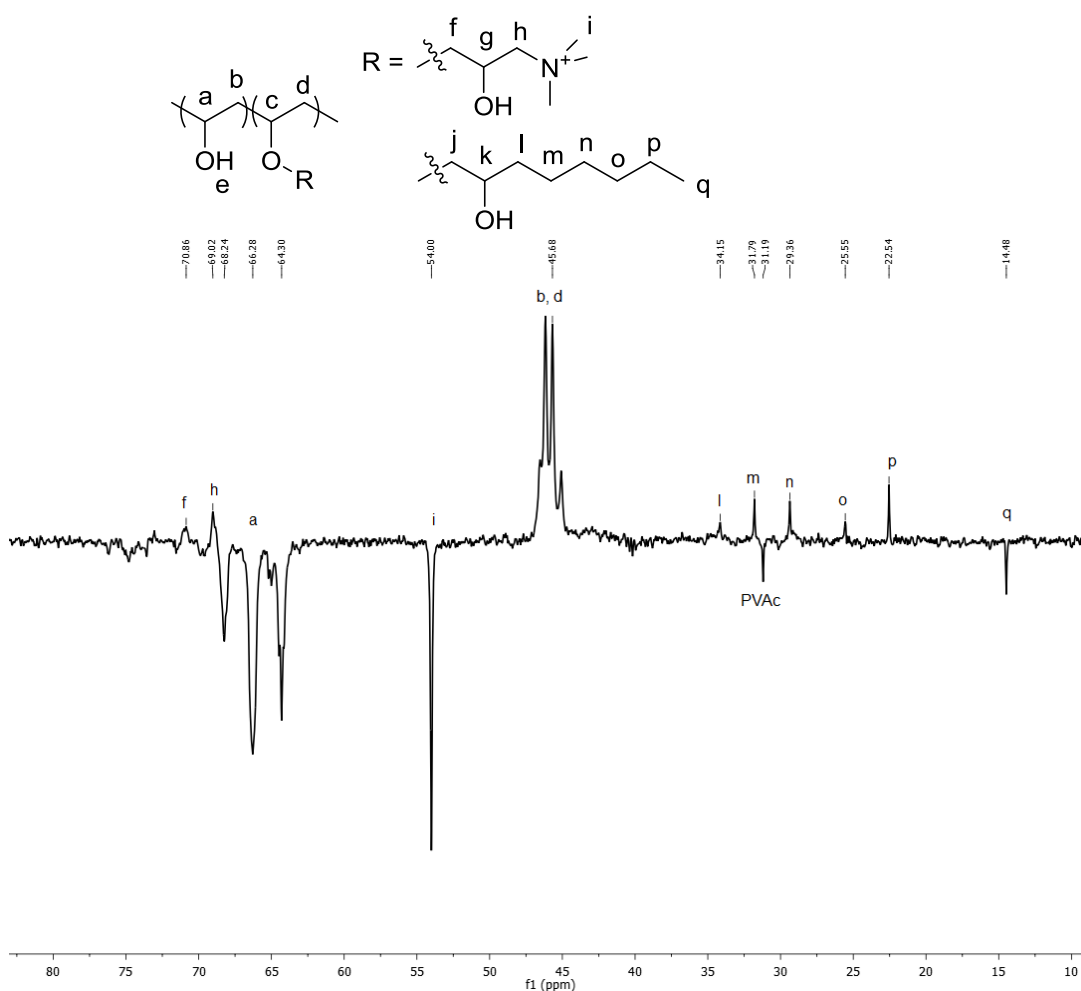


Figure 5.8: 100 MHz DEPT-135 NMR of P[(VA)-r-(VOE)-r-(VETMAC)] swollen gel in d_6 -DMSO

The DEPT-135 NMR spectrum of P[(VA)-r-(VOE)-r-(VETMAC)] is shown in Figure 5.8. The resonance at 14.5 ppm corresponds to methyl carbon atom in the alkyl chain (q). The

resonances at 22.5 ppm, 25.6 ppm, 29.4 ppm, 31.8 ppm and 34.2 ppm are assigned to the methylene carbon atoms in the alkyl chain (p), (o), (n), (m), and (l), respectively. The resonance at 31.2 ppm is attributed to the methyl carbon atom in PVAc. The resonance at 45.7 ppm is attributed to the methylene carbon atoms on the polymer backbone (b, d). The resonance at 54.0 ppm corresponds to the methyl carbon atoms adjacent to the quaternary carbon atom (i). The resonances at 64.4 ppm, 66.3 ppm and 68.2 ppm are attributed to the methine carbon atoms on the polymer backbone (a, c). The resonance at 69.0 ppm corresponds to methylene carbon atom adjacent to the quaternary nitrogen atom (h). The resonance at 70.9 ppm is attributed to the methylene carbon atom neighbouring the hydroxyl group in PVETMAC (f).

The %HS of P[(VA)-*r*-(VOE)-*r*-(VETMAC)] was determined to be 2.8% using Equation 5.1, which is greater than that for P[(VA)-*r*-(VOE)] (1.7%). This increase is within the experimental error due to the coalesced resonances in the ¹H NMR spectrum, Figure 5.8.

The addition of epoxyoctane is anticipated to decrease the charge density of the P[(VA)-*r*-(VETMAC)], because the molecular weight of P[(VA)-*r*-(VOE)-*r*-(VETMAC)] is greater. The CD was determined from Equation 5.2.

$$CD = 1000 \left(\frac{Q_c \times n_{poly} \times \%QNC}{m_{initial} + m_{\%QNC} + m_{\%HS}} \right) \quad \text{Equation 5.2}$$

Where CD is the charge density (meq g⁻¹), Q_c is the charge of the cationic subunit, n_{poly} is the moles of polymer (mol), %QNC is the quaternary nitrogen content, m_{initial} is the initial mass of polymer used (g). The m_{%QNC} or m_{%HS} are determined from Equation 5.3.

$$m_{\%RU} = MW_{added} \times (n_{poly} \times \%RU) \quad \text{Equation 5.3}$$

Where MW_{added} is the molecular weight of the substituent (g mol⁻¹) (*i.e.* MW_{added} = 115.6 g mol⁻¹ for %QNC; MW_{added} = 128.12 for %HS) and %RU is equivalent to the percentage of the repeat unit being determined (*i.e.* %QNC and %HS).

As expected, the CD of P[(VA)-*r*-(VOE)-*r*-(VETMAC)] decreased to 0.82 meq g⁻¹ from 0.88 meq g⁻¹ for P[(VA)-*r*-(VETMAC)].

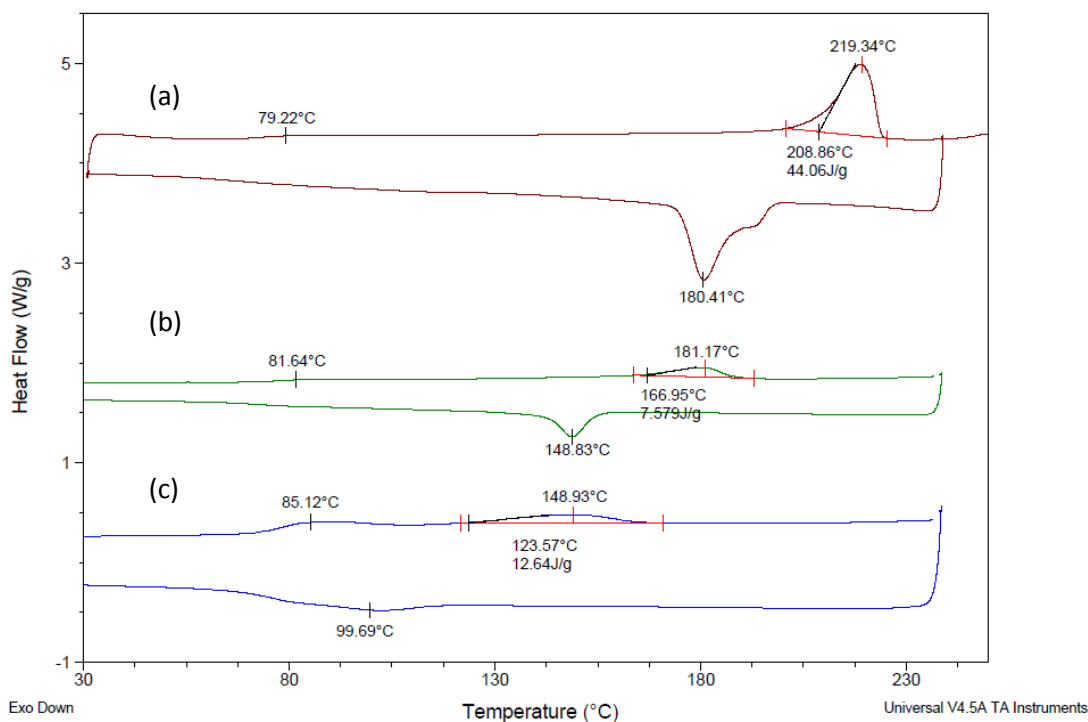
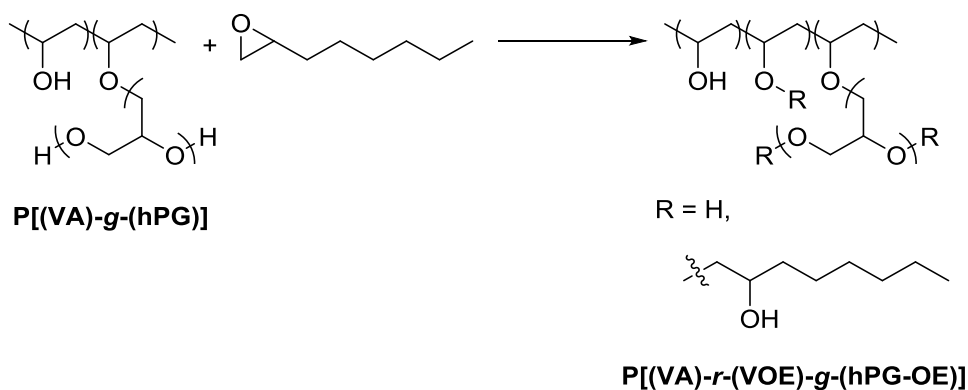


Figure 5.9: DSC thermograms of (a) PVA, (b) P[(VA)-r-(VETMAC)] and (c) P[(VA)-r-(VOE)-r-(VETMAC)]

A comparison of the DSC thermograms of PVA, P[(VA)-r-(VETMAC)] and P[(VA)-r-(VOE)-r-(VETMAC)] is shown in Figure 5.9. The T_m of PVA (Figure 5.9.a) at 219 °C decreases to 181 °C in P[(VA)-r-(VETMAC)] (Figure 5.9.b). Furthermore, with the addition of the alkyl chains in P[(VA)-r-(VOE)-r-(VETMAC)] (Figure 5.9.c) the T_m is decreased to 149 °C. This is due to the incorporation of flexible GTMAC and epoxyoctane, respectively. Moreover, the T_g of PVA (79 °C) and P[(VA)-r-(VETMAC)] (82 °C) remain the same, within the experimental error due to the difficulty of determining the T_g . However, the T_g increases to 85 °C for P[(VA)-r-(VOE)-r-(VETMAC)], due to the increased chain stiffness with the addition of the alkyl chain.

5.3.3. Synthesis of Poly[(vinyl alcohol)-*ran*-(vinyl, 2-hydroxy octyl ether)-*graft*-(hyperbranched polyglycerol-2-hydroxyoctyl ether)]

P[(VA)-*g*-(hPG)], with a mole fraction of hyperbranched polyglycerol (x_{hPG}) of 19%, was reacted with epoxyoctane to synthesise Poly[(vinyl alcohol)-*ran*-(vinyl, 2-hydroxy octyl ether)-*graft*-(hyperbranched polyglycerol-2-hydroxyoctyl ether)] (P[(VA)-r-(VOE)-*g*-(hPG-OE)]), Scheme 5.5. As observed with the previous reactions using epoxyoctane (Section 5.3.1 and 5.3.2), a precipitate formed during the reaction in the aqueous reaction solvent.



Scheme 5.5: Synthesis of P[(VA)-r-(VOE)-g-(hPG-OE)]

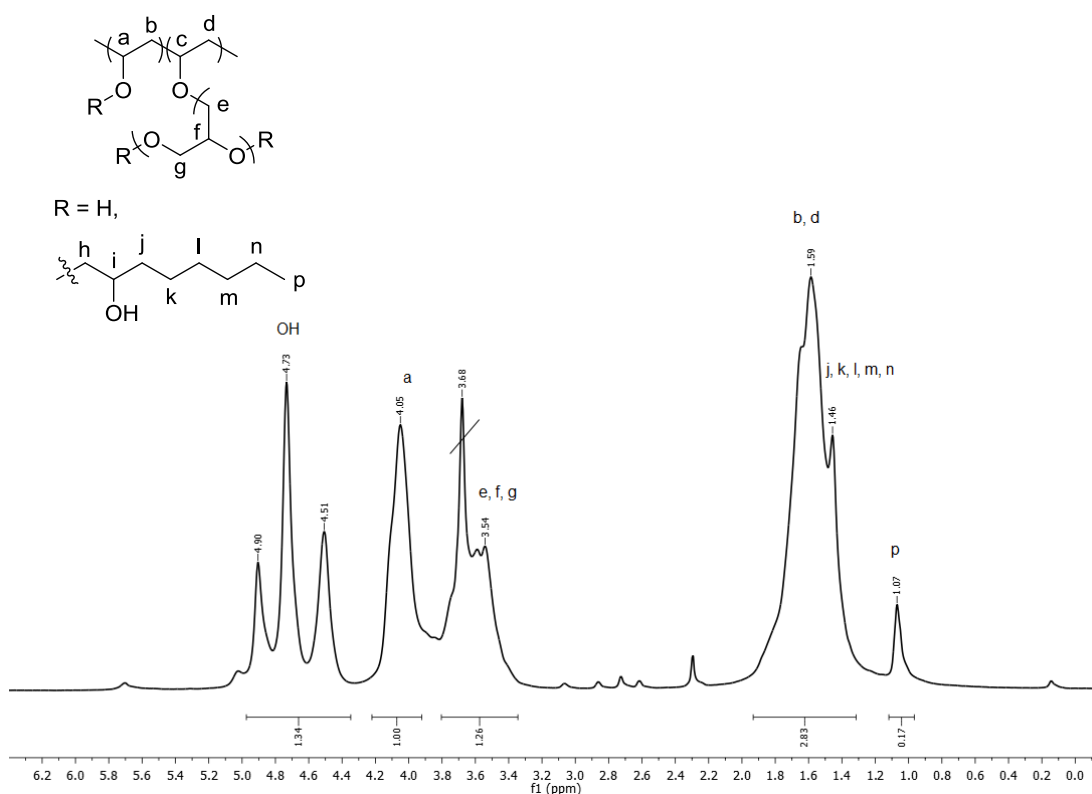


Figure 5.10: 400 MHz ^1H NMR spectrum of P[(VA)-r-(VOE)-g-(hPG-OE)] swollen in d_6 -DMSO

In the solid state ^1H NMR spectrum of P[(VA)-r-(VOE)-g-(hPG-OE)], shown in Figure 5.10, the resonances attributed to the alkyl chain are seen at 1.07 ppm for the methyl proton (p), 1.46 ppm for methylene protons (k, l, m, n) and for the methylene proton adjacent to the methine proton (j). The broad resonance at 1.31 - 1.98 ppm is attributed to the methylene protons on the polymer backbone (b, d). The broad resonance at 3.36 - 3.81 ppm

corresponds to the methylene and methine protons in the hPG chain (e, f, g). The resonance at 3.68 ppm within the broad resonance is due to residual water in d_6 -DMSO used to swell the sample. The broad resonance between 3.88 - 4.25 ppm is attributed to the methine protons in the polymer backbone (a, c). The triad of resonances at 4.51 ppm, 4.73 ppm and 4.90 ppm is due to the hydroxyl protons in the polymer.

The %HS of P[(VA)-*r*-(VOE)-*r*-(hPG-OE)] was determined, using Equation 5.1, to be 5.6%. The increase in %HS is potentially due to the increased amount of hydroxyl groups in the polymer. However, due to the coalesced resonances in the ^1H NMR spectrum accurate determination was not possible.

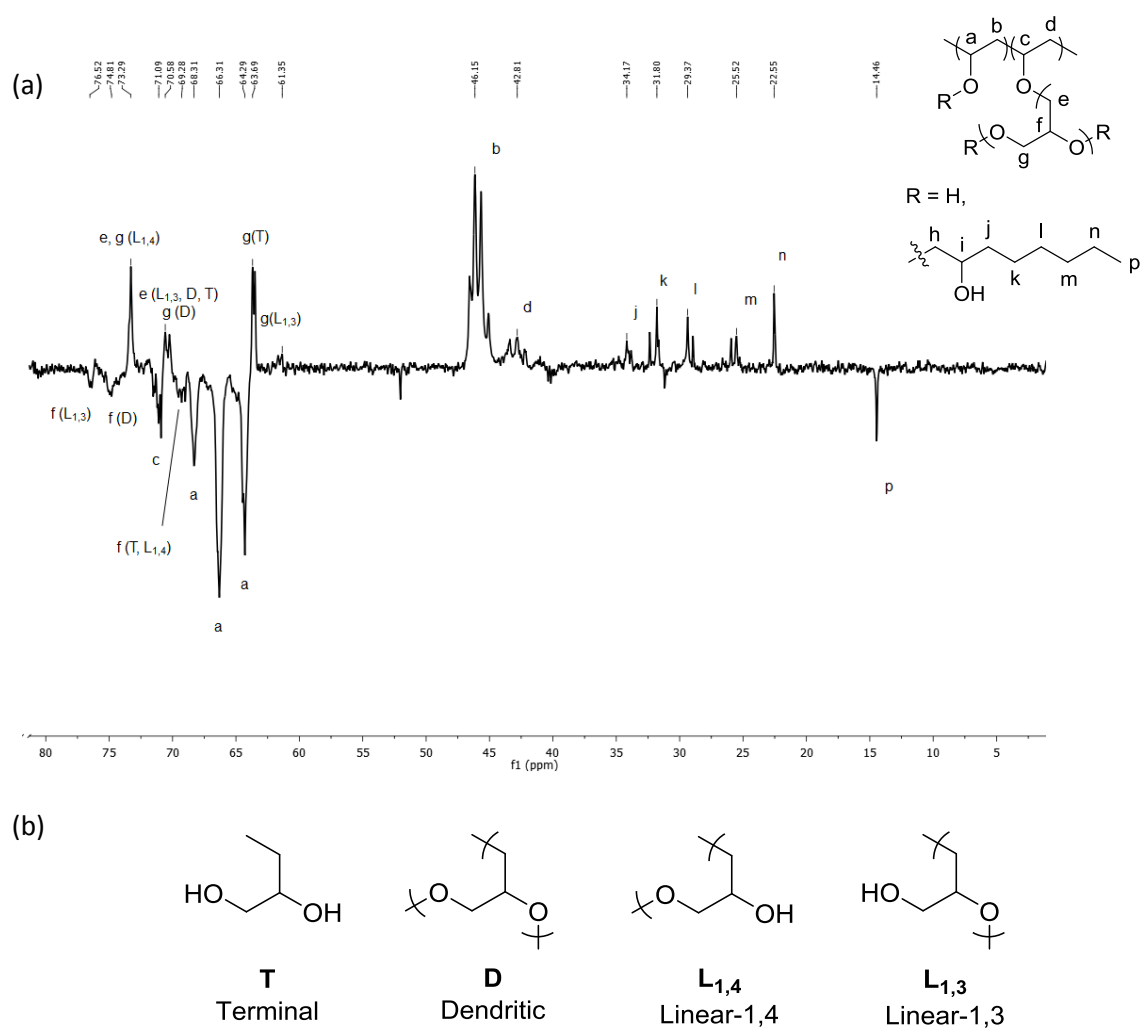


Figure 5.11: (a) 100 MHz DEPT-135 of P[(VA)-*r*-(VOE)-*g*-(hPG-OE)] swollen in d_6 -DMSO (b) structural units of hPG

The solid state DEPT-135 spectrum of P[(VA)-*r*-(VOE)-*g*-(hPG-OE)] is shown in Figure 5.11.a and the structural units of hPG can be seen in Figure 5.13.b. The resonance at 14.5 ppm is attributed to the methyl carbon in the alkyl chain (p). The resonances at 22.6 ppm, 25.5 ppm, 29.4 ppm, 31.8 ppm and 34.2 ppm correspond to methylene carbon atoms in the alkyl chain (n), (m), (l), (k) and (j), respectively. The resonances at 42.8 ppm and 46.2 ppm are assigned to the methylene carbon atoms on the polymer backbone (d) and (b), respectively. The resonances at 61.4 ppm and 63.4 ppm are attributed to the methylene carbon atoms in hPG (g, L_{1,3}) and (g, T), respectively. The resonances at 64.3 ppm, 66.3 ppm and 68.3 ppm correspond to the methine carbon atom on the polymer backbone (a). The resonance at 69.3 ppm is attributed to the methine carbon atoms in hPG (f, T; f, L_{1,4}). The resonance at 70.6 ppm is assigned to the methylene protons in hPG (e, L_{1,3}; e, T; e, D; g, D). The resonance at 71.1 ppm is attributed to the methine carbon atom on the polymer backbone (c). The resonance at 73.3 ppm corresponds to the methine carbon atoms in hPG (e, L_{1,4}; g, L_{1,4}). The resonances at 74.8 ppm and 76.5 ppm are assigned to the methine carbon atoms in hPG (f, D) and (f, L_{1,3}), respectively.

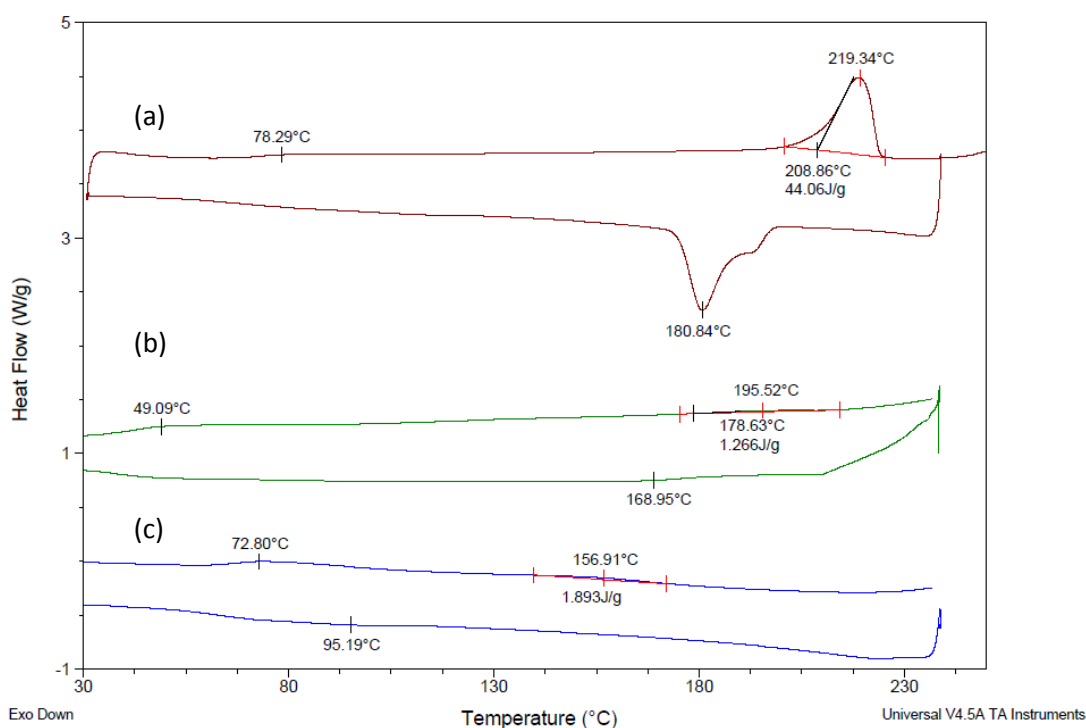
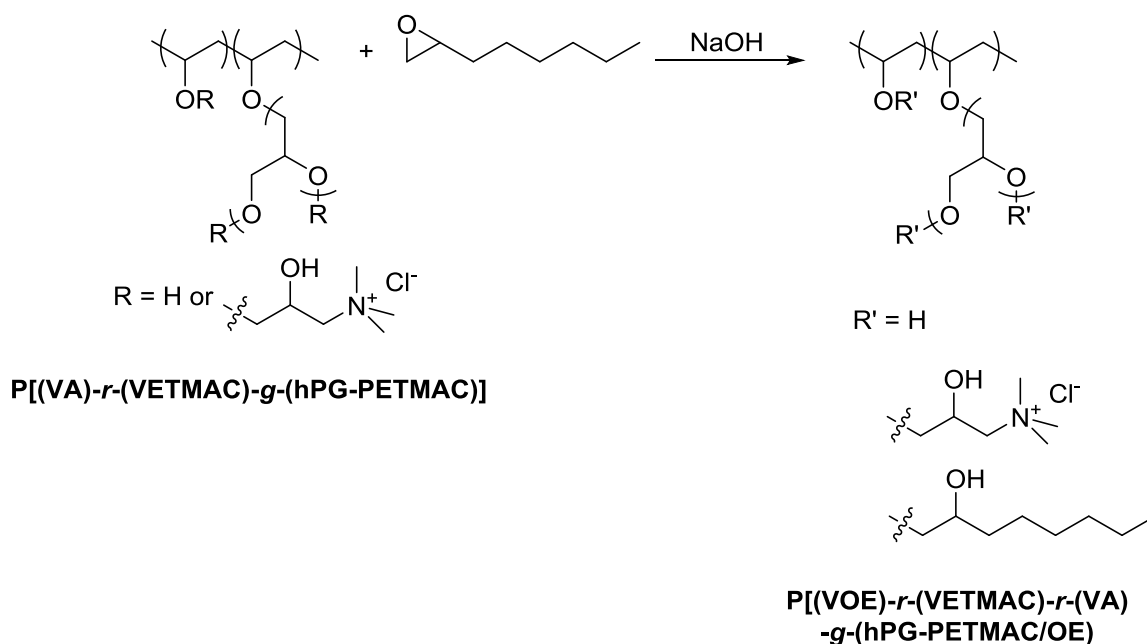


Figure 5.12: DSC thermograms of (a) PVA (b) P[(VA)-*g*-(hPG)] and (c) P[(VA)-*r*-(VOE)-*g*-(hPG-OE)]

A comparison of the DSC thermograms of PVA, P[(VA)-*g*-(hPG)] and P[(VA)-*r*-(VOE)-*g*-(hPG-OE)] is shown in Figure 5.12. The T_m of PVA (Figure 5.12.a) at 219 °C decreases to 195 °C in P[(VA)-*g*-(hPG)] (Figure 5.12.b). Furthermore, with the addition of the alkyl chains in P[(VA)-*r*-(VOE)-*g*-(hPG-OE)] (Figure 5.12.c), the T_m is decreased to 157 °C. This is due to the incorporation of flexible hPG and epoxyoctane, respectively. Moreover, the T_g decreases from 78 °C in PVA to 49.1 °C in P[(VA)-*g*-(hPG)] as the polymer becomes more flexible, however with the addition of the alkyl chains in P[(VA)-*r*-(VOE)-*g*-(hPG-OE)] the T_g increases to 73 °C as the stiffness of the chains increases.

5.3.4. Synthesis of Poly[(vinyl, 2-hydroxy octyl ether)-*ran*-(vinyl, 2-hydroxypropyl ether trimethylammonium chloride)-*ran*-(vinyl alcohol)-*graft*-(hyperbranched polyglycerol)-(2-hydroxypropyl ether trimethylammonium chloride)/(2-hydroxy octyl ether)]

P[(VA)-*r*-(VETMAC)-*g*-(hPG-PETMAC)] with a $x_{(hPG)}$ of 19% and a CD of 1.34 meq g^{-1} , was reacted with epoxyoctane to produce P[(VOE)-*r*-(VETMAC)-*r*-(VA)-*g*-(hPG-PETMAC/OE)], Scheme 5.6. As seen with the previous reactions a precipitate formed during the reaction.



Scheme 5.6: Synthesis of P[(VA)-*r*-(VOE)-*r*-(VETMAC)-*g*-(hPG-PETMAC-OE)]

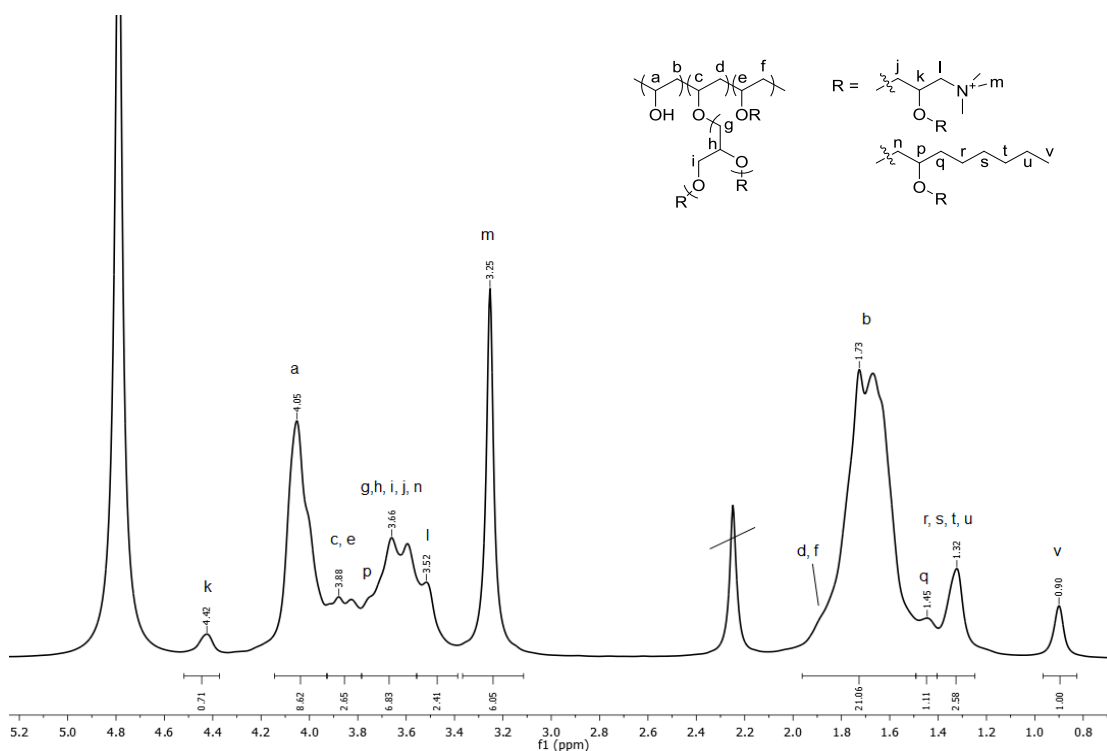


Figure 5.13: 700 MHz ^1H NMR spectrum of P[(VA)-*r*-(VOE)-*r*-(VETMAC)-*g*-(hPG-PETMAC-OE)] in D_2O

In the ^1H NMR spectrum of P[(VA)-*r*-(VOE)-*r*-(VETMAC)-*g*-(hPG-PETMAC-OE)] (Figure 5.13), the resonance at 0.90 ppm is assigned to the methyl proton in the polymer chain (v). The resonances at 1.32 ppm and 1.45 ppm are attributed to methylene protons in the polymer chain (r, s, t, u) and (q), respectively. The broad resonance between 1.49 - 1.94 ppm corresponds to the methylene protons in the polymer backbone (b, d, f). The resonance at 3.25 ppm is attributed to the methyl protons adjacent to the quaternary nitrogen atom (m). The resonance at 3.52 ppm is attributed to the methylene proton neighbouring the quaternary nitrogen atom (l). The broad resonance between 3.55 - 3.75 ppm corresponds to the methylene and methine protons in hPG (g, h, i) and the methylene protons neighbouring the ether linkage in the alkyl chain and GTMAC (j, n). The resonances between 3.78 - 3.92 ppm and 3.92 - 4.15 ppm are attributed to the methine protons in the polymer backbone (c, e) and (a), respectively. The resonance at 4.42 ppm is assigned to the methine proton in the GTMAC (k).

The %HS of P[(VA)-*r*-(VOE)-*r*-(VETMAC)-*g*-(hPG-PETMAC-OE)] was determined using Equation 5.1 to be 3.8%, which is less than 5.6% determined for P[(VA)-*r*-(VOE)-*g*-(hPG-OE)]. This decrease has been attributed to the decrease in hydroxyl content and increased

steric hindrance with the previous addition of GTMAC. The added hydrophobic character reduced the CD from 1.34 meq g^{-1} in P[(VA)-*r*-(VETMAC)-*g*-(hPG-PETMAC)] to 1.23 meq g^{-1} for P[(VA)-*r*-(VOE)-*r*-(VETMAC)-*g*-(hPG-PETMAC-OE)], the CD was determined by Equation 5.3.

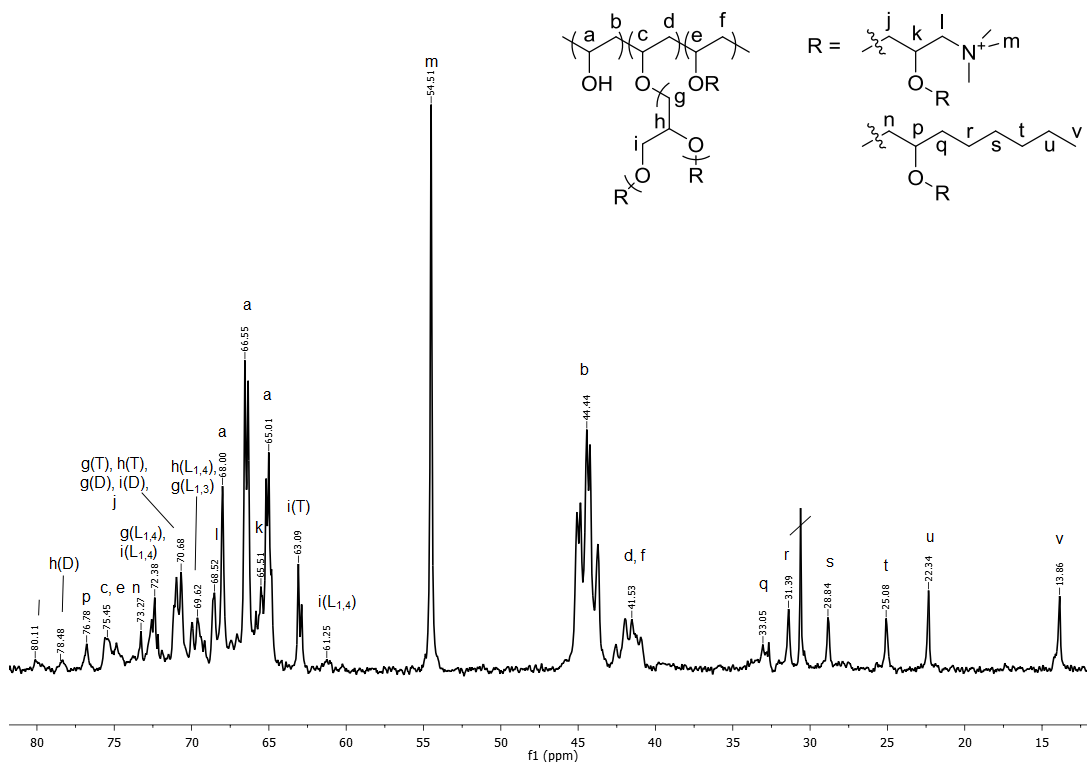


Figure 5.14: 176 MHz ^{13}C NMR spectrum of P[(VA)-*r*-(VOE)-*r*-(VETMAC)-*g*-(hPG-PETMAC-OE)] in D_2O

In the ^{13}C NMR spectrum of P[(VA)-*r*-(VOE)-*r*-(VETMAC)-*g*-(hPG-PETMAC-OE)] (Figure 5.14), the resonance at 13.9 ppm is attributed to the methyl carbon atoms in the alkyl chain (v). The resonances at 22.3 ppm, 25.1 ppm, 28.3 ppm, 31.4 ppm, 33.1 ppm are attributed to methylene carbon atoms in the alkyl chain (u), (t), (s), (r) and (q), respectively. The resonances at 41.5 ppm and 44.4 ppm correspond to the methylene carbon atoms in the polymer backbone (d, f) and (b), respectively. The resonance at 54.5 ppm is attributed to the methyl carbon atoms neighbouring the quaternary carbon atom (m). The resonances at 61.3 ppm and 63.1 ppm are attributed to the methylene carbon atoms in hPG (i, $\text{L}_{1,3}$) and (i, T), respectively. The resonances at 65.0 ppm, 66.6 ppm and 68.0 ppm are attributed to the methine carbon atoms on the polymer bone (a) and the resonance at 75.5 ppm is also attributed to methine protons on the polymer backbone (c, e). The resonance at 65.5 ppm

corresponds to the methine carbon atom in GTMAC (k) and the resonance at 68.5 ppm is attributed to the methylene carbon atom neighbouring the quaternary nitrogen atom (l). The resonance at 69.6 ppm is attributed to the methylene and methine carbon atoms in hPG (h, L_{1,4}; g, L_{1,3}) and the resonance at 70.7 ppm correspond carbon atoms in hPG (g, T; h, T; g, D; i, D) and the methylene carbon atom neighbouring the ether linkage in GTMAC (j). The resonance at 72.4 ppm is attributed to the methylene carbon atoms in hPG (g, L_{1,4}; i, L_{1,4}) and the resonance at 73.3 ppm is assigned to the methylene carbon atom neighbouring the ether linkage in the alkyl chain (n). The resonance at 76.8 ppm is attributed to the methine carbon atom in alkyl chain (p). The resonance at 78.5 ppm and 80.1 ppm are attributed to the methine protons in hPG (h, D) and (h, L_{1,3}), respectively.

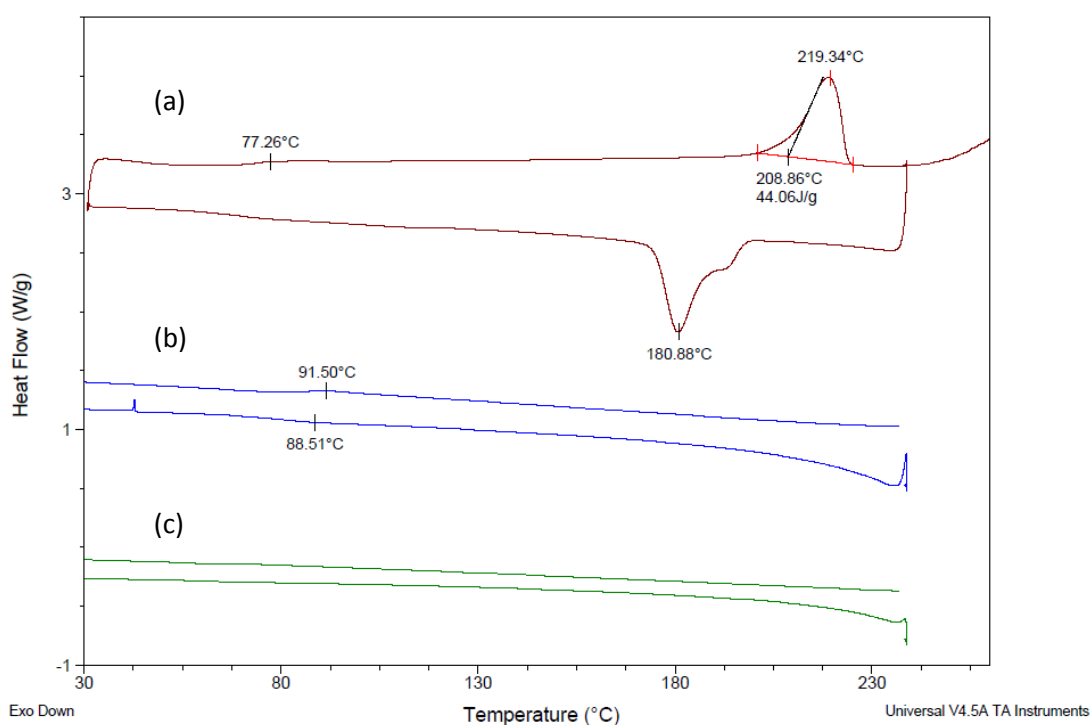


Figure 5.15: DSC thermogram of (a) PVA, (b) P[(VA)-r-(VETMAC)-g-(hPG-PETMAC)] (c) P[(VA)-r-(VOE)-r-(VETMAC)-g-(hPG-PETMAC-OE)]

A comparison of the DSC thermograms of PVA, P[(VA)-r-(VETMAC)-g-(hPG-PETMAC)] and P[(VA)-r-(VOE)-r-(VETMAC)-g-(hPG-PETMAC-OE)] is shown in Figure 5.15. For PVA (Figure 5.15.a) a T_m at 219 °C and T_g at 77 °C is observed and with the addition of hPG and GTMAC in P[(VA)-r-(VETMAC)-g-(hPG-PETMAC)] (Figure 5.15.b) no T_m is observed as the material becomes amorphous, and an increased T_g to 91.50 °C is also observed due to increased chain stiffness. Furthermore, with the addition of epoxyoctane in P[(VA)-r-(VOE)-r-

(VETMAC)-*g*-(hPG-PETMAC-OE)] (Figure 5.15.c) no thermal transitions can be observed by DSC analysis, this might due to the resolution of the thermogram.

5.3.5. Hydrophobic character analysis

The hydrophobicity of the synthesised PVA derivatives was compared based on their water solubility, polymer solutions were tested by preparing 10 mg mL⁻¹ solutions, Table 5.1.

Table 5.1: The aqueous solubility of 10 mg mL⁻¹ solutions of PVA derivatives at ambient temperature (RT), 80 °C and after cooling from 80 °C to RT

Entry	Polymer	RT	80 °C	Cooling to RT
1	PVA	✗	✓	✓
2	P[(VA)- <i>r</i> -(VOE)]	✗	✗	✗
3	P[(VA)- <i>r</i> -(VETMAC)]	✓	✓	✓
4	P[(VA)- <i>r</i> -(VOE)- <i>r</i> -(VETMAC)]	✗	✓	✗
5	P[(VA)- <i>g</i> -(hPG)]	✓	✓	✓
6	P(VOE- <i>r</i> -[VA- <i>g</i> -hPG-OE])	✗	✓	✗
7	P[(VA)- <i>r</i> -(VETMAC)- <i>g</i> -(hPG-PETMAC)]	✓	✓	✓
8	P[(VA)- <i>r</i> -(VOE)- <i>r</i> -(VETMAC)- <i>g</i> -(hPG-PETMAC-OE)]	✗	✓	✓

PVA is a water soluble polymer that requires heating for dissolution in water, but the polymer remains in solution after cooling the heated mixture to RT (Table 5.1, Entry **1**). The addition of alkyl chains results in P[(VA)-*r*-(VOE)] being only partially water soluble at 80 °C as only a small fraction of the material dissolved (Table 5.1, Entry **2**). This change in solubility behaviour shows the increase in hydrophobicity of the polymer.

P[(VA)-*r*-(VETMAC)] is completely water soluble at RT (Table 5.1, Entry **3**) whereas P[(VA)-*r*-(VOE)-*r*-(VETMAC)] is only soluble in water after heating (Table 5.1, Entry **4**). However, when the mixture was cooled to RT the solution solidified. The same change in solubility

behaviour is also observed for the modification of completely soluble at RT P[(VA)-*g*-(hPG)] (Table 5.1, Entry 5) to P(VOE-*r*-[VA-*g*-hPG-OE]) (Table 5.1, Entry 6), which is only in solution at elevated temperatures. Despite their solubility at 80 °C, a precipitate formed during the reactions to synthesise P[(VA)-*r*-(VOE)-*r*-(VETMAC)] and P[(VA)-*r*-(VOE)-*g*-(hPG-OE)]. This is because the saturation point of the mixtures is between 10 mg mL⁻¹ and the concentration of the reaction mixture (125 mg mL⁻¹).

P[(VA)-*r*-(VETMAC)-*g*-(hPG-PETMAC)] is completely soluble at RT in water (Table 5.1, Entry 7) but P[(VA)-*r*-(VOE)-*r*-(VETMAC)-*g*-(hPG-PETMAC-OE)] is not soluble at ambient temperature (Table 5.1, Entry 8). However, P[(VA)-*r*-(VOE)-*r*-(VETMAC)-*g*-(hPG-PETMAC-OE)] showed superior water solubility in comparison with the previously discussed hydrophobic polymers, as it remained in solution at RT after dissolution at 80 °C.

The contact angle of water on polymer films was also used to investigate the hydrophobicity. However, due to the partial solubility of the PVA derivatives in water the contact angle of the material decreased with time, as shown in Figure 5.16 for P[(VA)-*r*-(VOE)-*r*-(VETMAC)-*g*-(hPG-PETMAC-OE)]. Therefore, two values of the contact angle are quoted and discussed, at 0 s and after 10 s.

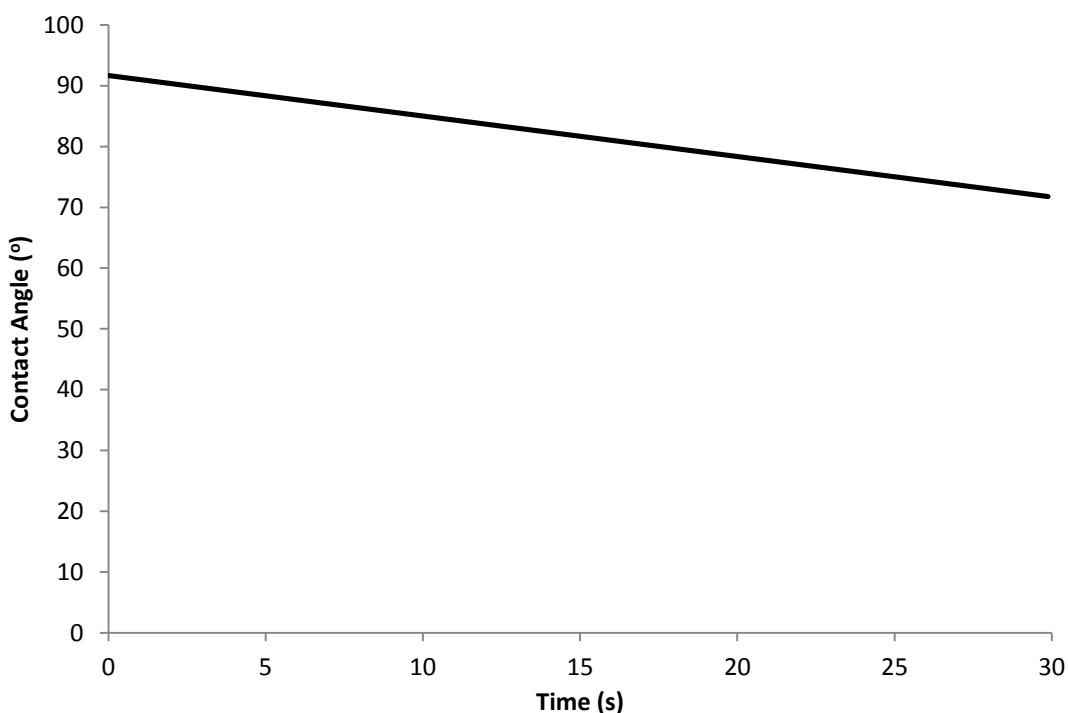


Figure 5.16: Change in contact angle with time for P[(VA)-*r*-(VOE)-*r*-(VETMAC)-*g*-(hPG-PETMAC-OE)]

A comparison between the contact angles of PVA and P[(VA)-*r*-(VOE)] is shown in Figure 5.17. The initial contact angle of PVA decreased from 63° to 39° after 10 s, Figure 5.17.1.A. However, the decrease in contact angle is within experimental error due to the large error bars. The same magnitude of decrease was observed with the inclusion of the alkyl chain in P[(VA)-*r*-(VOE)] as the contact angle decreased from 59° to 32° (Figure 5.19.1.B), but with more precision due to the smaller error bars. This magnitude in decrease was not expected based upon the decrease in solubility of P[(VA)-*r*-(VOE)] compared with PVA (Table 5.1, Entry **1** and **2**). This may possibly be due to the small %HS of P[(VA)-*r*-(VOE)] (1.7%), therefore the film surface was dominated by the presence of PVA, hence the two films display similar wetting behaviour. Furthermore, the difference between the error bars in Figure 5.17.A and 5.17.B is due to the non-uniform film surface observed for PVA in Figure 5.17.2 and Figure 5.17.3, in comparison with the film surface of P[(VA)-*r*-(VOE)] in Figure 5.17.4 and Figure 5.17.5.

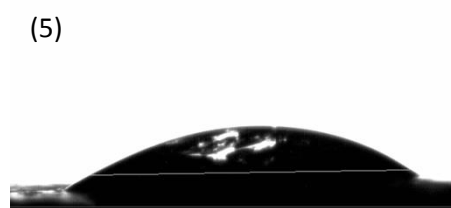
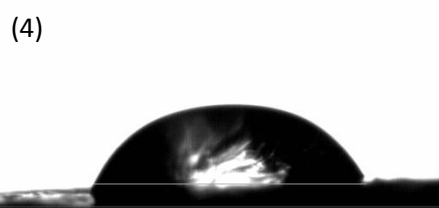
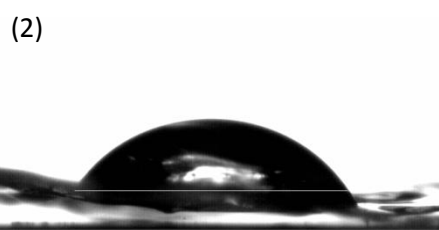
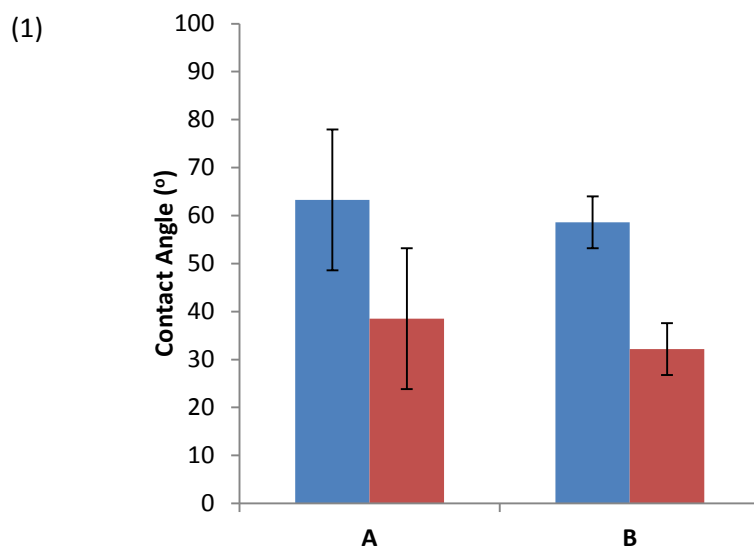


Figure 5.17: (1) Contact angle measurements after 0 s (blue bar) and 10 s (red bar) for (A) PVA (B) P[(VA)-r-(VOE)] (2) Initial contact angle of PVA (3) Contact angle after 10 s of PVA (4) Initial contact angle of P[(VA)-r-(VOE)] (5) Contact angle after 10 s of P[(VA)-r-(VOE)]

A comparison between the contact angles of P[(VA)-r-(VETMAC)] and P[(VA)-r-(VOE)-r-(VETMAC)] is shown in Figure 5.18. There is a negligible change in the initial contact angle of 73° for P[(VA)-r-(VETMAC)] (Figure 5.18.1.C, blue bar) and 72° for P[(VA)-r-(VOE)-r-(VETMAC)] (Figure 5.18.1.D, blue bar). Moreover, the same trend is observed for the contact angles measured after 10 s, as the change from 49° for P[(VA)-r-(VETMAC)] to 43° for P[(VA)-r-(VOE)-r-(VETMAC)] is observed within the experimental error. The lack of change in contact angle between Figure 5.18.1.C and Figure 5.18.1.D is probably due to the small %HS of P[(VA)-r-(VOE)-r-(VETMAC)] (1.7%), hence the two films display similar wetting behaviours.

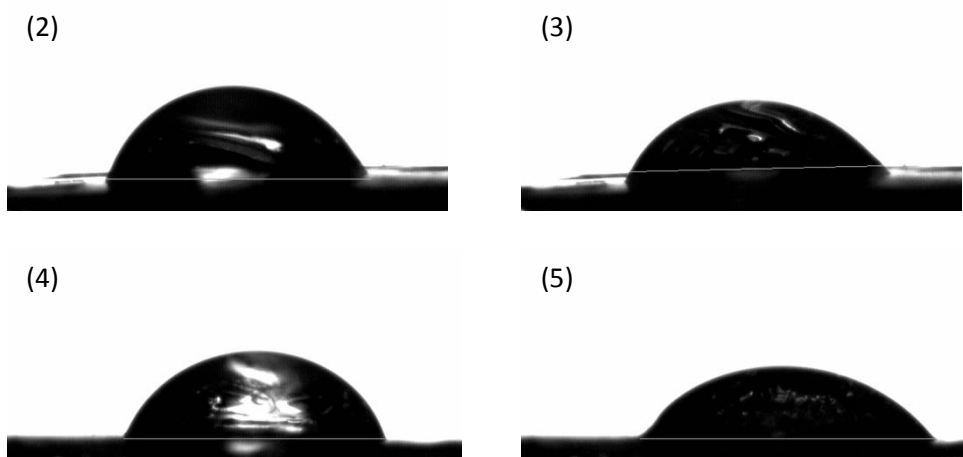
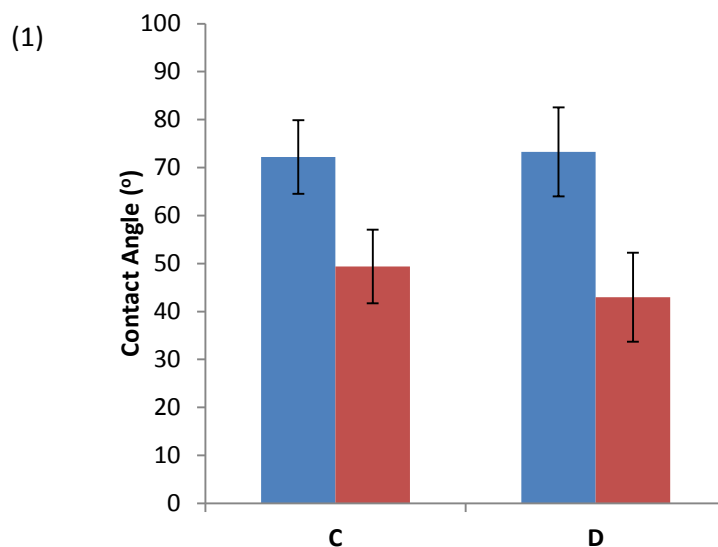


Figure 5.18: (1) Contact angle measurements after 0 s (blue bar) and 10 s (red bar) for (C) P[(VA)-r-(VETMAC)] (D) P[(VA)-r-(VOE)-r-(VETMAC)] (2) Initial contact angle of P[(VA)-r-(VETMAC)] (3) Contact angle after 10 s of P[(VA)-r-(VETMAC)] (4) Initial contact angle of P[(VA)-r-(VOE)-r-(VETMAC)] (5) Contact angle after 10 s of P[(VA)-r-(VOE)-r-(VETMAC)]

A comparison between the contact angles of P[(VA)-g-(hPG)] and P[(VA)-r-(VOE)-g-(hPG-OE)] is shown in Figure 5.19. The initial contact angle of 53° for P[(VA)-g-(hPG)] (Figure 5.19.1.E, blue bar) increased to 79° for P[(VA)-r-(VOE)-g-(hPG-OE)] (Figure 5.19.1.F, blue bar) with the introduction of the long alkyl chain. After 10 s the contact angle of 32° for P[(VOE)-r-(VA)-g-(hPG-OE)] was the same as the contact angle of 39° recorded for P[(VA)-g-(hPG)], which is within the experimental error.

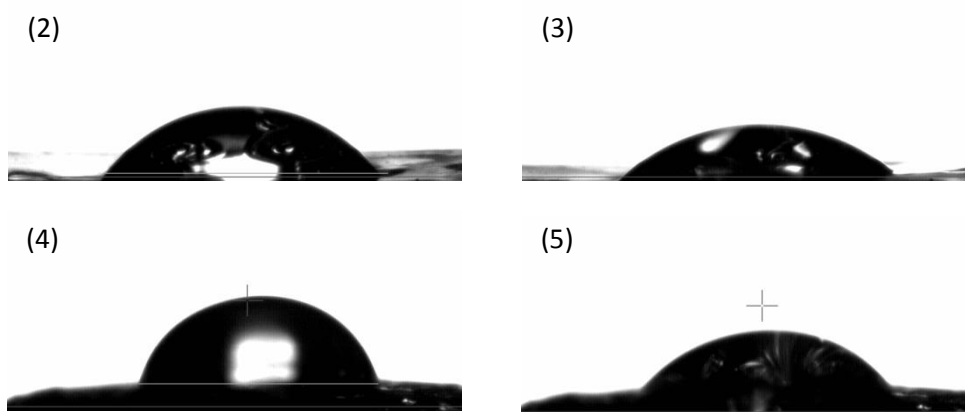
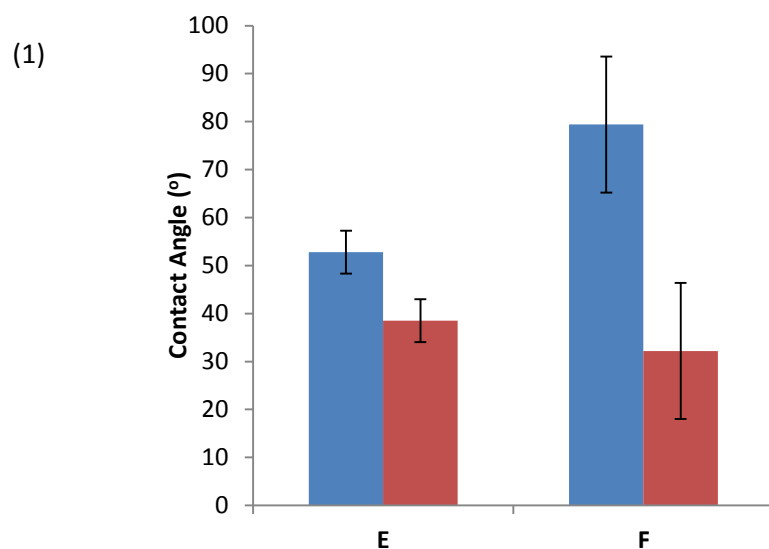
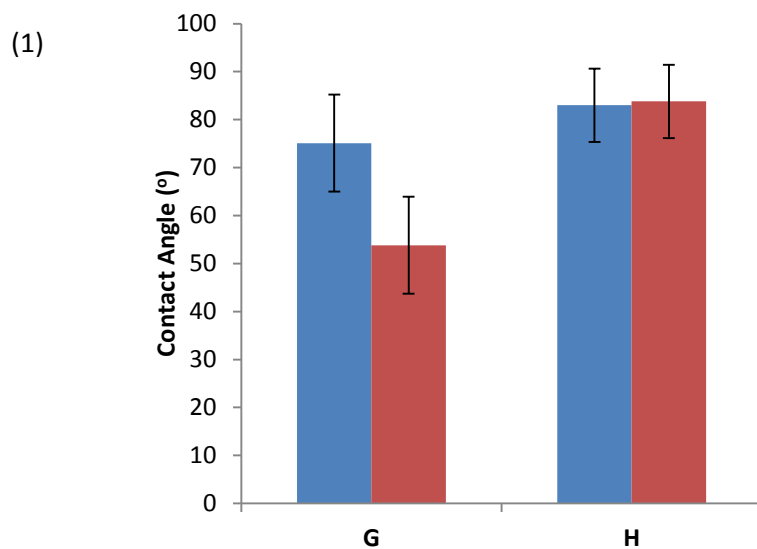


Figure 5.19: (1) Contact angle measurements after 0 s (blue bar) and 10 s (red bar) for (E) P[(VA)-g-(hPG)] (F) P[(VA)-r-(VOE)-g-(hPG-OE)] (2) Initial contact angle of P[(VA)-g-(hPG)] (3) Contact angle after 10 s of P[(VA)-g-(hPG)] (4) Initial contact angle of P[(VA)-r-(VOE)-g-(hPG-OE)] (5) Contact angle after 10 s of P[(VOE)-r-(VA)-g-(hPG-OE)]

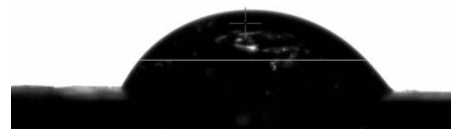
A comparison between the contact angles of P[(VA)-r-(VETMAC)-g-(hPG-PETMAC)] and P[(VA)-r-(VOE)-r-(VETMAC)-g-(hPG-PETMAC-OE)] is shown in Figure 5.20. The inclusion of the alkyl chains in P[(VA)-r-(VOE)-r-(VETMAC)-g-(hPG-PETMAC-OE)] (Figure 5.20.1.H) shows an increase in the initial contact angle to 83° from 75.1° for P[(VA)-r-(VETMAC)-g-(hPG-PETMAC)] (Figure 5.20.1.G). Interestingly, the contact angle of P[(VA)-r-(VOE)-r-(VETMAC)-g-(hPG-PETMAC-OE)] after 10 s is retained at 84°. Therefore, application of P[(VA)-r-(VOE)-r-(VETMAC)-g-(hPG-PETMAC-OE)] for shampoo formulations is predicted to be advantageous due to the increased hydrophobic character.



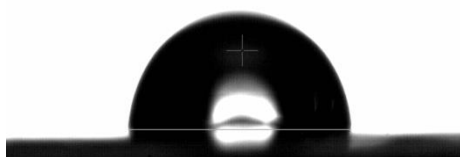
(2)



(3)



(4)



(5)

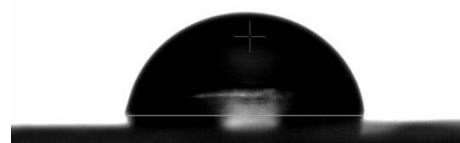


Figure 5.20: (1) Contact angle measurements after 0 s (blue bar) and 10 s (red bar) for (E) P[(VA)-*r*-(VETMAC)-*g*-(hPG-PETMAC)] (F) P[(VA)-*r*-(VOE)-*g*-(hPG-OE)] (2) Initial contact angle of P[(VA)-*r*-(VETMAC)-*g*-(hPG-PETMAC)] (3) Contact angle after 10 s of P[(VA)-*r*-(VETMAC)-*g*-(hPG-PETMAC)] (4) Initial contact angle of P[(VA)-*r*-(VOE)-*r*-(VETMAC)-*g*-(hPG-PETMAC-OE)] (5) Contact angle after 10 s of P[(VA)-*r*-(VOE)-*r*-(VETMAC)-*g*-(hPG-PETMAC-OE)]

Furthermore, Figure 5.21 shows the general trend that all the modifications on PVA increase the hydrophobicity of the material despite the change in water solubility observed for the sample.

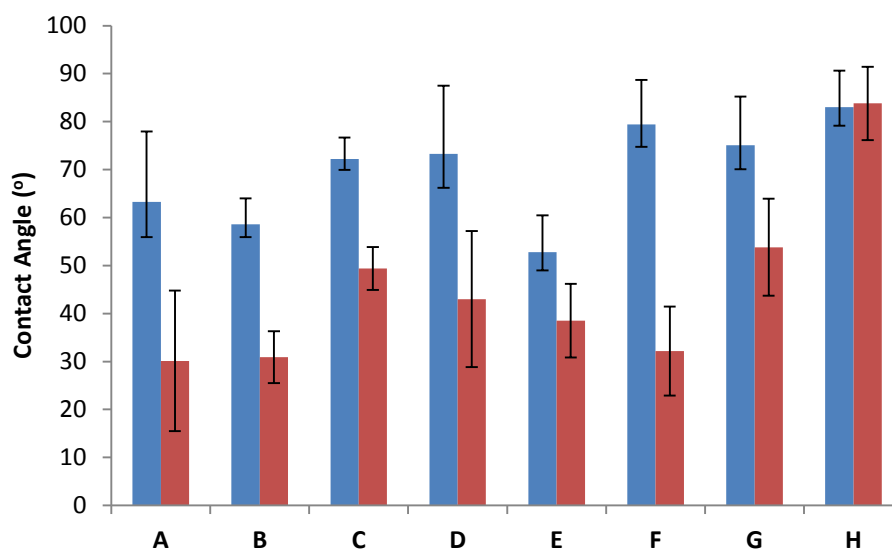


Figure 5.21: Contact angle measurements after 0 s (blue bar) and 10 s (red bar) for (A) PVA (B) P[(VA)-*r*-(VOE)] (C) P[(VA)-*r*-(VETMAC)] (D) P[(VA)-*r*-(VOE)-*r*-(VETMAC)] (E) P[(VA)-*g*-(hPG)] (F) P(VOE-*r*-(VA-*g*-hPG-OE)) (G) P[(VA)-*r*-(VETMAC)-*g*-(hPG-PETMAC)] (H) P[(VA)-*r*-(VOE)-*r*-(VETMAC)-*g*-(hPG-PETMAC-OE)]

5.4. Conclusion

Epoxyoctane was reacted with PVA to synthesise P[(VA)-*r*-(VOE)] with increased hydrophobicity. A %HS of 1.7% was determined by solution and solid state ^1H NMR spectroscopy. However, the recorded contact angles (initial and after 10 s) did not markedly differ. Epoxyoctane was reacted with P[(VA)-*r*-(VETMAC)] to synthesise P[(VA)-*r*-(VOE)-*r*-(VETMAC)] with a %HS of 2.8%, the addition of the alkyl chain reduced the charge density from 0.88 meq g^{-1} in P[(VA)-*r*-(VETMAC)] to 0.82 meq g^{-1} . Therefore, the addition of the alkyl chains does not significantly affect the CD. When epoxyoctane was reacted with the macroinitiator P[(VA)-*g*-(hPG)] to synthesise P(VOE-*r*-(VA-*g*-hPG-OE)), a %HS of 5.6% was recorded due to the increased availability of hydroxyl groups in comparison with PVA and P[(VA)-*r*-(VETMAC)] macroinitiators. In contrast with water insoluble P[(VA)-*r*-(VOE)], the incorporation of hydrophilic GTMAC and hPG in P[(VA)-*r*-(VOE)-*r*-(VETMAC)] and P(VOE-*r*-(VA-*g*-hPG-OE)), respectively, resulted in improved water solubility at 80°C . However, the solutions solidified at ambient temperature.

Epoxyoctane was reacted with P[(VA)-*r*-(VETMAC)-*g*-(hPG-PETMAC)] to synthesise the target material for shampoo formulations, P[(VA)-*r*-(VOE)-*r*-(VETMAC)-*g*-(hPG-PETMAC-

OE)]. The resulting polymer which dissolves in water at 80 °C and remains in solution at ambient temperature, has a %HS of 3.8% and the CD was determined to be 1.23 meq g⁻¹. Moreover, the contact angle of P[(VA)-*r*-(VOE)-*r*-(VETMAC)-*g*-(hPG-PETMAC-OE)] did not decrease with time unlike any of the previously discussed samples in the chapter.

5.5. References

- (1) Santos, O.; Johnson, E. S.; Nylander, T.; Panandiker, R. K.; Sivik, M. R.; Piculell, L. *Langmuir* **2010**, *26*, 9357.
- (2) Goddard, E. D. *J. Soc. Cosmet. Chem.* **1990**, *41*, 23.
- (3) Joshi, D. P.; Pritchard, J. G. *Polymer* **1978**, *19*, 427.
- (4) Marstokk, O.; Roots, J. *Polym. Bull.* **1999**, *42*, 527.
- (5) Aoi, K.; Aoi, H.; Okada, M. *Macromol Chem. Physic* **2002**, *203*, 1018.
- (6) Peppas, N. A.; Merrill, E. W. *J. Appl. Polym. Sci.* **1976**, *20*, 1457.

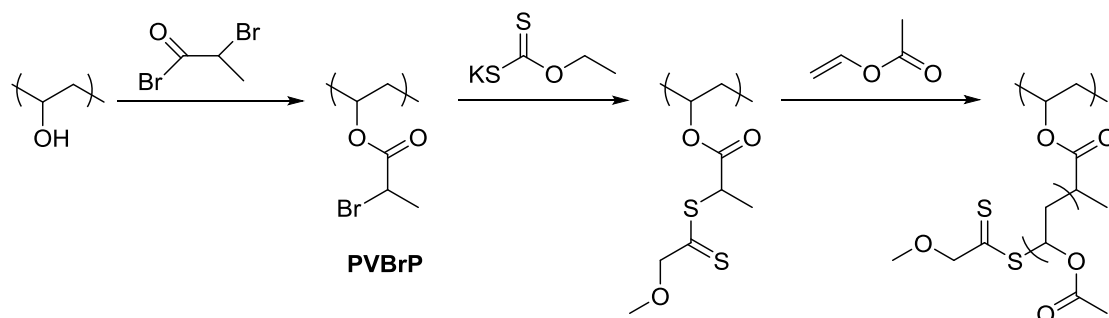
Chapter 6

**Synthesis and characterisation of
poly(vinyl alcohol)-based Reversible-
deactivation radical polymerisation
initiators**

6.1. Introduction

Graft copolymers containing a poly(vinyl alcohol) (PVA) backbone have previously been synthesised by redox initiated free radical polymerisation, using a range of monomers including acrylates and acrylamides.^{1,2,3} However, the graft copolymers synthesised using this technique are predominantly insoluble cross-linked materials.⁴

In an attempt to produce graft copolymers and avoid crosslinking, PVA has been modified to be a macroinitiator for reversible addition-fragmentation chain transfer (RAFT) polymerisation by Bernard *et al.*⁵ Vinyl acetate was then polymerised using the macroinitiator to synthesise poly[(vinyl alcohol)-*graft*-(vinyl acetate)] (P[(VA)-*g*-(VAc)]), Scheme 6.1. However, multimodal traces in size-exclusion chromatography (SEC) chromatograms were observed for the recovered polymers which were attributed to intermolecular and intramolecular termination.



Scheme 6.1: Synthesis of P[(VA)-*g*-(VAc)]

Poly(vinyl, 2-bromopropionate) (PVBBrP), synthesised as an intermediate during the synthesis of P[(VA)-*g*-(VAc)], can act as macroinitiator for reversible - deactivation radical polymerisation (RDRP). RDRP is a class of polymerisation that includes techniques such as atom transfer radical polymerisation (ATRP), which has been used to synthesise graft copolymers with styrene or butyl acrylate side chains using hydroxyethyl (meth)acrylate functionalised to contain an alkyl halide as an initiator. Polymers synthesised by this method have produced monomodal SEC chromatograms^{6,7}

In this chapter the synthesis of PVA-based initiators for RDRP will be discussed, containing varying ratios of PVA and initiating sites (PVBBrP).

6.2. Experimental

6.2.1. Materials

2-Bromopropionic acid ($\geq 99\%$), 1,4-dioxane ($\geq 99\%$), butanone ($\geq 99\%$), 88% low molecular weight (LMW) poly(vinyl alcohol) ($M_w = 1.8 \times 10^4 \text{ g mol}^{-1}$; 88% hydrolysed), dicyclocarbodiimide (DCC) (99%), magnesium sulphate (MgSO_4), dimethyl sulfoxide (DMSO), deuterated acetone (d_6 -acetone), deuterated chloroform (CDCl_3) and sodium bicarbonate (NaHCO_3) ($\geq 99.5\%$) were purchased from Sigma Aldrich and used without further purification. Dichloromethane (DCM), methanol (MeOH), acetone, hydrochloric acid (HCl), diethyl ether and sodium hydroxide (NaOH) were purchased from Fisher Scientific and used without further purification.

6.2.2. Instrumentation

^1H Nuclear magnetic resonance (NMR) spectra were recorded on a Bruker Avance-400 operating at 400 MHz or VNMRS-700 at 700 MHz. ^{13}C NMR spectra were carried out on a VNMRS-700 at 176 MHz.

Fourier transform infra-red spectroscopy (FT-IR) was performed using a Perkin Elmer 1600 Series FT-IR.

Molecular weight analysis of polymer samples was obtained using SEC on a Viscotek TDA 302 with triple detection (refractive index [RI], viscosity and light scattering), using 2 x 300 mL PLgel 5 μm C columns and dimethylformamide (DMF) (containing 0.1% w/v LiBr) as the eluent at a rate of 1 mL min^{-1} (70°C). The system was calibrated using polyethylene glycol standards.

Mass spectra were collected on a *LCT Premier XE* mass spectrometer and an Acquity UPLC (Waters Ltd, UK) using an atmospheric pressure solids analysis probe ionisation to ionise the material at 150°C .

DSC measurements were carried out using a TA Instruments DSC Q1000, samples were heated from -50 and 300°C at a rate of $10^\circ\text{C min}^{-1}$.

CHN Analysis of small molecules was obtained using an Exeter CE-440 elemental analyser.

Thermogravimetric analysis (TGA) measurements were collected using a Perkin Elmer Pyris 1 TGA samples were heated in N_2 to 500°C at a rate of $10^\circ\text{C min}^{-1}$.

6.2.3. Synthesis of 2-bromopropionic anhydride

DCC (11.0 g, 53.2 mmol) in DCM (100.0 mL) was stirred at 0 °C, in a round bottom flask (250 mL) with a mechanical stirrer. 2-bromopropionic acid (9.6 mL, 106.4 mmol) was added slowly at 0 °C. The reaction mixture was stirred for 4 h, acclimatising to room temperature. A white solid precipitated during the reaction which was removed by filtration under reduced pressure. The filtrate was washed with NaHCO_{3(aq)} (5 %wt, 3 x 50.0 mL). The organic layer was dried over MgSO₄ followed by filtration. The solvent was then removed under reduced pressure affording a dark yellow liquid, 2-bromopropionic anhydride (BPAnh). The values were in good agreement with the values in the literature.⁸

Yield = 4.89 g (32%). ¹H NMR (CDCl₃): δ (ppm): 1.89 (dd; 6H; J₁ = 6.88 Hz, J₂ = 0.76 Hz, CH₃), 4.47 (dq; 2H; J₁ = 6.92 Hz, J₂ = 1.28 Hz, CH). ¹³C NMR (CDCl₃): δ (ppm): 21.0 (CH₃), 39.3 (CH), 164.5 (COOC). MS: 288 [M+]. FT-IR ν (cm⁻¹): 2934 (ν C-H), 1816 (ν CO-O-CO), 1750 (ν CO-O-CO). CHN: Expected = %C = 25.03, %H = 2.8, %N = 0%; Measured = %C = 25.92, %H = 3.03, %N = 0.16. B.p. = 128 °C (at 1 atm).

6.2.4. Synthesis of poly[(vinyl, 2-bromopropionate)-*ran*-(vinyl, 2-butyral)]

88% LMW PVA (0.5 g, 10.0 mmol) was stirred in butanone (5.0 mL) at 80 °C, in a round bottom flask (50 mL) equipped with a water cooled condenser and a magnetic stirrer bar. BPAnh (3.6 g, 12.5 mmol) was added to the heterogeneous mixture. The resulting homogeneous purple reaction mixture was added to water precipitating a purple solid which was neutralised with NaHCO_{3(aq)} (5 %wt). The solid was purified by dissolving in acetone and adding to water. The purple solid product, poly[(vinyl, 2-bromopropionate)-*ran*-(vinyl, 2-butyral)] (P[(VBrP)-*r*-(VByl)]) was dried under reduced pressure.

Yield = 0.563 g (31%). ¹H NMR (d₆-acetone): δ (ppm): 0.90 (s, 3H, CCH₂CH₃), 1.08 (s, 2H, CCH₂CH₃), 1.21 (s, 3H, CH₃CCH₂), 1.32 (s, 3H, CH₃CCH₂), 1.43 (s, 2H, CHCH₂), 1.55 (s, 2H, CCH₂CH₃), 1.69 (s, 2H, CHCH₂), 1.79 (s, 3H, CH₃CHBr), 1.85 (s, 2H, CHCH₂), 1.98 (s, 3H, CH₃CO), 4.02 (m, 1H, CHCH₂), 4.53 (s, 1H, CH₃CHBr), 4.93 (s, 1H, CHCH₂), 5.14 (m, 1H, CHCH₂). ¹³C NMR (d₆-acetone): δ (ppm): 8.0 (CCH₂CH₃), 9.1 (CCH₂CH₃), 18.4 (CH₃CCH₂), 21.3 (COCH₃), 22.2 (CH₃CHBr), 25.1 (CH₃CH₂C), 27.3 (CH₃CCH₂), 36.6 (CH₃CH₂C), 38.7 (CHCH₂), 39.9 (CH₃CHBr), 42.1 (CHCH₂), 44.6 (CHCH₂), 65.7 (CHCH₂), 68.2 (CHCH₂), 70.3 (CHCH₂), 100.5 (C), 101.5 (C), 170.1 (CO), 170.7 (CO). FT-IR ν (cm⁻¹): 3302 (ν -OH), 2960 (ν C-H), 1732 (ν C=O), 1216 (ν C(OR)₂). SEC: M_p = 2.58 x 10⁴ g mol⁻¹, Đ = 1.94. T_d = 240 °C.

6.2.5. Synthesis of poly[(vinyl alcohol)-*ran*-(vinyl, 2-bromopropionate)]

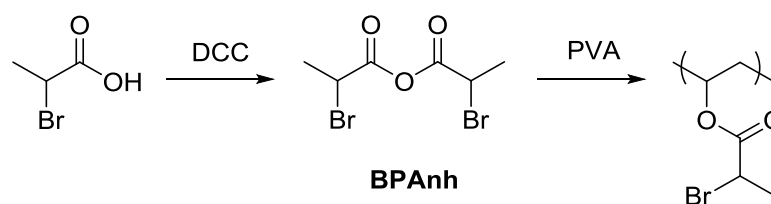
88% LMW PVA (0.15 - 3 g, 3 - 60 mmol) was stirred in 1,4-dioxane (10 - 30 mL) at 80 °C in a round bottom flask (50 - 100 mL) equipped with a water cooled condenser and magnetic stirrer bar. BPA_{nh} (1 - 20.73 g, 3.51 - 72.7 mmol, 120% or 200% mol) was added to the heterogeneous reaction mixture. The reaction proceeded to become a homogeneous purple mixture and was added into water precipitating a purple solid. The non-solvent was then neutralised with NaHCO_{3(aq)} (5 %wt). The solid was purified by dissolving in acetone and adding to water. The purple solid product, poly[(vinyl alcohol)-*ran*-(vinyl, 2-bromopropionate)] (P[(VA)-*r*-(VBrP)]) and was then dried under reduced pressure.

Yield = 6.71g (63%). ¹H NMR (d₆-acetone): δ (ppm): 1.29 (m, 6H, CH₃C), 1.54 (m, 3H, CH₃CH), 1.66 (m, 2H, CH₂CH), 1.80 (m, 3H, CH₃CH), 1.98 (m, 2H, CH₂CH), 2.09 (m, 3H, CH₃CO), 3.73 (m, 1H, CH₂CH), 4.53 (m, 1H, CHBr), 5.06 (m, 1H, CH₂CH). ¹³C NMR (d₆-acetone): δ (ppm): 16.3 (CH₃CH), 20.3 (CH₃CO), 24.3 (CH₃C), 29.8 (CH₃C), 38.9 (CH₂CH), 40.7 (CHBr), 42.8 (CH₂CH), 63.6 (CH₂CH), 69.2 (CH₂CH), 169.3 (CO), 169.7 (COCH₃). FT-IR ν (cm⁻¹): 2936(ν_{C-H}), 1728 (ν_{C=O}). SEC: M_p = 3.88 x 10⁴ g mol⁻¹, Đ = 3.92. T_d = 232 °C.

6.3. Results & Discussion

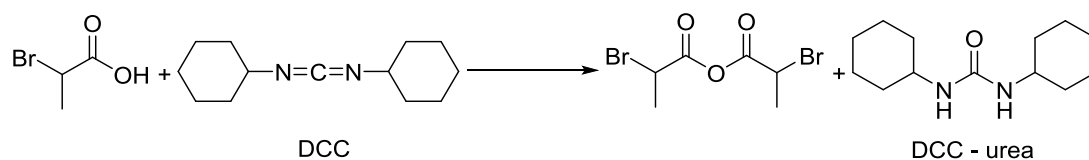
6.3.1. Synthesis of 2-bromopropionic anhydride

An alternative method to synthesise PVBrP, shown in Scheme 6.1, is proposed in Scheme 6.2 using BPA_{nh}. This was to make the method more robust to impurities by avoiding the use of 'dry' solvents, as 2-bromopropionyl bromide (used in Scheme 6.1) is highly reactive towards water.



Scheme 6.2: Synthesis of PVBrP using BPA_{nh}

BPA_{nh} was synthesised by Steglich esterification of 2-bromopropionic acid with DCC in dichloromethane, Scheme 6.3.



Scheme 6.3: Synthesis of BPAh by Steglich esterification

DCC-urea precipitated as the reaction proceeded indicating the formation of the anhydride bond. DCC-urea was removed by filtration at the end of the reaction. BPAh was purified by washing with $\text{HNaCO}_{3(\text{aq})}$ to remove unreacted 2-bromopropionic acid.

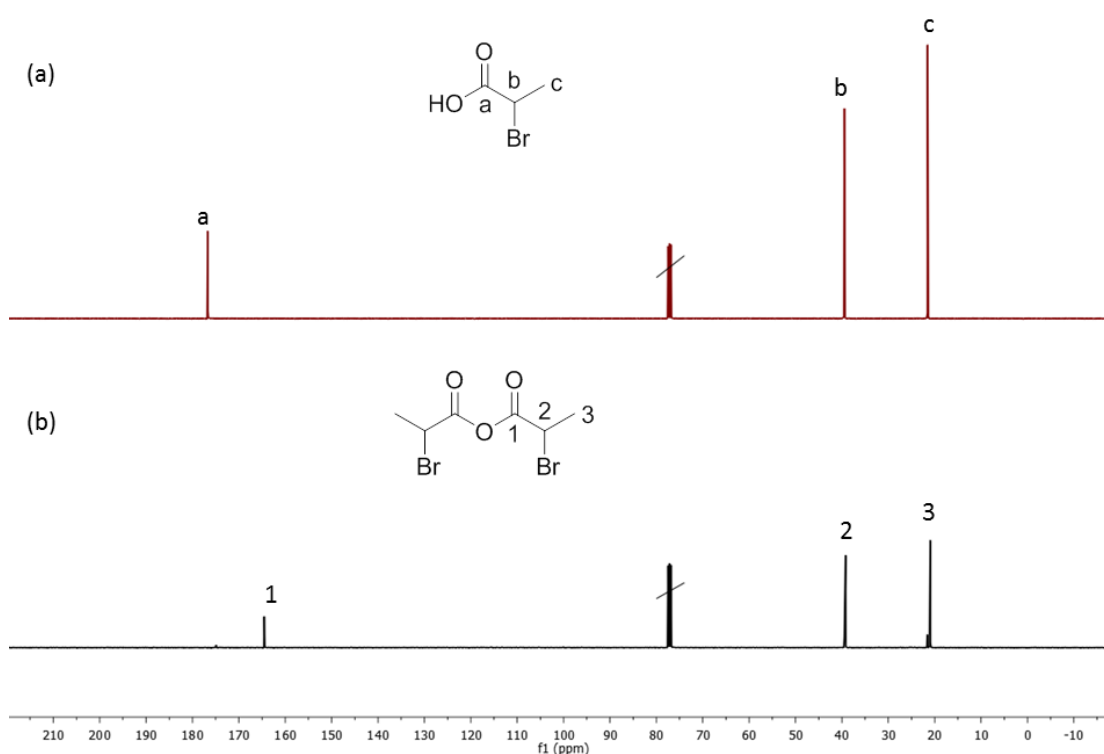


Figure 6.1: 176 MHz ^{13}C NMR spectra in CDCl_3 (a) 2-bromopropionic acid (b) BPAh

A comparison of the ^{13}C NMR spectra of 2-bromopropionic acid and BPAh is shown in Figure 6.1. The resonance at 174.0 ppm in Figure 6.1.a is attributed to the carboxylic acid carbon atom in 2-bromopropionic acid (a), whereas the resonance for the carbonyl carbon is shifted upfield to 164.5 ppm in Figure 6.1.b, showing formation of the anhydride (1). The methine carbon atom (2) corresponds to the resonance at 39.3 ppm and the methyl carbon atom (3) is assigned to resonance at 21.0 ppm in Figure 6.1.b.

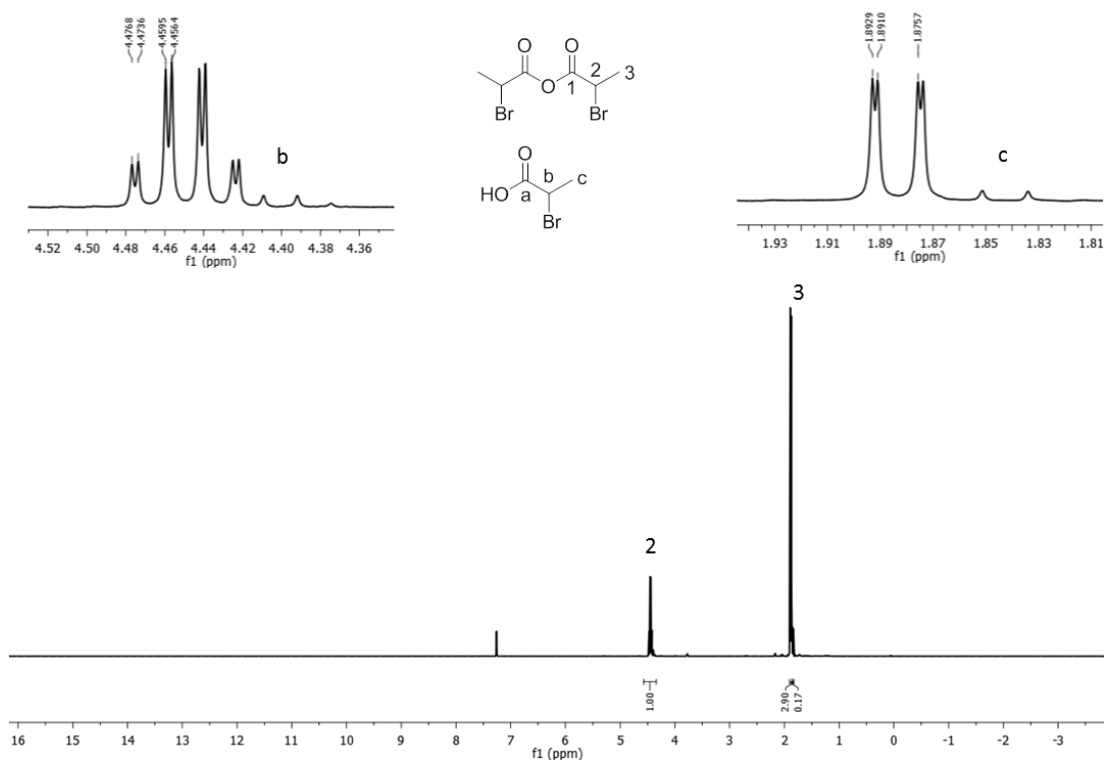


Figure 6.2: 400 MHz ^1H NMR spectrum of BPAnh in CDCl_3

In the ^1H NMR spectrum of BPAnh, shown in Figure 6.2, the resonance at 1.89 ppm is assigned to the methyl protons (3), the resonance is split into a double doublet (dd), due to the neighbouring methine proton attached to chiral centre. The resonance at 4.46 ppm is attributed to the methine proton (2), the resonance is split into a double quartet (dq), from the adjacent methyl protons attached to a chiral centre. Trace resonances corresponding to 2-bromopropionic acid, the starting material, are seen slightly upfield of the resonances assigned to the anhydride (e.g. 1.84 ppm [c] and 4.40 ppm [b]).

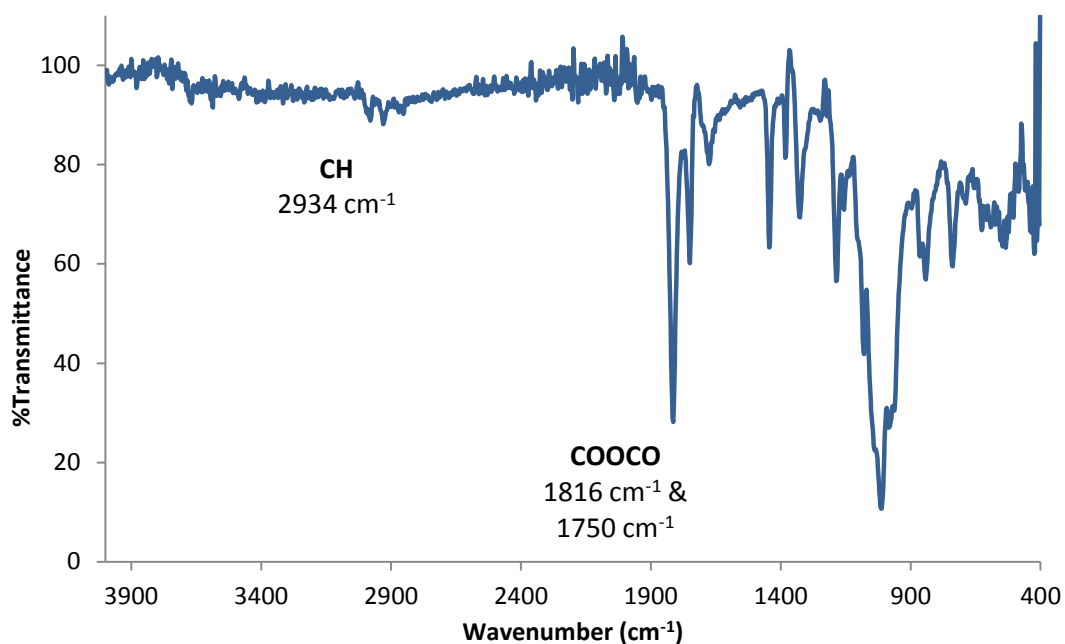


Figure 6.3: FT-IR spectrum of BPAh

The FT-IR spectrum (Figure 6.3) shows two signals separated by approximately 60 cm^{-1} at 1816 cm^{-1} and 1750 cm^{-1} , this is characteristic of an anhydride.

The atmospheric solids analysis probe (ASAP) mass spectrum, Figure 6.4, does not show the predicted mass at 287.88 g mol^{-1} for the product. However, a triplet of signals centred at 317.88 g mol^{-1} with an intensity ratio of 1:2:1 can be observed, this ratio is characteristic of a molecule containing two bromine atoms. No explanation for the 30 g mol^{-1} increase in molecular weight can be proposed.

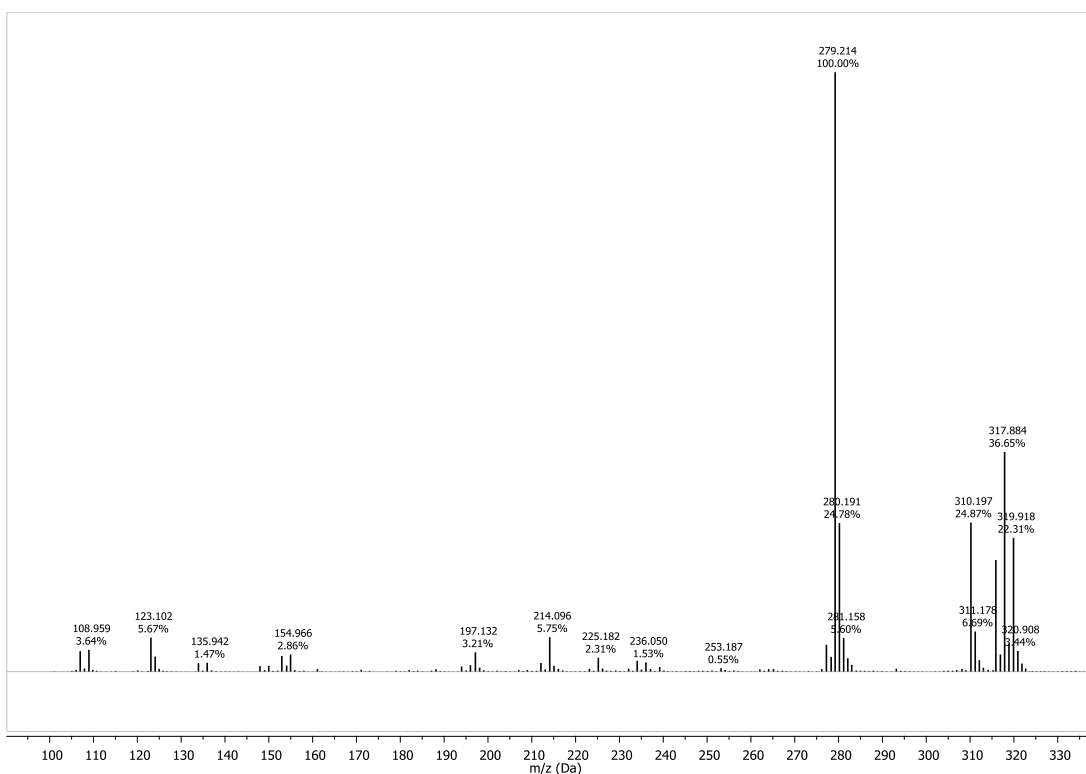
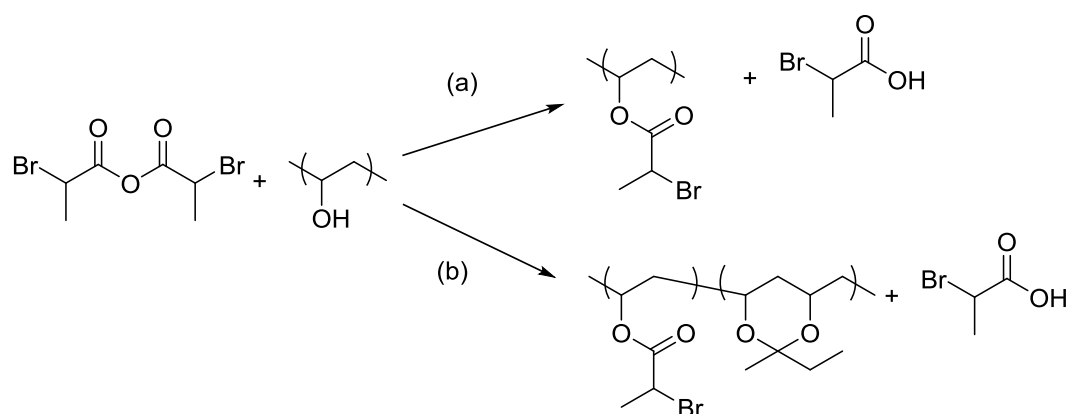


Figure 6.4: ASAP mass spectrum of BPAh

CHN analysis was carried out on BPAh with a found composition of %C = 25.92, %H = 3.03 and %N = 0.16. The ratios are in good agreement with the expected values (%C = 25.03, %H = 2.8 and %N = 0) indicating the successful synthesis of BPAh. However, the detection of nitrogen in the sample shows that DCC-urea remains in the sample, which also accounts for the slight increase in the found %C and %H than expected.

6.3.2. Synthesis of poly[(vinyl, 2-bromopropionate)-*ran*-(vinyl, 2-butyral)]



Scheme 6.4: Synthesis of P[(VBrP)-*r*-(VByI)] in butanone (a) proposed product (b) observed product

A heterogeneous mixture of 88% LMW PVA and BPA_nh in butanone was stirred for 24 h at 80 °C to synthesise PVBrP, Scheme 6.4.a. The reaction mixture proceeded to become homogeneous as the reaction proceeded and a purple solid was recovered *via* precipitation. The product of the reaction was analysed by ¹H NMR spectroscopy, Figure 6.5.

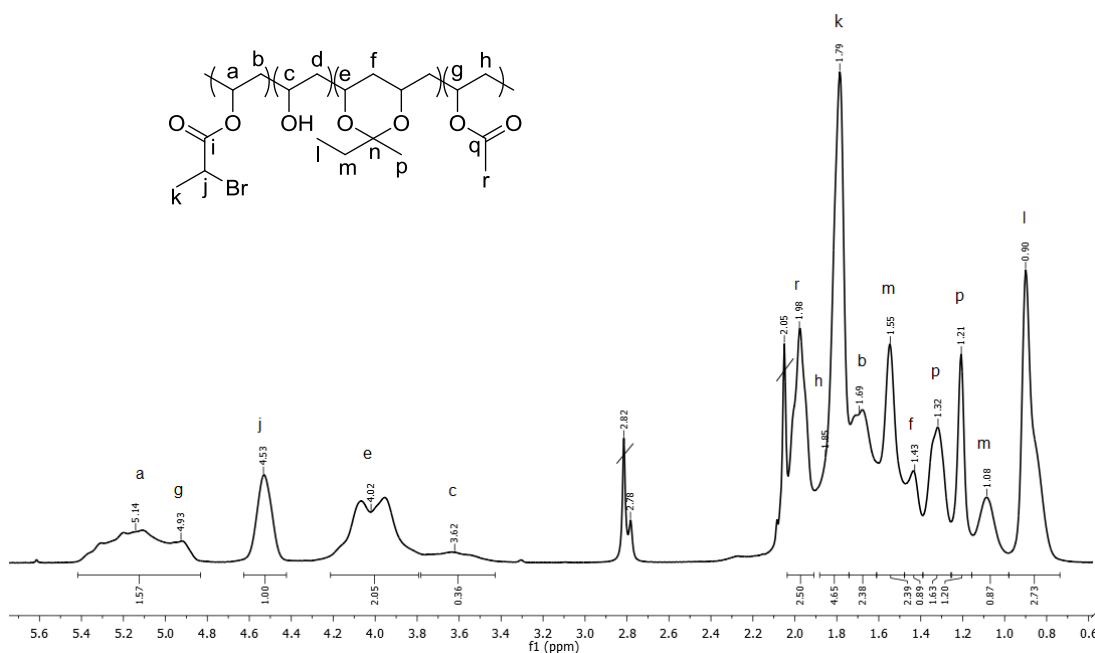


Figure 6.5: 400 MHz ¹H NMR spectrum of P[(VBrP)-r-(VByl)] in *d*₆-acetone

The resonances attributed to the PVBrP repeat unit are assigned to 1.79 ppm for the methyl proton (k); 4.53 ppm for the methine neighbouring the bromine atom (j); 1.69 ppm for the methylene proton on the polymer backbone (b); and 5.00 - 5.40 ppm for the methine proton on the polymer backbone (a). The correlation between the methyl protons and methine proton is highlighted in the ¹H - ¹H correlation spectroscopy (COSY) spectrum, Figure 6.6. A resonance at 3.62 ppm is attributed to the methine proton in unreacted PVA. The resonances assigned to the poly(vinyl acetate) (PVAc) repeat unit are at 1.21 ppm for the methyl proton (r); 1.85 ppm for the methylene protons on the backbone (h); and 4.93 ppm for the methine proton on the polymer backbone (g).

However, pure PVBrP was not synthesised as resonances corresponding to poly(vinyl, 2-butyril) (PVByl) repeat units can be assigned to resonances at 0.90 ppm for the methyl proton next to the methylene proton (l); 1.08 ppm and 1.55 ppm for the methylene proton neighbouring the quaternary carbon atom (m). The resonances at 1.21 ppm and 1.32 ppm are due to the methyl proton adjacent to the quaternary carbon atom (p). The resonances

at 1.43 ppm and at 4.02 ppm are attributed to the methylene proton (f) and the methine proton on the polymer backbone (e), respectively. The correlation between the methyl and methylene protons is highlighted in the $^1\text{H} - ^1\text{H}$ COSY spectrum, Figure 6.6. This indicates that butanone, the reaction solvent, has reacted with 88% LMW PVA and that the reaction proceeds *via* Scheme 6.4.b. Therefore, PVBrP synthesised using this method shall be referred to as P[(VBrP)-*r*-(VByl)].

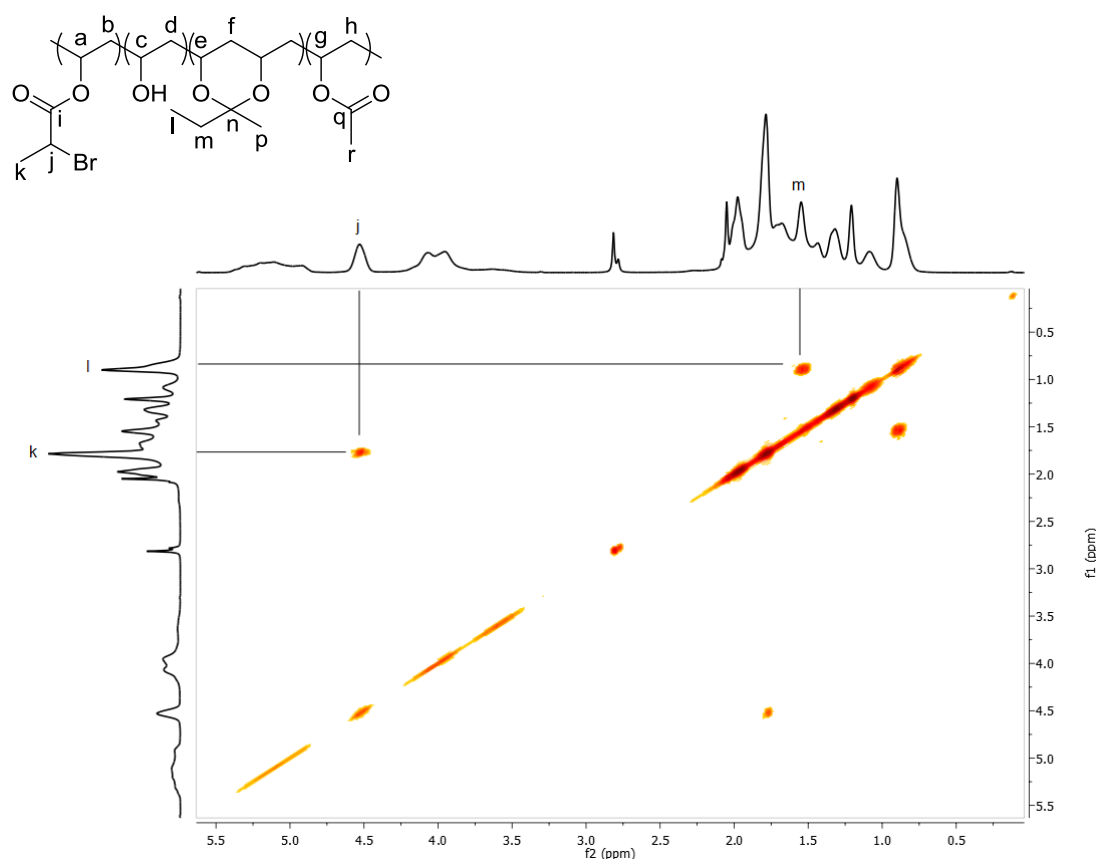


Figure 6.6: 700 MHz $^1\text{H} - ^1\text{H}$ COSY spectrum of P[(VBrP)-*r*-(VByl)] in d_6 -acetone

The characteristic stretch of a ketal functional group can be seen in the FT-IR spectrum of P[(VBrP)-*r*-(VByl)] (Figure 6.7) at 1200 cm^{-1} , supporting the formation of VByl. The stretch at 1738 cm^{-1} shows the ester linkage. Furthermore, a broad stretch is seen at 3326 cm^{-1} , characteristic of a hydroxyl group.

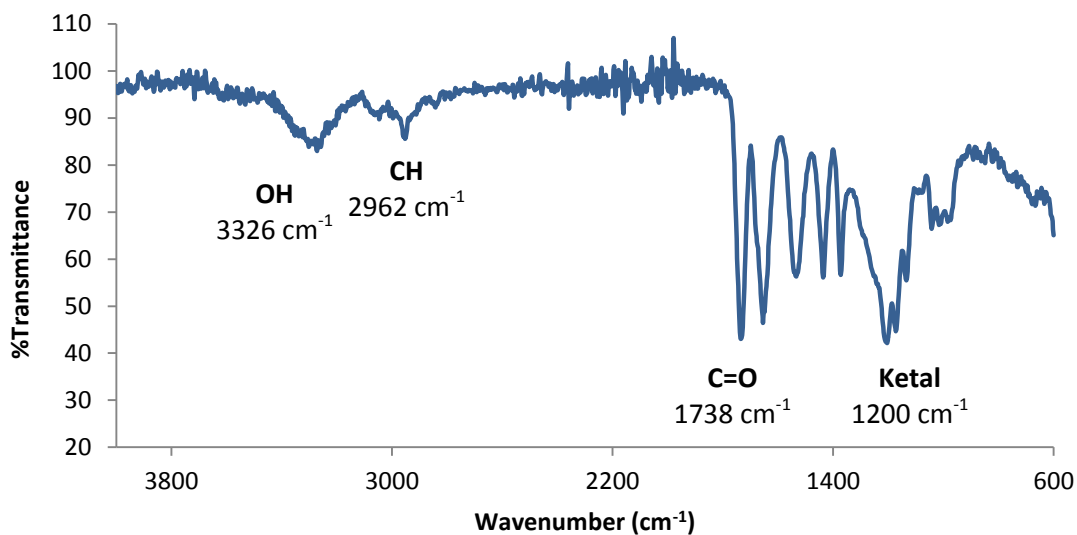


Figure 6.7: FT-IR spectrum of P[(VBrP)-*r*-(VByl)]

The ¹³C NMR spectrum of P[(VBrP)-*r*-(VByl)] is shown in Figure 6.8. Resonances attributed to the PVBrP repeat unit are at 22.1 ppm for the methyl carbon atom (k) and 39.8 ppm for the methine carbon atom adjacent to the bromine atom (j). The resonances at 41.9 ppm are for the methylene carbon atom on the polymer backbone (b), 70.1 ppm for the methine carbon atom on the polymer backbone (a) and 169.9 ppm for the carbonyl carbon atom (i).

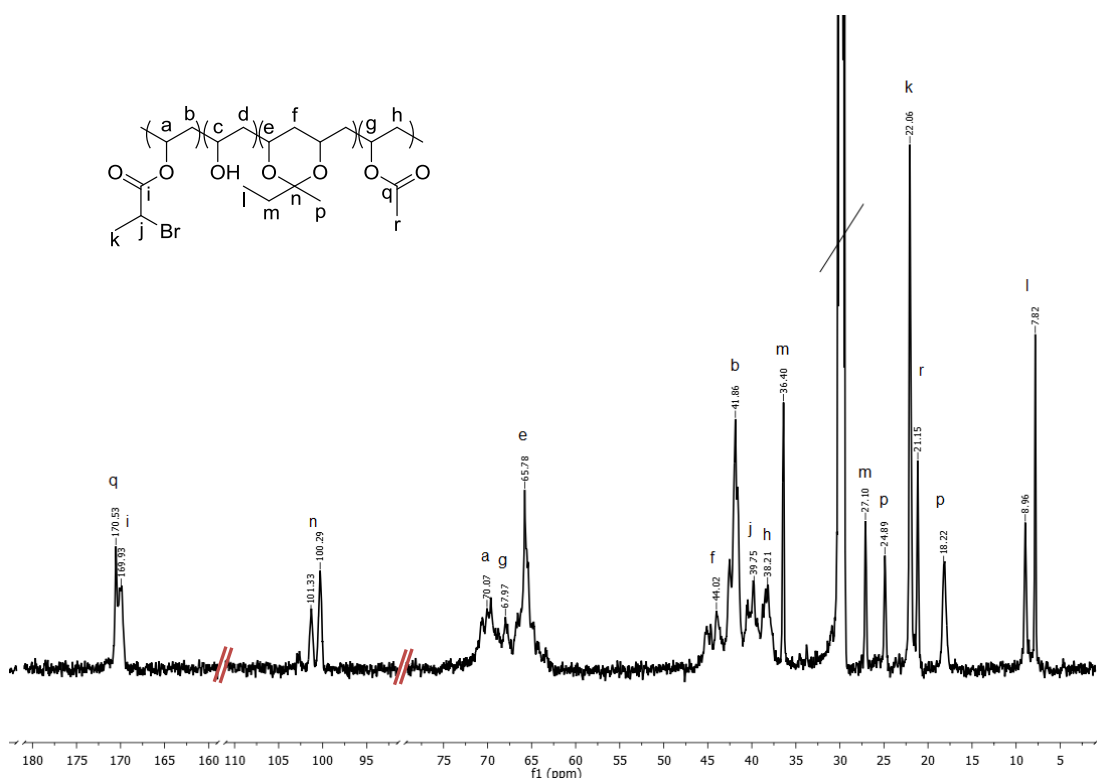


Figure 6.8: 176 MHz ^{13}C NMR spectrum of P[(VBrP)-*r*-(VByl)] in d_6 -acetone

The chiral centre in PVByl results in separate resonances at 7.8 ppm and 9.0 ppm for the methyl carbon atom (l); 18.2 ppm and 24.9 ppm for the methyl carbon atom neighbouring the quaternary carbon (p); 27.1 ppm and 36.4 ppm for the methylene carbon atom neighbouring the quaternary carbon atom (m). The carbon atoms on the polymer backbone in PVByl are attributed to the resonances at 44.0 ppm for the methylene carbon (f) and 65.8 ppm for the methine carbon atom (e). The quaternary carbon atom is attributed to the resonances at 100.3 ppm and 101.3 ppm (n), which correlates to the proton environments of PVByl in the $^1\text{H} - ^{13}\text{C}$ heteronuclear multiple-bond correlation (HMBC) spectrum, Figure 6.9.

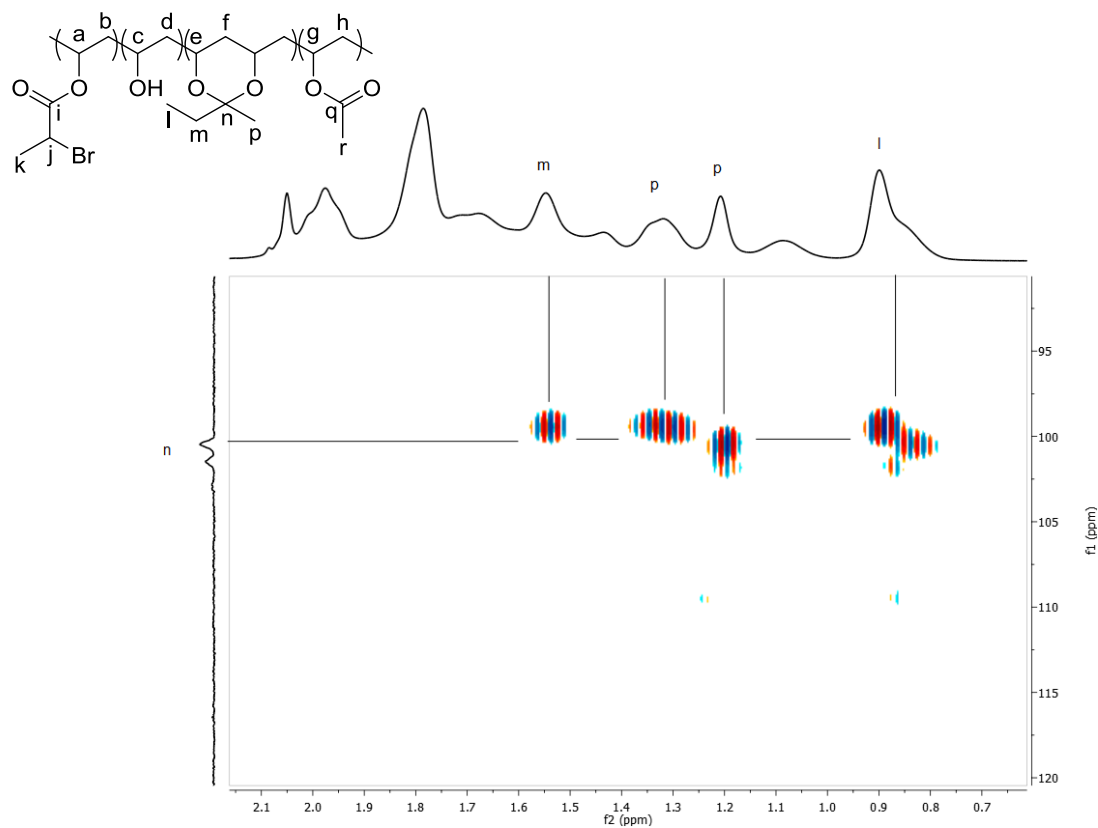


Figure 6.9: 176 MHz ^1H - ^{13}C HMBC spectrum of P[(VBrP)-*r*-(VByl)] in d_6 -acetone highlighting the correlations of the quaternary carbon atom

Resonances attributed to the PVAc repeat unit in Figure 6.9, are assigned to 21.2 ppm for the methyl carbon atom (r) and 38.2 ppm for the methylene carbon atom (h). Resonances at 68.0 ppm are attributed to the methine carbon atom on the polymer backbone (g) and 170.5 ppm to the carbonyl carbon atom (q). The two carbonyl carbon environments were assigned using the ^1H - ^{13}C HMBC spectrum, Figure 6.10.

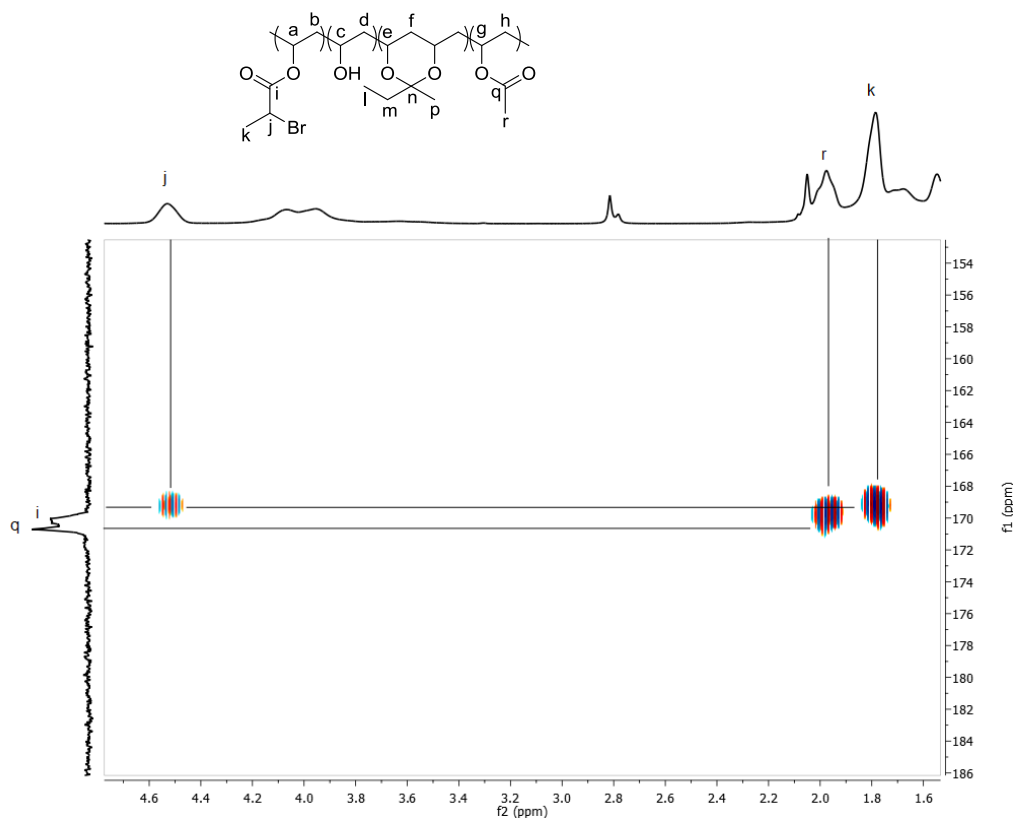


Figure 6.10: 176 MHz $^1\text{H} - ^{13}\text{C}$ HMBC spectrum of P[(VBrP)-*r*-(VByl)] in d_6 -acetone highlighting the correlations of the two carbonyl carbon environments

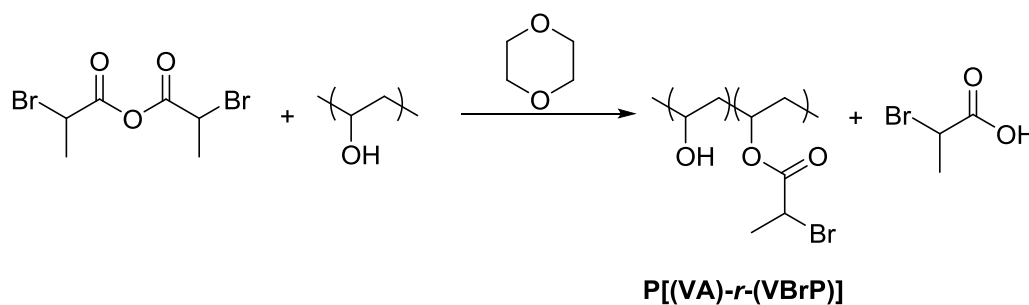
The composition of the copolymer is determined from the ratio of the integrals of the resonances in the ^1H NMR spectrum (Figure 6.5) attributed to PVBrP, PVA and PVByl, using Equation 6.1. The repeat unit to be determined is divided by the sum of the repeat units in the copolymer, the ratio is normalised to account for the degree of acetylation of PVA (12%).

$$\%RU = \frac{\left(\frac{\int RU_i}{n}\right)}{\sum \left(\frac{\int RU_i}{n_i}\right)} \times 0.88 \quad \text{Equation 6.1}$$

Where %RU is the percentage of the repeat unit, RU_i is the generic resonance corresponding to the selected repeat unit (*i.e.* $i = \text{PVBrP, PVA or PVByl}$); and $n =$ number of protons assigned to the resonance. For PVBrP proton environment (j) is used where $RU_i = 4.53$, $n = 1$; for PVA proton environment (c) is used where $RU_i = 3.62$, $n = 1$; and for PVByl proton environment (l) is used where $RU_i = 0.9$, $n = 3$. The composition of the polymer was determined to be 39:35:14:12 (PVBrP:PVByl:PVA:PVAc). P[(VBrP)-*r*-(VByl)] contains 35% PVByl which shows that the efficacy of this reaction is greatly diminished compared to the similar reaction to synthesise poly(vinyl chloroacetate) (PVCA) (discussed in Chapter 2)

which contains 3% PVByl. This could be due to the slower formation of PVBrP segments compared to that of PVCA, so the available time for PVByl to form increases therefore increasing the molar ratio of PVByl. Consequently a lower molar ratio of PVBrP in the product than predicted is determined. An alternative explanation to the low molar ratio of PVBrP, is the purity of BPA_h limits conversion, despite using a 20% molar excess of BPA_h.

6.3.3. Synthesis of poly[(vinyl alcohol)-*ran*-(vinyl, 2-bromopropionate)]



Scheme 6.5: Synthesis of PVBrP

In an attempt to increase the mole fraction of PVBrP in the macroinitiator, 1,4-dioxane was selected as an alternative solvent, based on solubility tests of P[(VBrP)-*r*-(VByl)], for the reaction between 88% LMW PVA and 120% molar ratio of BPA_h, Scheme 6.5. The heterogeneous reaction mixture became a homogeneous as the reaction proceeded, as observed for the synthesis of P[(VBrP)-*r*-(VByl)].

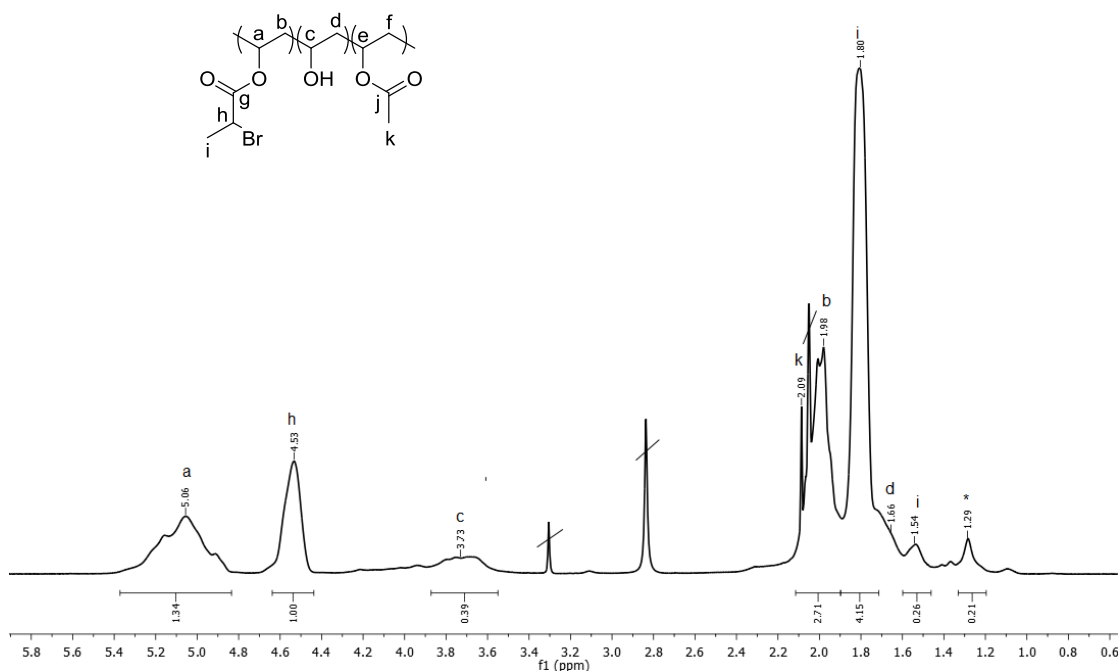


Figure 6.11: 176 MHz ¹H NMR spectrum of P[(VA)-*r*-(VBrP)] in *d*₆-acetone

In the ^1H NMR spectrum shown in Figure 6.11, resonances attributed to the PVBrP segments are observed at 1.54 ppm and 1.80 ppm are assigned to the methyl protons adjacent to the bromine atom (i) and at 4.53 ppm to the methine proton neighbouring the bromine atom (h). The resonances at 1.98 ppm and at 5.06 ppm are attributed to the methylene protons (b) and the methine protons on the polymer backbone (a), respectively. The resonance at 2.09 ppm is attributed to the methyl proton in the PVAc repeat unit (k). The resonances at 1.66 ppm and 3.73 ppm are attributed to methylene (d) and methine (c) on the polymer backbone of unreacted PVA. Therefore, the polymer will be referred to as P[(VA)-*r*-(VBrP)]. The assignments are in good correlation with those reported by Bernard *et al.*⁵

A stretching frequency at 1732 cm^{-1} corresponding to an ester linkage is observed in the FT-IR spectrum, Figure 6.12. However, due to the signal-to-noise ratio of the spectrum further characterisation is not reliable.

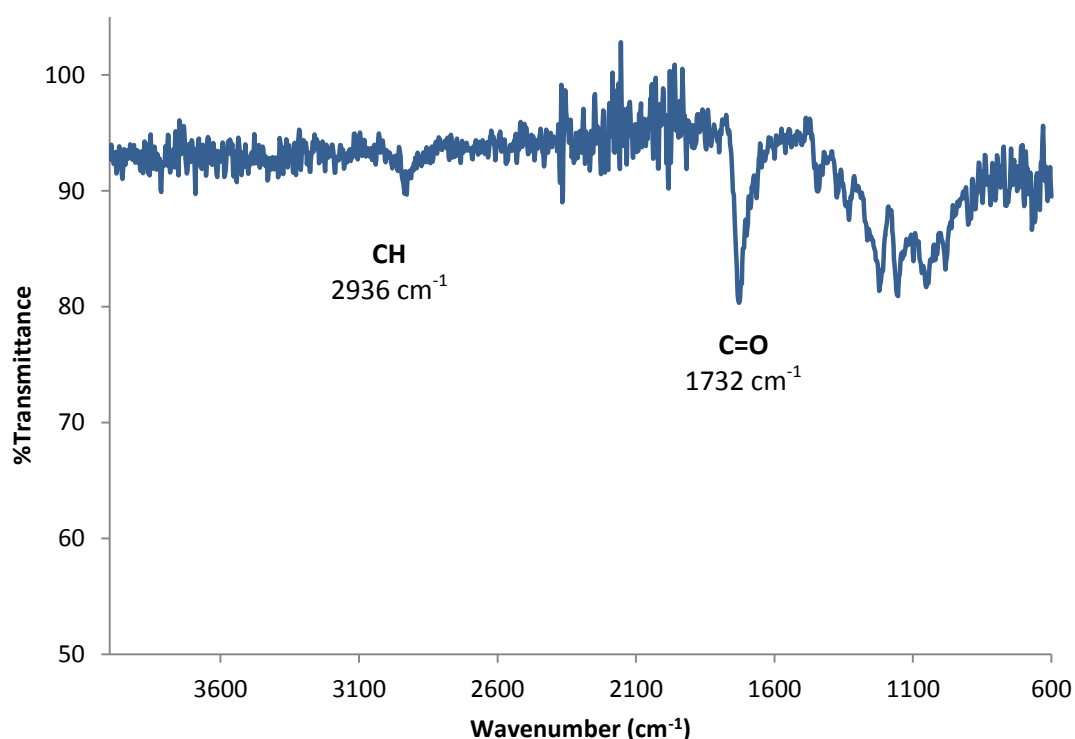


Figure 6.12: FT-IR spectrum of P[(VA)-*r*-(VBrP)]

P[(VA)-*r*-(VBrP)] sample was further characterised by ^{13}C NMR spectroscopy, Figure 6.13. The resonances at 16.3 ppm and 21.2 ppm are attributed to the methyl carbon atoms

adjacent to the bromine atom (i). The carbon atoms on the polymer backbone are attributed to 38.9 ppm for the methylene carbon atom (b) and 69.2 ppm for the methine carbon atom (a). The resonances at 40.7 ppm and 169.3 ppm are attributed to the methine carbon atom (h) and the carbonyl carbon in the PVBrP segments (g), respectively.

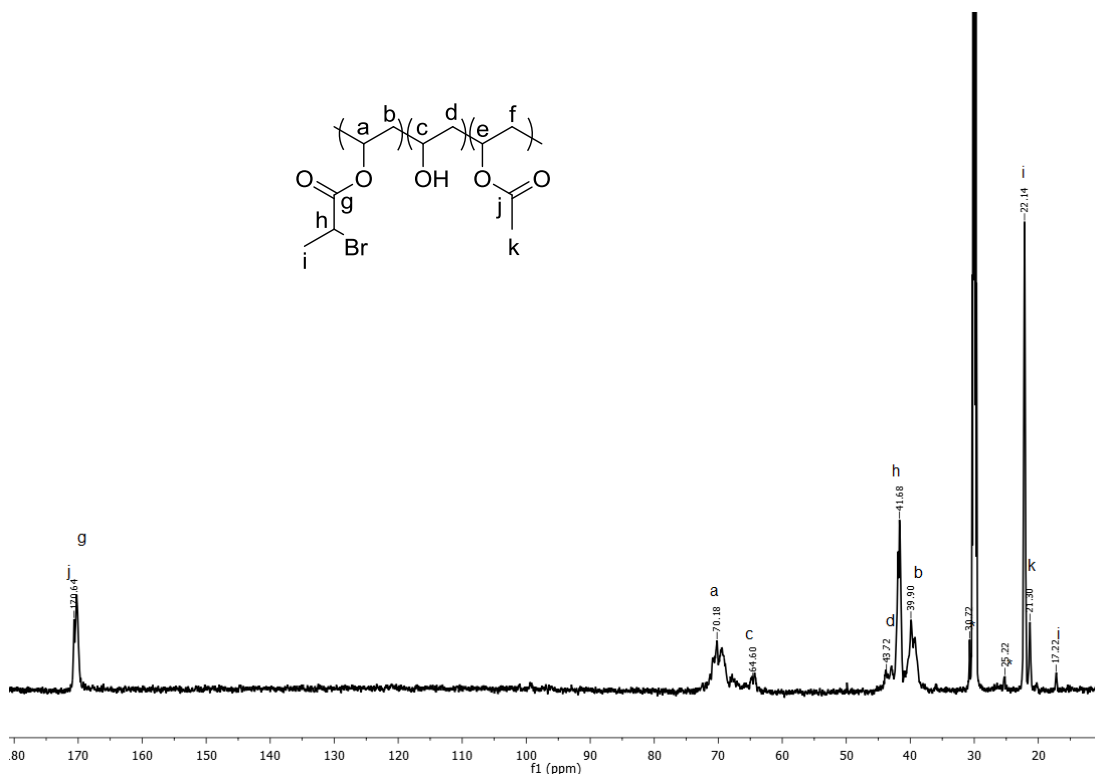


Figure 6.13: 176 MHz ^{13}C NMR spectrum of P[(VA)-r-(VBrP)] in d_6 -acetone

The resonances corresponding to PVAc are attributed to the resonances at 20.3 ppm for the methyl carbon atom (k) and 169.7 ppm for the carbonyl carbon atom (j). The resonances at 45.8 ppm and 63.6 ppm are attributed to the methylene (d) and methine (c) carbon atoms on the PVA backbone, respectively. The assignment of the resonances is supported by the ^1H - ^{13}C heteronuclear single quantum coherence (HSQC) spectrum, Figure 6.14.

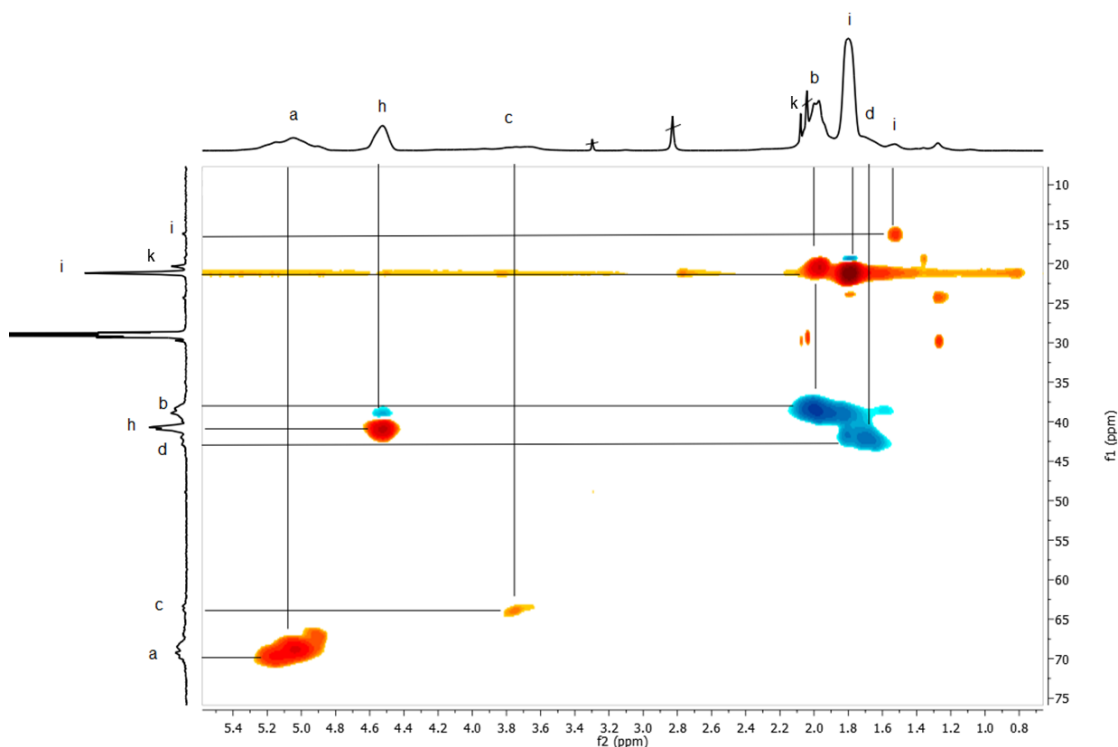


Figure 6.14: 176 MHz ^1H - ^{13}C HSQC spectrum of P[(VA)-*r*-(VBrP)] in d_6 -acetone

Furthermore, the ^1H - ^{13}C HMBC spectrum (Figure 6.15) reveals that the unattributed resonance at 1.29 ppm in the ^1H NMR spectrum (Figure 6.11.*), correlates to an unobservable resonance at 99.0 ppm in the ^{13}C NMR spectrum (Figure 6.13). No other ^1H NMR resonances correlate with the resonance at 99 ppm. Therefore, we propose that a ketal was formed and that poly(vinyl, 2-propyl) (PVPyl) was produced from the reaction between PVA and acetone, the non-solvent used during purification of P[(VA)-*r*-(VBrP)]. This side reaction was not observed in previous reactions using PVA and acetone (Chapters 2-5).

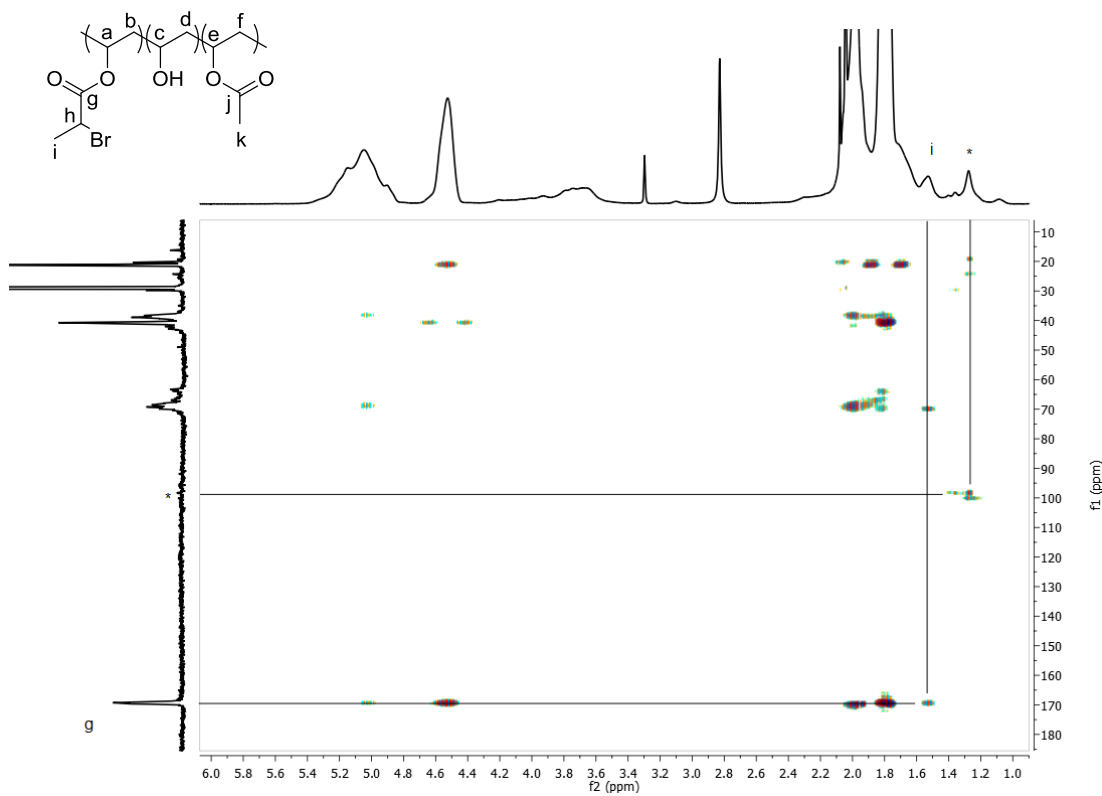


Figure 6.15: 176 MHz ^1H - ^{13}C HMBC NMR spectrum in d_6 -acetone highlighting the correlation between a quaternary carbon and carbonyl carbon atoms in $\text{P}[(\text{VA})\text{-}r\text{-}(\text{VBrP})]$

The normalised SEC chromatograms of the PVA and $\text{P}[(\text{VA})\text{-}r\text{-}(\text{VBrP})]$ are shown in Figure 6.16.

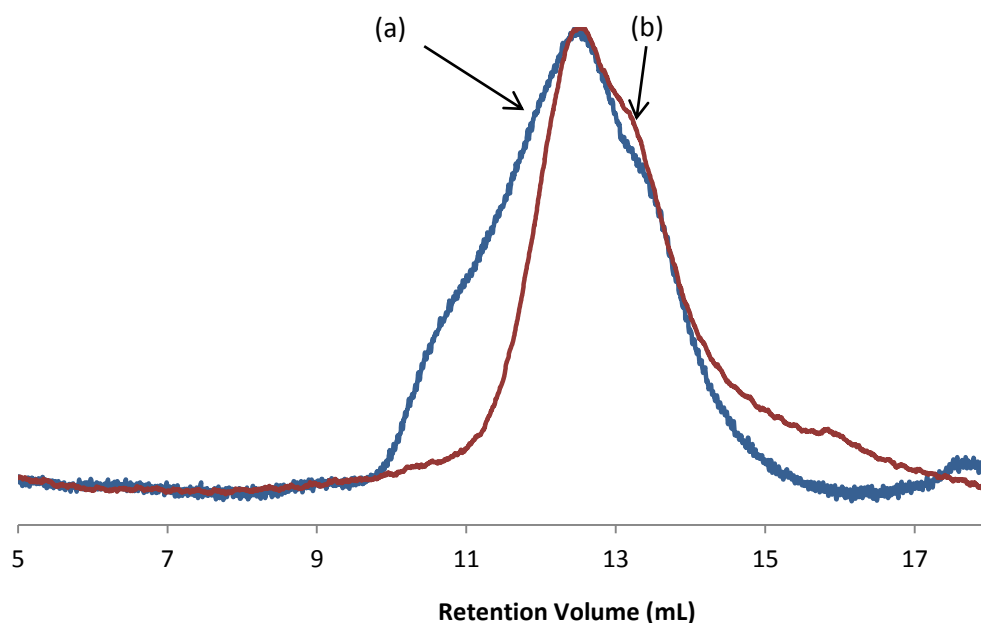


Figure 6.16: Plots of normalised RI vs retention volume for, (a) P[(VA)-*r*-(VBrP)] ($M_p = 3.99 \times 10^4 \text{ g mol}^{-1}$, $\mathcal{D} = 3.06$) (b) 88% LMW PVA ($M_p = 3.79 \times 10^4 \text{ g mol}^{-1}$, $\mathcal{D} = 1.82$)

The SEC analysis (Figure 6.16) shows an increase in the molecular weight (MW) upon the addition of BPA_{nh} to PVA (Figure 6.16.b) forming P[(VA)-*r*-(VBrP)] (Figure 6.16.b) based on the appearance of a high molecular weight shoulder. An increase in dispersity (\mathcal{D}) from 1.82 in 88% LMW PVA to 3.06 for P[(VA)-*r*-(VBrP)] is also observed indicating that all the PVA repeat units have not been modified. Moreover, an accurate MW cannot be obtained due to the hydrodynamic volumes of these complex structures in comparison to PEG standard samples used for calibration for SEC analysis.

The composition of the polymer was determined, using Equation 6.1, to be 62%:24%:12%:2% for PVBrP:PVA:PVAc:PVPyl. Therefore the mole fraction of initiating sites (PVBrP) was successfully increased from 46% in P[(VBrP)-*r*-(VByl)] to 62% in P[(VA)-*r*-(VBrP)].

The molar ratio of BPA_{nh} was increased from 120% to 200% with respect to hydroxyl groups in 88% LMW PVA, as unreacted PVA was observed in the P[(VA)-*r*-(VBrP)] structure. This was done to test the hypothesis that the composition of PVBrP was affected by the purity of BPA_{nh} as DCC-urea and 2-bromopropionic acid were detected in the material (Section 6.3.1).

When the molar excess of BPA_{nh} was increased, the mole fraction of PVBrP repeat units increased from 62% to 79% and no ketal formation could be observed in the ^1H NMR

spectrum, Figure 6.17, due to the absence of resonances at 0.90 ppm, 1.21 ppm, 1.29 ppm, 1.32 ppm and 1.55 ppm. The ^1H NMR spectrum was analysed in a similar manner to the previously shown spectrum of 62% P[(VA)-*r*-(VBrP)] in Figure 6.11.

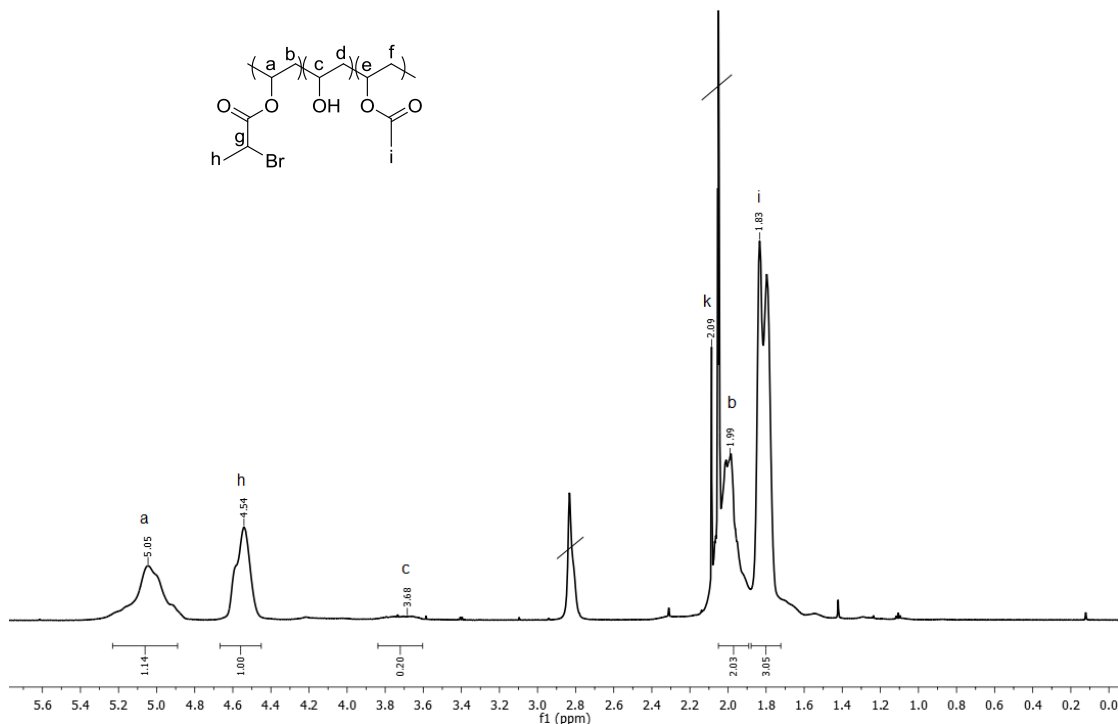


Figure 6.17: 700 MHz ^1H NMR spectrum of 79% P[(VA)-*r*-(VBrP)] in d_6 -acetone

The composition of the polymer was determined to be 79%:9%:12%:0% (PVBrP:PVA:PVAc:PVPyl), showing that the molar equivalents of BPA_nH can limit formation of PVBrP segments. Furthermore, Figure 6.18 compares the SEC chromatograms of 79% P[(VA)-*r*-(VBrP)] and 88% LMW PVA. The M_p has increased from $3.79 \times 10^4 \text{ g mol}^{-1}$ in 88% LMW PVA to $4.03 \times 10^4 \text{ g mol}^{-1}$ upon the addition of VBrP segments. Moreover, the \bar{D} of 1.8 remains the same indicating almost complete conversion of the PVA segments.

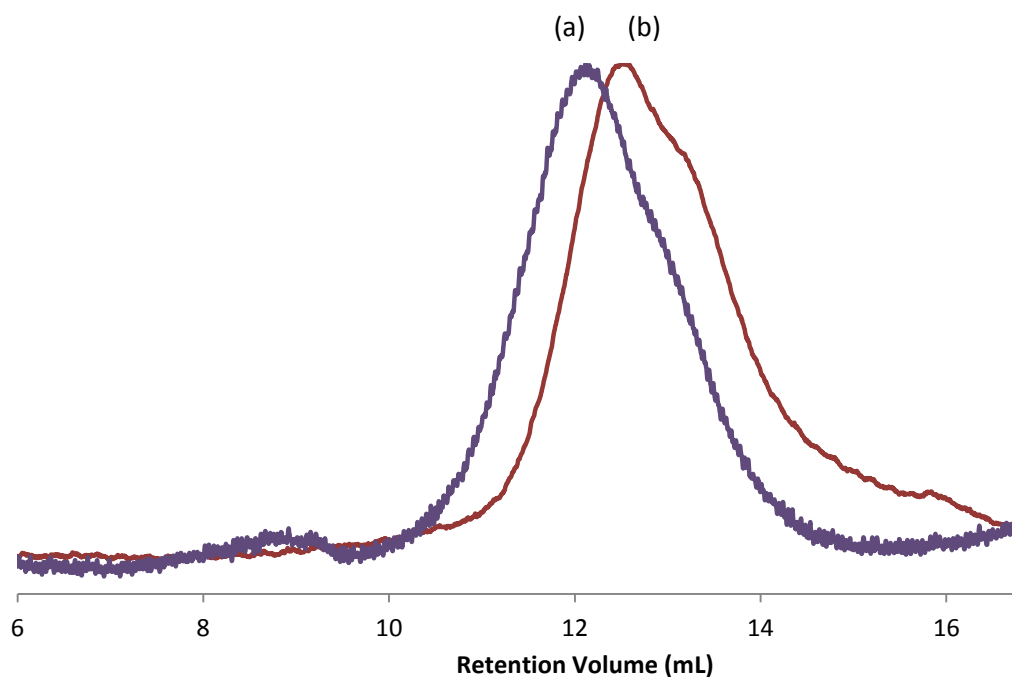


Figure 6.18: Plots of normalised RI vs retention volume for (a) 79% P[(VA)-*r*-(VBrP)] ($M_p = 4.03 \times 10^4 \text{ g mol}^{-1}$, $\mathcal{D} = 1.80$), and (b) 88% LMW PVA ($M_p = 3.79 \times 10^4 \text{ g mol}^{-1}$, $\mathcal{D} = 1.82$)

6.4. Conclusion

BPA_{nh} was synthesised *via* Steglich esterification of 2-bromopropionic acid using DCC. BPA_{nh} was then reacted with 88% LMW PVA in butanone to incorporate VBrP segments in the polymer structure for use as initiating sites. However, PVByl was formed during the reaction limiting the conversion of PVA groups to PVBrP. The resulting P[(VBrP)-*r*-(VByl)] has a composition of 39:35:14:18 (PVBrP:PVByl:PVA:PVAc).

A change in the reaction solvent from butanone to 1,4-dioxane eliminated the formation of PVByl and P[(VA)-*r*-(VBrP)] containing 62% PVBrP segments was synthesised. Increasing the molar quantity of BPA_{nh} increased the molar ratio of PVBrP segments to 79%.

6.5. References

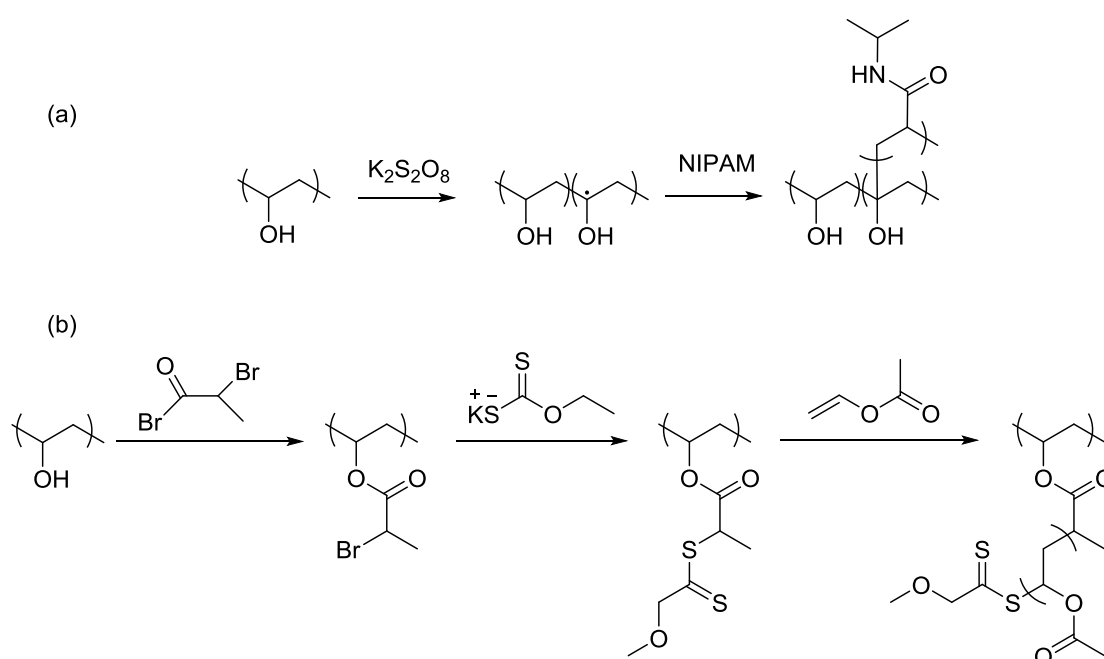
- (1) Liu, Y. H.; Liu, X. H.; Liu, Y. W.; Zhang, J. S.; Deng, K. L.; Liu, Z. J. *Polym. Int.* **2004**, *53*, 1611.
- (2) Lu, Y.; Jing, R.; Kong, Q. M.; Zhu, P. X. *J. Appl. Polym. Sci.* **2014**, *131*, 7.
- (3) Yang, J.; Hu, D. D.; Zhang, H. *React. Funct. Polym.* **2012**, *72*, 438.
- (4) Jabbari, E.; Karbasi, S. *J. Appl. Polym. Sci.* **2004**, *91*, 2862.
- (5) Bernard, J.; Favier, A.; Davis, T. P.; Barner-Kowollik, C.; Stenzel, M. H. *Polymer* **2006**, *47*, 1073.
- (6) Sumerlin, B. S.; Neugebauer, D.; Matyjaszewski, K. *Macromolecules* **2005**, *38*, 702.
- (7) Beers, K. L.; Gaynor, S. G.; Matyjaszewski, K.; Sheiko, S. S.; Moller, M. *Macromolecules* **1998**, *31*, 9413.
- (8) Bischoff, A.; Walden, P. *Chemische Berichte* **1894**, *27*, 2939

Chapter 7

**Reversible-deactivation radical
polymerisation of poly(vinyl alcohol)-
based initiators**

7.1. Introduction

The synthesis of graft copolymers containing a poly(vinyl alcohol) (PVA) backbone using redox initiators has been reported using different monomers and redox systems, *e.g.* methyl methacrylate with cerium ammonium sulphate;¹ acrylamide with ammonium persulfate and sodium bisulfite;² and N-isopropylacrylamide (NIPAM) with potassium peroxydisulfate (Scheme 7.1.a).³ Furthermore, PVA has been modified and used as a chain transfer agent for reversible addition-fragmentation chain transfer (RAFT) polymerisations (Scheme 7.1.b).⁴ However, both of these techniques suffer from bicomination termination, and has also produced cross-linked materials in the case of redox initiated polymerisations.^{1,5}



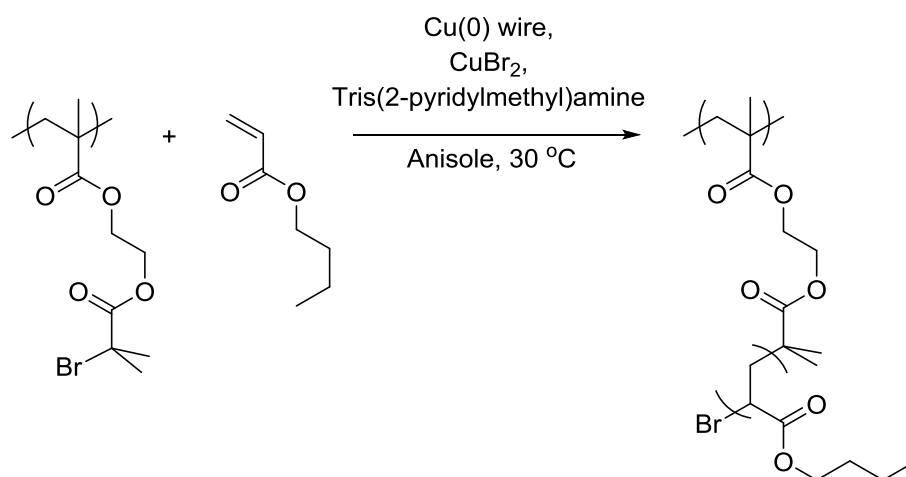
Scheme 7.1: Synthesis of PVA containing graft copolymers (a) Redox initiated NIPAM containing graft copolymer (b) Macro-chain transfer agent and vinyl acetate graft copolymer by RAFT

Various graft copolymers have been reported to be synthesised by reversible deactivation radical polymerisation (RDRP), predominately by atom transfer radical polymerisation (ATRP). Moreover, the monomodal size exclusion chromatography (SEC) traces have shown that molecular brushes without cross-linked side products were produced.^{6,7,8} However, monomer conversions have been kept low in the graft copolymerisations in order to avoid crosslinking.⁹

Single electron transfer-living radical polymerisations (SET-LRP) is a Cu(0) mediated RDRP technique. However, unlike ATRP, SET-LRP is proposed to proceed without the need for the

persistent radical effect because polymers with $\geq 99\%$ chain end functionality have been synthesised.^{10,11} Therefore, as bicombination termination can be avoided, SET-LRP could potentially be used to synthesise molecular brushes without the need to limit the monomer conversion.

The mechanism of Cu(0) mediated RDRP is contested between SET-LRP and supplemental activator and reducing agent (SARA)-ATRP (See Chapter 1, Section 1.3.2.1.2.). Furthermore, SARA-ATRP has been used to produce *n*-butyl acrylate comb polymers with molecular weights greater than $1 \times 10^6 \text{ g mol}^{-1}$, Scheme 7.2. The conversions of the polymerisations were $\leq 20\%$ despite reaction times $> 140 \text{ h}$ and the elongated polymer backbone architecture was imaged using atomic force microscopy (AFM).¹² Although SARA-ATRP has been used to synthesise graft copolymers, the SET-LRP methodology has not been used to synthesise graft copolymers, as far as we are aware.



Scheme 7.2: Synthesis of *n*-butyl acrylate graft copolymer by SARA-ATRP

In this chapter the synthesis of a range of graft copolymers using Poly[(vinyl alcohol)-*ran*-(vinyl, 2-bromopropionate)] (P[(VA)-*r*-(VBrP)]), with 62% and 79% initiating sites (VBrP), as macroinitiators for the SET-LRP of methyl acrylate (MA), hydroxyethyl acrylate (HEA) and NIPAM will be discussed.

7.2. Experimental

7.2.1. Materials

Copper (II) bromide (99%), bare copper wire (24 standard wire, diameter = 0.559 mm), tris(2-aminoethyl)amine (TREN) (96%), MA (99%, $\leq 100 \text{ ppm}$ monomethyl ether

hydroquinone), NIPAM (97%), dimethyl sulfoxide (DMSO) ($\geq 99.9\%$), methyl 2-bromopropionate (98%), magnesium sulphate and hydroquinone ($\geq 99\%$) were purchased from Sigma Aldrich and used without further purification. Diethyl ether was purchased from Fisher scientific and used without further purification.

HEA (96%) was purchased from Sigma Aldrich and purified by a method outlined by Percec *et al.*¹³ HEA_(aq) solution (20% v/v, 50 mL) was washed with hexane (10 x 20 mL) and NaCl (10 g) was then added to the aqueous layer. HEA was extracted with diethyl ether (4 x 20 mL). The organic layer was collected; hydroquinone (5 mg) was added and dried over magnesium sulphate. The mixture was filtered and the solvent was removed under reduced pressure.

The following polymers containing 12% acetate groups were used as macroinitiators: 79% P[(VA)-*r*-(PVB_rP)] with a composition of 79:9 (PVB_rP:PVA) and 62% (P[(VA)-*r*-(PVB_rP)]) with a composition of 62:26 (PVB_rP:PVA), were prepared following the methods outlined in Chapter 6.

7.2.2. Instrumentation

¹H nuclear magnetic resonance (NMR) spectra were recorded on a Bruker Avance-400 operating at 400 MHz or VNMRS-700 at 700 MHz. ¹³C NMR spectra were carried out on a VNMRS-700 at 176 MHz.

Fourier transform infra-red (FT-IR) spectroscopy was performed using a Perkin Elmer 1600 Series FT-IR.

Molecular weight analysis of polymer samples was obtained using SEC on a Viscotek TDA 302 with triple detection (refractive index [RI], viscosity and light scattering), using 2 x 300 mL PLgel 5 μ m C columns and DMF (containing 0.1% w/v LiBr) as the eluent at a rate of 1 mL min⁻¹ (70 °C). The system was calibrated using polyethylene glycol standards.

Thermogravimetric analysis (TGA) measurements were collected using a Perkin Elmer Pyris 1 TGA samples were heated in air or nitrogen (N₂) atmosphere to 500 °C at a rate of 10 °C min⁻¹.

Differential scanning calorimetry (DSC) measurements were carried out using a TA Instruments DSC Q1000 between -50 and 300 °C at a rate of 10 °C min⁻¹.

Molecular images were recorded by AFM. The micrographs were recorded on a Bruker Multimode 8 with a Nanoscope 5 control box using peak force tapping mode scan assist

and a 115 x 25 μm silicon tip on nitride lever with a 0.4 N m^{-1} spring constant. All measurements were corrected for the effective width of the cantilever.

The lower critical solution temperature (LCST) of poly[(vinyl alcohol)-*ran*-(vinyl 2-bromopropionate)-*graft*-(N-isopropylacrylamide)] (P[(VA)-*r*-(VBrP)-*g*-(NIPAM)]) was determined by UV-Vis Spectroscopy. A Varian Cary - 100 UV-Visible spectrophotometer coupled with a temperature controller was used. An aqueous polymer solution (1 mg mL^{-1}) was monitored at 270 nm as the temperature was increased at a rate of $1 \text{ }^\circ\text{C min}^{-1}$ from 15 $^\circ\text{C}$ to 45 $^\circ\text{C}$, before cooling at a rate of $1 \text{ }^\circ\text{C min}^{-1}$ to 15 $^\circ\text{C}$. The LCST was measured at the point when the transmittance began to decrease.

7.2.3. Synthesis of poly[(vinyl alcohol)-*ran*-(vinyl 2-bromopropionate)-*graft*-(methyl acrylate)]

A Schlenk tube sealed with a rubber septum was charged with MA (1.0 – 10.0 mL, 11.1 – 111.0 mmol). A solution of DMSO (0.5 – 5.0 mL) containing 62% or 79% P[(VA)-*r*-(VBrP)] (5.0 – 50.0 mg, 0.03 - 0.3 mmol), Cu(II)Br₂ in DMSO (10.7 – 110.0 μL , 5.9 M, 0.06 - 0.6 mmol) and TREN in DMSO (17.1 – 170.0 μL , 4.8 M, 0.1 - 0.8 mmol) was added to the Schlenk tube. The reaction mixture was bubbled with N_{2(g)} for 0.5 h at 25 $^\circ\text{C}$ and sealed in a N₂ atmosphere. A stirrer bar wrapped with Cu(0) wire (1.6 cm) was added to the reaction mixture. The reaction was stirred at 25 $^\circ\text{C}$ for 2.5 - 24 h. The stirrer bar wrapped in Cu(0) wire was removed to halt the reaction. The reaction was added to diethyl ether precipitating a white solid. The resulting poly[(vinyl alcohol)-*ran*-(vinyl 2-bromopropionate)-*graft*-(methyl acrylate)] (P[(VA)-*r*-(VBrP)-*g*-(MA)]) was dried under reduced pressure.

Conversion = 70%. ¹H NMR (CDCl₃): δ (ppm): 1.46 (m, 2H, CH₂CH), 1.63 (m, 2H, CH₂CH), 1.89 (m, 2H, CH₂CH), 2.26 (m, 1H, CH₂CH), 3.61 (m, 3H, CH₃). ¹³C NMR (CDCl₃): δ (ppm): 35.0 (CHCH₂), 41.4 (CHCH₂), 51.8 (CH₃), 174.9 (CO). FT-IR ν (cm⁻¹): 3402 (ν_{OH}), 2950 ($\nu_{\text{C-H}}$), 1728 ($\nu_{\text{C=O}}$). SEC: $M_p = 2.75 \times 10^5 \text{ g mol}^{-1}$, $D = 2.43$. $T_g = 21.00 \text{ }^\circ\text{C}$; $T_d = 352.08 \text{ }^\circ\text{C}$.

7.2.4. Synthesis of poly[(vinyl alcohol)-*ran*-(vinyl 2-bromopropionate)-*graft*-(hydroxyethyl acrylate)]

A Schlenk tube sealed with a rubber septum was charged with HEA (1.29 mL, 11.1 mmol). A solution of DMSO (0.5 mL) containing 62% P[(VA)-*r*-(VBrP)] (5 mg, 0.03 mmol), Cu(II)Br₂ in DMSO (10.7 μL , 5.9 M, 0.06 mmol) and TREN in DMSO (17.1 μL , 4.8 M, 0.08 mmol) was added to the Schlenk tube. The reaction mixture was bubbled with N_{2(g)} for 0.5 h at 25 $^\circ\text{C}$

and sealed in a N₂ atmosphere. A stirrer bar wrapped with Cu(0) wire (1.6 cm) was added to the reaction mixture. The reaction was stirred at 25 °C for 24 h. The stirrer bar wrapped in Cu(0) wire was removed to halt the reaction. The reaction was added to diethyl ether precipitating a white solid. The resulting poly[(vinyl alcohol)-*ran*-(vinyl 2-bromopropionate)-*graft*-(hydroxyethyl acrylate)] (P[(VA)-*r*-(VBrP)-*g*-(HEA)]) was dried under reduced pressure.

Conversion = 43%. ¹H NMR (D₂O): δ (ppm): 1.66 (m, 2H, CH₂CH), 1.81 (m, 2H, CH₂CH), 2.01 (m, 2H, CH₂CH), 2.44 (m, 1H, CH₂CH), 3.80 (m, 2H, COCH₂), 4.20 (m, 2H, CH₂OH). ¹³C NMR (CDCl₃): δ (ppm): 35.1 (CHCH₂), 42.3 (CHCH₂), 60.3 (COCH₂), 67.3 (CH₂OH), 177.3 (CO). FT-IR ν (cm⁻¹): 2952 (ν_{C-H}), 1724 (ν_{C=O}). SEC: M_p = 4.91 × 10⁵, Đ = 16.46. T_g = 13.92 °C; T_d = 357 °C.

7.2.5. Synthesis of poly[(vinyl alcohol)-*ran*-(vinyl 2-bromopropionate)-*graft*-(N-isopropylacrylamide)]

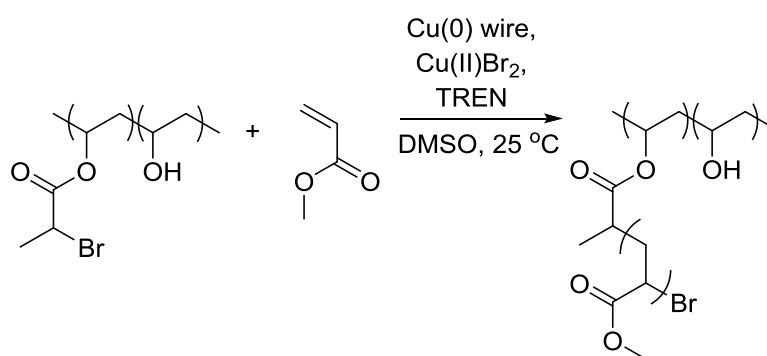
A Schlenk tube sealed with a rubber septum was charged with NIPAM (1.26 g, 11.1 mmol) and DMSO (1.1 mL). A solution of DMSO (0.5 mL) containing 62% P[(VA)-*r*-(PVBBrP)] (5 mg, 0.03 mmol), Cu(II)Br₂ in DMSO (10.7 μL, 5.9 M, 0.06 mmol) and TREN in DMSO (17.1 μL, 4.8 M, 0.08 mmol) was added to the Schlenk tube. The reaction mixture was bubbled with N_{2(g)} for 0.5 h at 25 °C and sealed in a N₂ atmosphere. A stirrer bar wrapped with Cu(0) wire (1.6 cm) was added to the reaction mixture. The reaction was stirred at 25 °C for 24 h. The stirrer bar wrapped in Cu(0) wire was removed to halt the reaction. The reaction was added to diethyl ether precipitating a white solid. The resulting P[(VA)-*r*-(VBrP)-*g*-(NIPAM)] was dried under reduced pressure.

Conversion = 12%. ¹H NMR (CDCl₃): δ (ppm): 1.13 (m, 6H, CH₃), 1.35 ppm (m, 2H, CH₂CH), 1.63 (m, 2H, CH₂CH), 1.81 (m, 2H, CH₂CH), 2.14 (m, 1H, CH₂CH), 2.31 (m, 1H, CH₂CH), 3.99 (m, 1H, NHCH) 6.48 (m, 1H, NH). ¹³C NMR (d₆-DMSO): δ (ppm): 22.4 (CH₃), 35.5 (CHCH₂), 41.6 (CHCH₂), 79.0 (CH), 173.5 (CO). FT-IR ν (cm⁻¹): 3416 (ν_{OH}), 3264 (ν_{NH}), 2974 (ν_{C-H}), 1636 (ν_{C=O}), 1536 (ν_{NH}). SEC: M_p = 3.32 × 10⁵ g mol⁻¹, Đ = 13.64. LCST = 36 °C, T_g = 136.10 °C; T_d = 294.17 °C.

7.3. Results & Discussion

7.3.1. Synthesis of poly[(vinyl alcohol)-*r*-(vinyl 2-bromopropionate)-*graft*-(methyl acrylate)]

62% and 79% P[(VA)-*r*-(VBrP)] were used as macroinitiators to polymerise MA under SET-LRP methodology to synthesise P[(VA)-*r*-(VBrP)-*g*-(MA)], Scheme 7.3. Cu(II)Br₂ was added to the reaction mixture as it deactivates the propagating chain, lowering the probability of termination at the beginning of the polymerisation before Cu(II)Br₂ is naturally produced; and the minimum length of Cu(0) wire was also selected. Both measures reduce the rate of the reaction and the number of active radicals in the reaction lowering the probability of termination and the formation of cross-linked materials during graft copolymerisations. DMSO was chosen as a solvent and TREN as a ligand to aid the disproportionation of Cu(I) to Cu(0) and Cu(II), which is integral in the SET-LRP mechanism.



Scheme 7.3: Synthesis of P[(VA)-*r*-(VBrP)-*g*-(MA)]

In the ¹H NMR spectrum of P[(VA)-*r*-(VBrP)-*g*-(MA)] shown in Figure 7.1, resonances due to poly(methyl acrylate) (PMA) are seen at 1.46 ppm, 1.63 ppm and 1.89 ppm the methylene protons on the polymer backbone (a); at 2.26 ppm for the methine proton (b) and at 3.61 ppm for the methyl proton (d).

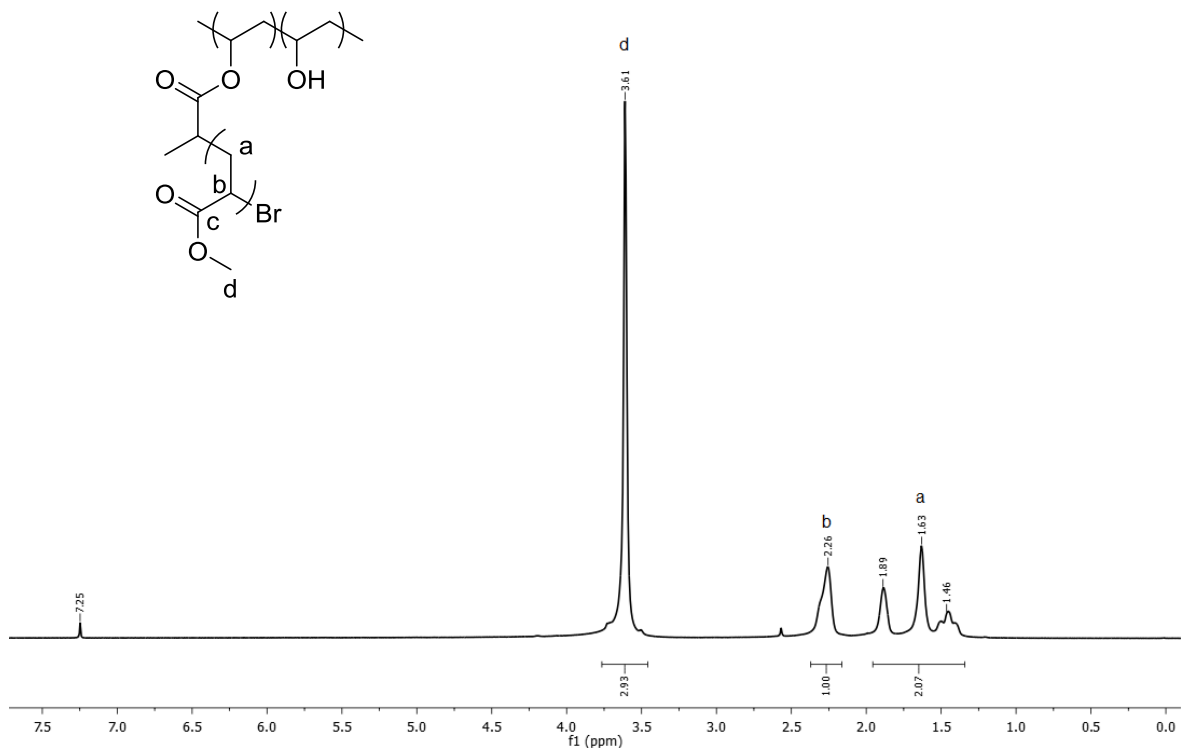


Figure 7.1: 700 MHz ^1H NMR spectrum of P[(VA)-*r*-(VBrP)-*g*-(MA)] in CDCl_3

In the ^{13}C NMR spectrum of P[(VA)-*r*-(VBrP)-*g*-(MA)] shown in Figure 7.2, resonances due to PMA are observed at 35.0 ppm which is attributed to the methine carbon atom on the polymer backbone (c). The resonance at 41.4 ppm corresponds to the methylene carbon atom on the polymer backbone (b). The resonance at 51.8 ppm is assigned to the methyl carbon atom (d). The resonance at 174.9 ppm is attributed to the carbonyl carbon atom (d). The results of the ^1H and ^{13}C NMR spectra clearly show the presence of PMA in the graft copolymer which could only be formed *via* the Cu(0) mediated RDRP using an alkyl halide initiator (Appendix 7.1).

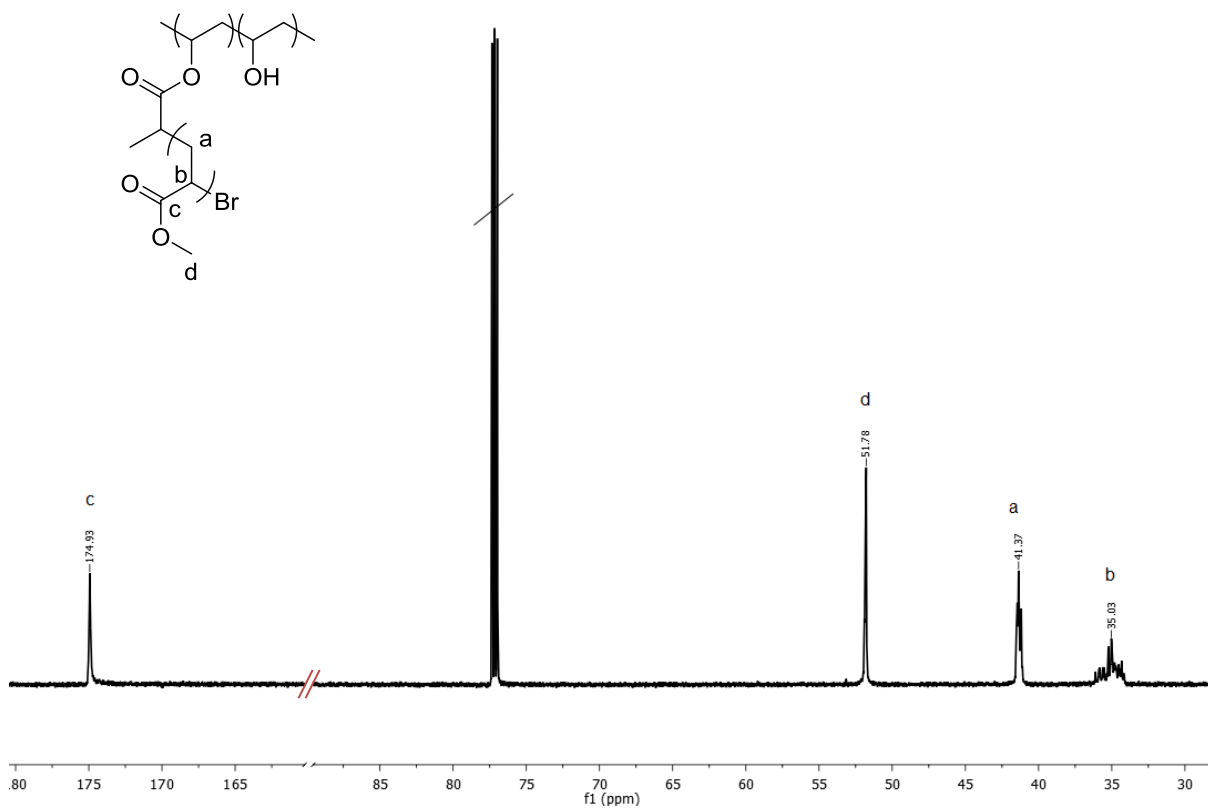


Figure 7.2: 176 MHz ^{13}C NMR spectrum of P[(VA)-*r*-(VBrP)-*g*-(MA)] in CDCl_3

The conversion is determined from the ratio between the resonances attributed to the monomer and the synthesised polymer, Equation 7.1.

$$\%conv = \frac{\left(\frac{\int poly}{N_i}\right)}{\left(\frac{\int poly}{N_i}\right) + \left(\frac{\int mon}{N_i}\right)} \quad \text{Equation 7.1}$$

Where %conv is the conversion, $\int poly$ is the integral of the resonance relating to the polymer (*i.e.* 2.32 ppm), $\int mon$ is the integral of the resonance relating to the monomer (*i.e.* 5.85 ppm), and N_i is the number of protons attributed to the resonance (*i.e.* N_{poly} is 1 and N_{mon} is 1).

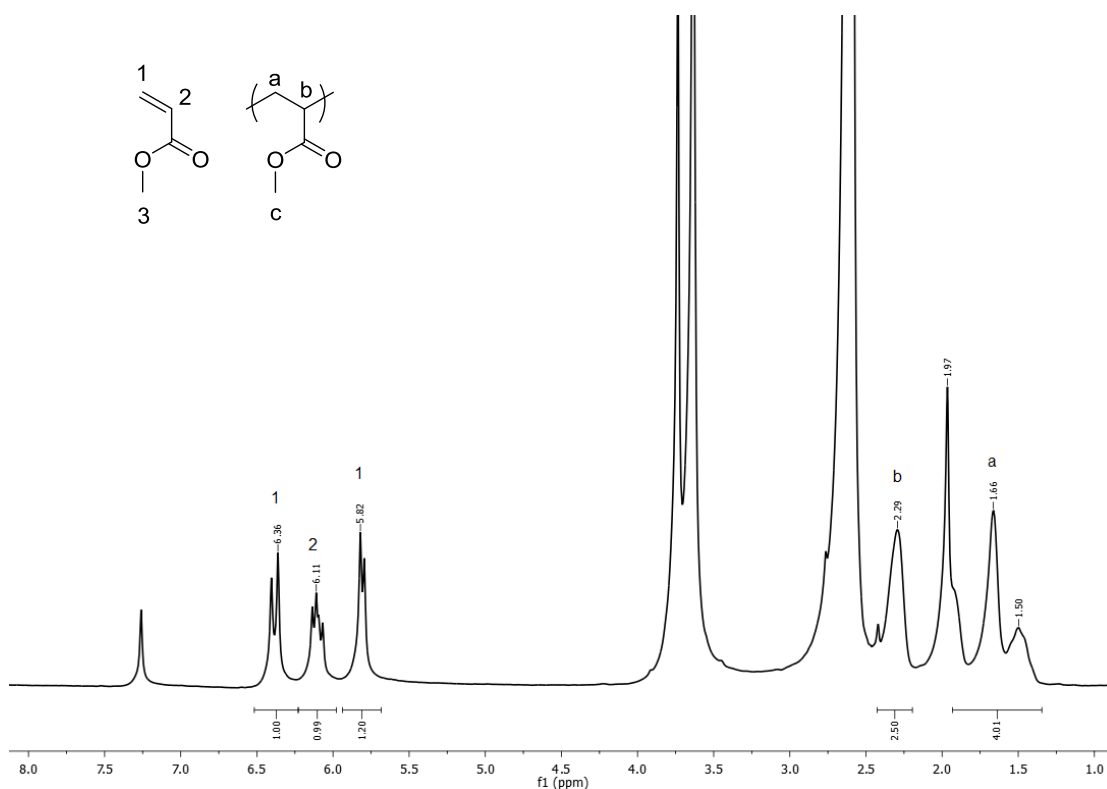


Figure 7.3: 400 MHz ^1H NMR of 79% P[(VA)-*r*-(VBrP)-*g*-(MA)] polymerisation mixture in CDCl_3

A %conv of 71% was determined for 79% P[(VA)-*r*-(VBrP)-*g*-(MA)] (Figure 7.3) and 46% for 62% P[(VA)-*r*-(VBrP)-*g*-(MA)], Appendix 7.2. The MW_{th} of the graft copolymers were determined using Equation 7.3. However, as the initiator efficiency (I_{eff}), was not determined experimentally, the I_{eff} was assumed to be 50% based on average I_{eff} of other graft copolymers.^{12,14}

$$MW_{th} = MW_{init} + \left(\%conv \times \left(\frac{n_{mon}}{n_{init}} \right) \times MW_{mon} \times N_G \right) \quad \text{Equation 7.2}$$

Where N_G is the number of grafted chains in the graft copolymer, which is determined from Equation 7.4.

$$N_G = \%PVB r P \times DP_{MI} \times I_{eff} \quad \text{Equation 7.3}$$

Where %PVB r P is the percentage of PVB r P repeat units in the macroinitiator (P[(VA)-*r*-(VBrP)]) and DP is the degree of polymerisation of the macroinitiator ($DP_{MI} = 409$). The MW_{th} of the two graft copolymers was therefore determined to be $352 \times 10^4 \text{ g mol}^{-1}$ for 79% P[(VA)-*r*-(VBrP)-*g*-(MA)] and $189 \times 10^4 \text{ g mol}^{-1}$ for 62% P[(VA)-*r*-(VBrP)-*g*-(MA)].

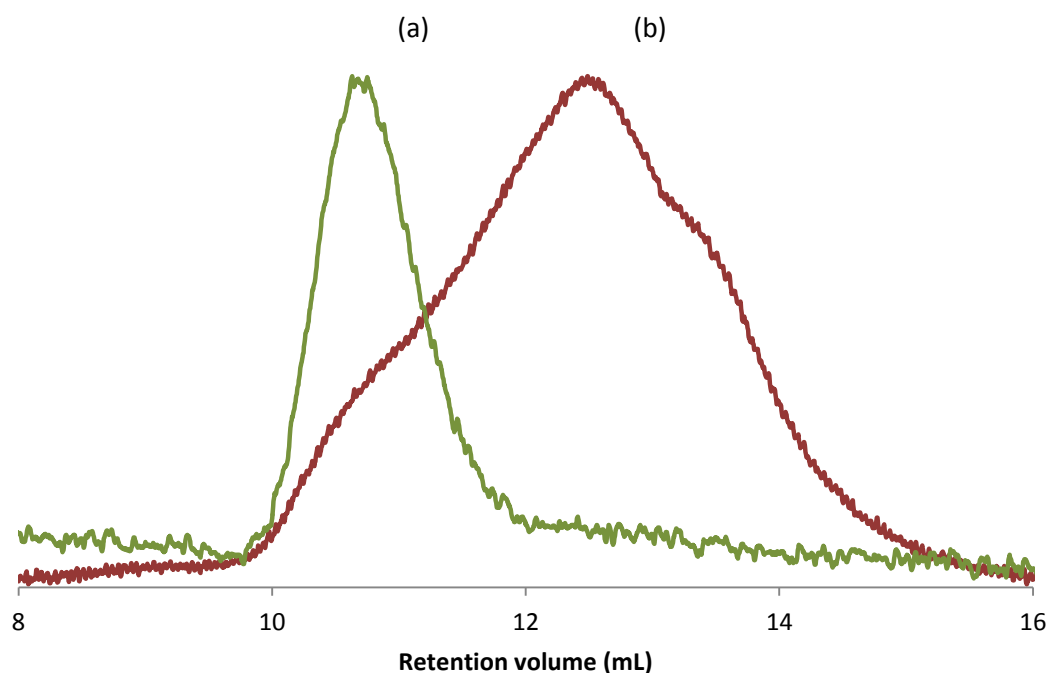


Figure 7.4: Plots of normalised RI vs retention volume (a) 62% P[(VA)-*r*-(VBrP)-*g*-(MA)] ($M_p = 2.75 \times 10^5 \text{ g mol}^{-1}$, $\mathcal{D} = 2.43$) (b) 62% P[(VA)-*r*-(PVBrP)] ($M_p = 3.99 \times 10^4 \text{ g mol}^{-1}$, $\mathcal{D} = 3.06$)

The normalised SEC chromatograms of 62% P[(VA)-*r*-(PVBrP)] and the resulting P[(VA)-*r*-(VBrP)-*g*-(MA)] are shown in Figure 7.4. An M_p of $2.75 \times 10^5 \text{ g mol}^{-1}$ was recorded for 62% P[(VA)-*r*-(VBrP)-*g*-(MA)] (Figure 7.4.a), which is much greater than the M_p of $3.99 \times 10^4 \text{ g mol}^{-1}$ of the macroinitiator, 62% P[(VA)-*r*-(PVBrP)] (Figure 7.4.b). This large increase in M_p shows that the graft copolymerisation was successful. The dispersity (\mathcal{D}) decreases from 3.06 for 62% P[(VA)-*r*-(PVBrP)] to 2.43 for the resulting P[(VA)-*r*-(VBrP)-*g*-(MA)] graft copolymer. This decrease in \mathcal{D} and largely monomodal response indicates that the graft copolymerisation proceeds in a controlled manner and the influence of the unreacted macroinitiator is diminished with the addition of the grafted chains. A comparison of the SEC chromatograms of 62% P[(VA)-*r*-(VBrP)-*g*-(MA)] and 79% P[(VA)-*r*-(VBrP)-*g*-(MA)] is shown in Figure 7.5.

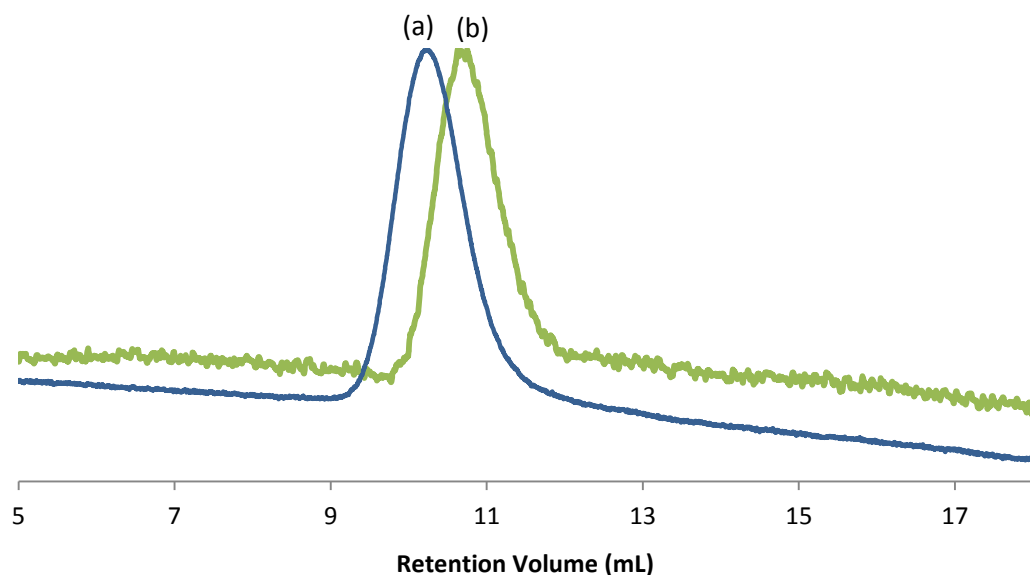


Figure 7.5: Plots of normalised RI vs retention volume for (a) 79% P[(VA)-*r*-(VBrP)-*g*-(MA)] ($M_p = 2.81 \times 10^5 \text{ g mol}^{-1}$, $\bar{D} = 2.69$) (b) 62% P[(VA)-*r*-(VBrP)-*g*-(MA)] ($M_p = 27.5 \times 10^4 \text{ g mol}^{-1}$, $\bar{D} = 2.43$) and

79% P[(VA)-*r*-(VBrP)-*g*-(MA)] (Figure 7.5.a) has a M_p of $2.81 \times 10^5 \text{ g mol}^{-1}$ which is slightly greater than the recorded M_p of $2.75 \times 10^5 \text{ g mol}^{-1}$ for 62% P[(VA)-*r*-(VBrP)-*g*-(MA)], in line with increasing the number of initiating sites. Furthermore, the \bar{D} of 2.69 for 79% P[(VA)-*r*-(VBrP)-*g*-(MA)] is similar to the \bar{D} of 2.43 for 62% P[(VA)-*r*-(VBrP)-*g*-(MA)], within experimental error, showing that the number of initiating sites has had little effect on the \bar{D} .

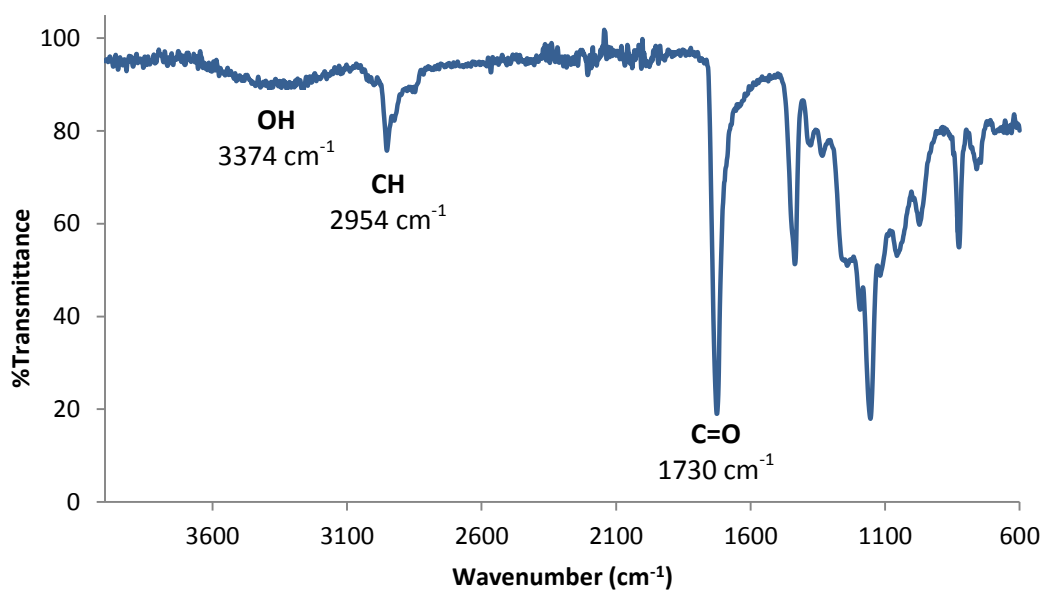


Figure 7.6: FT-IR spectrum of 62% P[(VA)-*r*-(VBrP)-*g*-(MA)]

The FT-IR spectrum of 62% P[(VA)-*r*-(VBrP)-*g*-(MA)] is shown in Figure 7.6. A small stretch at 3410 cm^{-1} is observed for 62% P[(VA)-*r*-(VBrP)-*g*-(MA)] which is characteristic of a hydroxyl group, this is potentially due to the PVA repeat units in the macroinitiator. Moreover, a stretch at 1726 cm^{-1} is observed which is attributed to the ester bonds.

A solution of 79% P[VA]-*r*-R(VBrP)-*g*-(MA)] in acetone (3×10^{-5} %wt) was spin cast onto mica to image single graft copolymer molecules by AFM, Figure 7.7.a. The highlighted oval shape is raised from the mica surface is believed to be a single molecule of P[(VA)-*r*-(VBrP)-*g*-(MA)]. The shape of the polymer reveals the graft copolymer architecture, as the grafted chains straighten the polymer backbone away from the entropically favoured globular coiled conformation of the macroinitiator.¹⁵

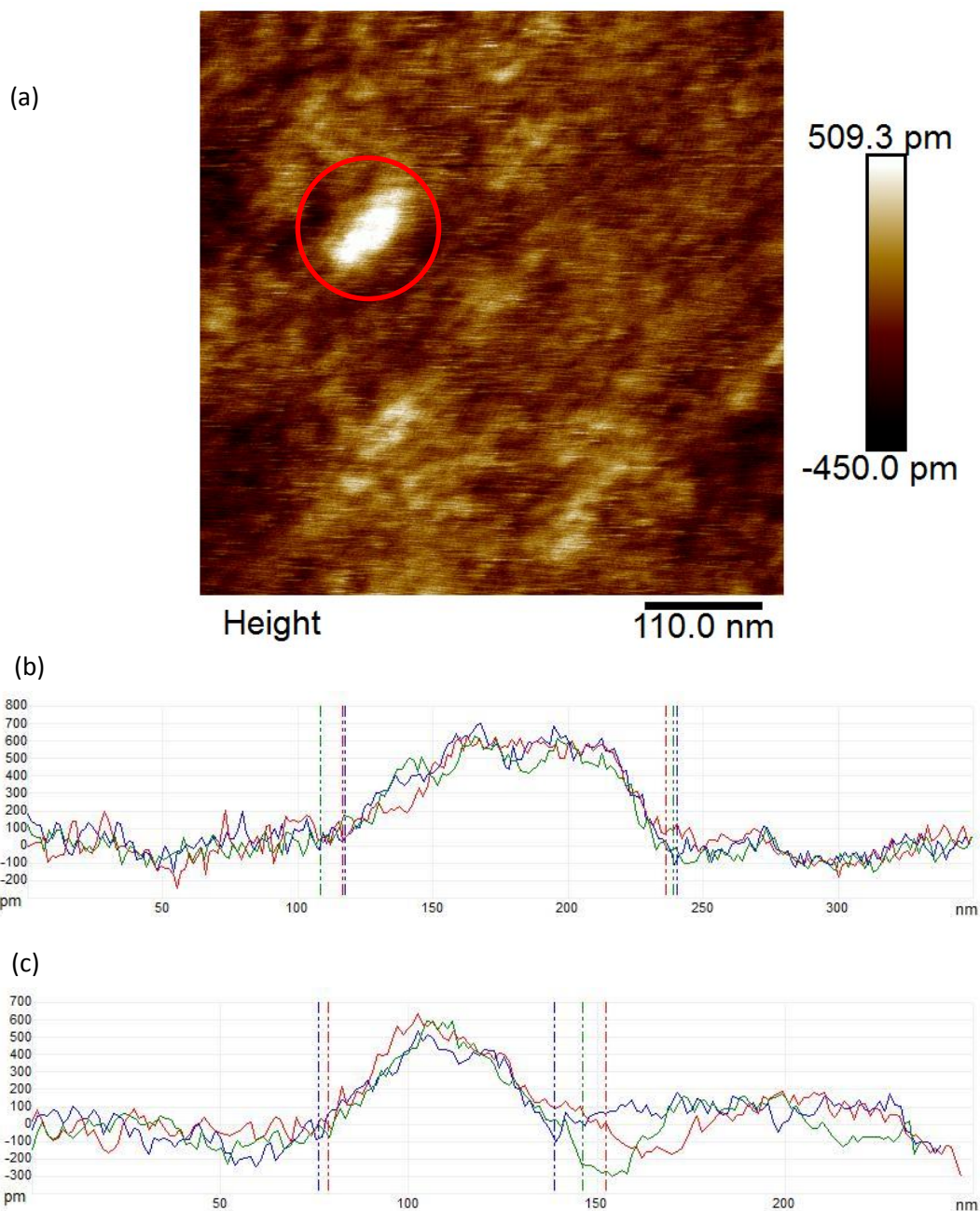


Figure 7.7: (a) AFM image of 79% P[VA]-*r*-R(VBrP)-*g*-(MA)] and height scale (b) cross section of the length of the polymer (c) cross section of the width of the polymer

The average length of 122 ± 6 nm and the width of 65 ± 6 nm for the graft copolymer were measured from cross sections of the molecule, shown in Figure 7.7.b and Figure 7.7.c, respectively. The DP was determined based on the average length of a sp^3 hybridised carbon - carbon bond using Equation 7.5.¹²

$$DP = \frac{l_{poly}}{l_0} \quad \text{Equation 7.4}$$

Where l_{poly} is the length or width of the polymer (nm) and l_0 is the length of a fully extended monomeric unit in a tetrahedral configuration (nm), ($l_0 = 0.25$ nm).¹² The DP of the length of polymer backbone in the graft copolymer was determined to be 488, which is in the range of the DP for PVA (≈ 409) determined from the data supplied from the retailer (Sigma Aldrich) and the D determined by SEC for 88% hydrolysed PVA (1.82; Chapter 6, Figure 6.16). A DP of 260 was determined for the width of the graft polymer chains, which equates to approximately a DP of 130 for the grafted chains on either side of the backbone. An MW_{th} can be approximated using Equation 7.5.

$$MW_{\text{th}} = MW_{\text{init}} + (DP_{\text{BB}} \times I_{\text{GC}} \times (MW_{\text{mon}} \times DP_{\text{GC}})) \quad \text{Equation 7.5}$$

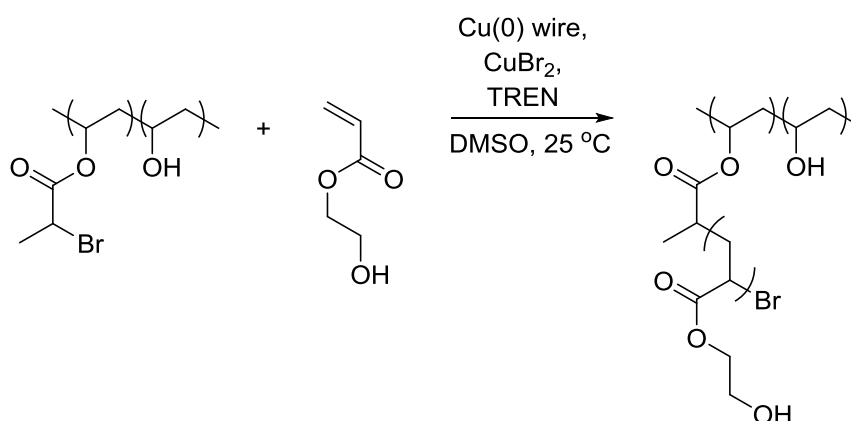
Where DP_{BB} is the degree of polymerisation of the backbone, MW_{mon} is the molecular weight of the monomer, DP_{GC} is the degree of polymerisation of the grafted chains and I_{GC} is the number of initiated chains determined by Equation 7.6.

$$I_{\text{GC}} = I_{\text{eff}} \times \%P\text{VBrP} \times DP_{\text{BB}} \quad \text{Equation 7.6}$$

The I_{eff} was again assumed to be 50% based on average I_{eff} of other graft copolymers.^{12,14} A MW_{th} of 2.31×10^6 g mol⁻¹ was determined, which is much greater than the M_p calculated by SEC (2.75×10^5 g mol⁻¹, Figure 7.4).

7.3.2. Synthesis of poly[(vinyl alcohol)-*ran*-(vinyl 2-bromopropionate)-graft-(hydroxyethyl acrylate)]

62% P[(VA)-*r*-(PVBrP)] was used as a macroinitiator for the polymerisation of HEA under SET-LRP conditions to synthesise P[(VA)-*r*-(VBrP)-*g*-(HEA)], Scheme 7.5.



Scheme 7.4: Synthesis of P[(VA)-*r*-(VBrP)-*g*-(HEA)]

The SEC chromatograms of P[(VA)-*r*-(VBrP)-*g*-(HEA)] and 62% P[(VA)-*r*-(PVBBrP)] are shown in Figure 7.8.

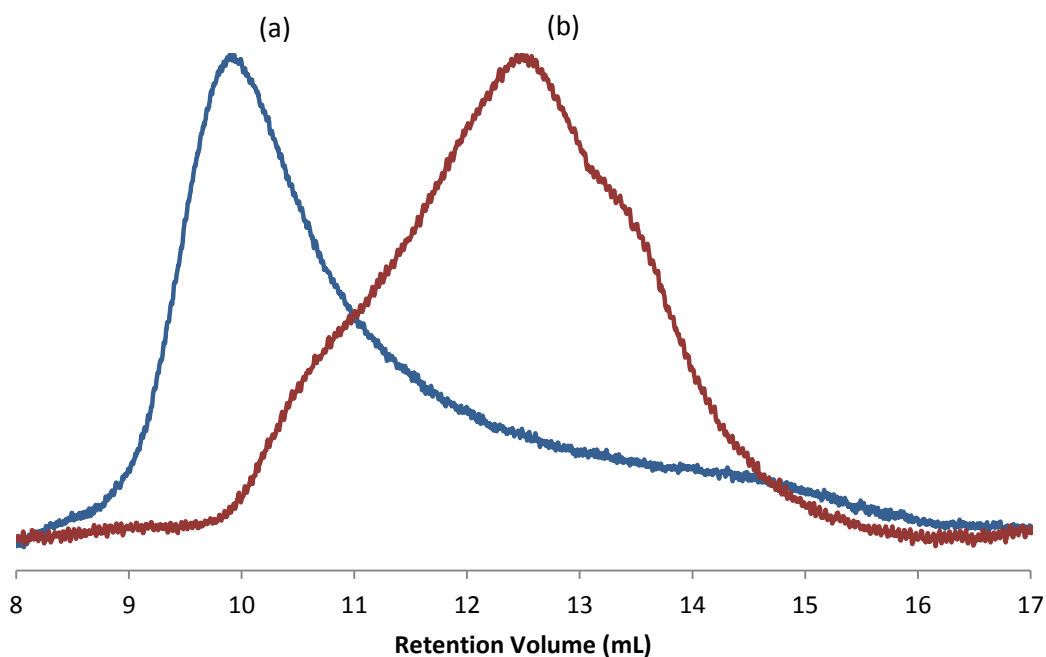


Figure 7.8: Plots of normalised RI vs retention volume for (a) P[(VA)-*r*-(VBrP)-*g*-(HEA)] ($M_p = 4.91 \times 10^5 \text{ g mol}^{-1}$, $\mathcal{D} = 16.46$) (b) 62% P[(VA)-*r*-(PVBBrP)] ($M_p = 3.99 \times 10^4 \text{ g mol}^{-1}$, $\mathcal{D} = 3.06$)

The M_p of the macroinitiator increases from $3.99 \times 10^4 \text{ g mol}^{-1}$ for 62% P[(VA)-*r*-(PVBBrP)] to $4.91 \times 10^5 \text{ g mol}^{-1}$ for the graft copolymer, P[(VA)-*r*-(VBrP)-*g*-(HEA)]. The \mathcal{D} of 16.46 of P[(VA)-*r*-(VBrP)-*g*-(HEA)] is due to a long low molecular weight tail, potentially because of the presence of unreacted 62% P[(VA)-*r*-(PVBBrP)] macroinitiator.

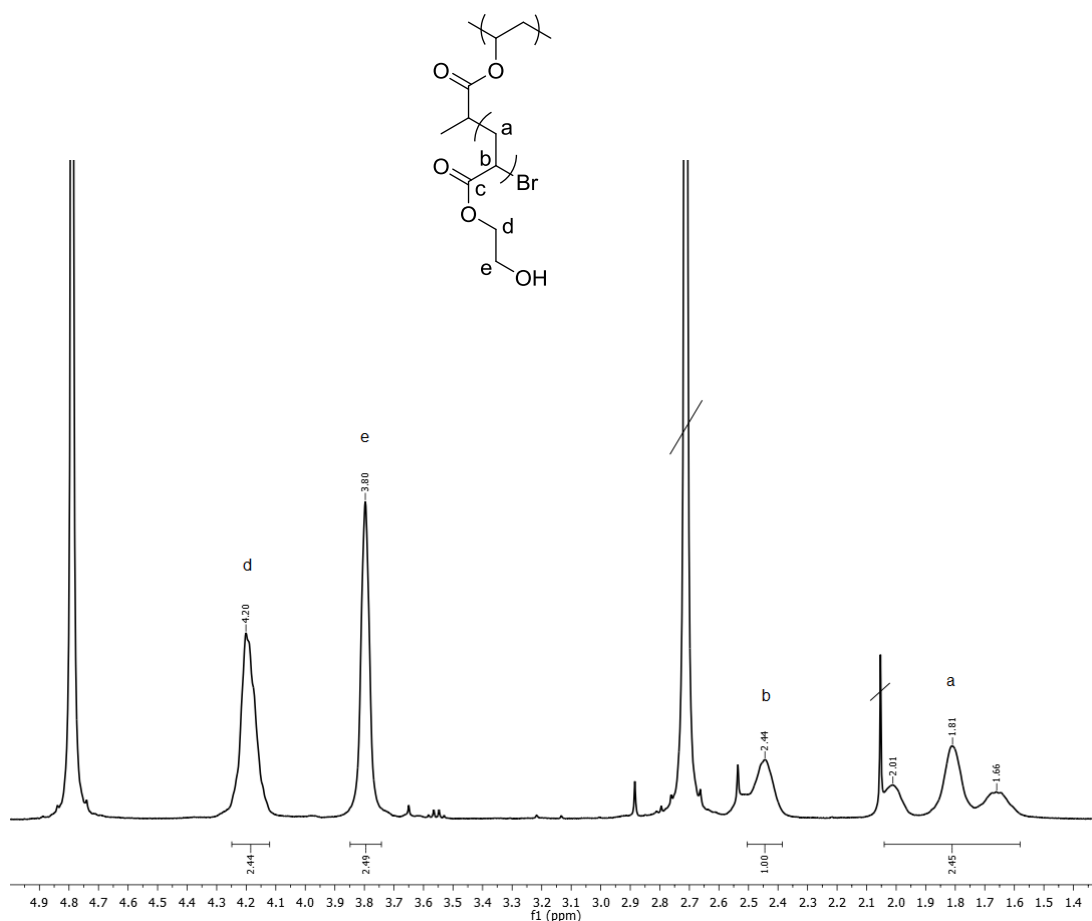


Figure 7.9: 400 MHz ^1H NMR of P[(VA)-*r*-(VBrP)-*g*-(HEA)] in D_2O

The ^1H NMR spectrum of P[(VA)-*r*-(VBrP)-*g*-(HEA)] is shown in Figure 7.9. The resonances at 1.66 ppm, 1.81 ppm and 2.01 ppm are attributed to the methylene protons on the polymer backbone (a). The resonance at 2.44 ppm is assigned to the methine protons on the polymer backbone (b). The resonances at 3.80 ppm and 4.20 ppm correspond to the methylene protons in the ethyl chain (e) and (d). The %conv of the polymerisation was determined using Equation 7.1 to be 43% from the ^1H NMR spectrum of the reaction mixture (Appendix 7.3).

Poly(hydroxyethyl acrylate) (PHEA) hydrogels are widely used in fields such as soft contact lenses.¹⁶ When unpurified HEA was used as the monomer in the polymerisation an insoluble material was produced, due to the unremoved diacrylate contaminants. The ability of cross-linked P[(VA)-*r*-(VBrP)-*g*-(HEA)] to act as a hydrogel was measured by immersing a dried sample in water for 48 h (1 %wt) at room temperature. The swelling ratio of the sample was determined using Equation 7.8.¹⁷

$$\text{Swelling ratio} = \frac{W_s - W_u}{W_s} \quad \text{Equation 7.7}$$

Where W_s is the saturated weight of the material and W_u is the unsaturated weight of the dried material. The swelling ratio was determined to be $50\% \pm 1\%$, Table 7.1.

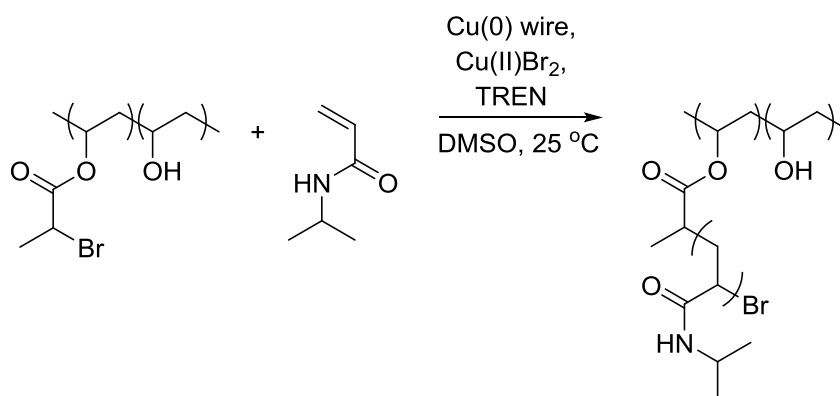
Table 7.1: The W_s , W_u and swelling ratio of 62% P[(VA)-*r*-(VBrP)-*g*-(HEA)] samples

Entry	W_s (g)	W_u (g)	Swelling Ratio
1	0.197	0.096	51%
2	0.194	0.097	50%
3	0.184	0.094	49%
Average			50% \pm 1%

Therefore, a greater swelling ratio was achieved than reported values for cross-linked PHEA samples (38%)¹⁸ and cross-linked PVA (< 40%).¹⁷

7.3.3. Synthesis of poly[(vinyl alcohol)-*ran*-(vinyl 2-bromopropionate)-*graft*-(N-isopropylacrylamide)]

NIPAM was polymerised under SET-LRP conditions using 62% P[(VA)-*r*-(PVBBrP)] as a macroinitiator to synthesise P[(VA)-*r*-(VBrP)-*g*-(NIPAM)], Scheme 7.6.



Scheme 7.5: Synthesis of P[(VA)-*r*-(VBrP)-*g*-(NIPAM)]

The SEC chromatograms of P[(VA)-*r*-(VBrP)-*g*-(NIPAM)] and 62% P[(VA)-*r*-(PVBBrP)] are shown in Figure 7.10.

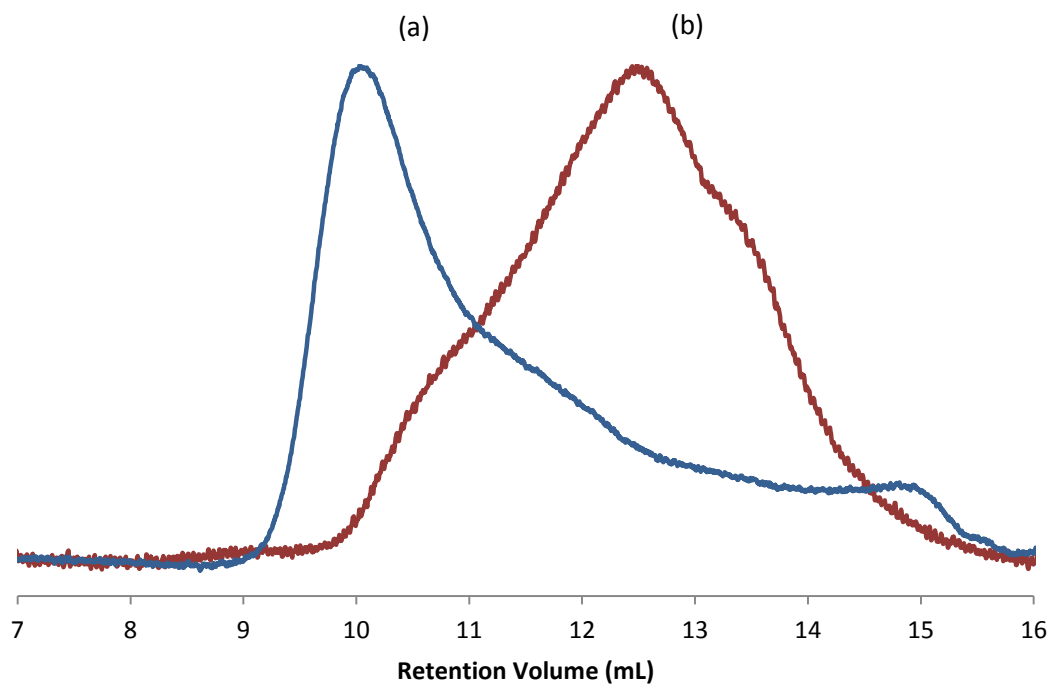


Figure 7.10: Plots of normalised RI vs retention volume for (a) P[(VA)-*r*-(VBrP)-*g*-(NIPAM)] ($M_p = 3.32 \times 10^5 \text{ g mol}^{-1}$, $\mathcal{D} = 13.64$) (b) 62% P[(VA)-*r*-(PVBBrP)] ($M_p = 3.99 \times 10^4 \text{ g mol}^{-1}$, $\mathcal{D} = 3.06$)

The M_p of P[(VA)-*r*-(VBrP)-*g*-(NIPAM)] graft copolymer was found to be $3.32 \times 10^5 \text{ g mol}^{-1}$ which is greater than the M_p of $3.99 \times 10^4 \text{ g mol}^{-1}$ for the macroinitiator, suggesting a successful graft copolymerisation reaction. The broad \mathcal{D} of 13.64 for P[(VA)-*r*-(VBrP)-*g*-(NIPAM)] is due to a long low molecular tail, potentially because of the presence of unreacted 62% P[(VA)-*r*-(PVBBrP)] macroinitiator. Furthermore, the interaction with the nitrogen atom in NIPAM and the catalyst (Cu(0) wire) could also affect the \mathcal{D} . This interaction is known to be capable of deactivating the catalyst, lowering the control over the polymerisation reaction.¹⁹

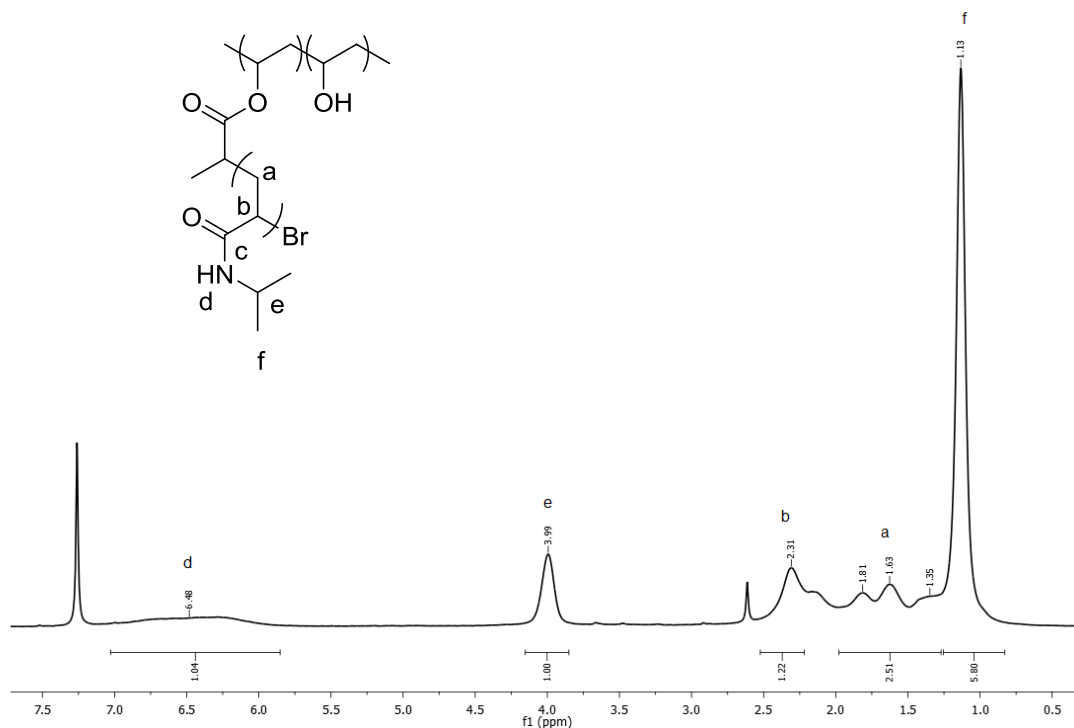


Figure 7.11: 400 MHz ^1H NMR spectrum of P[(VA)-*r*-(VBrP)-*g*-(NIPAM)] in CDCl_3

The ^1H NMR spectrum of P[(VA)-*r*-(VBrP)-*g*-(NIPAM)] is shown in Figure 7.11. The resonance at 1.13 ppm is due to the methyl protons (f), 3.99 ppm to the methine protons (e) and 6.48 ppm is to the amide proton (d). The protons on the polymer backbone are seen at 1.35 ppm, 1.63 ppm and 1.81 ppm due to the methylene protons (a); and 2.31 ppm to the methine proton on the polymer backbone (b).

A limited %conv of 12% was determined from Equation 7.1 using the ^1H NMR spectrum of the polymerisation mixture (Appendix 7.4). The decrease in %conv in comparison with the acrylate polymerisations (Section 7.3.1 and 7.3.2) might be due to the deactivation of the catalyst from the nitrogen atom contained in the monomer, NIPAM.¹⁹

Poly(N-isopropylacrylamide) (PNIPAM) is a known thermoresponsive polymer with a LCST of 32 °C in water, depending on the MW.²⁰ The LCST of P[(VA)-*r*-(VBrP)-*g*-(NIPAM)] was observed to be 32 °C by UV-Vis spectroscopy (Figure 7.12), by measuring the decrease in transmittance of the aqueous P[(VA)-*r*-(VBrP)-*g*-(NIPAM)] solution, as it became cloudy during the phase separation above the LCST.. The solution became transparent upon cooling, showing an LCST of 29 °C. The observed hysteresis of 3 °C is believed to be due to hydrogen bonding between the carbonyl and amide moieties of PNIPAM grafts in the

globule conformation limiting the dissociation process. The phase transition was found to be reproducible.

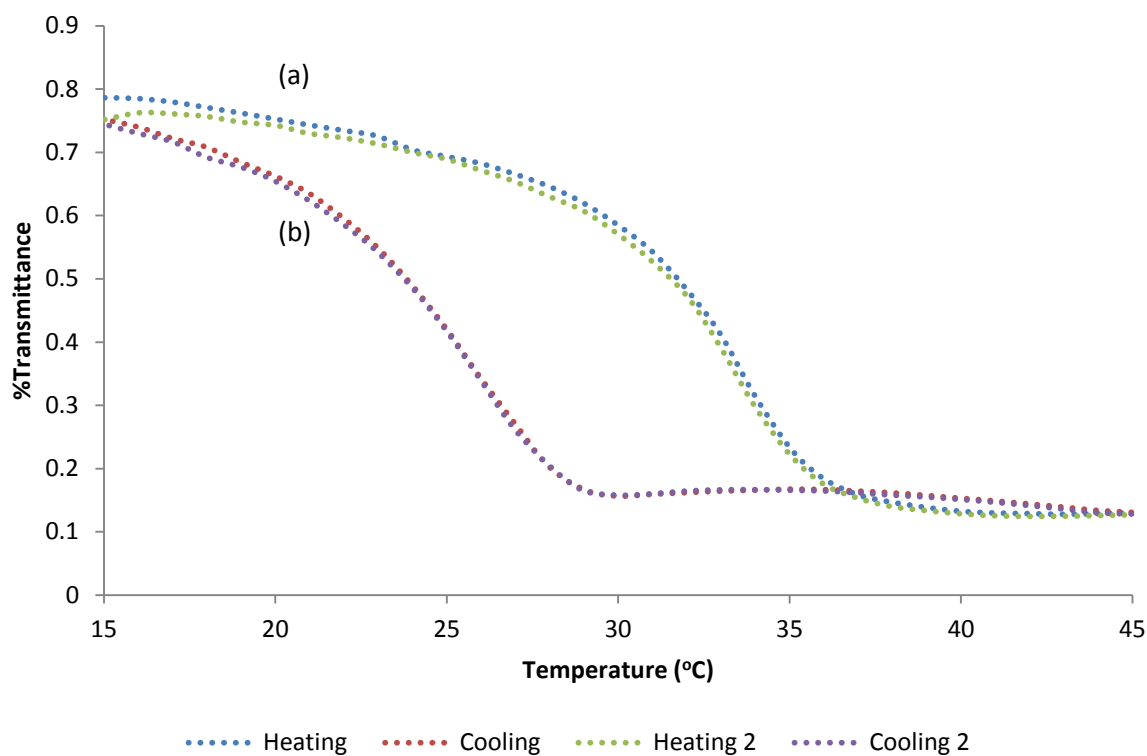


Figure 7.12: The change in transmittance of P[(VA)-r-(VBrP)-g-(NIPAM)] solution with temperature (a) heating (b) cooling

The LCST was also visually observed by heating an aqueous solution of P[(VA)-r-(VBrP)-g-(NIPAM)] (1 %wt) in a water bath above the LCST, which became cloudy and it then turned transparent again upon cooling below the LCST, Figure 7.13.

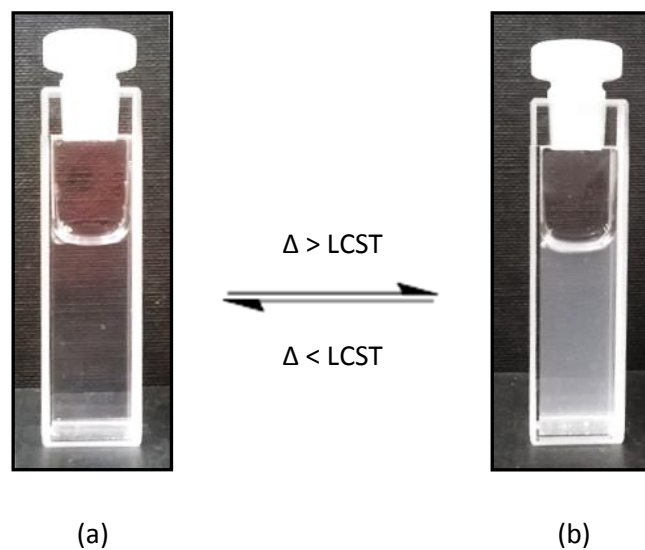


Figure 7.13: A 1 %wt aqueous solution of 62% P[(VA)-*r*-(VBrP)-*g*-(NIPAM)] at (a) 25 °C (b) 40 °C

7.4. Conclusion

The novel graft copolymer, P[(VA)-*r*-(VBrP)-*g*-(MA)] was synthesised under SET-LRP conditions with using P[(VA)-*r*-(PVBBrP)] as a macroinitiator, containing 62% or 79% initiating groups (VBrP). An M_p of $2.81 \times 10^5 \text{ g mol}^{-1}$ with a \mathcal{D} of 2.69 was determined from SEC for 79% P[(VA)-*r*-(VBrP)-*g*-(MA)]. However, a MW of $2.31 \times 10^6 \text{ g mol}^{-1}$ was determined for the graft copolymer using AFM. A %conv of 71% was determined which is much greater than quoted %conv for other RDRP graft copolymerisation techniques using to synthesise non-PVA based graft copolymers.¹² Furthermore, an M_p of $2.75 \times 10^5 \text{ g mol}^{-1}$ with a \mathcal{D} of 2.43 was determined for 62% P[(VA)-*r*-(VBrP)-*g*-(MA)].

P[(VA)-*r*-(VBrP)-*g*-(HEA)] was successfully synthesised using P[(VA)-*r*-(PVBBrP)] as a macroinitiator, containing 62% initiating groups (VBrP), under SET-LRP conditions to produce a water soluble graft copolymer with $M_p = 4.91 \times 10^5 \text{ g mol}^{-1}$ and $\mathcal{D} = 16.46$. The large \mathcal{D} is potentially due to unreacted macroinitiator. When the monomer (HEA) was not purified prior to polymerisation, an insoluble hydrogel was produced with a recorded water uptake of $50\% \pm 1\%$, which is greater than pure PHEA or PVA hydrogels.

P[(VA)-*r*-(VBrP)-*g*-(NIPAM)] was successfully synthesised using P[(VA)-*r*-(PVBBrP)] as a macroinitiator, containing 62% initiating groups (VBrP), under SET-LRP conditions to produce a thermoresponsive graft copolymer with a $M_p = 3.32 \times 10^5 \text{ g mol}^{-1}$ and $\mathcal{D} = 13.64$. The large \mathcal{D} is potentially due to unreacted macroinitiator. An LCST of 32 °C was observed for the graft copolymer. Furthermore, a 3 °C hysteresis was observed for P[(VA)-*r*-(VBrP)-*g*-

(NIPAM)], this is potentially due to the hydrogen bonding within the PNIPAM grafted chains in the globule conformation.

7.5. References

- (1) Chowdhury, P.; Pal, C. M. *Eur. Polym. J.* **1999**, *35*, 2207.
- (2) Lu, Y.; Jing, R.; Kong, Q. M.; Zhu, P. X. *J. Appl. Polym. Sci.* **2014**, *131*, 7.
- (3) Yang, J.; Hu, D. D.; Zhang, H. *React. Funct. Polym.* **2012**, *72*, 438.
- (4) Bernard, J.; Favier, A.; Davis, T. P.; Barner-Kowollik, C.; Stenzel, M. H. *Polymer* **2006**, *47*, 1073.
- (5) Liu, Y. H.; Liu, X. H.; Liu, Y. W.; Zhang, J. S.; Deng, K. L.; Liu, Z. J. *Polym. Int.* **2004**, *53*, 1611.
- (6) Beers, K. L.; Gaynor, S. G.; Matyjaszewski, K.; Sheiko, S. S.; Moller, M. *Macromolecules* **1998**, *31*, 9413.
- (7) Neugebauer, D.; Sumerlin, B. S.; Matyjaszewski, K.; Goodhart, B.; Sheiko, S. S. *Polymer* **2004**, *45*, 8173.
- (8) Runge, M. B.; Bowden, N. B. *J. Am. Chem. Soc.* **2007**, *129*, 10551.
- (9) Hadasha, W.; Klumperman, B. *Polym. Int.* **2014**, *63*, 824.
- (10) Lligadas, G.; Percec, V. *J. Polym. Sci. Polym. Chem.* **2007**, *45*, 4684.
- (11) Samanta, S. R.; Cai, R. L.; Percec, V. *J. Polym. Sci. Polym. Chem.* **2015**, *53*, 294.
- (12) Nese, A.; Li, Y. C.; Sheiko, S. S.; Matyjaszewski, K. *ACS Macro. Lett.* **2012**, *1*, 991.
- (13) Leng, X. F.; Nguyen, N. H.; van Beusekom, B.; Wilson, D. A.; Percec, V. *Polym. Chem.* **2013**, *4*, 2995.
- (14) Sumerlin, B. S.; Neugebauer, D.; Matyjaszewski, K. *Macromolecules* **2005**, *38*, 702.
- (15) Cowie, J. M. G.; Arrighi, V. *Polymers: Chemistry and Physics of Modern Materials, Third Edition*; Taylor & Francis, 2007.
- (16) Kopecek, J. *J. Polym. Sci. Polym. Chem.* **2009**, *47*, 5929.
- (17) Jabbari, E.; Karbasi, S. *J. Appl. Polym. Sci.* **2004**, *91*, 2862.
- (18) Castilla Cortázar, I.; Vidaurre, A.; Gallego Ferrer, G.; Monleón Pradas, M.; Gómez Ribelles, J. L.; Meseguer Dueñas, J. M. *J. of Non-Crystalline Solids* **2001**, *287*, 130.
- (19) Wever, D. A. Z.; Raffa, P.; Picchioni, F.; Broekhuis, A. A. *Macromolecules* **2012**, *45*, 4040.
- (20) Mark, J. E. *Polymer Data Handbook*; Oxford University Press, 1999.

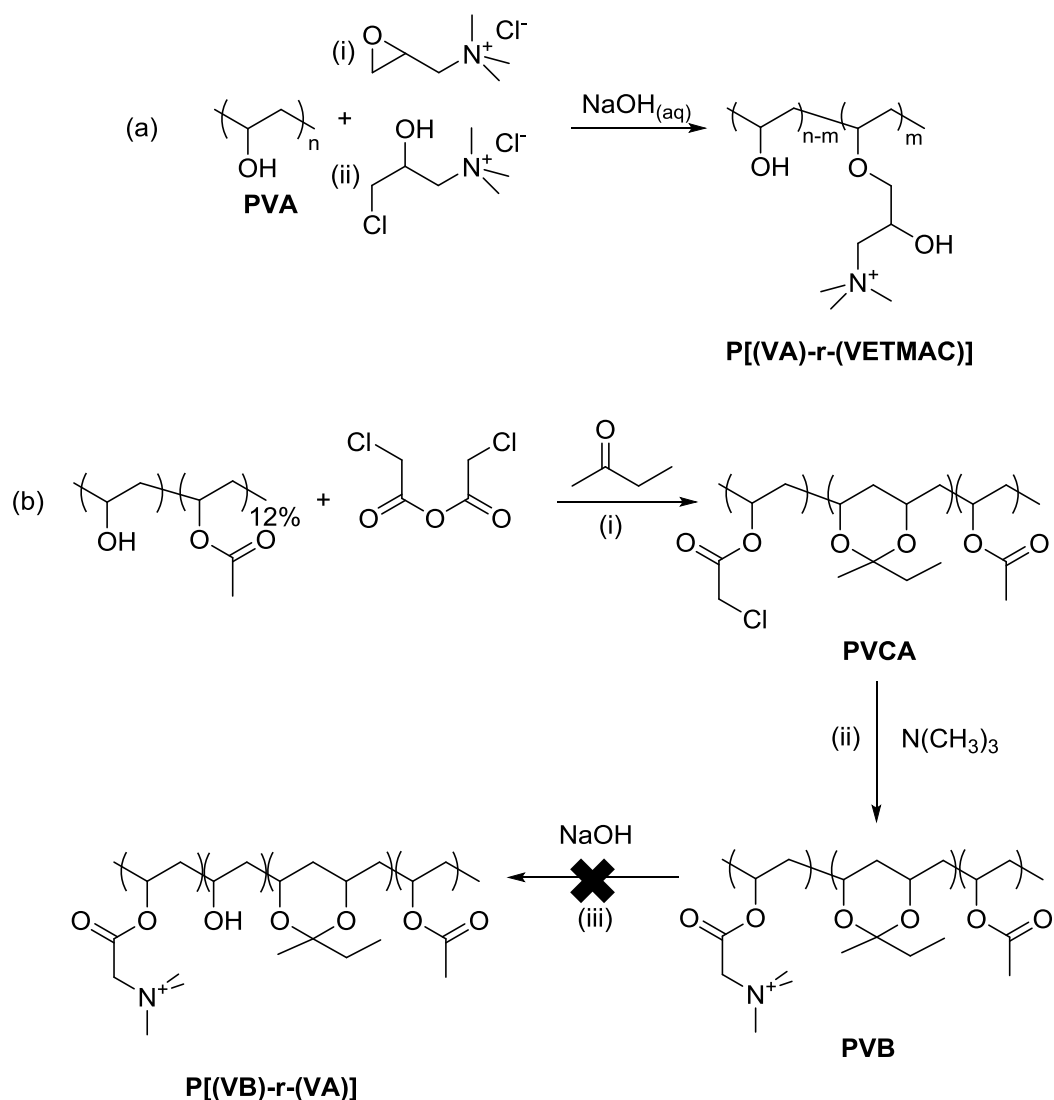
Chapter 8

Conclusions and future perspectives

8.1. Summary of work and general conclusions

The overall aim of the project was to synthesise a cationic polymer for potential use in personal products. Poly(vinyl alcohol) (PVA) was selected as a polymer backbone to be modified as it is a synthetic, water soluble, biocompatible and biodegradable polymer.

In Chapter 2, the methods already documented in the literature were followed to synthesise cationic PVA, before attempting improvements. Poly[(vinyl alcohol)-*ran*-(vinyl, 2-hydroxypropyl ether trimethylammonium chloride)] (P[(VA)-*r*-(VETMAC)]) was synthesised using PVA and either glycidyltrimethylammonium chloride (GTMAC) (Scheme 8.1.a.i) or 1,2-chlorohydroxypropyltrimethylammonium chloride (CHPTMAC) (Scheme 8.1.a.ii). An equation to determine the charge density (CD) based upon the quaternary nitrogen content (%QNC) was also derived. P[(VA)-*r*-(VETMAC)] synthesised using GTMAC produced greater CDs than when CHPTMAC was used. The molar equivalents of GTMAC and the addition of an inert diluent were investigated resulting in either small or no effect on the CD, respectively. Greater CDs than claimed in publications (1.7 meq g^{-1}) were achieved by slowing the rate of addition of GTMAC with a maximum CD of 2.5 meq g^{-1} being recorded.

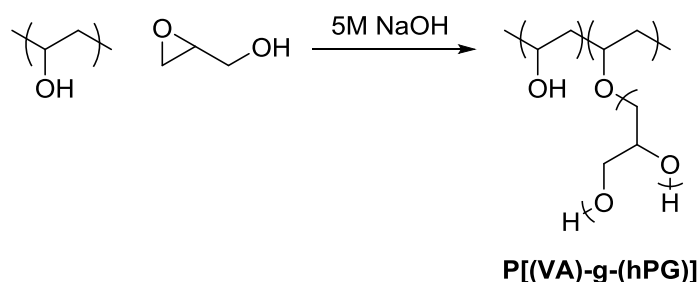


Scheme 8.1: (a) Synthesis of P[(VA)-r-(VETMAC)] using (i) GTMAC (ii) CHPTMAC; (b) (i) Synthesis of PVCA (ii) Synthesis of PVB (iii) Synthesis of P[(VA)-r-(VB)]

An alternative method was used to synthesise cationic PVA based on the synthesis of poly(vinyl betaine) (PVB) (Scheme 8.1.b). Initially, poly(vinyl chloroacetate) (PVCA) was successfully synthesised as an intermediate from the reaction of 88% hydrolysed PVA with chloroacetic anhydride (CAA) (Scheme 8.1.b.i). However, the formation of poly(vinyl butyral) (PVByl) segments was also observed due to the side reaction of PVA with butanone, used as the reaction solvent. PVB was then synthesised by the subsequent reaction of PVCA with trimethylamine (NMe_3) (Scheme 8.1.b.ii), to synthesise a copolymer with a composition of 85:3:12 for PVB:PVByl:PVAc with a CD of 5.3 meq g^{-1} . Controlling the CD of PVB by adjusting the molar equivalents of trimethylamine resulted in the formation of cross-linked materials by Williamson etherification between hydroxyl groups in PVA and chlorine atoms in PVCA. Therefore, an alternative route to control CD was attempted *via* the hydrolysis of PVB to synthesise poly[(vinyl alcohol)-*ran*-(vinyl betaine)] (P[(VA)-r-(VB)])

(Scheme 8.1.b.iii). However, the reaction was unsuccessful as this resulted in complete hydrolysis of PVB producing PVA.

In Chapter 3 a multifunctional graft copolymer was synthesised to increase the functionalisation potential of PVA. This was achieved by the ring-opening polymerisation of glycidol using PVA as a macroinitiator to synthesise poly[(vinyl alcohol)-*graft*-(hyperbranched polyglycerol)] (P[(VA)-*g*-(hPG)]), Scheme 2.



Scheme 8.2: Synthesis of P[(VA)-*g*-(hPG)]

PVA of different molecular weights were successfully used as macroinitiators for ROP of glycidol to synthesise the novel P[(VA)-*g*-(hPG)] with varying mole fractions of hyperbranched polyglycerol ($x_{(hPG)}$). P[(VA)-*g*-(hPG)] is soluble in water at room temperature unlike PVA, which requires heating for its dissolution.

P[(VA)-*g*-(hPG)] was synthesised using water as a solvent with a maximum $x_{(hPG)}$ of 42%, degree of substitution (%DS) of 20% and degree of branching (%DB) of 20%. The $x_{(hPG)}$ of P[(VA)-*g*-(hPG)] was increased by increasing the reaction temperature from 0 °C to 100 °C and the reaction time from 4 h to 24 h. Furthermore, an increase in $x_{(hPG)}$ was also observed for increasing molar equivalents of glycidol from 50% to 225% and addition time of glycidol from single addition to drop-wise over a 40 h time period. The increase in $x_{(hPG)}$ could also be achieved by increasing the concentration of PVA up to 5.68 mol L⁻¹ for LMW PVA or by using P[(VA)-*g*-(hPG)] as a macroinitiator for the ROP of glycidol.

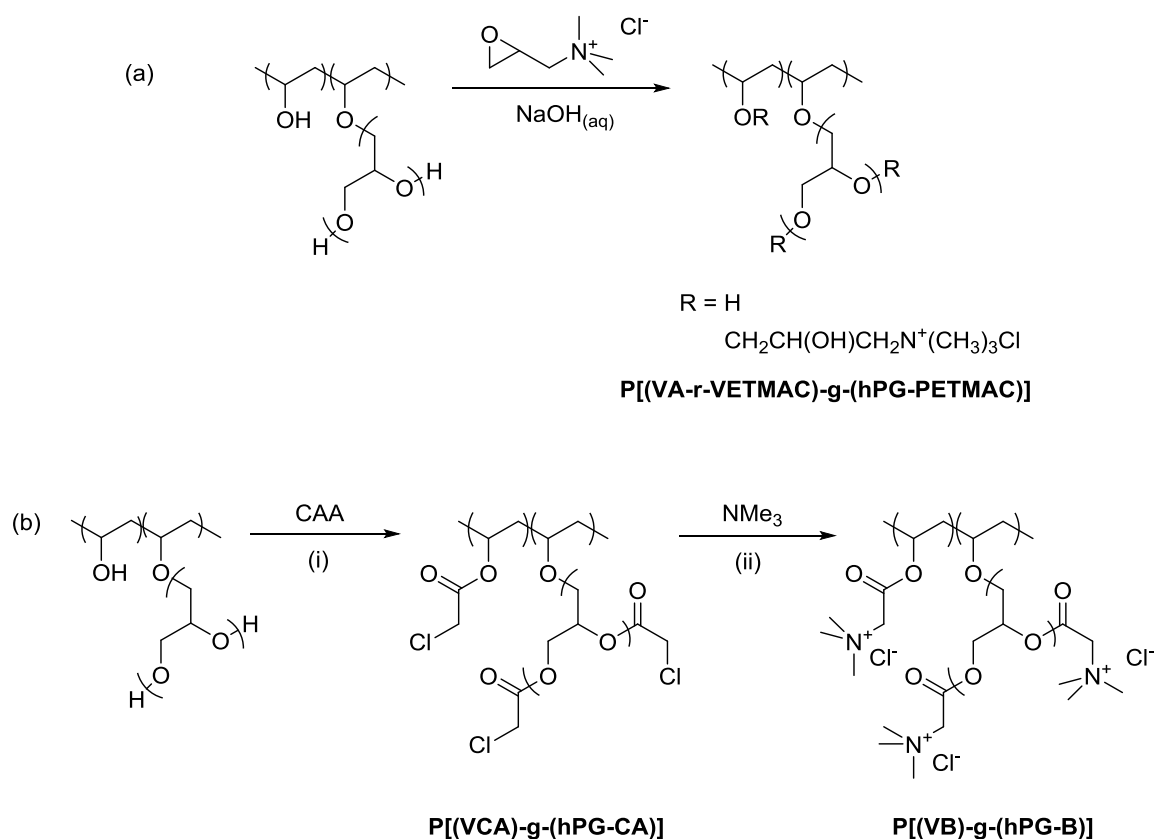
An increase in %DS coincided with an increase in the $x_{(hPG)}$. A small increase in %DB was observed with increasing temperature. A maximum in %DB was observed with increasing reagent addition time (31% after 12 h). The average %DB of P[(VA)-*g*-(hPG)] was 25%, indicating a slightly branched structure.

P[(VA)-*g*-(hPG)] was also synthesised in organic solvents with an $x_{(hPG)}$ of 45%, %DS of 19% and %DB of 19%. However, a discoloured product was recovered due to the side reaction between the solvent (dimethyl sulfoxide [DMSO]) and glycidol.

The χ_c of P[(VA)-g-(hPG)] decreased greatly in comparison with PVA, this is due to the disruption to the packing of polymeric chains from the addition of hPG. The T_m of P[(VA)-g-(hPG)] decreased with increasing $x(\text{hPG})$, this is due to the decrease in the χ_c . Furthermore, the change in degradation temperature of P[(VA)-g-(hPG)] compared with PVA was negligible.

PVA/hPG blends were produced; however the blends did not show the improved solubility, the change in melting point or the magnitude of the decrease in χ_c .

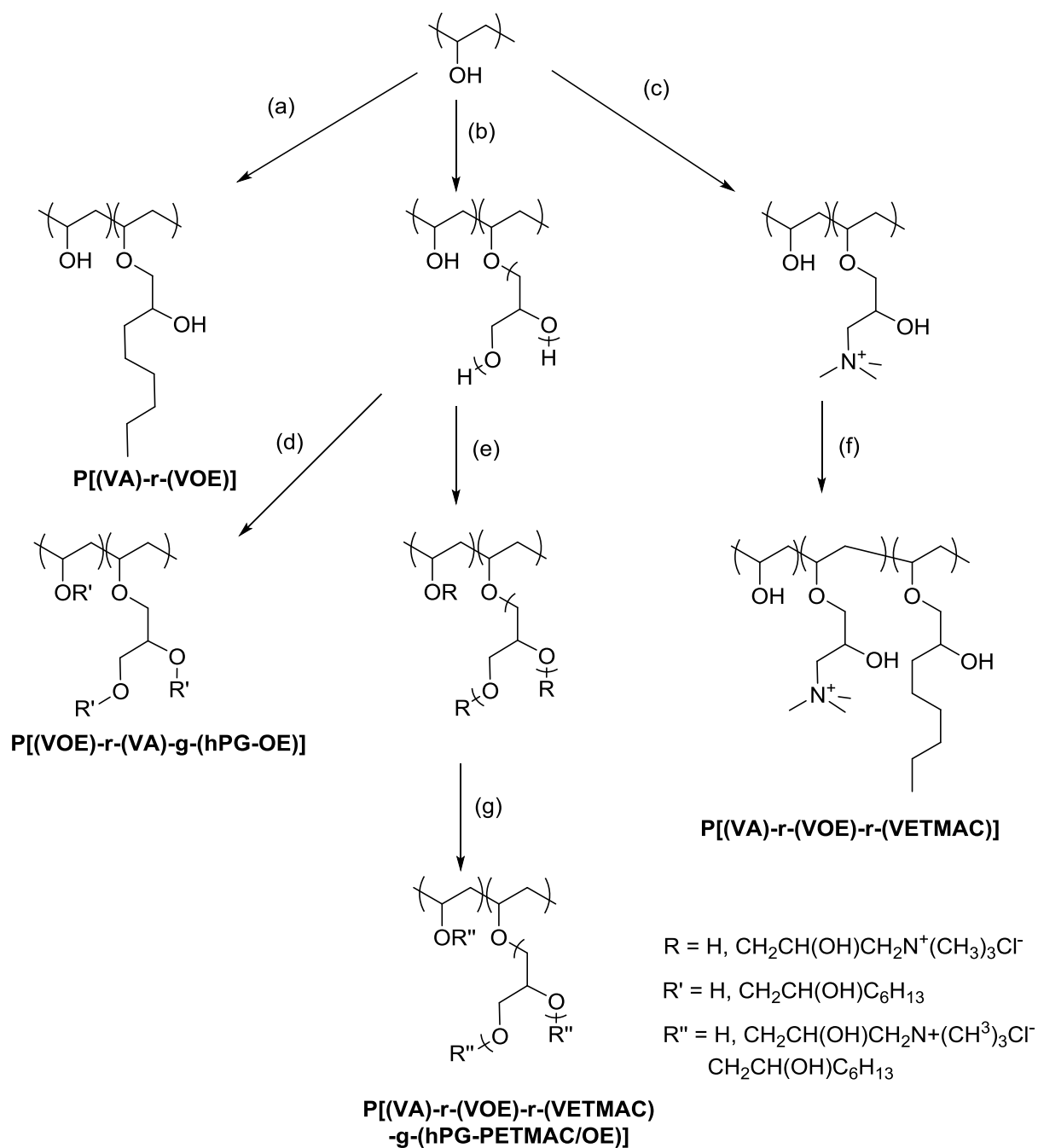
In Chapter 4, P[(VA)-g-(hPG)] was reacted with GTMAC to successfully synthesise poly[(vinyl alcohol)-ran—(vinyl, 2-hydroxypropyl ether trimethylammonium chloride)-graft-(hyperbranched polyglycerol-2-hydroxypropyl ether trimethylammonium chloride)] (P[(VA)-*r*-(VETMAC)-g-(hPG-PETMAC)]) (Scheme 8.3.a) and CDs greater than P[(VA)-*r*-(VETMAC)] (2.5 meq g⁻¹) were observed because of the increased availability of reactive hydroxyl moieties. The CD of these polymers increased with $x_{(\text{hPG})}$ of the P[(VA)-g-(hPG)] macroinitiator. The highest CD achieved was 5.81 meq g⁻¹.



Scheme 8.3: (a) Synthesis of P[(VA)-*r*-(VETMAC)-g-(hPG-PETMAC)] (b) (i) Synthesis of P[(VCA)-g-(hPG-CA)] (ii) Synthesis of P[(VB)-g-(hPG-B)]

P[(VA)-*g*-(hPG)] was reacted with CAA to synthesise poly[(vinyl chloroacetate)-*graft*-(hyperbranched polyglycerol 2-chloroacetate)] (P[(VCA)-*g*-(hPG-CA)]). However, complete conversion of all the hydroxyl groups in P[(VA)-*g*-(hPG)] was not achieved. The resulting P[(VCA)-*g*-(hPG-CA)] was quarternised with NMe₃ to synthesise poly[(vinyl betaine)-*graft*-(hyperbranched polyglycerol betaine)] (P[(VB)-*g*-(hPG-B)]). The composition of the polymer could not be determined, due to the coalesced resonances in the NMR spectra.

The hydrophobic interaction between a cationic polymer and anionic surfactants is integral in the deposition of silicone emulsion in shampoo formulations. Therefore in Chapter 5, epoxyoctane was reacted with PVA to synthesise poly[(vinyl alcohol)-*ran*-(vinyl, 2-hydroxy octyl ether)] (P[(VA)-*r*-(VOE)]) with increased hydrophobicity (Scheme 8.4.a). A degree of hydrophobic substitution (%HS) of 1.7% was determined by solution and solid state ¹H NMR spectroscopy. However, the recorded contact angles (initial and after 10 s) did not markedly differ. Epoxyoctane was reacted with P[(VA)-*r*-(VETMAC)] to synthesise poly[(vinyl alcohol)-*ran*-(vinyl, 2-hydroxy octyl ether)-*ran*-(vinyl, 2-hydroxypropyl ether trimethylammonium chloride)] (P[(VA)-*r*-(VOE)-*r*-(VETMAC)]) with a %HS of 2.8% (Scheme 8.4.f), the addition of the alkyl chain reduced the charge density from 0.88 meq g⁻¹ in P[(VA)-*r*-(VETMAC)] to 0.82 meq g⁻¹ in P[(VA)-*r*-(VOE)-*r*-(VETMAC)]. Therefore, the addition of the alkyl chains does not appear to significantly affect the CD. When epoxyoctane was reacted with the macroinitiator P[(VA)-*g*-(hPG)] to synthesise poly[(vinyl alcohol)-*ran*-(vinyl, 2-hydroxy octyl ether)-*graft*-(hyperbranched polyglycerol-2-hydroxyoctyl ether)] (P[VOE-*r*-(VA-*g*-hPG-OE)]) (Scheme 8.4.d), a %HS of 5.6% was recorded due to the increased availability of hydroxyl groups in comparison with PVA and P[(VA)-*r*-(VETMAC)] macroinitiators. In contrast with partially water soluble P[(VA)-*r*-(VOE)] at 80 °C, the incorporation of hydrophilic GTMAC and hPG in P[(VA)-*r*-(VOE)-*r*-(VETMAC)] and P[VOE-*r*-(VA-*g*-hPG-OE)], respectively, resulted in improved water solubility at 80 °C. However, the solutions solidified at ambient temperature.

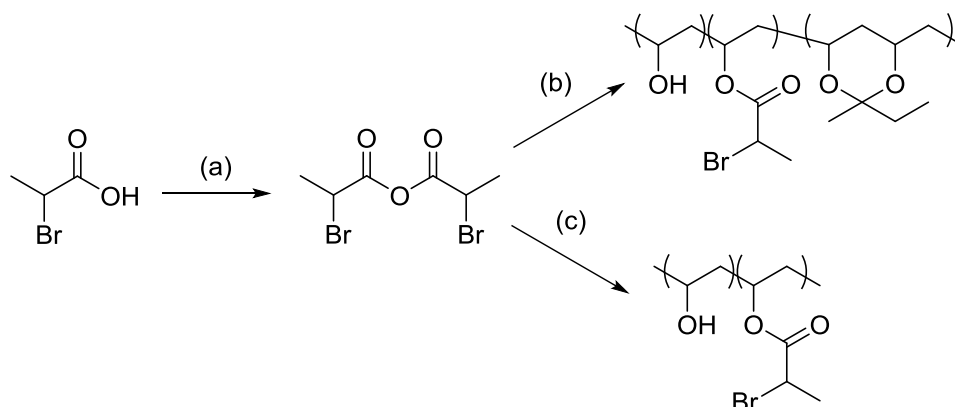


Scheme 8.4: (a) Synthesis of P[(VA)-r-(VOE)] (b) Synthesis of P[(VA)-g-(hPG)] (c) Synthesis of P[(VA)-r-(VETMAC)] (d) Synthesis of P[(VOE)-r-(VA)-g-(hPG-OE)] (e) Synthesis of P[(VA)-r-(VETMAC)-g-(hPG-PETMAC)] (f) Synthesis of P[(VA)-r-(VOE)-r-(VETMAC)] (g) Synthesis of P[(VA)-r-(VOE)-r-(VETMAC)-g-(hPG-PETMAC/OE)]

Epoxyoctane was reacted with P[(VA)-r-(VETMAC)-g-(hPG-PETMAC)] to synthesise the target material for shampoo formulations, poly[(vinyl, 2-hydroxy octyl ether)-*ran*-(vinyl, 2-hydroxypropyl ether trimethylammonium chloride)-*ran*-(vinyl alcohol)-*graft*-(hyperbranched polyglycerol)-(2-hydroxypropyl ether trimethylammonium chloride)/(2-hydroxy octyl ether)] (P[(VA)-r-(VOE)-r-(VETMAC)-g-(hPG-PETMAC-OE)]) (Scheme 8.4.g).

The resulting polymer which dissolves in water at 80 °C and remains in solution at ambient temperature, has a %HS of 3.8% and the CD was determined to be 1.23 meq g⁻¹. Moreover, the contact angle of P[(VA)-*r*-(VOE)-*r*-(VETMAC)-*g*-(hPG-PETMAC-OE)] did not decrease with time unlike any of the epoxyoctane containing polymers over a 10 s time period.

As well as the synthesis of cationic polymers for personal products the synthesis of graft copolymers was also investigated. In Chapter 6, the synthesis of PVA-based macroinitiators for single electron transfer (living radical polymerisation) (SET-LRP) was discussed. 2-Bromopropionic anhydride (BPA_{nh}) was synthesised *via* Steglich esterification of 2-bromopropionic acid using dicyclocarbodiimide (DCC). BPA_{nh} was then reacted with 88% LMW PVA in butanone to incorporate poly(vinyl, 2-bromopropionate) (PVBrP) segments in the polymer structure for use as initiating sites. However, PVByl was formed during the reaction limiting the conversion of PVA groups to PVBrP. The resulting poly[(vinyl, 2-bromopropionate)-*ran*-(vinyl, 2-butyral)] (P[(VBrP)-*r*-(VByl)]) has a composition of 39:35:14:18 (PVBrP:PVByl:PVA:PVAc), based on the ¹H NMR analysis.

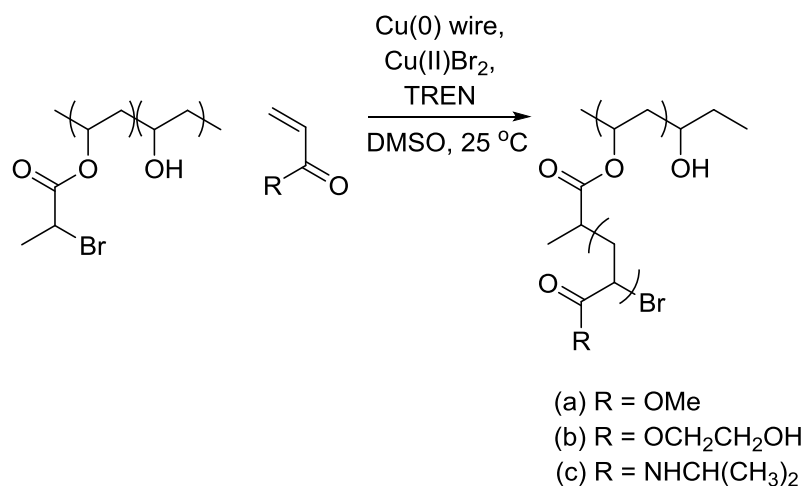


Scheme 8.5 (a) Synthesis of BPA_{nh} (b) Synthesis of P[(VBrP)-*r*-(VByl)] (c) Synthesis of P[(VA)-*r*-(VBrP)]

A change in the reaction solvent from butanone to 1,4-dioxane eliminated the formation of PVByl, and poly[(vinyl alcohol)-*ran*-(vinyl, 2-bromopropionate)] (P[(VA)-*r*-(VBrP)]) containing 62% PVBrP segments was synthesised. Increasing the molar quantity of BPA_{nh} increased the molar ratio of PVBrP segments to 79%.

In Chapter 7, a range of novel graft copolymers were synthesised using P[(VA)-*r*-(PVBrP)] as a macroinitiator, with varying compositions; Cu(0) wire, as a catalyst; tris(2-aminoethyl)amine (TREN), as a ligand; and Cu(II)Br₂, to reduce the initial radical concentration of the reaction mixtures, TREN was used instead of Me₆-TREN to limit the radical concentration. The novel graft copolymer, poly[(vinyl alcohol)-*ran*-(vinyl, 2-bromopropionate)-*graft*-(methyl acrylate)] (P[(VA)-*r*-(VBrP)-*g*-(MA)]) was synthesised using

methyl acrylate and P[(VA)-*r*-(PVBBrP)] as a macroinitiator, containing 62% or 79% initiating groups (VBrP) (Scheme 8.6.a). An M_p of $2.81 \times 10^5 \text{ g mol}^{-1}$ with a \mathcal{D} of 2.69 was determined from SEC for 79% P[(VA)-*r*-(VBrP)-*g*-(MA)]. However, a molecular weight (MW) of $2.31 \times 10^6 \text{ g mol}^{-1}$ was determined for the graft copolymer using AFM. A conversion (%conv) of 70% was determined which is much greater than quoted %conv for supplemental activator and reducing agent – atom transfer radical polymerisation (SARA-ATRP) graft copolymerisation technique used to synthesise poly(*n*-butyl acrylate) with a poly(methacrylate) backbone.² Furthermore, an M_p of $2.75 \times 10^5 \text{ g mol}^{-1}$ with a \mathcal{D} of 2.43 was determined for 62% P[(VA)-*r*-(VBrP)-*g*-(MA)].



Scheme 8.6: SET-LRP of P[(VA)-*r*-(PVBBrP)] to synthesise (a) P[(VA)-*r*-(VBrP)-*g*-(MA)] (b) P[(VA)-*r*-(VBrP)-*g*-(HEA)] (c) P[(VA)-*r*-(VBrP)-*g*-(NIPAM)]

Poly[(vinyl alcohol)-*ran*-(vinyl, 2-bromopropionate)-*graft*-(hydroxyethyl acrylate)] (P[(VA)-*r*-(VBrP)-*g*-(HEA)]) was successfully synthesised using hydroxyethyl acrylate (HEA) monomer and P[(VA)-*r*-(PVBBrP)] as a macroinitiator, containing 62% initiating groups (VBrP), under similar SET-LRP conditions to produce a water soluble graft copolymer with $M_p = 4.91 \times 10^5 \text{ g mol}^{-1}$ and $\mathcal{D} = 16.46$ (Scheme 8.6.b). The large \mathcal{D} is potentially due to unreacted macroinitiator. When the monomer (HEA) was not purified prior to polymerisation, an insoluble hydrogel was produced with a recorded water uptake of $50\% \pm 1\%$, which is greater than pure poly(hydroxyethyl acrylate) or PVA hydrogels.

Poly[(vinyl alcohol)-*ran*-(vinyl, 2-bromopropionate)-*graft*-(N-isopropylacrylamide)] (P[(VA)-*r*-(VBrP)-*g*-(NIPAM)]) was successfully synthesised using N-isopropylacrylamide monomer and P[(VA)-*r*-(PVBBrP)] as a macroinitiator, containing 62% initiating groups (VBrP), under similar SET-LRP conditions to produce a thermoresponsive graft copolymer with a $M_p = 3.32 \times 10^5 \text{ g mol}^{-1}$ and $\mathcal{D} = 13.64$ (Scheme 8.6.c). The large \mathcal{D} is potentially due to unreacted

macroinitiator. An LCST of 36 °C was observed for the graft copolymer, which is 4 °C greater than the LCST of Poly(NIPAM), this is potentially due to the macroinitiator containing hydrophilic PVA segments. Furthermore, a 5 °C hysteresis of the LCST for P[(VA)-*r*-(VBrP)-*g*-(NIPAM)] was observed, this is potentially due to the hydrogen bonding within the PNIPAM grafted chains in the globule conformation.

8.2. Preliminary evaluation of poly(vinyl alcohol)-based materials applicability for use with shampoo formulations

In Chapters 2, 3, 4 and 5, polymers for use in personal products were synthesised. Polymer samples of P[(VA)-*g*-(hPG)] and P[(VA)-*r*-(VETMAC)-*g*-(hPG-PETMAC)] were sent to Ashland Inc. (New Jersey, USA), one of the sponsors of the project, for physical properties test. Preliminary tests have shown that hair tresses coated with P[(VA)-*g*-(hPG)] and kept in a room of 90% relative humidity at 32 °C retain their curl better than hair tresses coated with PVA (Figure 8.1).

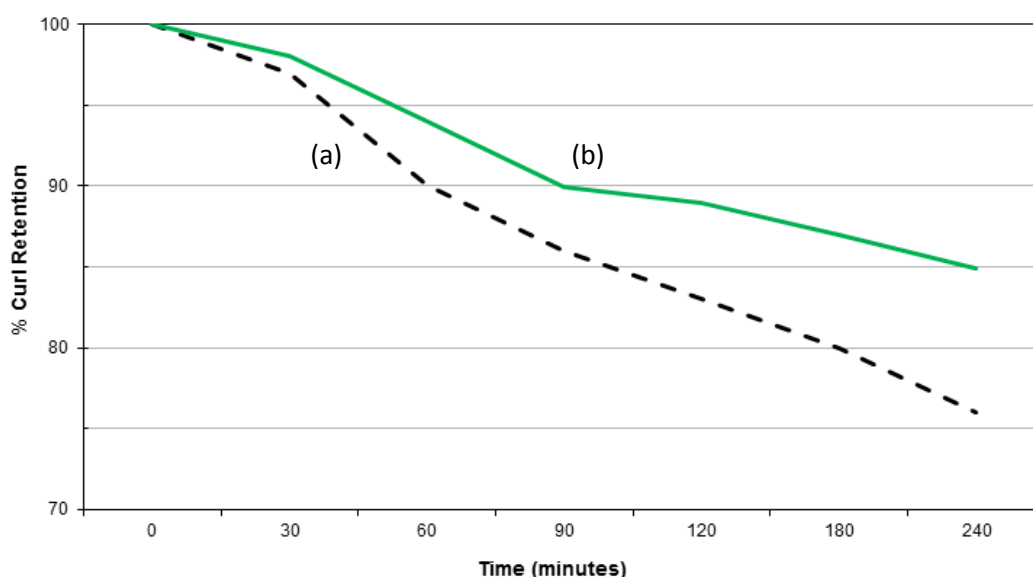


Figure 8.1: Curl retention test of (a) PVA (b) P[(VA)-*g*-(hPG)]

Furthermore, two judges from Ashland Inc. performed qualitative test in a temperature and humidity controlled room on curled hair tresses treated with polymer solutions (5 %wt) of PVA, P[(VA)-*g*-(hPG)] and P[(VA)-*r*-(VETMAC)-*g*-(hPG-PETMAC)]. The hair tresses were subjectively compared on a numeric scale between 0 and 10 for shine/lustre, stiffness, crunch, curl snap, manageability, residual polymer and static. P[(VA)-*g*-(hPG)] (red bar) and P[(VA)-*r*-(VETMAC)-*g*-(hPG-PETMAC)] (green bar) both compare favourably with PVA (blue bar) in regards to lack of sample left upon treated hair tresses and on a comb. Moreover,

P[(VA)-*r*-(VETMAC)-*g*-(hPG-PETMAC)] shows largely superior stiffness and curl snap compared to the other two samples.

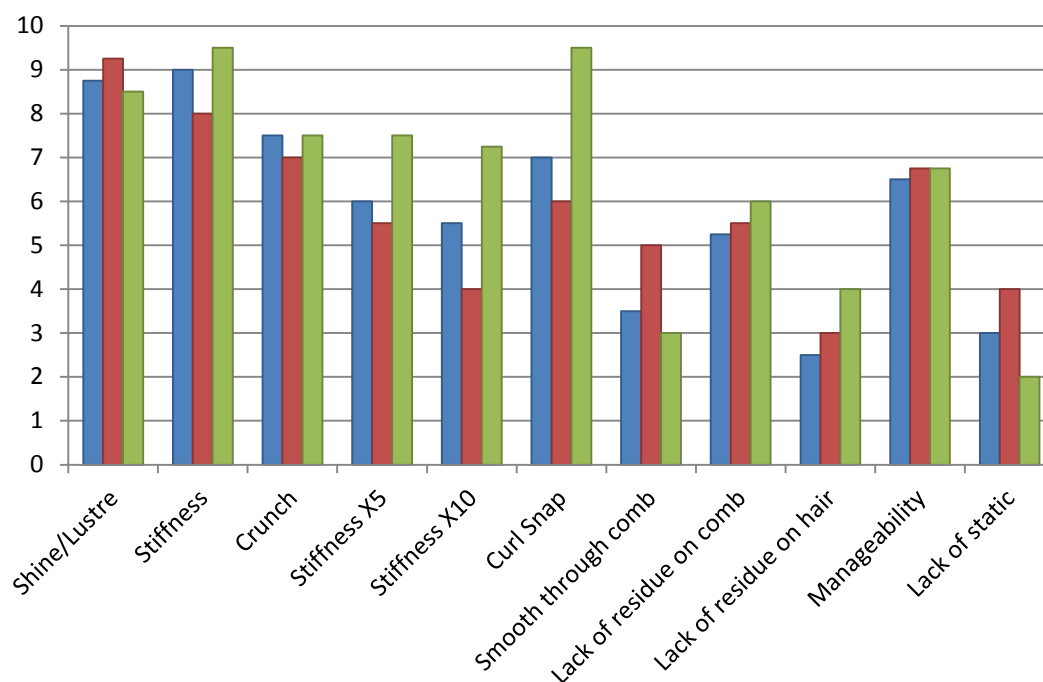


Figure 8.2: The qualitative rankings of (a) PVA (blue bar) (b) P[(VA)-*g*-(hPG)] (red bar) (c) P[(VA)-*r*-(VETMAC)-*g*-(hPG-PETMAC)] (green bar)

8.3. Future perspectives

8.3.1. Application evaluation

However, more extensive testing is required to establish the true efficacy of these materials. This can be done by modelling the deposition and desorption behaviour of the cationic polymer onto a silica surface, using *in situ* ellipsometry. The layer thickness of the polymer and silicone emulsion at different surfactant concentrations and after rinsing can be recorded following a method outlined by Picullel *et al.*³ This would reveal the maximum amount of silicone emulsion deposited, and how completely it is removed from the surface. Tests of the shampoo formulations on hair samples are also required to inform on the physical properties imbued onto washed hair. As the amount of silicone emulsion is not the only determiner, *e.g.* the conformation of the coacervate can affect the imbued properties. Moreover, the critical aggregation concentrations can be determined by changes in turbidity of an aqueous cationic polymer solution with increasing surfactant concentration, following a method outlined by Johnson *et al.*⁴ The results of these tests can then influence further developments to maximise performance and the role of the different component parts have.

8.3.2. Synthetic work

Aside from more testing of the prepared materials, the synthesis of P[(VA)-*g*-(hPG)] in DMSO could be further investigated as a greater $x_{(hPG)}$ was recorded than when the ROP was carried out using water as a solvent. The main aims of this investigation would be to increase the length of the grafted chains and to establish whether a white polymer could be synthesised, which is preferential for clear shampoo formulations.

As P[(VA)-*g*-(hPG)] is a versatile functional polymer its application is not limited to personal products. PVA is used in food packaging, therefore the efficacy of P[(VA)-*g*-(hPG)] for use in food packaging could be investigated. A cross-linked material could be prepared by using citric acid as a crosslinker (previously used for PVA)⁵ whilst maintain the biocompatibility of the material. Furthermore, modifications of hPG with small molecules (*e.g.* sulphates and amines) to synthesise ionic polymers or amphiphilic polymers (*e.g.* fatty acids) for drug delivery have also been carried out.^{6,7} These methods could be applied to P[(VA)-*g*-(hPG)] as well.

The synthesis of the macroinitiators and graft copolymers synthesised in Chapters 6 and 7 could also be investigated. A larger range of macroinitiator composition could be established, by modifying the molar ratio of BPAnh used. The initiator efficiency is required for accurate determination of the MW. This could be determined by hydrolysis to remove the ester linkage connected the graft copolymers; the MW of the grafted chain can then be used to determine the initiator efficiency.² Synthesising graft copolymers with greater MW could be attempted by either increasing the length of the polymer backbone by using PVA with a greater MW, or by targeting longer grafted polymer chains.

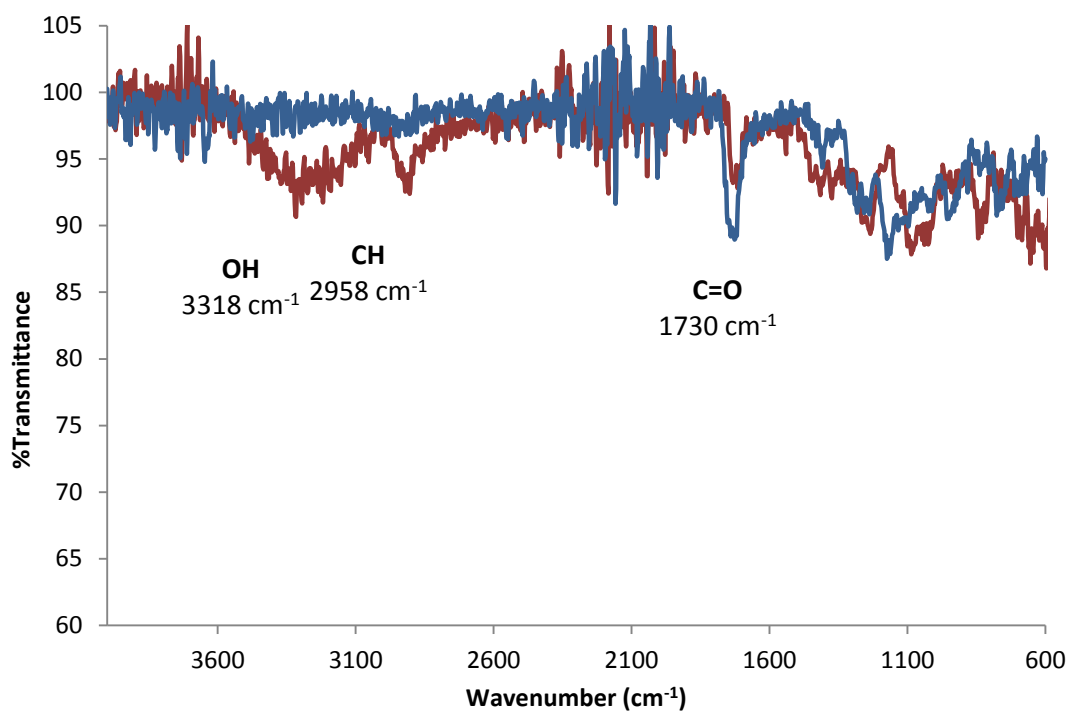
The composition of the graft copolymers could be further altered to include different monomers depending on the potential application, such as vinylbenzyl chloride and the subsequent graft copolymer could be quarternised with NMe₃ to produce a cationic polymer. Copolymer grafted chains could also be targeted, for instance, acrylic acid could be incorporated into the side chains of P[(VA)-*r*-(VBrP)-*g*-(NIPAM)] to include pH responsivity to the material.⁶

8.3. References

- (1) Fatehi, P.; Xiao, H. N.; van de Ven, T. G. M. *Langmuir* **2011**, *27*, 13489.
- (2) Nese, A.; Li, Y. C.; Sheiko, S. S.; Matyjaszewski, K. *ACS Macro Lett.* **2012**, *1*, 991.
- (3) Clauzel, M.; Johnson, E. S.; Nylander, T.; Panandiker, R. K.; Sivik, M. R.; Piculell, L. *ACS Appl. Mater. Interfaces* **2011**, *3*, 2451.
- (4) Svensson, A. V.; Huang, L.; Johnson, E. S.; Nylander, T.; Piculell, L. *ACS Appl. Mater. Interfaces* **2009**, *1*, 2431.
- (5) Musetti, A.; Paderni, K.; Fabbri, P.; Pulvirenti, A.; Al-Moghazy, M.; Fava, P. *J. Food Sci.* **2014**, *79*, E577.
- (6) Jones, C. D.; Lyon, L. A. *Macromolecules* **2000**, *33*, 8301.

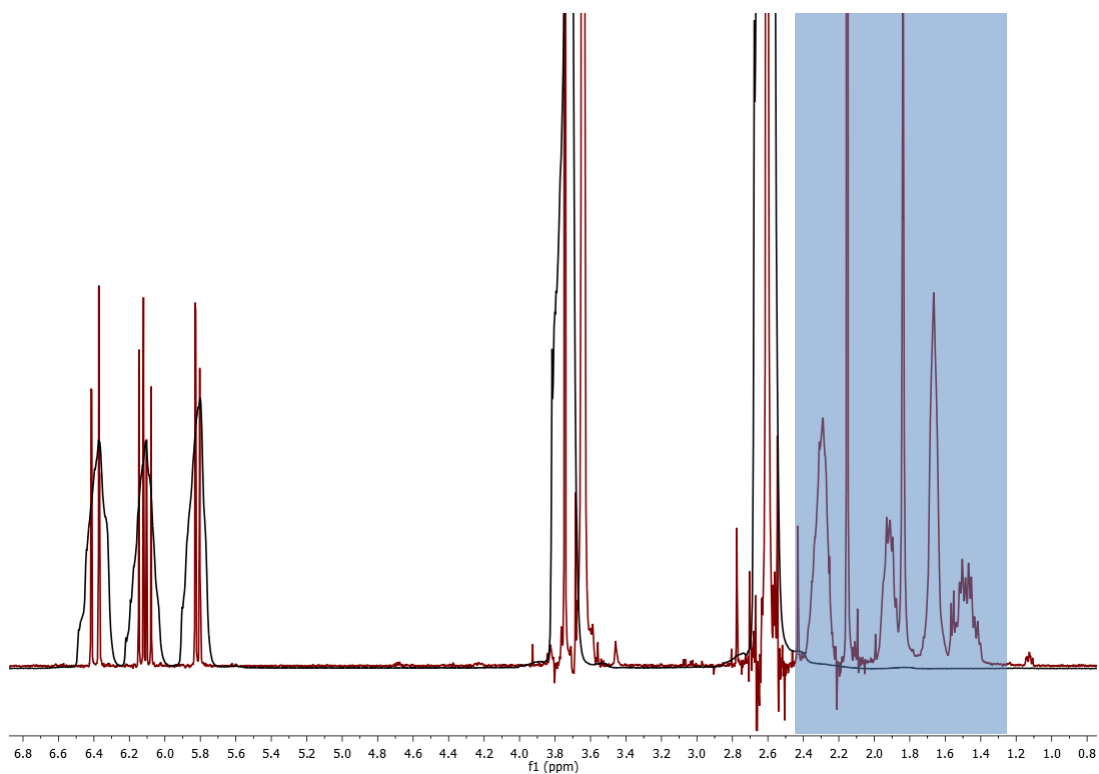
Appendix

Appendix 1 - Appendices for Chapter 2

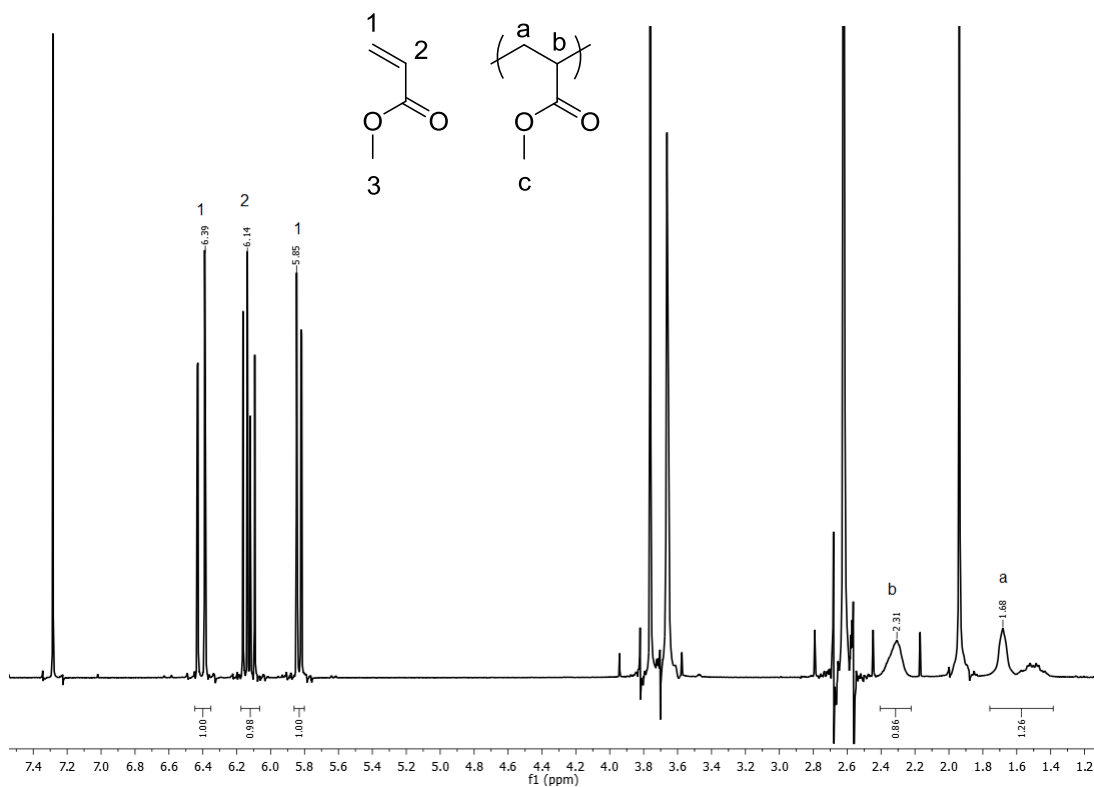


Appendix 2.1: FT-IR spectrum of PVCA (—) and 88% hydrolysed PVA (—)

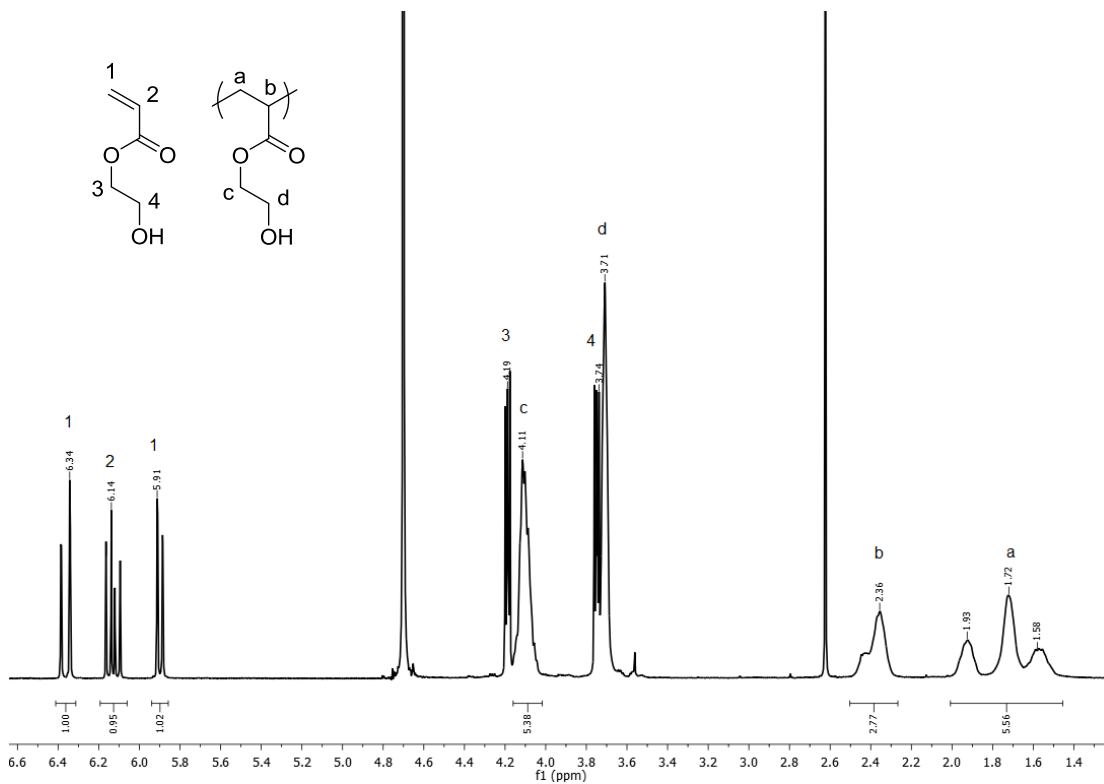
Appendix 2 - Appendices for Chapter 7



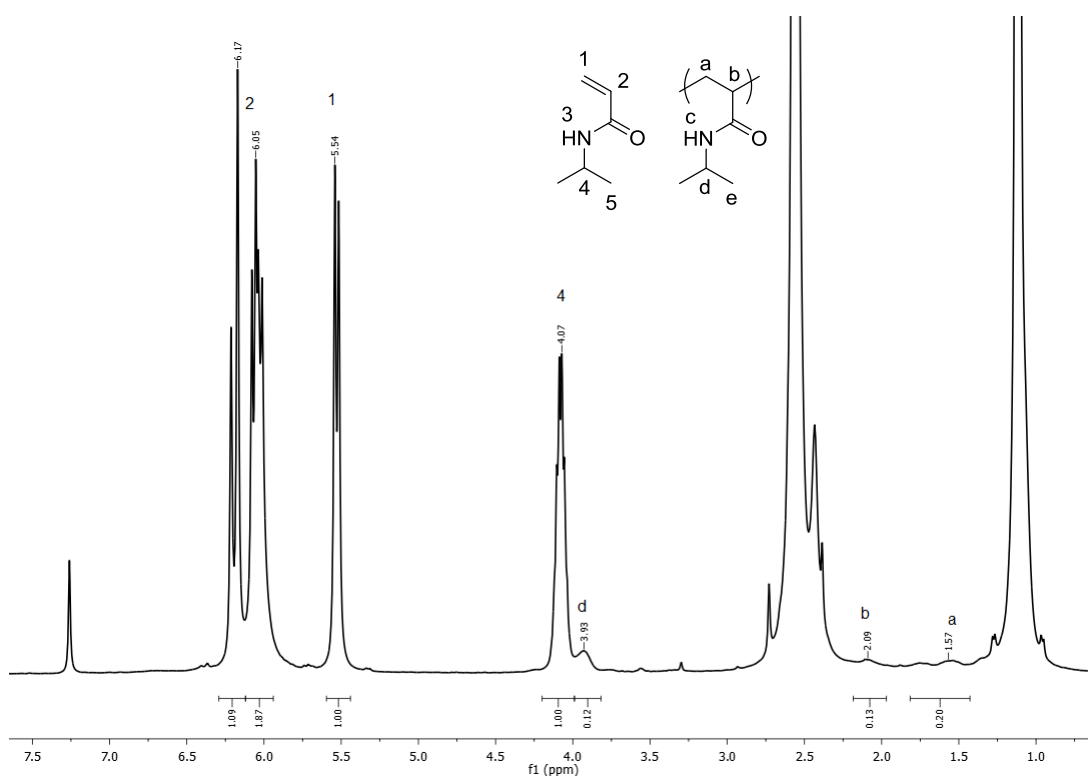
Appendix 7.1: 400 MHz ¹H NMR spectra in CDCl₃ of reaction mixtures of blank (—) and PMA (—); the ppm range where resonances corresponding to the polymer backbone is highlighted



Appendix 7.2: 400 MHz ¹H NMR of 62% P[(VA)-*r*-(VBrP)-*g*-(MA)] polymerisation mixture in CDCl₃



Appendix 7.3: 400 MHz ¹H NMR of P[(VA)-*r*-(VBrP)-*g*-(HEA)] polymerisation mixture in CDCl₃



Appendix 7.4: 400 MHz ^1H NMR of P[(VA)-*r*-(VBrP)-*g*-(NIPAM)] polymerisation mixture in CDCl_3